DETERMINING THE ROLE OF GROWTH DIFFERENTIATION FACTOR-6 (GDF6) IN THE DEVELOPMENT OF THE CORONAL SUTURE

By

Dawn Elizabeth Clendenning

Dissertation

Submitted to the Faculty of the

Graduate School of Vanderbilt University

in partial fulfillment of the requirements for

the degree of

DOCTOR OF PHILOSOPHY

in

Human Genetics

May, 2012

Nashville, Tennessee

Approved:

Professor Douglas P. Mortlock

Professor Ela W. Knapik

Professor Michelle Southard-Smith

Professor Patricia Labosky

Professor Xiangli Yang

To my parents, Bill and Kathy, for their love, sacrifice, and encouragement
and
To my husband, Jeremy; my best friend and love of my life

ACKNOWLEDGEMENTS

The work presented in this dissertation was supported in part by the NIH Genetics Training Grant (T32GM080178) and the NIH Developmental Biology Training Grant (T32HD07502). Thanks to my committee for pushing me to be a better scientist: Ela Knapik (committee chair), Michelle Southard-Smith, Xiangli Yang, and Trish Labosky. You are all inspirations for women in science. I would like to especially thank my mentor, Doug Mortlock, whose door was always open. Doug has an enthusiasm for science that is contagious and his eternal optimism that any experiment can work served as a great encouragement. Thank you for providing me with a project that fostered my love for development!

I would also like to thank the past and present members of the Mortlock lab: Yue Hou, Ron and Kelly Chandler, Nyk Reed, Eva Broeckelmann, and Steve Pregizer. My lab mates were always willing to lend a hand or baby-sit my mice! Your insights and discussions at lab meetings contributed greatly to my work. Thanks to the students and faculty of the Program in Human Genetics and the Program in Developmental Biology for your time and investment in my education.

We gratefully thank Dr. Robert Maxson and Nancy Wu for the training in bead implantation and culture methods; and for many helpful discussions. Also, Michelle Southard-Smith for allowing me to monopolize her cryostat for months on end. Special thanks to my Grove City College biology professors: Dr. Sodergren, Dr. Ray, Dr. Jones, Dr. Shaw, and Dr. Jenkins, for teaching me that I do not need to compromise my faith in order to do good science.

I would like to thank my sisters, Katie and Bonnie, for celebrating every passed qualifying exam and committee meeting with me, even if you didn't really know what a qualifying exam or committee meeting were. Thank you to my Grandmom Foehr, who asked me every Sunday for the past five years what I did this week in research.

To my daughter, Miriam: you have brought more joy to my life than I could have ever imagined. Although you won't remember, we spent many days in the mouse room before you were born and then your first week of life writing this thesis together.

I would like to thank my best friend and the love of my life, my husband, Jeremy. He came with me to this strange world south of the Mason-Dixon line and has listened to endless practice talks about "cranial sutures". Without your daily support, humor, and encouragement, I would have never made it through grad school. I look forward to the next exciting chapter in our lives together!

I would like to dedicate this body of work to my parents, Bill and Kathy, who instilled in me a love for the natural world. You have given countless sacrifices to give to me an education, and I want you to know they have not gone unnoticed or unappreciated. I hope I have made you proud.

Finally, I would like to give thanks to my Lord and Savior, who created a world of beauty, where there will always be things to inspire awe and new questions to be asked.

TABLE OF CONTENTS

LIST OF TABLES

LIST OF FIGURES

LIST OF APPENDICES

CHAPTER I

INTRODUCTION

Cranial sutures

Anatomy and origins of the cranial vault

The mammalian calvaria, or skull vault, houses and protects the brain and sensory organs. It is composed of five main flat bones, including pairs of the frontal, parietal, and squamosal bones, and the anterior portion of the occipital bone. Flexible joints composed of fibrous connective tissue separate the cranial bones. These are termed the cranial sutures. Although sutures are found throughout the skull, there are five major sutures in the cranial vault. These include the sagittal suture (between the paired parietal bones), coronal suture (between the frontal and parietal bones), lambdoid suture (between the parietal and occipital bones (the occipital is also referred to as the interparietal bone in the murine skull)); squamosal suture (between the squamosal and parietal bones), and the metopic/interfrontal suture (between the paired frontal bones) (Fig 1.1).

The cranial sutures are not simply a space between the bones, but a complex structure made of multiple components. These include: 1) the differentiated bones; 2) the bone fronts, which are regions of proliferating and differentiating osteoblasts lining the edges of the advancing bones, 3) the suture mesenchyme, which remains undifferentiated; 4) the periosteum; and 5) the dura (Fig 1.2). Each of these components provides signals that are necessary for the formation and maintenance of a newly formed suture.

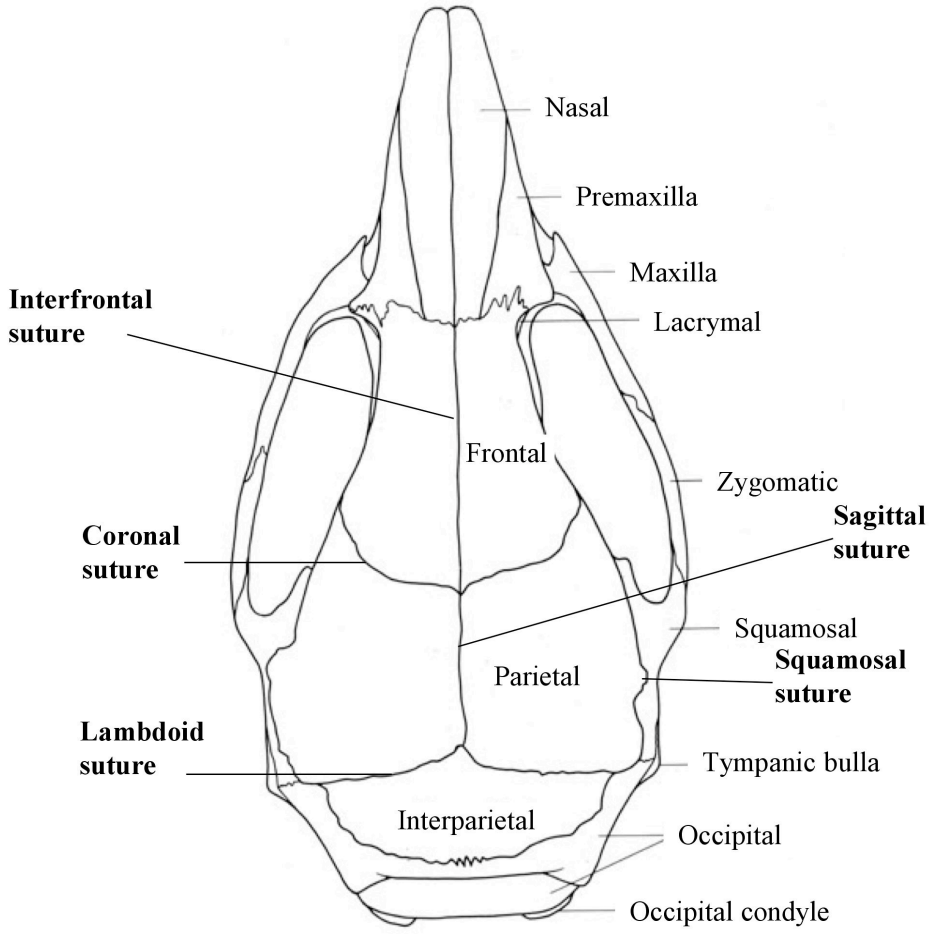

Figure 1.1. Cranial bones and sutures. The mammalian skull is composed of paired frontal, parietal, and squamosal bones, plus the anterior portion of the occipital bone (the occipital is also known as the interparietal bone in mice). These bones form through intramembranous ossification, which occurs without a cartilage intermediate. Separating the cranial bones are flexible joints known as the cranial sutures. These include the interfrontal suture (separating the paired frontal bones), sagittal suture (separating the paired parietal bones), coronal suture (separating the frontal and parietal bones), squamosal suture (separating the parietal and squamosal bones), and lambdoid suture (separating the parietal and interparietal/occipital bones). The sutures are the main sites for cranial growth during development.

Adapted from The Anatomy of the Laboratory Mouse, Margaret J. Cook 1965.

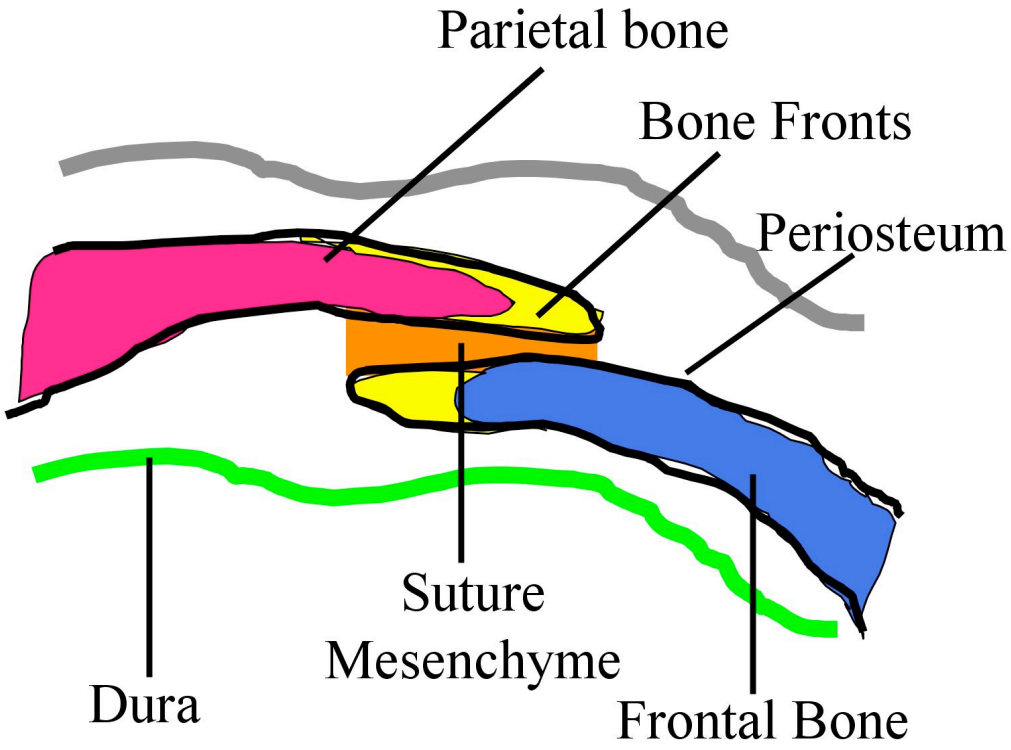

Figure 1.2. Components and structure of the suture. The suture is composed of: 1) the differentiated bones (here the frontal bone, blue; parietal bone, red); 2) the bone fronts (yellow), which contain the proliferating and differentiating osteoblasts; 3) the undifferentiated suture mesenchyme (orange); 4) the periosteum (black); and 5) the dura (green).

Along with fontanelles (the soft spots in a newborn's head), the sutures provide flexible joints for the compression of the calvaria during passage through the birth canal. However, as the calvaria grows after birth, the fontanelles quickly diminish, but the sutures remain (Rice, 2008). The sutures are the main sites for cranial growth during development. These dynamic structures also act as shock absorbers, prevent separation of the cranial bones, and accommodate room for the rapidly growing brain (Cohen, 2005).

The cranial bones are of mixed origin, being derived from both the cranial neural crest and the paraxial mesoderm. The neural crest is a distinct ectoderm population in vertebrates. A portion of these cells migrate off the crest of the neural tube into multiple regions of the developing embryo, differentiating into structures including cranial ganglia, cartilage, bone, and connective tissue (Knecht and Bronner-Fraser, 2002). The paraxial mesoderm is a cell population located on either side of the neural tube. During development they pinch off into a defined number of somites and go on to form the vertebrae, ribs, and skeletal muscle (Gilbert, 2003).

Origin of cranial tissues in mice: The exact contribution of the neural crest and mesoderm to each of the bones and sutures was highly controversial. Bones were sometimes assigned different origins depending on the lab or method of study. Historically, fate-labeling methods used to map neural crest contributions have included dye labeling and β-galactosidase retroviral infection. A more definitive genetic methodology was developed utilizing the *Wnt1-Cre* and *R26R* mouse lines (Fig 1.3A). In the *Wnt1-Cre* transgenic mice, Cre recombinase is expressed under the control of the

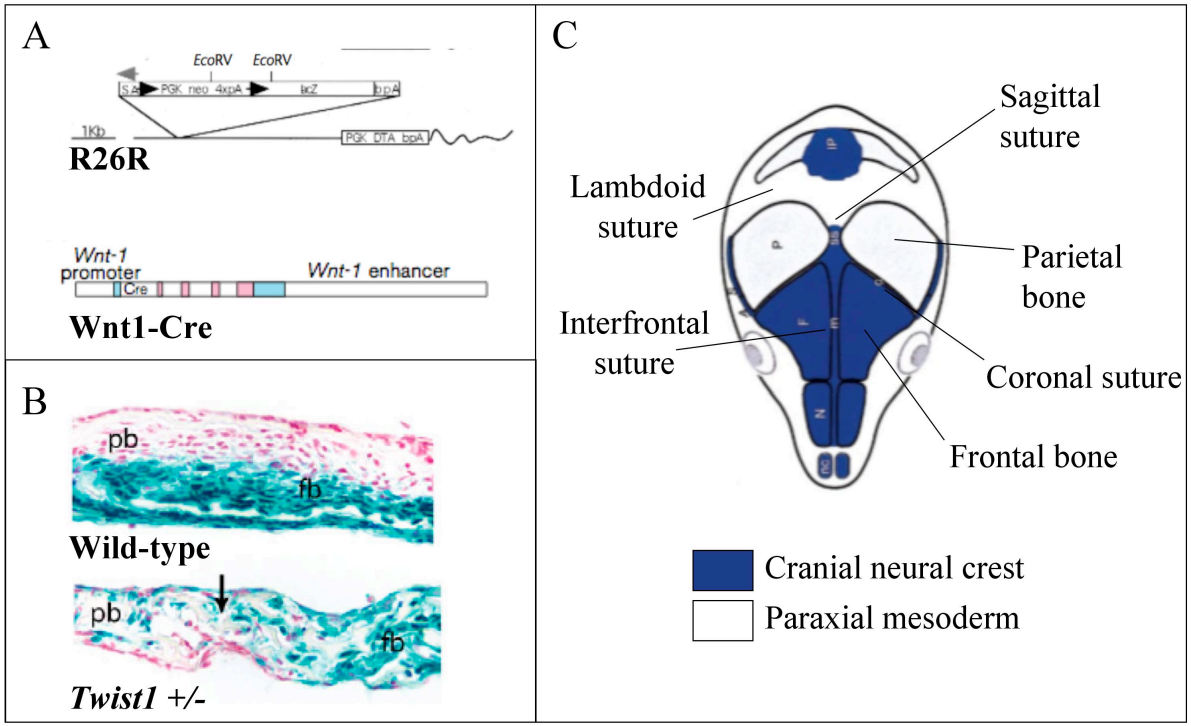

Figure 1.3. Fate mapping of the cranial bones. A) (Above) Structure of the *R26R* locus, which stably expresses ß-galactosidase upon Cre-mediated recombination. (Below) The *Wnt1-Cre* transgene, which expresses *Cre* under the control of the *Wnt1* promoter and enhancer. When expressed together, they stably label derivates of the neural crest with *lacZ*. Adapted from Soriano 1999 and Danielian et al. 1998. B) (Above) *Wnt1-Cre* and *R26R* labeling of a wild-type coronal suture reveals a distinct boundary between the frontal bone cells (labeled with *lacZ*) and the cells of the parietal bone. (Below) In the *Twist1* mutant there is a mixing of the frontal and parietal bone cells (arrow) at sites of coronal craniosynostosis. Adapted from Merrill et al. 2006. C) Origins of each of the cranial bones and sutures in the mammalian skull as determined by fate mapping studies using the *Wnt1-Cre* and *R26R* mouse lines. The nasal, frontal, and interparietal bones are derived from the cranial neural crest (blue) along with the interfrontal suture and a portion of the sagittal suture. The parietal and occipital bones and the lambdoid and coronal sutures are derived from the paraxial mesoderm. Adapted from Jiang et al. 2002. fb, frontal bone; pb, parietal bone.

Wnt1 promoter and enhancer (Danielian et al., 1998). *Wnt1* is expressed transiently in the neural plate, dorsal neural tube, and early migrating neural crest cells, and is silenced after the neural crest migrates away from the neural tube (Jiang et al., 2000). The skeletogenic cranial neural crest cells in the branchial arches, which contribute to the facial and cranial bones, are all derived from *Wnt1*-expressing cells (Jiang et al., 2002). The *R26R* mouse line expresses β-galactosidase from the ROSA26 locus following Cre-mediated recombination (Soriano, 1999). ROSA26 is a ubiquitously expressed locus, and therefore, the combination of *R26R* and *Wnt1-Cre* alleles together results in expression of β-galactosidase in migrating neural crest cells and their derivatives. Once a *R26R*-carrying cell undergoes Cre-mediated recombination it will stably express β-galactosidase, allowing labeling of neural crest-derivatives throughout development.

These tools demonstrated that the frontal bone and the underlying dura in mice are derived from the neural crest, with the parietal bone derived entirely from the paraxial mesoderm (Jiang et al., 2002). The boundary between rudiments of the frontal and parietal bones, the future site of the coronal suture (CS), is evident in mouse embryos as early as embryonic day (E) 9.5, at the end of neural crest migration (Jiang et al., 2002). The interfrontal suture mesenchyme and a portion of the sagittal suture extending from the frontal bones are also neural crest-derived, whereas the remaining sutures are mesoderm-derived (Fig 1.3C). Therefore, the CS and a portion of the sagittal suture form at interfaces between cell populations of different embryonic origins. In contrast, the interfrontal suture is formed at the junction between two neural crest-derived bones with a neural crest-derived suture, with no involvement of the mesoderm (Fig 1.3C) (Jiang et al., 2002)

Origins of cranial tissues in other vertebrates: Due to their quick reproductive cycle and large number of progeny, zebrafish are an attractive model organism for developmental research. Although not historically used to study cranial development and the suture, zebrafish do have a highly similar cranial anatomy compared to humans and mice (Quarto and Longaker, 2005), including the presence of interfrontal, coronal, sagittal, and lambdoid sutures. The origins of the bones are also the same, with frontal bones derived from cranial neural crest and parietal bones derived from paraxial mesoderm.

The arrangement of the cranial bones and sutures in zebrafish is not conserved across all vertebrate species. Although the mammalian frontal bones are now believed to be derived from the cranial neural crest, the frontal bones in avians have a dual neural crest/mesoderm origin, and therefore the boundary between the two does not form at a cranial suture (Evans and Noden, 2006). However, it theorized that early in avian evolution, the frontal and parietal fused into a single bone, which extend as far back as the cerebellum (Morriss-Kay, 2001). Frogs do in fact have a single frontal-parietal bone, but it is composed entirely of neural crest origin (Hanken and Gross, 2005). Although the cranial bones may be anatomically similar, this does not mean they are also evolutionarily homologous.

Mice are an optimal model system for study of the human coronal suture because of the homology between mice and human in the origins of the cranial bones and the possibility that tissue origin has a critical impact on the development of the cranial suture. Also, the genetic tools available in mice for fate mapping this cell population make mice an ideal model organism for studying human suture development.

Intramembranous ossification and development of the cranial sutures

The flat bones of the skull vault form through the process of intramembranous ossification. In contrast to the endochondral ossification of the long bones (Fig 1.4A), intramembranous ossification occurs without a cartilage intermediate and instead, osteoblasts differentiate directly from mesenchymal cells (Fig 1.4B). An exception is the occipital bone: the anterior portion forms through intramembranous ossification while the posterior portion forms through endochondral ossification (Fig 1.4C). In mice, the anterior and posterior portions form two separate bones, the interparietal and occipital bones respectively (Fig 1.1). However, in the majority of humans, the anterior and posterior portions form from multiple ossification centers that fuse into a single occipital bone (Shapiro and Robinson, 1976).

In addition to the flat bones of the skull, portions of the clavicle, mandible, maxilla, scapula, and pelvis all form through intramembranous ossification. It was previously hypothesized that all intramembranous bones were neural crest-derived and endochondral bones were derived from the mesoderm. However, this was contradicted by the mesoderm-derived parietal bone, which forms through intramembranous ossification (Jiang et al., 2002), and areas of the shoulder girdle and cervical vertebrae that are neural crest-derived and form endochondral bone (Matsuoka et al., 2005). Instead, portions of the bones in the neck and shoulder region have the same origins as the muscles at the site of attachment (Matsuoka et al., 2005).

The ossification of the cranial vault begins with the migration of mesenchymal cells to positions between the surface ectoderm and the brain (Lenton et al., 2005).

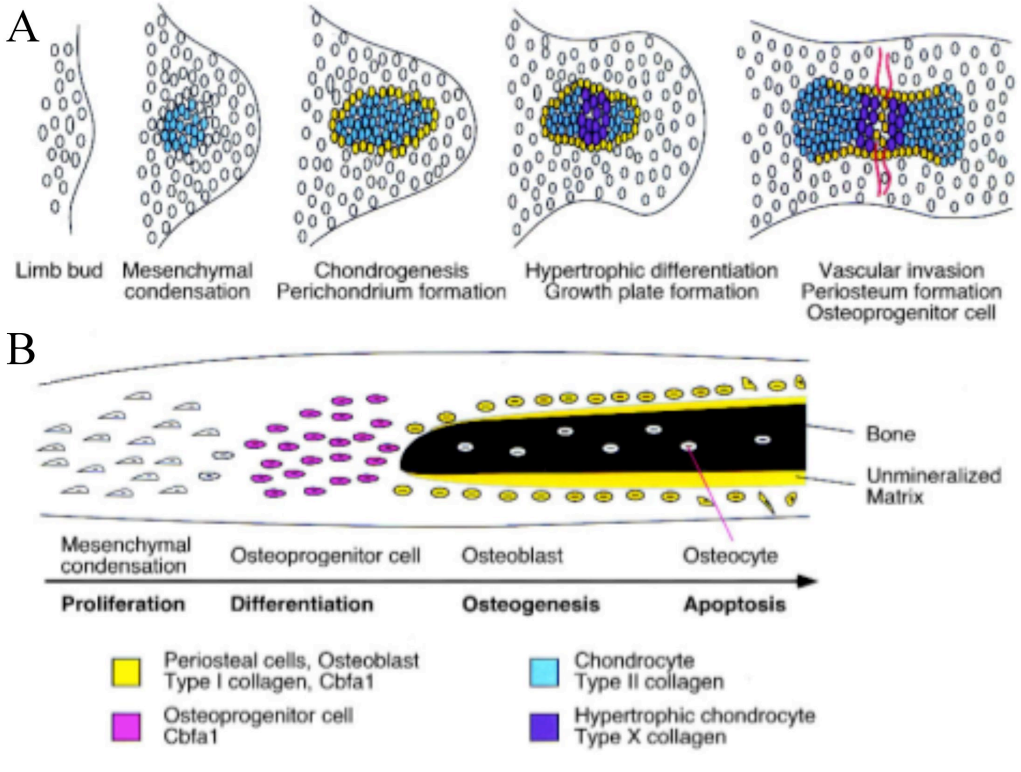

C

Endochondral bones
Ethmoid
Hyoid
Sphenoid
Malleus, Incus, Stapes
Intramembranous bones
Frontal
Parietal
Lacrimal
Nasal
Palatine
Combination
Occipital
Temporal
Maxilla
Mandible
Zygomatic

Figure 1.4. Comparison of endochondral and intramembranous ossification. (A) Endochondral ossification begins with the formation of a mesenchymal condensation, expressing *type II collagen* (blue). Cells differentiate into chondrocytes, which hypertrophy and express *type X collagen* (purple). Progression to the mature growth plate accompanies development of the perichondrium (yellow) and the formation of a center of ossification containing osteoblasts (yellow). (B) In intramembranous ossification, mesenchymal cells differentiate directly into osteoprogenitor cells expressing *Cbfa1* (pink) and then to mature osteoblasts (yellow) that deposit bone matrix. Osteoblasts either die by apoptosis or are embedded in the matrix, becoming osteocytes. Adapted from Ornitz and Marie, 2002. (C) List of cranial bones that form through intramembranous ossification, endochondral ossification, or a combination of the two.

Interactions between the epithelia and the mesenchyme lead to mesenchymal condensations, or blastemas, which are the precursors to each of the bones in the cranial vault (Opperman, 2000). Bone morphogenetic proteins (BMPs) expressed in the epidermis are hypothesized to send an osteogenic signal to the cranial mesenchyme through activation of *Cbfa1*, a transcription factor (Fig 1.4). *Cbfa1* transforms mesenchymal cells into osteoblasts by activating bone-specific genes, including *osteocalcin* and *osteopontin* (Ducy et al., 1997). When these blastemas reach a critical size, the cells begin to differentiate into osteoblasts, secreting collagens, proteoglycans, and other bone-related proteins to begin mineralization (Lana-Elola et al., 2007). For each bone there is a center of ossification where the process begins and radiates out peripherally, separating the mesenchyme into the inner dura and the outer ectoperiosteal layers (Opperman, 2000).

The ossification centers for the paired bones (frontal and parietal) form close to the skull base, then radiate upward and outward until they meet at the interfrontal and sagittal sutures. The sutures are formed as the leading edges of the bone begin to approximate one another. The advancing bone fronts that will generate the CS first meet at the most lateral aspects of the calvaria and progress "zipper-like" upwards toward the cranial midline (toward the sagittal suture). Thus, during development, the more lateral regions of the CS are generally more histologically mature than the medial (Rice, 2008). Interestingly, interactions with the neural crest-derived meninges is required for the intramembranous ossification of the parietal bone, but not the frontal bone (Jiang et al., 2002).

As the bone fronts meet, the leading edges of the bones either abut or overlap. Bones that meet along the midline (at the sagittal and interfrontal sutures) abut each other, while the bones that meet perpendicular to the midline (at the coronal and lambdoid sutures) overlap. A theory as to why these different orientations exist is that they are suited for the mechanical forces applied to different planes during passage through the birth canal where the sutures along the midline are more likely to undergo mechanical forces with equal magnitude on either side, while the coronal and lambdoid sutures are more likely to experience unequal forces (Cohen, 2005). At the CS, the bones are pre-patterned to overlap, as seen at the boundary between the neural crest and paraxial mesoderm (Fig 1.2, Fig 1.3b). Even prior to the onset of ossification, the frontal bone rudiment always underlies the parietal at the CS (Jiang et al., 2002).

Where the sagittal and lambdoid sutures form over easily defined areas of the brain, the bridge between the cerebral hemispheres and the bridge between the cerebrum and cerebellum respectively, the CS overlies no visible landmarks (Jiang et al., 2002). The mechanisms that control where the sutures form are yet unknown. Some have hypothesized that it forms as a response a growth factor gradient generated by the approximation of the advancing ossification centers, while other have proposed that the region is pre-patterned by surrounding tissues, such as the dura, one of the three outermost meningeal layers covering the brain (Lenton et al., 2005). There are several genes known to be expressed in the dura, including *Fgfr1, Fgfr2, Fgfr3, Bmp4, Bmp7, Msx1, Msx2, Fgf2, and Fgf9* (Opperman, 2000). Mutations in some of these genes are also associated with craniosynostosis.

Once the suture is formed, the majority of bone growth occurs at its osteogenic fronts. A small number of suture mesenchymal cells that immediately flank the osteogenic fronts can differentiate and be recruited into growing bones, while mesenchymal cells occupying the center of the suture are not incorporated into the growing bones and remain undifferentiated (Lana-Elola et al., 2007). In order for growth to continue and the suture to remain open, these cells need to remain in an undifferentiated state. The ossifying cranial bones are capable of both appositional and resorptive growth, per the demands of the growing brain and also in response to pathologies, such as hydrocephalus or craniosynostosis (Rice, 2008). An active suture is characterized by a budge of undifferentiated mesenchymal cells, also referred to as a blastema. As cranial expansion slows around three weeks after birth in mice, the number of cells which line the suture declines, and the suture begins to narrow and become more fibrous (Opperman, 2000).

Craniosynostosis

In mice, all sutures remain open for the lifespan of the animal, with the exception of the posterior interfrontal suture, which begins to fuse around twenty-five days after birth in mice (Opperman, 2000). Interestingly, this suture is homologous to the human metoptic suture, which fuses in the first few years of life and is also the only suture to be composed of tissues entirely of neural crest origin (Jiang et al., 2002). All other sutures in humans remain open until the third or fourth decade of life, but in some cases can persist into the seventh (Furuya et al., 1984).

Craniosynostosis is characterized by the premature fusion of one or more of the cranial sutures and occurs in approximately 1 in 2,000 live births. The two largest contributors to cranial vault growth, the sagittal and CS, are also the most common sites of synostosis; in 40-60% of craniosynostosis cases the sagittal suture is affected, in 20-30% of cases the CS is affected, and only 5-10% are due to metopic suture fusion (Kabbani and Raghuveer, 2004). Because the interfrontal/metopic suture normally undergoes fusion postnatally in both humans and mice, it is often used as a model for craniosynostosis, to study the events that initiate the transition between a patent, functional suture, to a fused structure.

The size of the human brain increases 2.5-3 times in the first two years of life (Kabbani and Raghuveer, 2004) and therefore the cranial vault needs to grow accordingly. Virchow's law states that the synostosis of a suture leads to termination of growth perpendicular to the site of fusion, and compensatory growth increases parallel to the site of fusion. This produces a predictable dysmorphic head shape depending on the identity of the fused suture (Slater et al., 2008) (Fig 1.5). For example, fusion of the CS results in a short anterior-posterior diameter with a flat forehead and increased skull height (Fig 1.5C) while a sagittal fusion produces an elongated skull (Fig 1.5B) (Kabbani and Raghuveer, 2004). Unlike changes in head shape caused by trauma or fetal positioning, abnormal head shapes caused by craniosynostosis get worse with growth and a palpable ridge is found at the site of the fused suture (Kabbani and Raghuveer, 2004). Other complications associated with craniosynostosis can include hydrocephalus, airway defects, and increased intracranial pressure that can result in deafness, blindness, seizures, or developmental delays (Cohen, 2005; Morriss-Kay and Wilkie, 2005).

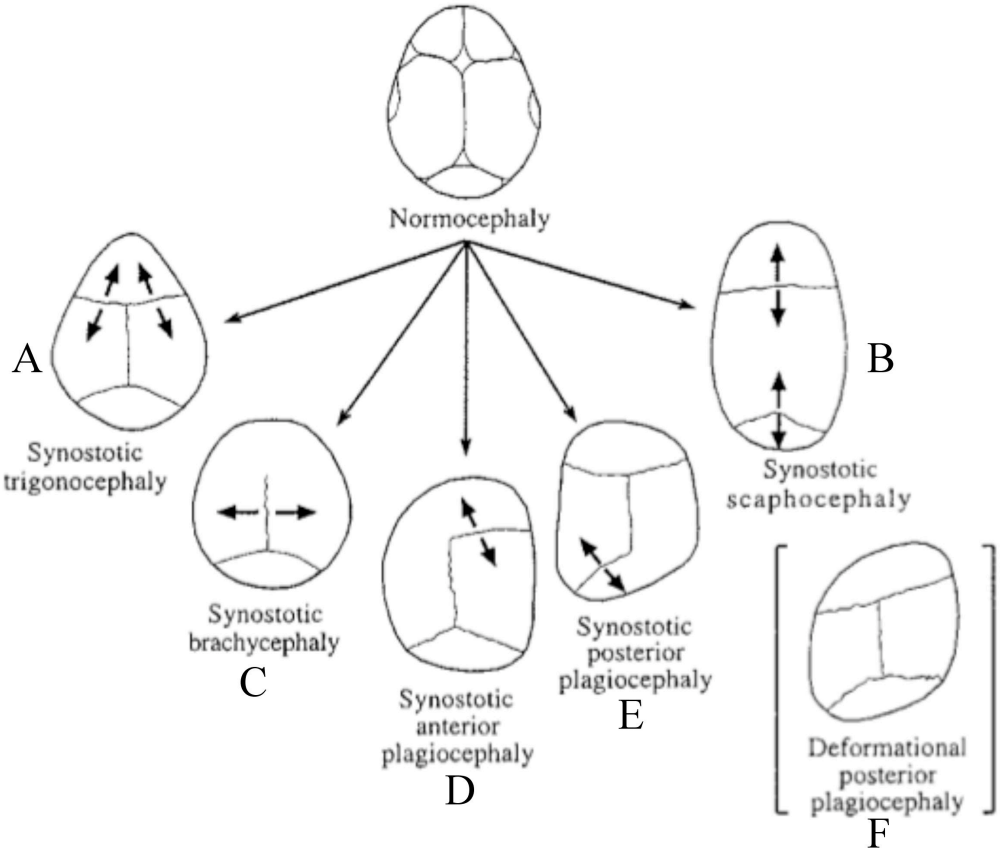

Figure 1.5. Dysmorphic skull shapes produced by craniosynostosis.
Craniosynostosis of a suture stops growth perpendicular to the site of fusion, and compensatory growth increases in the other sutures in order to maintain the volume of the skull vault. Fusion of the A) metopic, B) sagittal, C) bilateral coronal, D) unilateral coronal, and E) lambdoid sutures produce a predictable head shape. These differ from deformation caused by fetal position (F) in that craniosynostosis gets increasingly worse over time and palpable ridges can be felt over the sites of suture fusion.

Adapted from Cohen 2005.

These defects are surgically corrected through a cranioectomy or remodeling of the cranial vault by excising, trimming, and reshaping the bones. Most surgeries are performed at four to eight months of age due to the malleability of the bone, the rapid healing potential, and because the growth of the brain during this time stimulates bone remodeling (Kabbani and Raghuveer, 2004). However, most surgeons will intervene immediately if there is evidence of increased intracranial pressure (Warren and Longaker, 2001). Historically, surgeries involved a strip craniectomy to remove the fused suture, followed by removal and reshaping of the cranial bones in order to correct secondary deformities caused by the craniosynostosis (Warren and Longaker, 2001). However, since the defect that originally led to craniosynostosis is still present, craniectomies often result in re-fusion of the cranial bones and repeat surgeries. In addition, these are major surgeries, with a two percent mortality rate and complications that include seizures, blood loss, and hypothermia (Slater et al., 2008). Therefore a more thorough understanding of the genes and mechanisms that underlie the craniosynostosis phenotype could aid in the generation of more targeted and effective treatment strategies.

Genetic etiology of craniosynostosis

Cases of craniosynostosis are classified as either isolated non-syndromic cases or associated with over 150 syndromes, including Pfeiffer's disease, Apert's syndrome, and Crouzon's disease (Kabbani and Raghuveer, 2004). However, approximately 70% of craniosynostosis cases are isolated with no known etiology and no other associated phenotypes (Passos-Bueno et al., 2008). Craniosynostosis clearly can have a genetic component, with overall familial reoccurrence ranging from 6% (in sagittal fusion) to

14% (in coronal fusion). Family pedigrees have revealed inheritance patterns of autosomal dominant, autosomal recessive, and X-linked inheritance (Passos-Bueno et al., 2008). Sagittal craniosynostosis presents with a strong male prevalence (3.5:1), while coronal craniosynostosis cases are about 60-70% female (Boyadjiev, 2007). There have been great advances in the last decade in the identification of specific gene mutation associated with craniosynostosis of the suture, providing great insight into suture biology. A few notable genes identified in humans include *FGFR1, FGFR2, FGFR3, NELL-1, AXIN-2, TWIST, EFNB1,* and *MSX2* (Table 1.1).

Mechanisms of suture fusion

There are several known mechanisms leading to premature fusion of a suture. These may affect not just the formation of the suture structure, but also the maintenance of a patent suture through development. These mechanisms include changes in proliferation, apoptosis, or differentiation of the suture mesenchyme or bone fronts and failure to form a tissue boundary.

Proliferation and Differentiation: Heterozygous mutations in the *Fibroblast Growth Factors* (*FGF*s) and their receptors (*FGFR*s) account for the majority of nonsyndromic craniosynostosis cases where the etiology is known. These mutations are mostly gain-of-function mutations resulting in increased affinity between the ligand and the receptor, decreased specificity for receptor-ligand interactions, or increased receptor stabilization (Table 1.1). In general, these mutations have been associated with increased cell proliferation in the osteogenic fronts, leading to craniosynostosis (Lenton et al., 2005).

Table 1.1. Known craniosynostosis genes, their associated syndromes, mutation types, and mechanism that leads to suture fusion.

Gene	Syndromes	Change	Mechanism	References
MSX2	Boston-type Craniosynostosis	Gain of function	Proliferation Cell mixing	Lenton 2005 Merrill *et al*. 2006
TWIST1	Saethre-Chotzen Syndrome	Nonsense/ Deletions Loss of function	Differentiation Cell mixing	Merrill *et al*. 2006 Yoshida *et al*. 2005
FGFR1	Pfeiffer Syndrome	Missense Gain of function	Proliferation Differentiation	Iseki *et al*. 1999 Lenton 2005
FGFR2	Crouzon, Apert, Jackson-Weiss, and Pfeiffer Syndromes	Missense Gain of function	Proliferation Differentiation Apoptosis	Chen *et al*. 2003 Iseki *et al*. 1999 Lenton 2005 Mansukhani *et al*. 2003
FGFR3	Crouzon and Muenke Syndrome	Missense Gain of function	Proliferation Differentiation	Lenton 2005
EFNB1	Craniofrontonasal Syndrome	Missense, frameshift Loss of function	Cell mixing	Merrill *et al.* 2006
NELL-1	Non-syndromic unilateral coronal craniosynostosis	Loss of function	Proliferation Differentiation Apoptosis	Ting *et al.* 1999 Zhang *et al.* 2002
AXIN-2	Non-syndromic metopic craniosynostosis	Loss of function	Proliferation Differentiation	Liu *et al.* 2007 Yue *et al.* 2005

Studies in wild-type sutures in mice revealed *Fgfr2* expression in proliferating osteoprogenitor cells in the bone fronts, at a site mutually exclusive of *osteopontin* expression, an early marker for osteoblasts differentiation. FGF2 protein was localized to the regions low in *Fgfr2* expression, and was associated with increases in expression of the differentiation markers *osteopontin* and *osteonectin*, reduced proliferation, and increased *Fgfr1* expression. As differentiation progressed, *Fgfr2* was downregulated and *Fgfr1* was upregulated, suggesting that signaling through *Fgfr2* mainly played a role in proliferation, while *Fgfr1* signaling regulated osteogenic differentiation (Iseki et al., 1999).

Axin-2 is a negative regulator of the canonical WNT pathway and is required for reduction of β-catenin during osteoblast development (Liu et al., 2007). *Axin-2* is highly expressed in the cranial neural crest, including the cranial bone fronts and sutures. The targeted loss of *Axin2* results in craniosynostosis, with the postnatal fusion of both the Jugum Limitan (the suture that separates the frontal and nasal bones) and the interfrontal suture (Yu et al., 2005). For both of these sutures, all components (the suture mesenchyme and the bones) are derived from the cranial neural crest. The deficiency in *Axin-2* resulted in increased proliferation of the osteoprogenitor pool and thus increased intramembranous ossification (Yu et al., 2005). As an inhibitor of WNT signaling, the loss of *Axin-2* resulted in the accumulation of β-catenin in the membrane, a process inhibited by Noggin. Therefore, a BMP signal, initially induced by WNT signaling due to the loss of *Axin2*, controlled β-catenin localization to the plasma membrane in mature osteoblasts. This increased β-catenin induced cell-cell interactions, promoting osteogenic differentiation. Furthermore, haploinsufficiency for β-catenin rescued the suture defects

in *Axin-2* homozygous mutant mice (Liu et al., 2007). Therefore, *Axin-2* deficiency promotes suture fusion by affecting both the proliferation and differentiation of osteogenic cells.

Apoptosis: Apoptosis is hypothesized to contribute to premature suture fusion in multiple ways. In histological analysis of patients with craniosynostosis have revealed both increased and decreased apoptosis in sutures actively fusing. Apoptotic bodies were observed in the bone fronts flanking normal sutures (Furtwangler et al., 1985). In this location, apoptosis is thought to control the population of proliferating and differentiating cells. There is evidence that as the posterior interfrontal suture undergoes predictable fusion in postnatal development, there is a dramatic decline in the number of apoptotic cells in the bone fronts of the paired frontal bones compared to the anterior interfrontal suture, which remained patent (Agresti and Gosain, 2005).

In contrast, others have hypothesized that an increased rate of apoptosis contributes to fusion of a suture by reducing the number of cells occupying the suture space and bringing the bone fronts in closer proximity. This appears to be in the case in mutation Ser252Trp of *FGFR2,* which is associated with the craniosynostosis syndrome, Apert Syndrome. The corresponding mutation, when introduced in mice, resulted in coronal craniosynostosis and reduced bone formation due to increased apoptosis of the osteogenic cells. This resulted in the physical contact of the frontal and parietal bones (Chen et al., 2003). Studies in human and mouse calvaria cell lines demonstrated that increased expression of *FGF-2* resulted in increased apoptosis. The introduction of human-associated Apert FGFR2 mutations into cell lines both inhibited differentiation and increased apoptosis (Mansukhani et al., 2000).

Boundary formation: The formation of boundaries is a common theme throughout development and is necessary for the proper patterning of structures. Boundaries form during the segmentation of the presomitic mesoderm into individual somites, between the hindgut and the foregut, and the larval wing imaginal discs in *Drosophila* (Dahmann et al. 2011). Sometimes boundaries are not created by differences in origin, but instead a boundary set by gene expression. For example, expression of *wingless* and *apterous* in the *Drosophila* larval wing disc establish the dorso-ventral boundary, which activates *vestigial* expression at that boundary to stimulate wing patterning and growth (Williams et al., 1994).

Some human cases of coronal craniosynostosis were found to result from a failure to form the boundary between the neural crest-derived frontal bone and the paraxial mesoderm-derived parietal bone. Saethre-Chotzen syndrome in humans is caused by a heterozygous loss of function in *TWIST1*, a highly conserved transcription factor (Merrill et al., 2006). Using the neural crest lineage tracing system in *Wnt1-Cre* and *R26R* lines, Merrill and colleagues examined the boundary between these two bones at the CS in mice. They found that while the boundary between the neural crest and paraxial mesoderm remained distinct in wild-type mice, *Twist1*+/- mice exhibit cell mixing, with migration of neural crest-derived cells into the paraxial mesoderm (Fig 1.3B) (Merrill et al., 2006). This phenotype was first evident at E14.5, corresponding to the timepoint when ephrin-A2 and ephrin-A4, members of a group of proteins known to be involved in boundary formation and the inhibition of cell mixing, are transiently expressed in normal mice. Ephrin-A2 and ephrin-A4 are localized to a single layer of cells on the ectocranial side of the early frontal bone, where the frontal bone will eventually overlap with the

parietal bone. EphA4 was found in two layers of cells flanking that of ephrin-A4. In *Twist1* mutant mice, the ephrin-A2 and eprhrin-A4 localization was retracted anteriorly and away from the suture while the two layers of EphA4 was merged into one (Merrill et al., 2006). Likewise, several heterozygous mutations in *EFNA4* and *EFNB1* have been identified in patients with non-syndromic craniosynostosis and craniofacial syndromes *(*Merrill et al., 2006*)*. The authors speculated that *Twist1* interacts with *Msx2*, the underlying gene in Boston-type craniosynostosis, to control the expression of the *ephrins* (Merrill et al., 2006). The expression domain of *Msx2* in the calvarial mesenchyme of the frontal bone was expanded in the *Twist1+/-* mutant. Crossing *Twist1+/-* to *Msx2+/-* mice rescued the suture defect, restoring the boundary and expression of the ephrins.

Multiple mechanisms: The underlying mechanisms in the *Twist1* mutant cannot be attributed only to failed boundary formation. Further evidence suggests that *Twist1* may be involved in separate mechanisms at different points in development. Haploinsufficency or inhibition of *Twist1* expression resulted in decreased cell proliferation in the suture mesenchyme and increased osteogenic differentiation in the bone fronts (Yoshida et al., 2005). This suggests that the gene may play an early role not only in the proper guidance of the migrating neural crest population to form the boundary between the neural crest-derived frontal bone and the paraxial mesoderm-derived parietal bone, but also a later role in the maintenance of the suture structure as development progresses.

Fusion in the *Twist1* mutant occurs postnatally two weeks after birth. Surprisingly, between postnatal days (P) 9 and 11, chondrocytes were visible within the CS along with the upregulation of cartilage markers (Behr et al., 2011). This was

followed by ossification through the CS, suggesting that craniosynostosis was, at least in part, due to endochondral ossification of the suture mesenchyme. Previous studies demonstrated a similar mechanism contributing to the normal closure of the posterior interfrontal suture (Sahar et al., 2005). This is particularly interesting because endochondral ossification does not normally contribute to ossification of the cranial bones, and also because the sutures have different origins: the interfrontal suture is neural crest-derived and the CS is mesoderm derived (Jiang et al., 2002). In the posterior interfrontal suture (Sahar et al., 2005) and the sagittal suture (Behr et al., 2010), fusion was temporally correlated with a decrease in WNT signaling, presumably by inhibiting *Twist1*, a target of the WNT pathway, and suggesting similar interactions occur in the CS.

Although *Msx2* was associated with boundary formation in the *Twist1* mutant, genetic analyses suggest overlapping phenotypes. Gain of function mutations in *Msx2* produced premature suture fusion in mice and humans, whereas loss of function mutations caused calvarial ossification defects with persistent frontal foramina. This foramina defect was thought to result from defects in the differentiation and proliferation of the neural crest-derived frontal bone mesenchyme (Ishii et al., 2003). *Twist1*+/- mice also presented with persistent foramina, and the defect was exacerbated in *Twist1+/-; Msx2+/-* compound mutants (Ishii et al., 2003). The authors concluded that in the case of frontal bone growth, *Msx2* (a target of the BMP pathway) and *Twist1* (a target of the FGF pathway) did not function within a linear pathway, but instead through integration of two separate pathways to control the differentiation and patterning of the frontal bone.

Nell-1 was first identified in a candidate screen to identify genes overexpressed in the sutures of craniosynostosis patients. *Nell-1*, hypothesized to be a signal peptide

involved in intramembranous ossification (Lenton et al., 2005), is expressed in the bone fronts and suture mesenchyme (Ting et al., 1999). Transgenic mice over-expressing *Nell-1* presented with fusion of the interfrontal and sagittal sutures and partial fusion of the CS. Histological analysis of these mice revealed both increased differentiation and reduced proliferation at the suture, while *in vitro* analysis demonstrated the ability of *Nell-1* to stimulate differentiation and mineralization in calvarial osteoblast cell lines. Furthermore, *Nell-1* expression was associated with increased apoptosis of osteoblasts in the bone fronts of fusing sutures (Zhang et al., 2002).

Clearly, there is evidence that many craniosynostosis-associated genes can play a role in multiple mechanisms involved in the formation and maintenance of the suture structure at different times in development, and that there is no one definitive cause of premature suture fusion.

Interaction of craniosynostosis pathways

It is becoming increasingly clear that the dynamics of suture development and signaling cannot be described by a simple mechanism. The story is further complicated through interactions between different pathways, as depicted in Figure 1.6. An example of this is *Twist1,* which is negatively regulated by E protein, a basic helix-loop-helix transcription factor. Id protein, a helix-loop-helix factor that lacks the basic domain, binds to E proteins to prevent Twist1/E protein heterodimers (Connerney et al., 2006). The expression of Id protein in the bone fronts is induced by BMP signaling, and

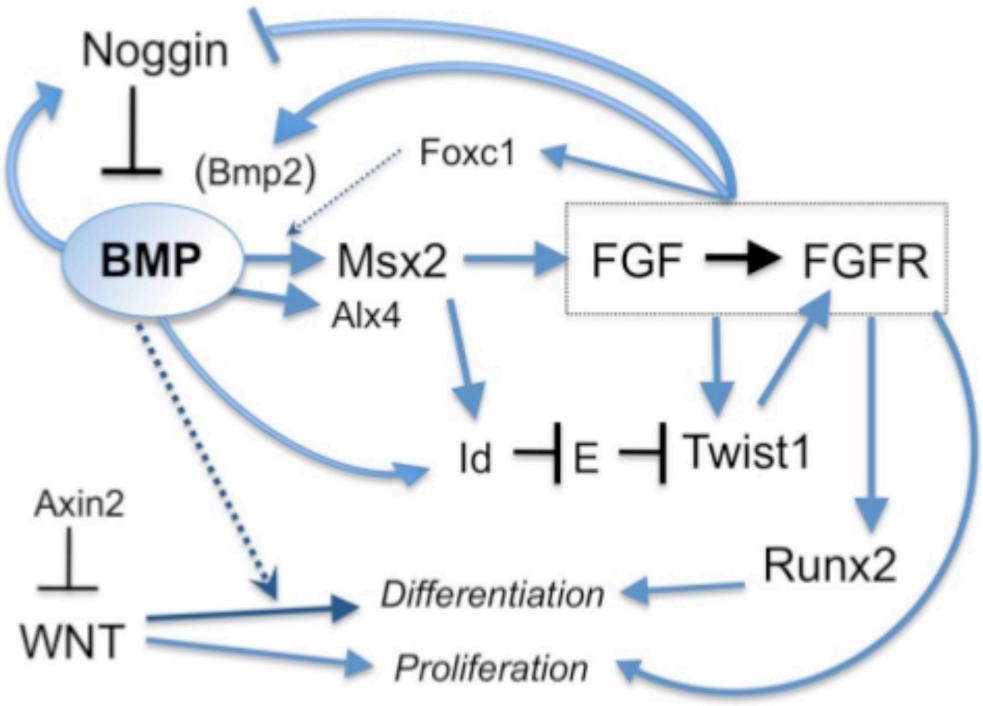

Figure 1.6. Signaling dynamics and interacting pathways in the development and maintenance of the suture. Demonstration of the complex interaction of multiple pathways involved in suture development. For example, BMP signaling intersects with the pathway involved in boundary formation at the coronal suture through *Msx2* and also through Id protein, which restricts the formation of *Twist1* heterodimers. Therefore, a perturbance in an one of these pathways could impact BMP, FGF, or WNT signaling.

Diagramed by Doug Mortlock.

therefore BMP signaling indirectly enhances *Twist1* function even though *Twist1* itself is regulated by the FGF pathway (Connerney et al., 2006). Another transcription factor, Foxc1, is required for BMP-mediated regulation of *Alx4* and *Msx2*, but its expression is also induced by FGF2 in calvarial mesenchyme, thereby integrating the FGF and BMP pathways independently of *Twist1* (Rice et al., 2005). There is also evidence that FGFs can induce BMP expression in the calvaria through a *Runx2*-dependent mechanism (Choi et al., 2005).

Axin-2, which is a regulator of WNT signaling, is involved in the proliferation and differentiation of osteogenic cells at the suture. Although its effects on proliferation are independent of BMPs, it promotes osteogenic differentiation in a positive feedback loop with BMPs (Liu et al., 2007). All these data suggest that a change within a single pathway can have large repercussions on overall signaling within the suture and bone fronts.

Beyond the suture mesenchyme

Multiple signals are required to maintain a suture in an undifferentiated state. These signals are not only derived from the suture mesenchyme and bone fronts, but also from the underlying dura mater and periosteal layers. There is a great deal of evidence that the dura mater plays a critical role in cranial morphogenesis. Although it is not required to establish the suture, it provides a signal(s) required for suture maintenance. In one study the position of the dura was altered such that the dura mater underlying the anterior interfrontal suture (which normally remains patent) was moved to a new position under the posterior interfrontal suture (which normally fuses). In this study, the posterior

interfrontal suture remained patent and the anterior interfrontal suture fused. This suggests that once the suture is initiated, the underlying dura mater is altered, possibly by inducing the dura to prevent the sending of osteogenic signals to the suture mesenchyme. Osteoblasts cultured with dural cells undergo a greater degree of differentiation, particularly when dural cells are used that are derived from below the posterior interfrontal suture (Warren et al., 2003b). This is likely due to paracrine signaling emitted from the dura mater which signals to the suture and bone fronts.

Although much less focus has been placed on the periosteum compared to the dura, there is evidence that it also plays a role in the dynamics at the suture. Removal of the periosteum from neonatal rats led to the consistent fusion of the entire interfrontal suture, and occasionally the coronal and sagittal sutures (Moss, 1960). During calvariectomies of neonatal rabbits, the cranial bones and sutures reformed at the correct anatomical positions, but this process was dependent upon a continuous, undamaged periosteum at the site (Mabbutt and Kokich, 1979). Additionally, the overlying ectoderm induces the underlying neural crest-derived cells to ossify in the frontal bone in chick (Tyler, 1983); specifically, BMP signals from the head epidermis are thought to induce the neural crest-derived cells to form bone by causing them to express *Runx2*, a gene involved in osteoblast differentiation (Ducy and Karsenty, 2000).

Bone morphogenetic proteins

Classification and signaling

The BMPs are a subgroup of the Transforming Growth Factor-Beta (TGFβ) family of growth factors. Almost a third of the TGFβ family is comprised of BMPs, with over twenty different proteins identified (Fig 1.7A) (Ducy and Karsenty, 2000). The members of the BMP family are referred to as BMPs, osteogenic proteins, cartilage-derived morphogenetic proteins, or growth differentiation factors (GDFs) (Ducy and Karsenty, 2000). They are divided into subgroups based on amino acid sequence comparison. Two of these subgroups, BMP2/4 and BMP5/6/7/8 are found in many organisms, including worms and flies. Members within each group share 74-92% identity in the amino-acid sequence in the C-terminal signaling region, while members share 40-60% identity across families (Storm et al., 1994).

BMPs were named by Urist *et al* for their ability to induce bone formation when planted ectoptically (Urist, 1965). BMP-2, -4, -5, -6, -7, and –9 are known as the most osteogenic BMPs, whereas BMP3 appears to antagonize BMP signaling (Xiao et al., 2007). Despite their name, BMPs are involved in many developmental processes, including cell proliferation and differentiation, apoptosis, mesoderm formation and patterning, neural patterning, morphogenesis, and organogenesis (Ducy and Karsenty, 2000; Hogan, 1996).

BMPs are synthesized as large precursors and cleaved at Arg-X-X-Arg consensus sites to form carboxy-terminal mature dimers (Ducy and Karsenty, 2000). The core of

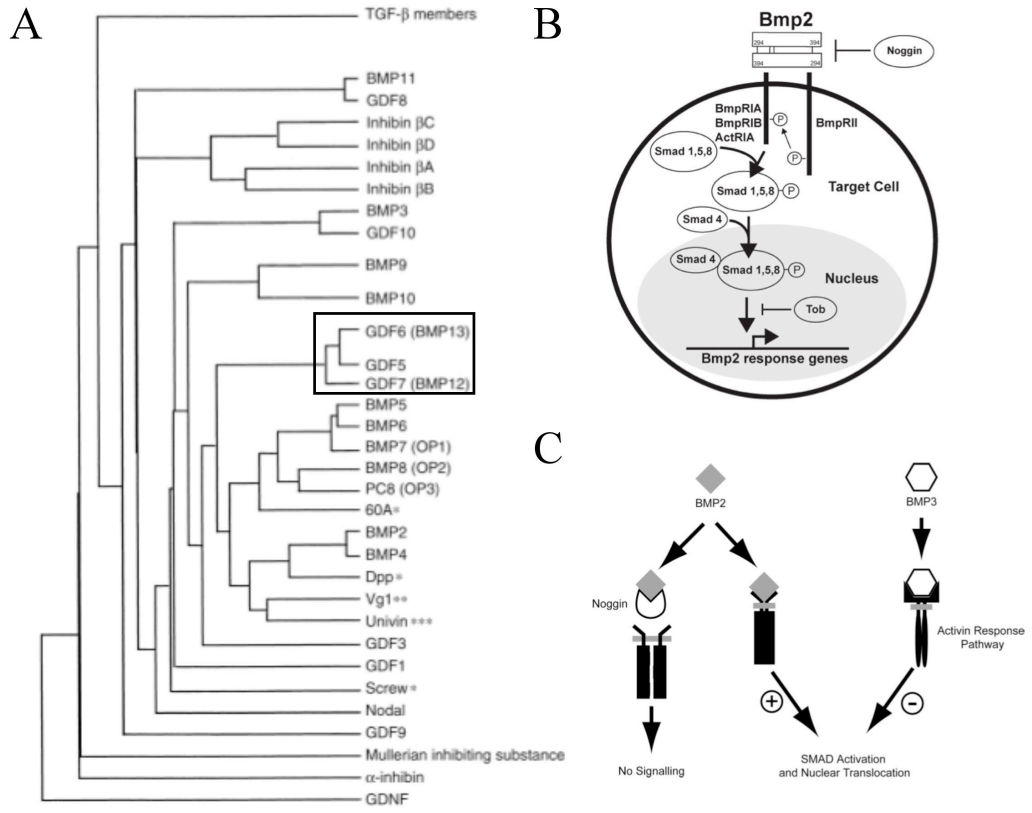

Figure 1.7. The Bone Morphogenetic Protein family and signaling mechanism. A) The BMP family tree with the GDF subfamily highlighted in the box. Adapted from Ducy and Karsenty, 2000. B) Generalized signaling pathway for BMP family members. BMP dimers bind to heterodimeric serine-threonine kinase transmembrane receptors, termed Type I and Type II receptors. The Type II receptors transphosphorylates the Type I receptor, activating the Type I kinase, which in turn activates the Smad proteins 1/5/8. The Smad proteins then translocate to the nucleus where they activate a set of target genes. C) Mechanisms of antagonism of BMP signaling. Where the BMP antagonist Noggin inhibits signaling by binding to the BMP ligand, and thereby preventing ligand-receptor interactions, BMP3 inhibits by competing for interaction with the receptors. Adapted from Nacamuli et al. 2005.

each monomer consists of six cysteine residues that reside in the C-terminal domain of all members of the BMP family (Ducy and Karsenty, 2000) with a seventh cysteine domain used to dimerize with a second monomer (Xiao et al., 2007). This distinguishes BMPs from other members of the TGFβ family, which generally have nine conserved cysteines in the mature region (Hogan, 1996). Prior to secretion, BMP monomers consist of an amino-terminal signal peptide, a prodomain, and mature carboxy terminal peptide. After the signal peptide is cleaved, the precursor protein is glycosylated and dimerized (Xiao et al., 2007).

Upon secretion, the prodomain is cleaved. Mature BMPs are secreted as homodimers or heterodimers and then bind to heterodimeric transmembrane receptors (Fig 1.7B). These serine-threonine kinase receptors have been termed type I and type II receptors. The type II receptors with BMP-binding ability include the type II BMP receptor (BMPR-II) and activin receptors (ActRIIa and ActR-IIb). They also bind three type I receptors, type IA and type IB receptors (BMPR1a and BMPR1b) (Xiao et al., 2007). At least *in vitro*, a given BMP can recognize more than one type II receptor, and therefore have the ability to interact with multiple type I receptors. The type II receptors also have the ability to bind to different ligands with different affinities, providing yet another regulatory mechanism to the BMP pathway (Hogan, 1996).

Upon binding of the BMP ligand, the constitutively active type II receptor transphosphorylates the type I receptor, leading to the activation of type I receptor kinases (Xiao et al., 2007). This is followed by the activation of the Smad proteins; Smad 1, 5, and 8 (Ducy and Karsenty, 2000), which are then recruited to a common mediator and co-Smad, Smad 4 (Xiao et al., 2007). The Smad proteins then translocate

to the nucleus where they activate a set of target genes (Ducy and Karsenty, 2000). Smads can bind to DNA directly or in cooperation with other transcription factors or bind and displace nuclear factors from their DNA binding sites (Canalis et al., 2003). Little is known about this set of downstream genes that are targeted by BMP signaling, although there is evidence for the activation of the Hox genes by BMPs in *Drosophila*, mice, and chick model systems (Hogan, 1996).

BMP signaling can be inhibited by antagonists, including Cerbarus, Dan, Gremlin, Chordin, and Noggin, all which bind different BMPs with varying specificities and prevent interaction with their receptors (Fig 1.7C) (Xiao et al., 2007). For example, Noggin preferentially binds to BMP2 and BMP4 over BMP7 (McMahon et al., 1998). Intracellularly, BMP signaling can be blocked by inhibitory Smads that can bind and activate the receptors, but are unable to activate downstream genes (Canalis et al., 2003).

Growth differentiation factor (Gdf) subfamily

The Growth Differentiation Factors (GDFs) 5, 6, and 7 are a highly conserved subset of the BMP family of signaling molecules. Unlike other members of this family, the GDF group is not known for their bone-inducing ability, but for their critical role in limb joint formation and chondrogenesis (Storm and Kingsley, 1999). In mice, the *Gdf* genes are some of the earliest markers of limb joint formation and are expressed in stripes corresponding to sites where joint formation will later occur. The expression of the Gdfs in the limbs usually represents a subset of the joints in the structures, with some overlap between members of the subfamily, and some sites of unique expression. For example, *Gdf5* expression overlaps with *Gdf6* in the elbow and carpal joints at E13.5, but only

Gdf5 is expressed in shoulder, metacarpophalangeal, and interphalangeal joints (Settle et al., 2001). A similar expression pattern is observed in the knee (Fig 1.8F-G). In limbs, *Gdf7* is only expressed in a stripe across the proximal interphalangeal joint (Fig 1.8H, arrow). The GDF5/6/7 subgroup is highly conserved, sharing 80-86% identity (Storm et al., 1994) but is only found in vertebrate organisms.

The receptors utilized by the Gdf family were identified by their ability to activate a BMP-responsive promotor construct and phosphorylate Smad1 in MC3T3 cells (Mazerbourg et al., 2005). Gdf5, Gdf6, and Gdf7 can all utilize the type I receptors BMPRIa and BMPRIb and the type II receptors BMPR-II and ActRIIa to activate the Smad1/5/8 pathway. This receptor usage is shared with several other members of the BMP family, including BMP2 and BMP4 (Mazerbourg et al., 2005). It is difficult to determine if these are the only receptors utilized by the Gdf family, since mutant embryos lacking either of the receptors BMPR-II and BMPRIa both suffer early embryonic lethality due to failed gastrulation and mesoderm formation, respectively. The BMPRIb homozygous mutant mouse presents with only defects in cartilage formation of the limbs (Yi et al., 2000) while the phenotype for ActRIIa homozygous mutant mice are characterized by only a hypoplastic mandible (Matzuk et al., 1995). Due to the lack of other abnormal phenotypes in the BMPRIa and ActRIIa homozygous mutant mice, it is likely there is some redundancy between the known BMP receptors or with receptors yet to be characterized.

Despite the high conservation between members of the Gdf family, they present with surprisingly distinct phenotypes. Mice lacking the sub-family member *Gdf7* have no known skeletal defects, although *Gdf7* does play a role in the development of the

seminal vesicles and spinal cord interneurons (Lee et al., 1998; Settle et al., 2001). The *Gdf5* gene is mutated in the brachypodism (*bp)* mouse, which results in reduced length of several long bones of the limb, and fusions of the first two bones in most of the digits (Storm et al., 1994). Homozygous mutations in *Gdf5* disrupt up to 30% of the joints in the limbs (Storm and Kingsley, 1996). The proposed functions of *Gdf5* include the regulation of joint formation in the limb and cartilage formation in the sternum (Storm and Kingsley, 1996).

The Gdf6 homozygous mutant phenotype

Gdf6, also known as BMP-13 and CDMP2, resides on human chromosome 8q22.1 and chromosome 4qA1 in mice and is comprised of two exons. The *Gdf6* mutant mouse was generated by replacing the second exon, which includes the entire mature signaling region and a portion of the pro-region, with a neomycin cassette (Settle et al., 2001). On a 129/SvJ and C57BL/6J mixed background, *Gdf6* homozygous mutants were able to survive to weaning. However, the number of surviving mice was less than the expected 1/4. The reduction in *Gdf6-/-* progeny likely occurred at the perinatal period, since normal Mendelian genotype ratios were found at E18.5 (Settle et al., 2001).

Like *Gdf5*, *Gdf6* is expressed in stripes across skeletal condensations before they are separated into distinct elements by the joints. *Gdf6* is expressed in the carpal joints and elbow of the forelimb, and likewise the ankle joints and knee of the hindlimb, from E13.5-E14.5 (Settle et al., 2001). *Gdf6-/-* mice present with fusions of the second, third, and central carpals in the wrist (Fig 1.8A, A'). In the ankle, the second and third tarsals

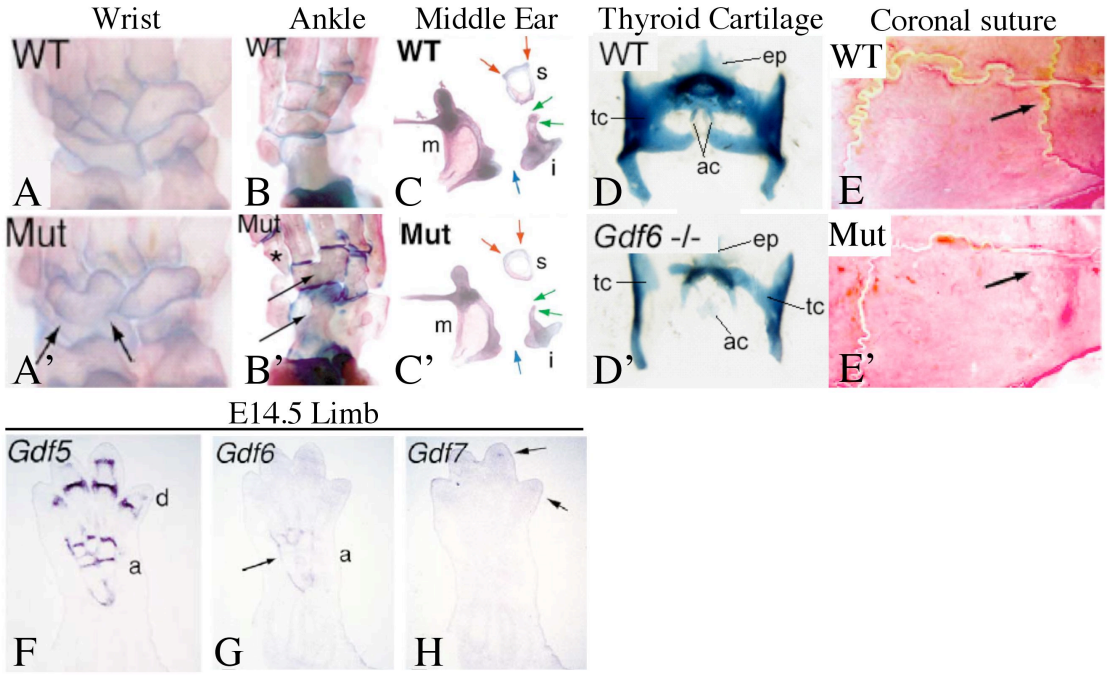

Figure 1.8. Skeletal phenotypes of the *Gdf6* mutant mouse. Defects include: A, A') fusion of the second, third, and central carpals of the wrist (arrows); B, B') fusion of the second and third tarsals (upper arrow) and the central tarsal and the talus (lower arrow), and shortening of the first distal tarsal (asterix); C,C') increased gaps and altered articulations in the malleus, incus, and stapes bones of the middle ear; D, D') hypoplasia of the thyroid cartilage and epiglottis and fusion of the arytenoid cartilages; E, E') craniosynostosis of the coronal suture (arrow). Members of the Gdf family are expressed in joints, including the joints of the ankle (F, G) and the interphalangeal joints of the digits (F, H). a, ankle; ac, arytenoid cartilage; d, interphalangeal joints of the digits; ep, epiglottis; i, incus; m, malleus; s, stapes; tc, thyroid cartilage.

All panels adapted from Settle *et al* 2003 except for D and D' (J. Witherspoon and D.P.

Mortlock, unpublished)

are fused (Fig 1.8B, B' upper arrow), along with the central tarsal and the talus (Fig 1.8B, B' lower arrow), with shortening of the first distal tarsal (Fig 1.8B, B' asterix) (Settle et al., 2001).

The bones of the wrist and ankle form from larger precursors that divide into separate skeletal elements. As early as E14.5, these early condensations in the *Gdf6-/-* mouse fail to separate into individual elements at sites of bone fusion, pointing to a very early role of *Gdf6* in joint development. However, early markers for joint formation, including *Gdf5* and *PTHrP*, are observed at the site of future joint fusion, albeit at reduced or restricted levels, pointing to an initial start of the joint formation process that fails to progress in the *Gdf6-/-* mouse (Settle et al., 2003).

In addition to the joints, defects were also observed in the middle ear bones, the malleus, incus, and stapes (Fig 1.8C, C'). The gaps between the malleus and the incus (Fig 1.8C, C' blue arrows) and the incus and the stapes (Fig 1.8C, C' green arrows) bones were increased in the *Gdf6-/-* mouse. There were also changes in the shape of each bone; for example, the stapes lost the processes that articulate with the oval window (Fig 1.8C, C' red arrows). *Gdf6* is normally expressed between each of the bones and where the stapes meets the oval window. Here, *Gdf6* appears to function primarily in cartilage growth and cell proliferation, as evidenced by the reduced proliferation in regions where the bones oppose one another, with no changes in proliferation of cells in the interior of the cartilage elements (Settle et al., 2003).

Another characteristic feature of the *Gdf6-/-* mouse was hypoplasia of the thyroid cartilage and epiglottis. The arytenoid cartilages, which are normally paired, were fused (Fig 1.8D, D'). *Gdf6* was not expressed in the cartilage element itself, but instead in the

mesenchyme adjacent to the thyroid cartilage and in the vocal cords at E14.5 (Mortlock et al., 2003).

The *Gdf6-/-* mice also lack the CS, the joint that separates the frontal and the parietal bones of the skull (Fig 1.8E, E'). This suggests that *Gdf6* may be a candidate gene for craniosynostosis and may play a critical role in the development or maintenance of the CS.

Evidence for BMP involvement in suture development

The contribution of BMPs to skull vault development has been little explored due to the fact that homozygous mutants for key BMP family members are often embryonic lethal; *Bmp2* homozygous mutant mice generally die by E10.5 with defects in amnion and heart development (Zhang and Bradley, 1996), *Bmp4* homozygous mutant mice die by E9.5 due to failed mesoderm differentiation (Winnier et al., 1995), and *Bmp7* homozygous mutant mice are perinatal lethal due to defects in kidney development (Dudley et al., 1995). However, *Bmp2*, *Bmp4*, and *Bmp7* are all expressed in the cranial bone rudiments at some point during calvarial development. Both *Bmp4* and *Bmp2* are expressed in the osteogenic fronts, and *Bmp4* is further expressed in the suture mesenchyme and the dura mater underlying the suture mesenchyme (Slater et al., 2008).

There have been several abnormal suture phenotypes associated with the effectors of BMP signaling. *Alx4, FoxC1*, and *Msx2* are BMP-responsive transcription factors. Mutants for each of these genes have a defect in frontal bone formation (Antonopoulou et al., 2004; Rice et al., 2003). Furthermore, *Msx2* mutant mice have a reduction in the size of the frontal bone rudiment (Ishii et al., 2003), and *Msx1/Msx2* compound mutants had

complete failure of frontal and parietal bone formation (Han et al., 2007). *Msx2* contains a BMP-responsive enhancer with a consensus site for Smad binding that controls the temporal and spatial pattern of BMP-dependent transcription (Brugger et al., 2004). As described previously, *Msx2* was ectopically expressed in the *Twist1* mutant CS, resulting in the mixing of the boundary between the frontal and parietal bone and coronal craniosynostosis (Merrill et al., 2006).

The conditional deletion of *Bmp4* in the neural crest produced a frontal foramen phenotype similar to that of *Msx2* (Maxson and Ishii, 2008). Furthermore, *Noggin* is expressed postnatally in patent but not fusing rat sutures, and down-regulated in the posterior interfrontal suture, which normally fuses in rats by P45. At this same timepoint, *Noggin* continued to be expressed in the sagittal and CSs, which remained patent. *Bmp4* was also expressed in the suture mesenchyme and bone fronts of both patent and fusing posterior interfrontal sutures. Although *Noggin* is an antagonist of BMP signaling, BMPs actually stimulated *Noggin* expression. Recombinant human BMP2 protein-coated beads placed in calvarial explants induced the expression of Noggin (Rice et al., 2005). Furthermore, primary calvarial osteoblasts expressed *Noggin* in a dose-dependent manner when treated with Bmp4 (Warren et al., 2003a). The suppression of *Noggin,* despite *Bmp4* stimulation, may be achieved through FGF2, which was only expressed in the posterior interfrontal suture. This is indeed the case. Injection of an FGF2-expressing adenovirus into the CS suppressed *Noggin* expression and produced suture fusion. Gain of function mutations in *FGFR2* associated with Apert's and Crouzon craniosynostosis syndromes also inhibited Noggin protein production in the suture and blocked Bmp4-mediated stimulation of *Noggin* expression (Warren et al., 2003a). Together these data

suggest a role for *Noggin* in the maintenance of suture patency and may be part of an underlying mechanism in FGF and FGFR-associated craniosynostosis.

Bmp3 is another antagonist of *Bmp4* and *Bmp2* signaling that functions by activating a TGF-β/activin-specific pathway. If activin and BMP signaling cascades are activated in the same cell, the strength of each signal will reflect competition for Smad 4, a common factor in both pathways (Candia et al., 1997). Therefore, activin is thought to act as an antagonist to the BMP pathway (Fig 1.7 C). Overexpression of *Bmp3* resulted in increased *Msx2,* and reduced ALP activity and *osteocalcin* expression (Nacamuli et al., 2005). *Bmp3* expression differs between the sutures. In the murine posterior interfrontal suture, which undergoes postnatal fusion, the expression of *Bmp3* decreased over time. However, in the sagittal suture, which remains patent, *Bmp3* expression increased over time. These differences between the sutures were most notable during the period in which the posterior interfrontal suture was undergoing fusion (Nacamuli et al., 2005). Interestingly, the *Bmp3-/-* mouse had no abnormal suture phenotype or any abnormal skeletal phenotype for that matter, other than increased bone density during adulthood (Daluiski et al., 2001). However, this might be attributed to redundancy with other BMP antagonists, including Noggin.

THESIS OVERVIEW

Although craniosynostosis is a fairly common birth defect, affecting 1 in 2,000 infants, the field of study has been restricted to the study of a small, defined group of genes, with much of the literature focused on the *Fgf* receptors, *Twist*, and *Msx2*. The known genes associated with craniosynostosis can explain only a minority of patient cases. Although BMPs are expressed in the suture region, and are historically known for their roles in skeletogenesis and patterning, *Gdf6* is the only member of the BMP family to be directly associated with abnormal suture fusion, in part due to the common lethality of BMP homozygous mutant mice. *Gdf6* is itself an understudied member of the BMP family. The information known about *Gdf6* is restricted to the mutant phenotype, some sites of expression at specific timepoints in development, the *cis*-regulation of the gene, and receptor usage. Little is known about genes the downstream signaling and how *Gdf6* interacts with other members of the BMP family. The study of *Gdf6* in relation to the suture may provide a large opportunity not only to understand how *Gdf6* could explain, or at least contribute to, a portion of craniosynostosis cases with an unknown etiology, but also would further advance the understanding the functions of *Gdf6*, the Gdf subfamily, and BMPs in general.

This project began with a simple phenotype in the *Gdf6* homozygous mutant mouse: the failure to form the CS. From there, the goal of the project was to gain a more thorough developmental understanding of how *Gdf6* contributes to the formation of this structure. This was to be done through the analysis of when and where *Gdf6* is expressed

during cranial development, the mechanism leading to craniosynostosis of the CS, and possible interactions between *Gdf6* and other members of the BMP family.

Chapter II describes the precise timepoint in development when a suture defect is first apparent in the *Gdf6*-/- embryo, in addition to exploring each of the known mechanisms that could lead to suture fusion (such as changes in the proliferation, apoptosis, or differentiation of the cells of the osteogenic bone fronts and suture mesenchyme or failure to form the boundary between the neural crest-derived frontal bone and paraxial mesoderm-derived parietal bone). Using bead implantation methods, we demonstrate the *in vivo* effects of *Gdf6* in the frontal bone primordia.

The goal of Chapter III was to determine if *Gdf6* was interacting with fellow BMP family member, *Bmp4*, in the development of the CS through genetic crosses of heterozygous mice. Chapter IV summaries the additional phenotypes found in the crosses between *Gdf6* and *Bmp4,* which together demonstrate a unique relationship between *Gdf6* and *Bmp4*. Finally, Chapter V explores the relationship between *Gdf6* and its antagonist *Noggin*, which has known functions in the maintenance of suture patency.

CHAPTER II

THE BMP LIGAND GDF6 PREVENTS DIFFERENTIATION OF CORONAL SUTURE MESENCHYME EARLY IN CRANIAL DEVELOPMENT

Introduction

The mammalian skull is composed of five main flat bones separated by joints known as the cranial sutures. These sutures are composed of fibrous connective tissue and act as the main sites for cranial growth during development. As the cranial vault expands, bone is deposited at the growing edges of the bone (the bone fronts), while the suture mesenchyme remains undifferentiated. Sutures provide flexible joints for passage through the birth canal, act as shock absorbers, prevent separation of the cranial bones, and accommodate room for the rapidly growing brain (Cohen, 2005). With the exception of the metopic suture, human sutures normally do not fuse until the third or fourth decade of life (Furuya et al., 1984), when the undifferentiated mesenchyme of the suture space becomes obliterated by bone.

Craniosynostosis is defined as the premature fusion of one or more of the cranial sutures and occurs in approximately 1 in 2,500 live births (Wilkie, 1997). When a suture fuses prematurely, cranial growth ceases perpendicular to the site of fusion, producing a dysmorphic skull shape. When the calvarial vault does not expand sufficiently to accommodate the rapidly growing brain, increased intracranial pressure can occur (Kabbani and Raghuveer, 2004). Coronal craniosynostosis can result from a failure to form the boundary between the neural crest-derived frontal bone and the paraxial mesoderm-derived parietal bone. This failed mechanism is evident as a mixing of the

two tissue populations at sites of suture fusion, as seen in the *Twist1* mutant mouse (Merrill et al., 2006). It is thought that *Twist1* works with *Msx2* to control the localization of ephrin-A2 and ephrin-A4, which are known to play roles in boundary formation at the frontal/parietal junction (Merrill et al., 2006). Several additional mechanisms could lead to fusion of a cranial suture. These include changes in proliferation, apoptosis, or the rate of differentiation of the suture mesenchyme or at the leading edges of the ossifying bone.

For example, gain of function mutations in *FGFRs* are associated with craniosynostosis in humans. Studies in normal mice found *Fgfr2* expression in proliferating osteoprogenitor cells surrounding the ossifying bones while *Fgfr1* is expressed in the frontal and parietal developing bone. As differentiation progresses, *Fgfr2* is down-regulated and *Fgfr1* is upregulated, suggesting that signaling through FGFR2 mainly plays a role in proliferation, while FGFR1 signaling regulates osteogenic differentiation (Iseki et al., 1999).

GDFs 5, 6, and 7 are members of the BMP family of secreted signaling molecules. The GDF subgroup (GDF5/6/7) is highly conserved in vertebrates and has a known critical role in limb joint formation and chondrogenesis (Storm and Kingsley, 1999). *Gdf6* homozygous mutant mice display multiple joint defects, including fusions of tarsal and carpal bones, morphological abnormalities in the malleus, incus, and stapes bones of the middle ear, and hypoplasia of the thyroid cartilage. In addition to these defects, *Gdf6*-/- mice lack the CS (Settle et al., 2003). However, the detailed expression pattern of *Gdf6* along with the onset of cranial suture fusion is not reported.

Gdf5 is the gene associated with brachypodism in mice and is hypothesized to function mainly in the stimulation of cartilage development, growth, and maturation (Storm and Kingsley, 1999). Therefore, *Gdf5* can be viewed as promoting aspects of endochondral bone growth. *Gdf5* and *Gdf6* share approximately 80% identity in the mature signaling region (Storm et al., 1994) and therefore it is likely the *Gdf5* and *Gdf6* operate by similar mechanisms. Like *Gdf5, Gdf6* can promote chondrogenic differentiation *in vitro* (Nochi et al., 2004). This makes the craniosynostosis phenotype in the *Gdf6*-/- mouse particularly interesting because unlike the long bones, the cranial bones form through intramembranous ossification without a cartilage intermediate. Therefore, the mechanism of *Gdf6* function in the CS may be drastically different than its function in the other joints.

The aim of this study was to gain a more thorough developmental understanding of craniosynostosis in the *Gdf6*-/- mouse and the underlying cause of suture fusion. We found that CS fusion occurs in the *Gdf6*-/- mouse before the first evidence of cranial bone ossification is observed at E14.5, with changes in early osteogenic markers detected prior to the onset of ossification. Our data suggest that *Gdf6* may self-regulate its expression in the developing frontal bone primordium. Additionally, fusion in the *Gdf6*-/- mouse is not due to a failure to form the boundary properly between the frontal and parietal bones, or changes in cell survival or proliferation, but is likely due to a failure of the suture mesenchyme to remain in an undifferentiated state.

Materials and Methods

Mouse crosses

The *Gdf6*-/- mouse (Settle et al., 2003) was a gift from Dr. David Kingsley and was backcrossed onto a C57BL/6J background for more than 10 generations. The *Gdf6*-/- allele appears to be perinatal lethal on this background, since no *Gdf6-/-* adults or weanlings were found during the described crosses, although normal Mendelian ratios were present at late embryonic stages (not shown). Therefore, all timepoints in which the *Gdf6-/-* phenotype was analyzed were collected prenatally. For fate mapping experiments, *Gdf6*+/- mice were crossed to *R26R*+/- (Soriano, 1999) to produce *Gdf6+/-; R26R+/-* compound heterozygotes, which were then crossed to *Wnt1Cre*+/- (Danielian et al., 1998); *Gdf6*+/- mice. The *Wnt1-Cre* line was maintained on a CD1 background. Embryonic age was determined through detection of the vaginal plug, with noon of that day observed as E0.5. Animal protocols (M/09/293 and M/04/381) were approved by the Institutional Animal Care and Use Committee at Vanderbilt University.

DNA preparations and Genotyping

DNA preparations were collected using tail snips (from postnatal mice) or yolk sacs (from embryos), which were placed in a 1.5 ml microcentrifuge tube. 0.7 ml of lysis buffer [100 mM Tris-HCl pH 8.5, 5 mM EDTA pH 8.0, 0.2% sodium dodecyl sulfate (SDS), 200 mM NaCl] with 125 ug freshly added Proteinase K (RPI). Preparations were digested overnight in a 55^{o}C water bath. 0.5 ml of phenol:chloroform:isoamyl alcohol (Sigma) was added in the hood, vortexed, and spun

down at maximum speed (13,000 rpm) for 5 minutes. 400 ul of the aqueous (upper) phase was transferred to a new 1.5 ml microcentrifuge tube containing 800 ul 100% ethanol and 40 ul of 3M sodium acetate. The preparation was mixed by inverting several times (a clump of DNA was visible) and centrifuged at maximum speed for 10 minutes. The supernatant was removed by decanting. 500 ul of 70% ethanol was added to the tube and the preparation was spun again at maximum speed for 5 minutes. All remaining ethanol was removed with a pipette tip. The DNA pellet was resuspended in 200 ul of Tris-EDTA (TE) pH 7.4.

Genotyping for *Gdf6* was carried out using a set of primers to amplify a 176 base pair fragment of the mature region of the *Gdf6* wild-type allele [Type6 F2 5'-AGCTCTTGGTCATGGATGTTTCTC-3' and Type6 R2 5'-CTGATGTAGCCCTTCCACCTTTC-3'] and a second set to amplify a 310 base pair product from the neomycin resistance cassette [N2F 5'-TGGAGAGGCTATTCGGCTATGAC-3' and N2R 5'-TACTTTCTCGGCAGGAGCAAGG-3'] from the mutant allele. The PCR program used for these primers included the following steps: 94^{o}C for 2 minutes, 35x [94^{o}C for 30 seconds, 63^{o}C for 1 minute, 72^{o}C for 40 seconds], and a final extension at 72^{o}C for 5 minutes.

The *Wnt1-Cre* line was genotyped using the following primers: Primer 1 5'-ATTCTCCCACCGTCAGTACG-3' and Primer 2 5'-CGTTTTCTGAGCATACCTGGA-3' (Chai et al., 2000) to amplify a 475 base pair produce from the transgene. The amplification conditions were as follows: 94°C for 2 min, 35x [94°C for 1 minute, 55°C for 2 minutes, 72°C for 90 seconds], and a final extension at 72°C for 5 minutes. The

R26R line was genotyped using the primers: 5'-AAAGTCGCTCTGAGTTGTTAT-3', 5'-GCGAAGAGTTTGTCCTCAAGG-3', and 5'-GGAGCGGGAGAAATGGATATG-3' that together generate a 500 base pair wild-type allele and a 250 base pair mutant allele (Soriano, 1999). The cycling conditions were: 94°C for 2 minutes, followed by 35 cycles of [94°C for 30 seconds, 53°C for 45 seconds, 72°C for 90 seconds], and a final extension at 72°C for 5 minutes. The homozygous *R26R* mice are viable, fertile, and have no obvious deficits, and therefore the line was eventually maintained with a mating pair of two homozygous *R26R* mice, with all progeny also being homozygous. Therefore, no further genotyping was required.

Whole-mount skeletal preparations

E18.5 embryos were collected and skinned, saving the yolk sac for genotyping. Each embryo was placed in a 50 ml conical tube filled with 95% ethanol for 2 days. Skeletal preparations were then moved to alcian blue staining solution for 7-10 days. To prepare the alcian blue staining, the solution [20% glacial acetic acid (Sigma) and 0.15 mg/ml alcian blue 8GX (Sigma) in 95% ethanol] was incubated in a 37^{o}C water bath then stirred vigorously on a stir plate for approximately 1 hour in order to help dissolve the blue stain. Skeletal preparations were then de-stained for 2 days in 95% ethanol. Carcasses were rinsed with tap water, soaked in 0.5% potassium hydroxide (KOH) with 400 ul of alizarin red stock solution [5 mg/ml alizarin red, 0.5% KOH in dH2O]. The solution initially had a dark pink color, which lightened as the skeletal preparations absorbed the stain. Preparations were incubated in alizarin red/ 0.5% KOH solution for 2 days. Samples were rinsed with tap water and transferred to graded glycerol series (25%,

50%, 70%, 80%, 90%, 100% glycerol (VWR) in phosphate-buffered saline (PBS) pH 7.4). All incubations were performed on a shaker. Specimens were imaged under a dissection microscope in a dish of water (if prior to storage in glycerol) or 100% glycerol (if after storage in glycerol). When imaged in glycerol, the skeletal preparations and glycerol solution were rocked overnight to avoid streaking of the glycerol.

E14.5/E15.5/E16.5. The same protocol was used as described above for E18.5 skeletons with the following exceptions: 1) 0.25% KOH was used for clearing and alizarin red staining, and 2) No skinning was necessary as stain was able to penetrate to the ossified tissues.

Whole-mount and slide in situ *hybridization*

The *Gdf6* RNA probe was generated by cloning a PCR fragment using the primers 5'- AAGCATGGAAGGAGGATGAAAGGG- 3' and 5'-CGACCTCCAGTAACTTTAGTGTTGTCA –3', targeting the *Gdf6* 3' untranslated region, into the pGEM-Teasy vector (Promega) (probe developed by Dr. Kelly Chandler). The plasmid template was linearized with NotI for the antisense probe and SpeI for the sense probe. RNA probes were labeled with digoxigenin labeled dUTPs (Roche) through an *in vitro* transcription reaction using 1 ug of linearized DNA template and Sp6 polymerase (NEB), to generate the antisense probe, and T7 (NEB) for the sense probe. Reaction was incubated for 2 hours at 37^{o}C (T7) or 40^{o}C (Sp6). Probe concentration was determined by running a small aliquot on a gel alongside a DIG-labeled RNA ladder and comparing band intensity by Quantity One gel imaging software.

For whole-mount *in situ* hybridization, embryos were collected at E10.5 and E11.5, fixed for 24 hours in 4% paraformaldehyde (PFA) at 4^{o}C, followed by dehydration through a graded methanol series (25%, 50%, 75%, 80%, 90% methanol in H_2O, 100% methanol) and stored at –20^{o}C for no longer than 1 week prior to carrying out *in situ* hybridization protocol. Embryos were re-hydrated in series of methanol/ PBT (PBS pH 7.4 and 0.1% Tween-20) (25%, 50%, 75% methanol in PBT, 100% PBT) then bleached with 6% hydrogen peroxide in PBT for 1 hour, rocking at room temperature. Samples were then protease-treated with 10 ug/ml of Proteinase K (RPI) in PBS for 12 minutes (for E10.5 embryos) to 15 minutes (for E11.5). The permeablization step was stopped with 2 mg/ml glycine, then post-fixed with 4% PFA/ 0.2% glutaraldehyde (ICN)/ 0.1% Tween-20. Embryos were then transferred to 2 ml cryovials of (pre)hybridization solution [50% formamide (Invitrogen), 5X SSC pH 4.5, 10 ug/ml yeast tRNA (Sigma), 10 ug/ml heparin (Sigma), 15% H_2O, 1% SDS] and incubated at 65^{o}C for 1 hour in a rotating hybridization oven. Fresh hybridization solution was transferred to the cryovials along with 200 ng/ml of *Gdf6* RNA probe. Samples were incubated overnight at 65^{o}C in a rotating hybridization oven.

The following day, samples were washed 3x30 minutes with Solution 1 [50% formamide (Invitrogen), 5X SSC pH 4.5, 1% SDS] followed by 2x30 minute washes with Solution 2 [50% formamide, 5X SSC pH 4.5] at 65^{o}C rotating in the hybridization oven. Samples were washed 3x with TBST [TBS and 0.1% Tween-20] then blocked with 10% normal sheep serum (Jackson Immunological Research Labs) in TBST for 90 minutes at room temperature, rocking. This was followed by application of an anti-DIG antibody (anti-digoxigenin-AP, Fab fragments, Roche) at a 1:1500 dilution in normal sheep serum

and blocked overnight at 4°C after the antibody was preabsorbed in embryo powder. The next 2 days were a series of TBST washes at room temperature. On the fifth day, the embryos were washed with NTMT [100 mM NaCl, 100 mM Tris pH 9.5, 50 mM $MgCl_2$, and 0.1% Tween-20] and the *in situ* was developed with BM Purple AP Substrate (Roche). For the *Gdf6 in situ* probe, development took to 5 hours depending on the level of background staining. For each timepoint, embryos were from the same litter and stained for an equal length of time.

For slide *in situ* hybridization, embryos were collected at E12.5 and fixed overnight in 4% PFA, rocking at 4°C. After equilibrating embryos in 50% sucrose, embryos were embedded in Tissue-Tek O.C.T. compound (Sakura Finetek) and frozen sections were collected at 18 um and placed on 3-aminopropyltriethozysilane-treated slides. Sections were treated with 3% hydrogen peroxide for 25 minutes at room temperature in order to inactivate endogenous enzyme activity, then post-fixed with 4% PFA for 20 minutes on ice. This was followed by treatment with 15ug/ml Proteinase K (RPI) for 1 minute. Slides were post-fixed in 4% PFA, then treated for acetylation [1.2% triethanolamine (Sigma) and 0.25% acetic anhydride in H_2O]. 30 ng of *Gdf6* RNA probe per slide was diluted in hybridization mix [40% formamide, 5X SSC pH 7.0, 1 mg/ml ssDNA, 1 mg/ml tRNA (Sigma) in H_2O], heated to 80°C, then cooled on ice. The probe was applied to each slide, covered with a parafilm coverslip cut to the dimensions of the slide, and placed into a humidification chamber. The chamber was sealed with electrical tape and then placed in hybridization oven at 65°C overnight.

The next day the slides were washed with decreasing concentrations of SSC (5X, 0.2X), then incubating in a blocking solution [10 mg/ml Blocking Reagent (Roche) in B1

[11.6 g/L maleic acid, 8.7 g/L sodium chloride, 7 g/L sodium hydroxide, in H_2O, pH 7.5] for 1 hour. The slides were then incubated in a 1:5000 dilution of anti-DIG antibody in B1 for 1 hour. This was followed by 2x15 minute washes in B1, then a 5 minute wash in B3 [50 mM Tris pH 9.5, 100 mM NaCl, 5 mM $MgCl_2$ in H_20]. Slides were incubated in developer [100 mM Tris pH 9.5, 100 mM NaCl, 100 g/L polyvinyl alcohol (PVA), in H_2O] that was heated until the PVA went into solution, then supplemented with 3 mM $MgCl_2$, 0.28 mg/ml nitro-blue tetrazolium chloride (NBT, Bio-rad) and 0.15 mg/ml 5-bromo-4-chloro-3'-indolyphosphate p-toluidine (BCIP, Bio-rad)] and allowed to develop overnight at room temperature. Slides were then rinsed with water before being coverslipped with Aquamount.

Histology

Embryos were dissected in 1X PBS and fixed for 60 min at 4° in 10% neutral buffer formalin (Sigma). Embryos were then decapitated, bisected sagittally, the skin removed, and fixed for another 15 minutes. Embryos were then washed 3x30 minutes with Wash Buffer [2mM $MgCl_2$, 0.01% deoxycholic acid, 0.02% nodidet-P40 (NP-4) (Roche), 23 mM monobasic sodium phosphate pH 7.3, 77 mM dibasic sodium phosphate pH 7.3 in H_2O], rocking at room temperature. Enough X-gal stain [0.6 mg/ml X-gal (Sigma) in dimethylformamide, 0.2 mM K-ferrocyanide, 0.2 mM K-ferricyanide, 1mM Tris pH 7.5, in Wash Buffer] was applied to cover the embryo and incubated overnight, rocking at room temperature. The next day, embryos were washed 3x1 hour with 1X PBS, then post-fixed with 4% PFA.

Whole-mount lacZ-stained specimens were further stained in a 0.5% KOH/ alizarin red solution overnight. Specimens to be sectioned were dehydrated through ethanol series (25%, 50%, 70%, 80%, 100% ethanol in H_2O), followed by 3x30 minute washes with Citrosolv clearing agent (Fisher). Samples were then rocked at 55^{o}C in 50% Citrisolv and 50% paraffin for 1 hour, then 100% paraffin for 1 hour rocking at 55^{o}C overnight. Samples were then incubated at 55^{o}C in vacuum oven for 1 hour prior to embedding. 10 μM sections were collected on Superfrost slides (Fisher) and counterstained with nuclear fast red (Vector Laboratories). Slides were dehydrated then coverslipped using Cytoseal (Fisher).

Alkaline Phosphatase (ALP) Staining

For whole-mount ALP staining, E12.5 embryonic heads were fixed in 4% PFA pH 7.4 in PBS overnight. The head was bisected sagittally, the brain removed, and then fixed for an additional 1 hour. Samples were washed 3x10 minutes with 1XPBS, 2x5 minutes with TBST, then 2x5 minutes with NTMT on ice. Embryos were then stained 1/2X ALP staining solution [180 ug/ml NBT and 9 ug/ml BCIP in NTMT] for at least 2 hours on ice, or until background started to develop. When the staining was complete, embryos were rinsed with 1X PBS then post-fixed overnight at 4^{o}C.

For transverse sections, embryos were collected at E14.5 and fixed overnight at 4^{o}C in 4% PFA. After equilibrating embryos in 50% sucrose, embryos were embedded in Tissue-Tek O.C.T. compound (Sakura Finetek) and frozen sections were collected at 18 um and placed on 3-aminopropyltriethozysilane-treated slides. Slides were baked on a slide warmer for 2 hours then stored at –80^{o}C until ready for staining. Slides were then

brought to room temperature and washed briefly in 1X PBS, then incubated for 10 minutes in acetone. Slides were washed 3x3 minutes in TBST, transferred to glass slide containers, and washed 3x3 minutes in NTMT. All washes were performed at 4°C. Slides then staining with 1X ALP staining solution [375 ug/ml NBT, 188 ug/ml BCIP in NTMT] for 10-15 minutes, depending on the timepoint (E12.5 takes less time then E14.5). Slides were washed briefly 3x with H_2O, counterstained with nuclear fast red (Vector Labs H-3403), then coverslipped with Aquamount.

Immunohistochemistry

Immunohistochemistry for phospho-histone-H3 (Ser10) (Cell Signaling) and cleaved caspase-3 (Asp175) (Cell Signaling) was carried out on cryosections. Slides were fixed in neutral buffer formalin for 20 minutes at 4°C, then treated with 0.3% H_2O_2 in methanol for 30 minutes at room temperature to quench endogenous peroxidase activity. Sections were circled with a PAP pen and blocked with 5% normal goat serum (Vector Labs)/ 0.05% Triton X-100 in PBS for 2 hours in a humidity chamber. The block solution was replaced with diluted primary antibody in blocking solution (phospho-histone-H3 1:200, cleaved caspase-3 1;12,800) and incubated overnight at 4°C in a humidity chamber.

The next day sections were incubated in a 1:200 dilution of biotinylated rabbit secondary antibody for 1 hour at 4°C in a humidity chamber. The secondary antibody was then replaced with ABC solution (Vector Laboratories, catalogue number SK-4100) for 30 minutes at room temperature in humidity chamber. DAB solution (Vector Labs) was applied to sections and allowed to develop before excess background started to form.

Sections were then dehydrated (70%, 95%, 100% ethanol), rinsed with Citrisolv, mounted with Cytoseal, and coverslipped.

In the analysis of proliferation and apoptosis, positive cells were counted in the suture region (composing the frontal and parietal bones plus the suture) at the same magnification. At least 5 sections from 3 separate embryos for each genotype were analyzed. Differences in the number of proliferating or apoptotic cells were tested for significance using a Student's T-test with a p-value<0.05 deemed as significant.

3-Aminopropyltriethoxysilane Treatment of Slides

Superfrost slides (Fisher) were placed in a slide holder and washed with dish-washing detergent for 30 minutes followed by a 30 minute wash in running tap water. Slides were then washed in distilled water in large slide cassettes for 2x5 minutes, then 2x5 minute washes of 95% ethanol. Slides were air-dried for 10 minutes and then incubated in a fresh 2% solution of 3-aminopropyltriethanoxysilane in acetone for 5 seconds followed by 2 brief washes with water. Slides were finally dried overnight on slide warmer at 42^{o}C and stored at room temperature.

Agarose Bead Preparation

Approximately 20 ul of Affi-gel blue agarose beads (100-200 mesh, Bio-rad) were transferred into a microcentrifuge tube with 500 ul 1X PBS. Beads were resuspended by flicking the tube, then spun down briefly. The supernatant was removed and the wash repeated. Either 0.1% BSA or 100 ng/ul protein was added to the beads,

then incubated at 37°C for 30 minutes. Beads were stored on ice until ready for implantation. Treated beads can be stored at 4°C for up to 1 month.

Gdf6 bead implantation experiment

E12.5 embryos were collected and placed (still inside the yolk sac) into a 60x15mm cell culture dish (Falcon) filled with BGJb medium (GIBCO) treated with 100U/ml penicillin and streptomycin and supplemented with 0.1% BSA. Embryos were stored temporarily in a 37°C 5% CO_2 incubator until bead implantation. Embryos were removed one at a time and placed in their own dish filled with media. Yolk sacs were collected for genotyping. Embryos were transferred to culture dishes filled with 2% agarose as a stable surface to hold the embryo still during the implantation procedure. Embryos were decapitated at the jaw line to remove the mandible. This allows for more efficient absorption of the media into the head throughout the culture period. Beads soaked in 0.1% BSA or 100ng/ul recombinant mouse Gdf6 protein were implanted under the skin into the suture region on the left side of the head (right side served as a control) using a mouth pipette with drawn glass needles. The CS has no visible external landmarks at this stage, so the best way to approximate the implantation site was at an angle from the embryonic eye. The bead implantation methodology is summarized in the panels B and C of Figure 2.1. Embryo heads were placed neck-side down onto a square of filter paper (Supor 0.45 um filters, Pall Life Sciences). The filter paper was placed on a wire mesh grid (stainless steel type 304 mesh #60, smallparts.com) cut into the shape of a triangle with bent corners in order to sit snugly into the central well of the organ culture dish (Falcon). The central well of organ culture dish was filled with media, while the

outer chamber was filled with 1X PBS. Media was at the level of the wire mesh grid so the media was absorbed into the filter paper but the embryo was not submerged. The specimens were incubated at 37^{o}C for 48 hours, the media was changed once at 24 hours, then the specimens were post-fixed in 4% PFA and embedded into O.C.T. for cryosectioning.

Test of protein function and validation of bead implantation methodology

In order to test the functionality of the recombinant proteins, beads soaked in BSA (control), Bmp4 (R&D), and Noggin (R&D) were implanted to the E13.5 limb, where all are known to have effects on limb and joint development. The same methodology was applied as for a cranial implantation. Bead effects were determined by staining the limbs with alcian blue, which highlighted the cartilage condensations (Fig 2.1A). While the bead soaked in BSA appeared to have no effect on the surrounding cartilage in the area immediately surrounding the bead, the Bmp4 bead appeared to slightly increase cartilage formation in the region surrounding the bead. The Noggin- soaked bead appeared to inhibit cartilage formation in the localized region around the bead.

A second assay was performed to further validate that the recombinant proteins were indeed active. Limb bead implantations were repeated. Limbs were fixed in 4% PFA for 24 hours, staged in 30% sucrose overnight, then embedded in O.C.T. Limbs were sectioned at 18 um, dried for 2 hours, then stored at –80^{o}C. Limbs sections then underwent slide *in situ* hybridization using probes for *ColIIa* (Appendix B) (Metsaranta et al., 1991), a marker for cartilage formation (Fig 2.1A). The antisense probe was

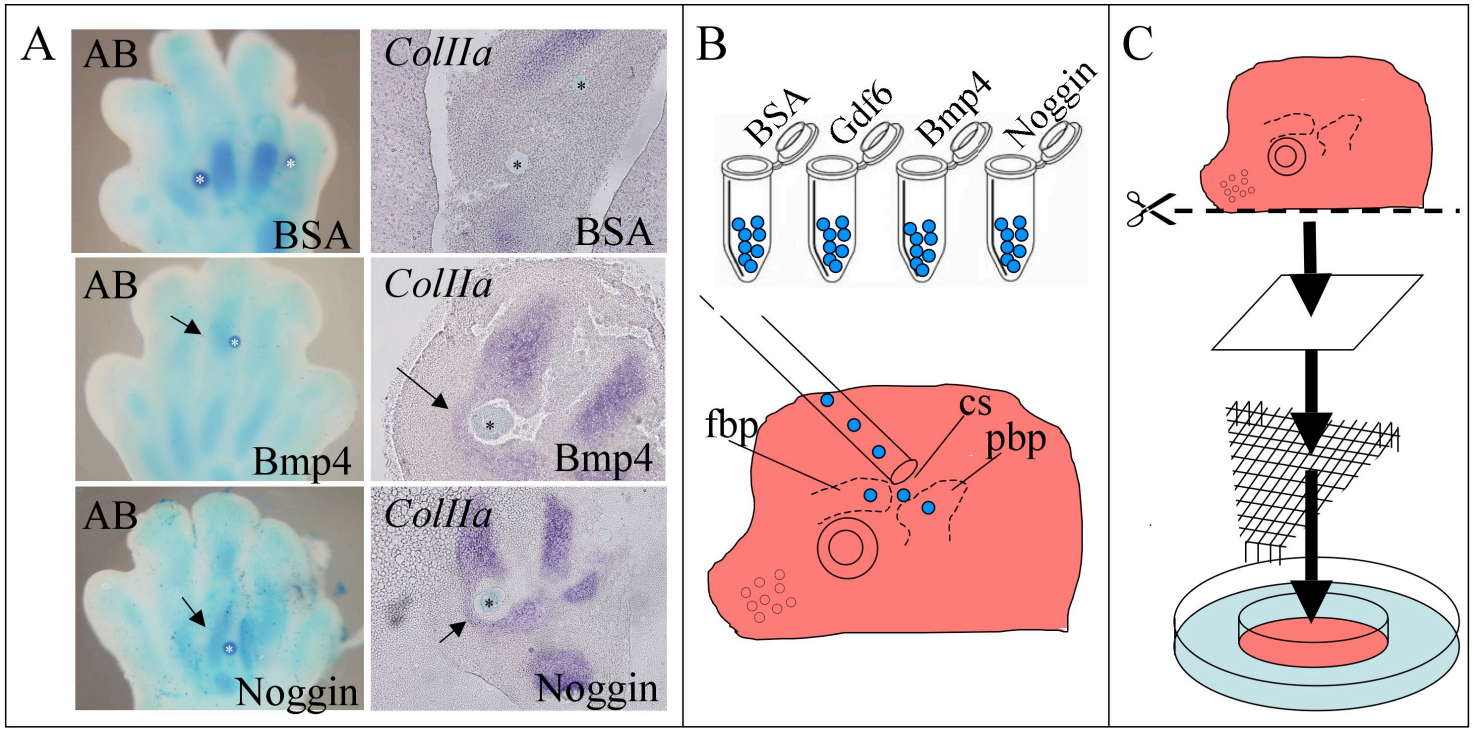

Figure 2.1. Methodology and validation of bead implantation and organ culture. A) Beads soaked in BSA, Bmp4, and Noggin were implanted into the E12.5 limb in order to test bioactivity of the recombinant protein. Activity was assessed through staining with alcian blue (AB) (left) and *in situ* hybridization for *ColIIa*, and marker for cartilage formation (right). The asterix indicates the location of the bead. B) Beads soaked in BSA (control) and protein (Gdf6, Bmp4, and Noggin) were implanted in the suture region of E12.5 embryo head using a drawn glass needle and a mouth pipette. C) Embryos were decapitated at the jaw line to remove the mandible, placed onto filter paper and a wire mesh grid, then into an organ culture dish. The central chamber of the organ culture dish was filled with BGJb media supplemented with 100 U/ml penicillin and streptomycin and 0.1% BSA. Embryos were cultured for 48 hours. AB, alcian blue; cs, coronal suture; fbp, frontal bone primordia; pbp, parietal bone primordia.

generated by linerizing the plasmid with EcoRI restriction enzyme followed by RNA transcription reaction using T7 RNA polymerase. The BSA implanted bead appeared to have no affect on local *ColIIa* expression where the Bmp4 bead appeared to increase the expression of *ColIIa* in the area immediately surrounding the bead. For Noggin, the same affect seen in the alcian blue staining was also seen in the limb, with *ColIIa* expression inhibited in the area occupied by the bead, and also a more localized reduction of *ColIIa* expression was observed in several cell layers surrounding the bead. These two assays together provided evidence that the proteins were functional and the bead implantation method was valid for changing gene expression and morphology even over a short culture period.

Results

Gdf6-/- *coronal suture fuses early in development*

The entire CS was absent in the *Gdf6*-/- mouse (Fig 2.2B), with complete penetrance (not shown). This defect was not observed in wild-type (Fig 2.2A) or *Gdf6* heterozygote littermates through embryonic development and postnatal life (not shown). To determine the timepoint during development at which the suture first became fused, *Gdf6-/-* embryos were collected at various stages and stained with alizarin red. At E14.0, ossification centers were not yet visible in embryos stained with alizarin red. By E14.5, frontal and parietal bones were visible as two separate ossification centers. The nascent CS was apparent in the wild-type embryo (Fig 2.2E,G) as the gap between the two bones. Yet in *Gdf6*-/- embryos, a single continuous ossification center was present (Fig 2.2F,H).

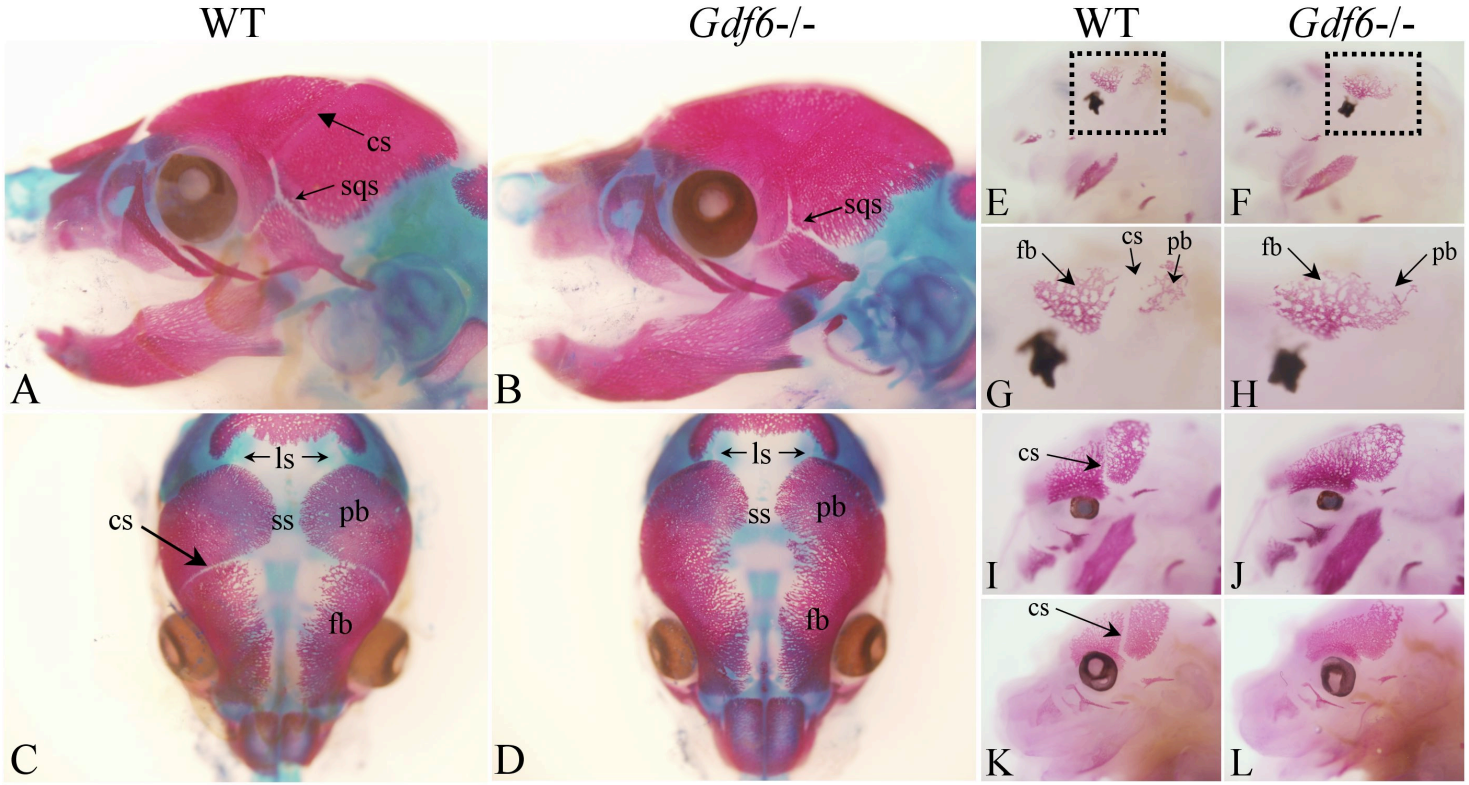

Figure 2.2. Analysis of coronal suture development in wild-type and *Gdf6-/-* embryos with alizarin red. The coronal suture separates the frontal and parietal bones in wild-type embryos (A, C), but is lacking in the *Gdf6-/-* embryo (B, D), while the squamosal (B), sagittal, and lambdoid (D) sutures are normal. At E14.5, the early coronal suture separates the frontal and parietal ossification centers in wild-type embryos (E, G) but is fused in the *Gdf6*-/- embryo (F,H). The frontal and parietal bones fuse into one continuous bone in the *Gdf6*-/- at E15.5 (J) and continue to fuse along its entire length as ossification progress toward the midline at E16.5 (L). fb, frontal bone; pb, parietal bone, cs, coronal suture; ls, lambdoid suture; sqs, squamosal suture

Analysis of multiple *Gdf6-/-* embryos at E13.5-14.5 failed to identify visibly separate sites of alizarin staining for frontal and parietal rudiments (not shown).

At E15.5, the frontal and parietal bones were fused into one continuous bone in the *Gdf6*-/- embryo (Fig 2.2J), while the bones remained separated by the CS in the wild-type (Fig 2.2I) embryo. The CS continued to fuse along its entire length as ossification progresses outward in the *Gdf6-/-* embryo through E16.5 (Fig 2.2L) and E18.5 (Fig 2.2B). The sagittal, lambdoid, and squamosal sutures (Fig 2.2B,D) remained unaffected in *Gdf6*-/- mice throughout embryonic development and adult life.

At the macroscopic level, the ossification centers and suture in *Gdf6+/-* embryos appear to develop identically to wild-type embryos with regards to the onset of ossification and size of the bones (not shown). This data suggests that *Gdf6* plays a role in CS formation at or prior to the onset of ossification.

Gdf6-/- *embryo has normal suture boundary formation*

Coronal craniosynostosis can result from a failure to form a proper boundary between cells of the neural crest-derived frontal bone and the paraxial mesoderm-derived parietal bone. The formation of this boundary involves the cooperation of *Twist1* and *Msx2* to control of the expression domains of *ephrin-A2*, *ephrin-A4*, and *EphA4* (Merrill et al., 2006). Ephrin signaling are hypothesized to inhibit cell mixing and provide guidance cues for migrating cell populations (Poliakov et al., 2004). Failed boundary formation is evident as a mixing of the two tissue populations in the *Twist1* mutant (Merrill et al., 2006).

To determine whether a similar cell mixing was the cause of the craniosynostosis in the *Gdf6-/-* embryos, we visualized the suture boundary the *Wnt1-Cre; R26R* lines, which together stably label derivates of the neural crest (Jiang et al., 2002), including the frontal bone. At E16.5, CS fusion was evident in whole-mount stained *Gdf6*-/- embryos (Fig 2.3A-D). Transverse sections showed the presence of ossified bone across the boundary between the frontal and parietal bones in the *Gdf6*-/- embryo (Fig 2.3F, arrow), while the suture remained open and undifferentiated in wild-type (Fig 2.3E, arrow). Also of note was a general thinning of the bone in this region of the *Gdf6*-/- (Fig 2.3F) along with the loss of the characteristic suture mesenchyme blastema, seen in wild-type embryos (Fig 2.3E, arrow). In the regions of the frontal bone more distal to the suture, there was no obvious thinning of the *Gdf6-/-* bone compared to wild-type (not shown).

In the *Gdf6-/-* embryo, ossified tissue disrupted the boundary between the frontal and parietal domains (as seen in Fig 2.3F) making it difficult to determine if cells have crossed the normal boundary. Therefore embryos were examined at E14.5, when portions of the *Gdf6*-/- calvaria were not yet ossified through the suture. Coronal sections through the region of the presumptive CS reveal that although the *Gdf6*-/- embryo lacked an identifiable suture, the cellular boundary between the frontal and parietal bones remained distinct just like the wild-type suture (Fig 2.3G,H). We could find no evidence of cell mixing between these tissue populations. There was no obvious difference between wild-type and *Gdf6*+/- embryos with regards to the suture boundary (not shown). Furthermore, we observed a surprisingly uniform and continuous surface between the frontal and parietal bones of *Gdf6-/-* mice, where the suture should reside (Fig 2.3D, H).

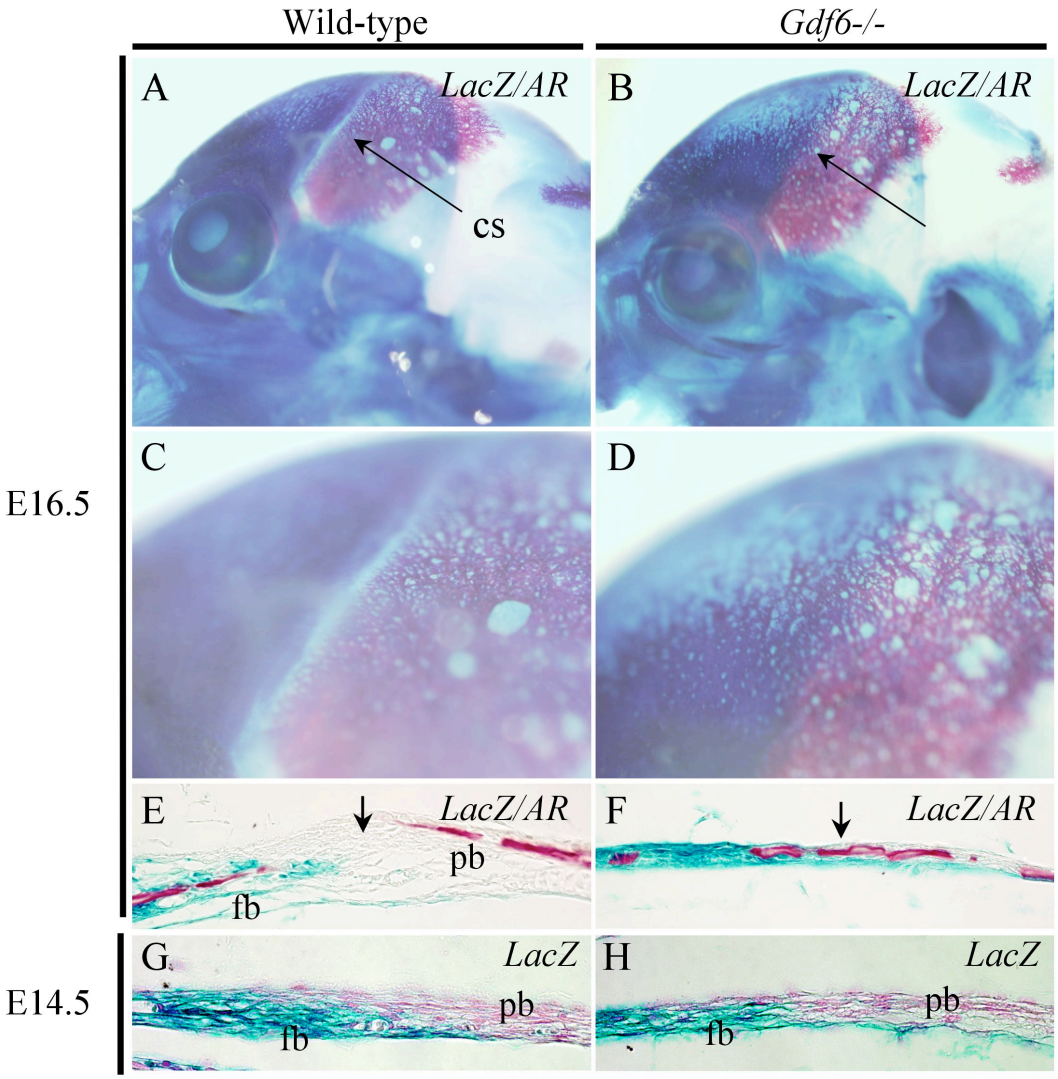

Figure 2.3. **Analysis of boundary formation in *Gdf6-/-* embryos**. E16.5 *Wnt1Cre+/-; R26R+/-; Gdf6+/+* (A,C) and *Wnt1Cre+/-; R26R+/-; Gdf6-/-* (B,D) embryos stained for lacZ, to label the frontal bone, followed by alizarin red to highlight the parietal bone. Sections through the *lacZ*/alzarin red stained embryos show the boundary between the labeled frontal bone and unlabeled parietal bone at the site of the wild-type suture (E, arrow), with bone continuing through the suture boundary in the *Gdf6-/-* embryo (F, arrow). E14.5 *Wnt1Cre+/-; R26R+/-; Gdf6+/+* (G) and *Wnt1Cre+/-; R26R+/-; Gdf6-/-* (H) embryos stained with Xgal and counterstained with nuclear fast red. In both the wild-type and *Gdf6-/-* coronal sutures, the boundary is distinct, with no evidence of cell mixing. AR, alizarin red; cs, coronal suture; fb, frontal bone; pb, parietal bone.

Gdf6-/- *and* Gdf6+/- *embryos present with pre-ossification changes in the suture*

Whole-mount staining for alkaline phosphatase (ALP) activity, an early osteoblasts marker, in the wild-type E12.5 embryo highlighted the frontal and parietal bone primordia with the CS in between (Fig 2.4A, arrow). In the *Gdf6+/-* embryo, an increase in ALP activity within the suture bridges the gap between the frontal and parietal primordia. This was the first evidence of abnormal activity in the *Gdf6+/-* mouse suture despite that *Gdf6+/-* mice do develop normal CSs. This points to a dosage effect, where the loss of *Gdf6* does increase ALP activity in the suture, but this slightly increased differentiation does not reach the threshold required for fusion of the suture.

The appearance of the parietal bone ossification center appears approximately 12 hours after the appearance of the frontal bone ossification center (Han et al., 2007). In many cases, the *Gdf6-/-* embryos at E12.5 had a further delay in appearance of the parietal primordia compared to wild-type and *Gdf6+/-* littermates, according to the initiation of ALP activity (Fig 2.4C, arrow). However, at stages when comparable levels of ALP activity are observed in the frontal and parietal bones, a strong continuous level of ALP activity bridges the gap between the two bone primordia of *Gdf6-/-* embryos (Fig 2.4D, arrow). This suggests a failure to form or maintain the undifferentiated mesenchyme that occupies a wild-type CS.

Transverse sections through the E12.5 wild-type suture also highlighted the frontal and parietal bone primordia, with the presumptive CS in between, seen as the gap in ALP activity (Fig 2.5A). In *Gdf6+/-* embryos, ALP activity extended through the presumptive suture region (Fig 2.5B), revealing a reduction of the undifferentiated suture

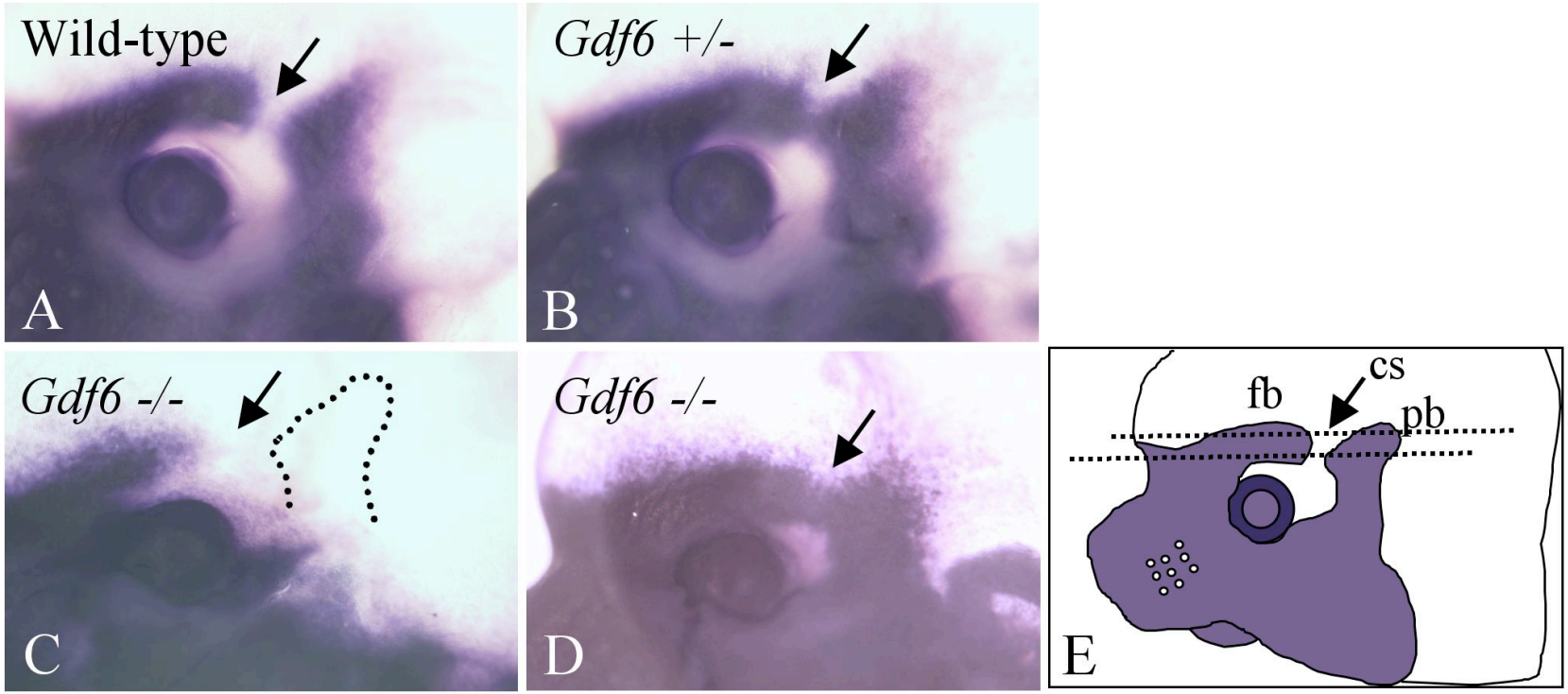

Figure 2.4. Whole-mount alkaline phosphatase staining of E12.5 embryo. Whole-mounting staining for ALP activity at E12.5 highlights the location of the frontal and parietal bone primordia with the coronal suture occupying the undifferentiated space between the two (A,E arrows). In the *Gdf6*+/- embryo, there is in increase in ALP activity within the suture mesenchyme, bridging the gap between the two primordia (B, arrow). *Gdf6*-/- embryos often had a delay in differentiation of the parietal bone rudiment (C, dotted line). When ALP activity in *Gdf6*-/- embryos were comparable to the rudiments in wild-type embryos, the suture mesenchyme was completely differentiated, with a continuous level of ALP staining between the frontal and parietal bone primordia (D, arrow). Cs, coronal suture; fb, frontal bone; pb, parietal bone.

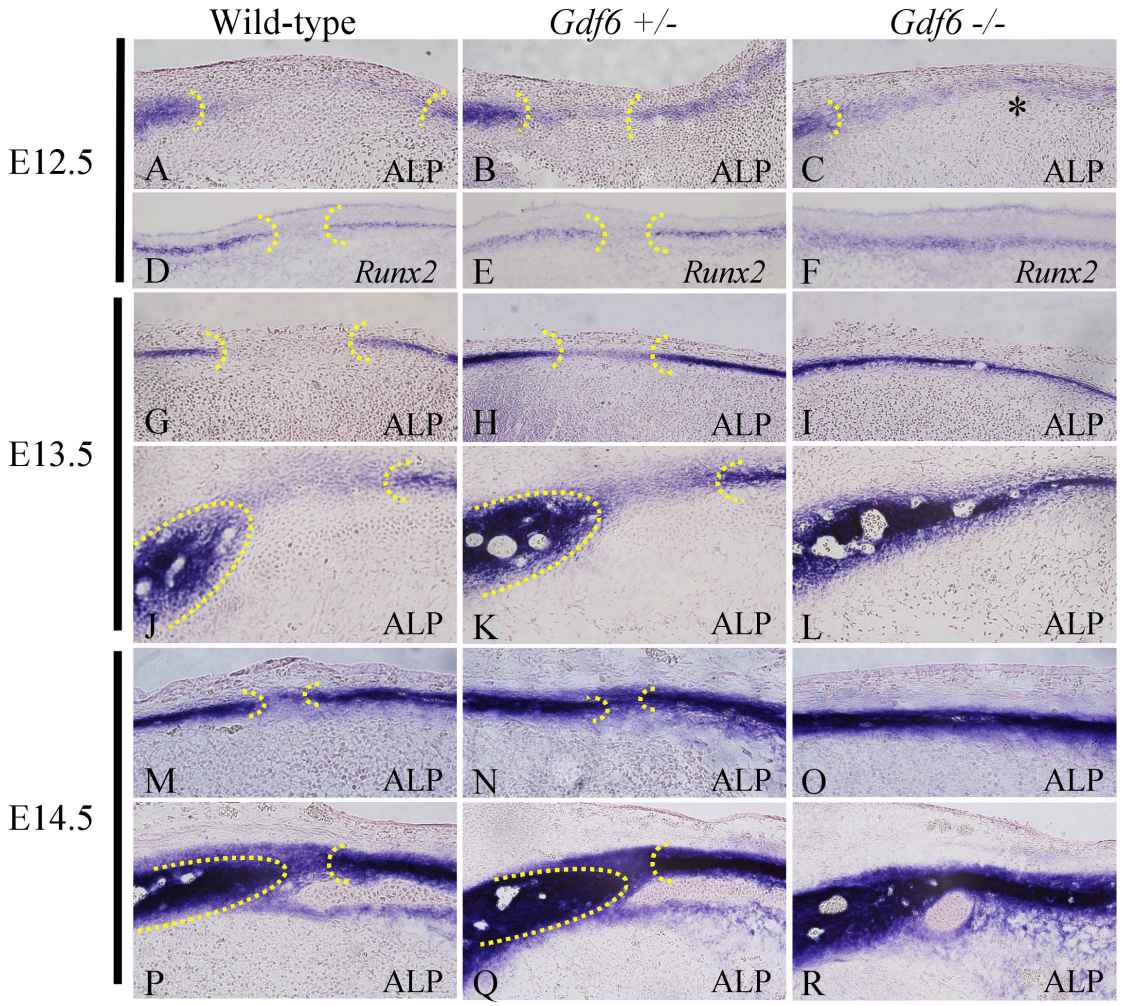

Figure 2.5. Alkaline-phosphatase staining in the presumptive suture. Transverse sections through the E12.5 wild-type suture show a gap in ALP activity between the frontal and parietal bones (A). The width of the gap is reduced in the *Gdf6*+/-, with an increase in ALP activity within the suture mesenchyme (B). In the *Gdf6*-/-, there is a continuous line of ALP activity through the region, with a reduction in ALP activity in the parietal portion of the fused bone (C). Similar changes in ALP staining were observed in the E13.5 and E14.5 rostral (G-I, M-O) and caudal (J-L, P-R) coronal sutures and through *in situ* hybridization for *Runx2* (D-F).

mesenchyme seen in the wild-type suture. In addition, the suture gap width was reduced in the *Gdf6*+/- embryos compared to wild-type (Fig 2.5B). In the *Gdf6*-/- embryos, after the frontal bone primordium there was continuous ALP staining through the region where the suture should have formed (Fig 2.5C). In comparison to the wild-type and *Gdf6*+/- embryos, the *Gdf6*-/- embryos lacked the increase in ALP activity found in the parietal bone (Fig 2.5C, asterix), although it was maintained in the frontal portion of the fused bone primordia. This confirms not only a loss of the undifferentiated suture mesenchyme, but also a delay in parietal bone differentiation was observed in *Gdf6*-/- embryos.

Differentiation of the suture mesenchyme was also examined by expression of *Runx2*, another marker for early bone differentiation. *Runx2* is required for the commitment of mesenchymal stem cells into osteoblasts. It is a master regulator of genes including *collagen type I*, *bone sialoprotein*, *osteopontin*, *TGFβ*, and *osteocalcin* (Marie et al., 2008). Like ALP*, Runx2* marked the presumptive frontal and parietal bones, with a gap of undifferentiated mesenchyme in between (Fig 2.5D). Again, the distance between the frontal and parietal rudiments was reduced in the *Gdf6*+/- embryo (Fig 2.5E). In the *Gdf6*-/- embryo, *Runx2* was expressed continuously through the suture region (Fig 2.5F).

These observations were confirmed at both caudal (closer to the eye) (Fig 2.4E, lower dotted line) and rostral (newly formed) (Fig 2.4E, upper dotted line) levels of the presumptive CS by ALP activity at E13.5 and E14.5 (caudal Fig 2.5J-L, P-R and rostral Fig 2.5G-I, M-O). These data all suggest an increase in osteogenic differentiation of the cells in the developing suture of the *Gdf6*+/- embryos and *Gdf6*-/-

embryos, and also a dosage effect, where the differentiation in the *Gdf6*+/- embryos is an intermediate level between wild-type and *Gdf6*-/- embryos.

A decrease in both the intensity (Fig 2.5C,I) and span (not shown) of ALP activity in the parietal bone rudiment of *Gdf6*-/- embryos was observed, suggesting a decrease in the rate of differentiation in this structure. This was also observed in the alizarin red staining of E14.5 embryos, with a reduction of the size of the *Gdf6*-/- parietal bone ossification center compared to wild-type and *Gdf6*+/- embryos *(not shown)*. This could be a potential secondary effect of loss of the suture, or a direct effect of the loss of *Gdf6*.

Suture fusion not due to changes in proliferation or apoptosis in the suture region

In principle, suture fusion could result from changes in the number of cells in the suture or bone fronts proliferating or undergoing apoptosis, thereby increasing or decreasing the number of cells in the pre-osteogenic pool. Between E14.0 and E14.5, the frontal and parietal rudiments in the *Gdf6*-/- embryo were first visible by alizarin red staining as a single fused ossified element (Fig 2.2F,H). Therefore the sutures of wild-type, *Gdf6*+/-, and *Gdf6*-/- littermates were examined prior to fusion at E13.5 through immunohistochemistry. Adjacent sections were stained for ALP activity in order to help localize the suture (Fig 2.6A-F). Immunohistochemistry for phospho-histone H3 (Fig 2.6A'-C') revealed a significant difference ($p=0.039$) in the proliferation of cells in the suture region between wild-type and *Gdf6*+/- embryos, however no difference was detected between wild-type and *Gdf6*-/- or *Gdf6*+/- and *Gdf6*-/- sutures (Fig 2.6G).

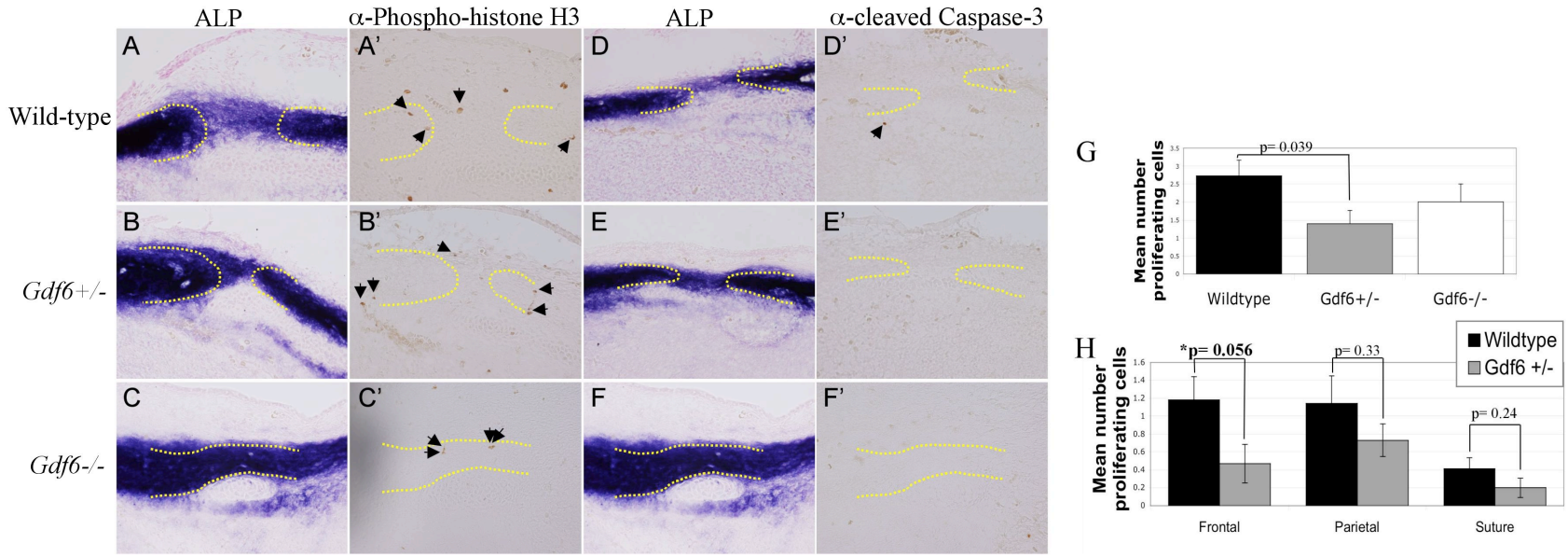

Figure 2.6. **Analysis of cell proliferation and apoptosis in the E13.5 coronal suture**. Adjacent sections stained for ALP activity, highlighting the location of the frontal and parietal bones (A-F dotted yellow lines), and immunohistochemistry for phospho-histone H3 (A'-C') or cleaved caspase-3 (D'-F'). Positive cells are marked with arrows. (G) Quantification of the total number of proliferating cells counted in the suture region. (H) Quantification of the number of proliferating cells counted in each separate component of the suture region; the frontal bone, parietal bone, and suture mesenchyme. The number of proliferating cells in each separate region of the suture was not counted for *Gdf6-/-* embryos since there is no suture mesenchyme and the border between the frontal and parietal bones cannot be distinguished. N=3 embryos for each genotype and antibody treatment with at least 5 sections per embryo quantified. Differences the number of proliferating cells per suture region were analyzed using a t-test with a p value<0.05 deemed as significant.

We also compared the number of proliferating cells separately in each tissue of the suture; the suture mesenchyme, the frontal bone, and parietal bone (Fig 2.6H). The number of proliferating cells in the *Gdf6-/-* embryo was not examined by region because there is no suture mesenchyme and the boundary between the frontal and parietal portions of the fused bone cannot be distinguished. However, we did observe a decrease in the number of proliferating cells in the *Gdf6+/-* frontal bone compared to wild-type that was trending toward significance (p=0.056). This could be attributed to the increased rate of differentiation in the suture of *Gdf6+/-* embryos, reducing the pool of pre-osteogenic proliferating cells, or a direct affect of *Gdf6* on frontal bone proliferation. No difference between the frontal bones of wild-type and *Gdf6+/-* embryos was observed in other assays. Although there was reduced proliferation also in the *Gdf6+/-* parietal bone and suture mesenchyme compared to wild-type, the difference did not reach the level of significance (p=0.33, p=0.24).

Cell proliferation was also examined at E12.5, the timepoint when erroneous differentiation of the suture mesenchyme is first visible by increased ALP activity (Fig 2.5). Although no suture mesenchyme is present in the *Gdf6-/-* embryo, at E12.5, the boundary between the frontal and parietal bone can be distinguished due to the increased ALP activity in the frontal bone (Fig 2.7A). Still we found no significant difference in the number of proliferating cells between the wild-type and *Gdf6-/-* embryos in the entire suture region (p=0.18) nor between wild-type and *Gdf6+/-* or *Gdf6+/-* and *Gdf6-/-* embryos (Fig 2.7B). The number of proliferating cells counted separately in the frontal bone, suture mesenchyme, and parietal bone (Fig 2.7C) was also not significant.

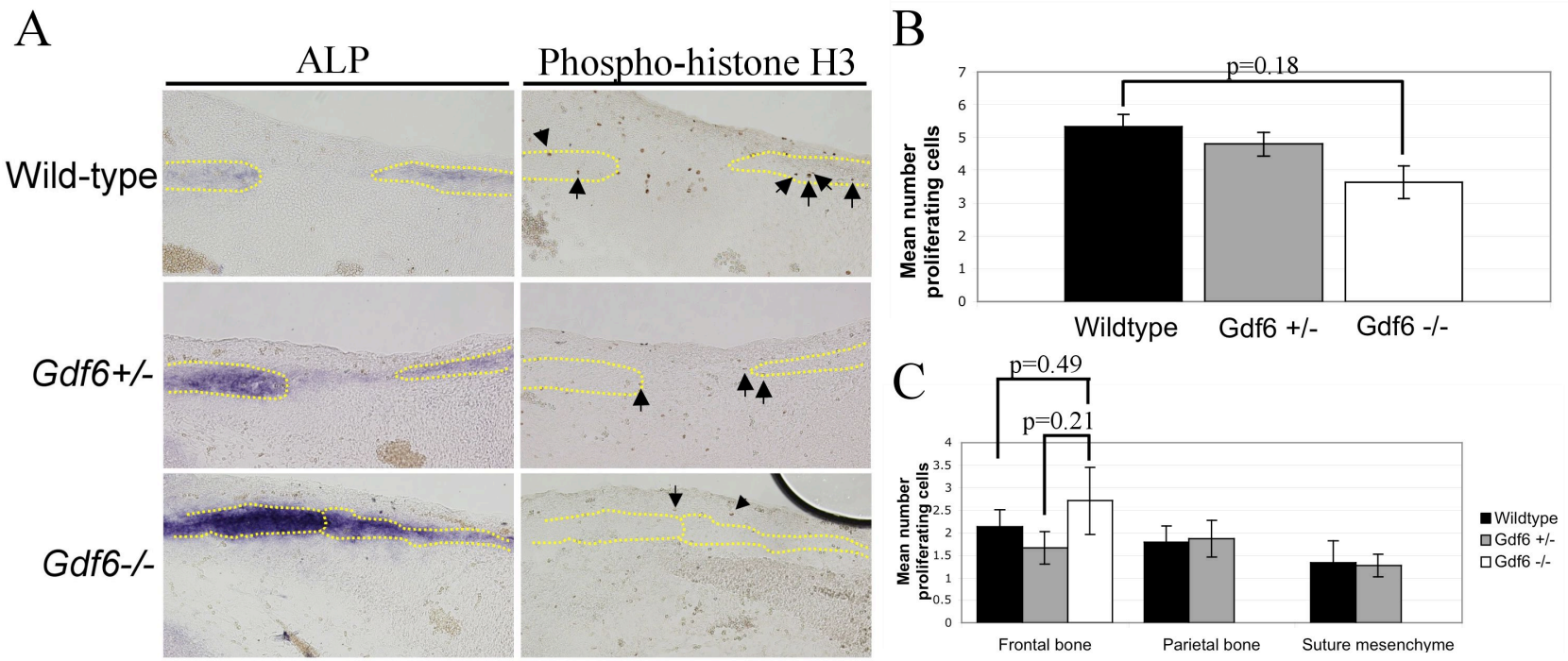

Figure 2.7. Analysis of cell proliferation in the E12.5 coronal suture. (A) Adjacent sections stained for ALP activity, highlighting the location of the frontal and parietal bones (dotted yellow lines), and immunohistochemistry for phospho-histone H3. Example positive cells are marked with arrows. (B) Quantification of the total number of proliferating cells counted in the suture region. (C) Quantification of the number of proliferating cells counted in each separate component of the suture region; the frontal bone, parietal bone, and suture mesenchyme. The number of proliferating cells in the suture mesenchyme and parietal bone were not counted for *Gdf6-/-* embryos since the boundary between the two cannot be distinguished. N=3 embryos for each genotype with at least 5 sections per embryo quantified. Differences the number of proliferating cells per suture region were analyzed using a t-test with a p value<0.05 deemed as significant.

Unlike E13.5, at E12.5 we detected no difference between the wild-type and *Gdf6*+/- suture regions (Fig 2.7B) or specifically in the frontal bone (Fig 2.7C). Therefore, no differences in proliferation are evident at the time when the suture mesenchyme begins to differentiate. This supports the idea that reduced proliferation in the frontal bone of *Gdf6*+/- embryos at E13.5 is a secondary affect of increased differentiation of osteoprogenitor cells and not a contributing factor to fusion of the suture.

To study cell death at the suture we used cleaved-caspase 3 immunohistochemistry. Few to no apoptotic cells were detectable in the suture mesenchyme or bone front at this timepoint in development (Fig 2.6D'-F'), and likewise, no significant difference between genotypes was found (not shown). Previous reports have suggested that apoptotic cell death is first detectable in the CS at E16 (Rice et al., 1999), and therefore apoptotic activity at the timepoint of the *Gdf6*-/- phenotype is not likely a contributing factor in normal suture development or the craniosynostosis pathology.

Gdf6 is expressed in the frontal bone primordia

By E10.5, the neural crest/paraxial mesoderm boundary and future site of the CS, has already formed (Jiang et al., 2002). In order to pinpoint the pattern of *Gdf6* expression during cranial development, we performed *in situ* hybridization on embryos at E9.5-E14.5. *Gdf6* mRNA was first detected in the developing cranial region in a triangular-shaped area just anterior to the eye at E10.5 (Fig 2.8A-C, arrow). This corresponded closely with the neural crest-derived frontal bone rudiment, as labeled in

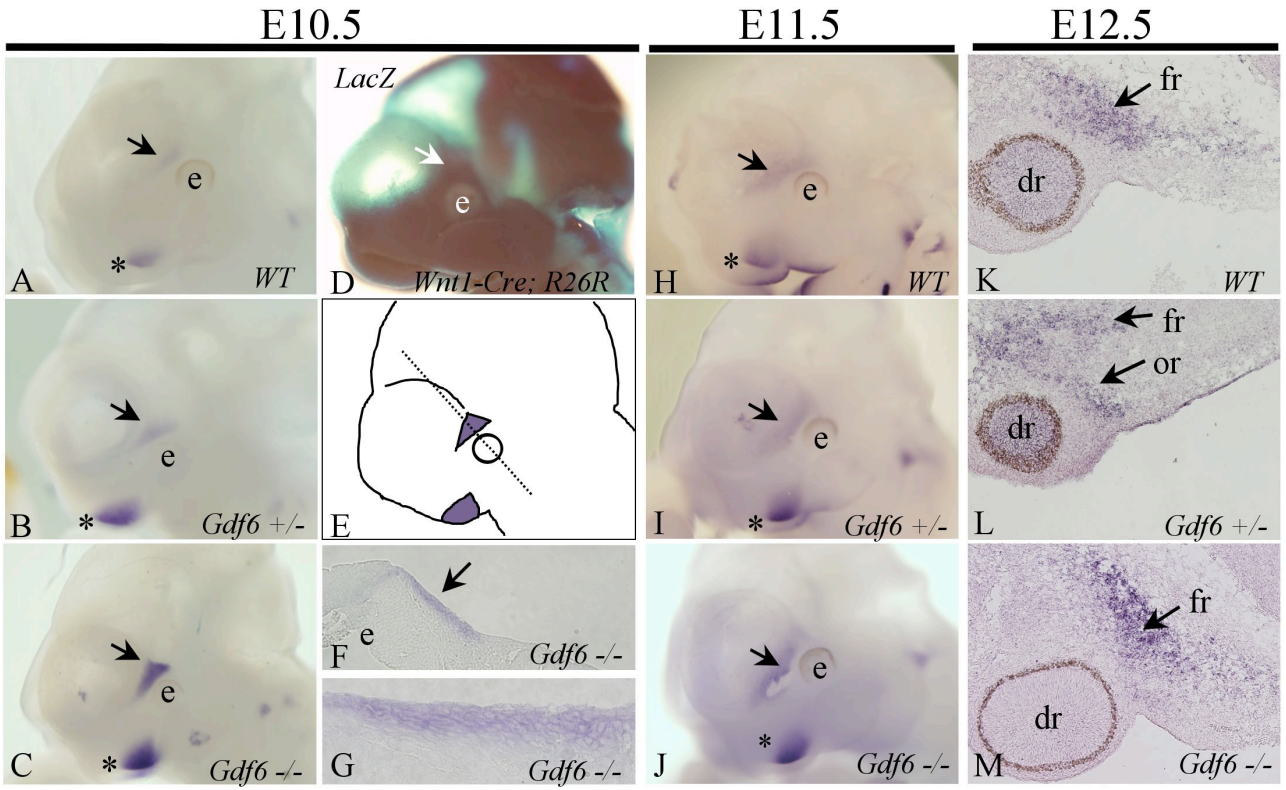

Figure 2.8. Expression of *Gdf6* in early cranial development. *In situ* hybridization for *Gdf6* at E10.5 (A-C, F,G), E11.5 (H-J), and E12.5 (K-M). *Gdf6* is expressed in the frontal bone primordia (arrow), which is labeled as neural crest-derived in the *Wnt1-Cre; R26R* embryos (D, white arrow). *Gdf6* transcript is expressed more strongly in the *Gdf6-/-* embryo (C, J) than either the wild-type (A, H) or *Gdf6+/-* embryo (B, I), in both the frontal bone rudiment (arrow) and branchial arches (asterix). In transverse cross section through the eye and frontal bone primordia at E10.5 (dotted line, E), *Gdf6* is expressed in several layers of mesenchyme underlying the surface ectoderm (F, G). At E12.5, *Gdf6* continues to be expressed in the frontal bone rudiment, in addition to the dorsal retina (K-L) and orbital bone rudiment (L). Expression of *Gdf6* in the dorsal retina seen in the wild-type and *Gdf6+/-* embryos (K,L) is absent in the *Gdf6-/-* embryo (M). dr, dorsal retina; e, eye; fr, frontal rudiment; or, orbital bone rudiment.

Wnt1-Cre; R26R embryos (Fig 2.8D, arrow). *Gdf6* was expressed in the frontal bone rudiment at E11.5 (Fig 2.8H-J), as the rudiment begins to grow and expand. Transverse sections through the E10.5 frontal rudiment (Fig 2.8E, dotted line) reveal this expression anterior to the eye was localized to several layers of mesenchyme underlying the surface ectoderm (Fig 2.8F,G). At E12.5, *Gdf6* continued to be exclusively expressed in the frontal bone rudiment (Fig 2.8K-M, arrow), with no evidence of expression in the suture mesenchyme or parietal bone rudiment. By E14.5, when fusion of the ossification centers was first visible by alizarin red staining, *Gdf6* is no longer expressed in the suture region (Fig 2.9).

The *Gdf6* mutant mouse was generated by replacing a large portion of the second exon, containing the entire mature signaling region (Fig 2.10A, red track), with a *neomycin* cassette. Although no functional Gdf6 protein can be made from the *Gdf6-/-* allele, the mutant *Gdf6* transcript was detected by our *in situ* RNA probe, which targets the 3' UTR of *Gdf6* (Fig 2.10A, green track). *In situ* hybridization revealed that *Gdf6* transcripts were still present in *Gdf6*-/- embryos (Fig 2.8C, J, M). Interestingly, the *Gdf6* transcript was more highly expressed in *Gdf6*-/- embryos than in either wild-type or *Gdf6*+/- embryos, with staining in *Gdf6*+/- embryos at intermediate levels (Fig 2.8A-C, H-I). Increased staining was also observed for *Gdf6* in the branchial arches (Fig 2.8, A-C, H-I asterix) and in the orbital bone rudiment (Fig 2.6L) of wild-type, *Gdf6+/-,* and *Gdf6-/-* embryos, each with increased *in situ* signal in the *Gdf6-/-* embryos.

These observations suggest that *Gdf6* expression may be self-regulated in the frontal bone, brachial arches, and orbital bone by a negative feedback loop. Thus, in wild-type embryos, when functional Gdf6 protein is produced, there might be a negative

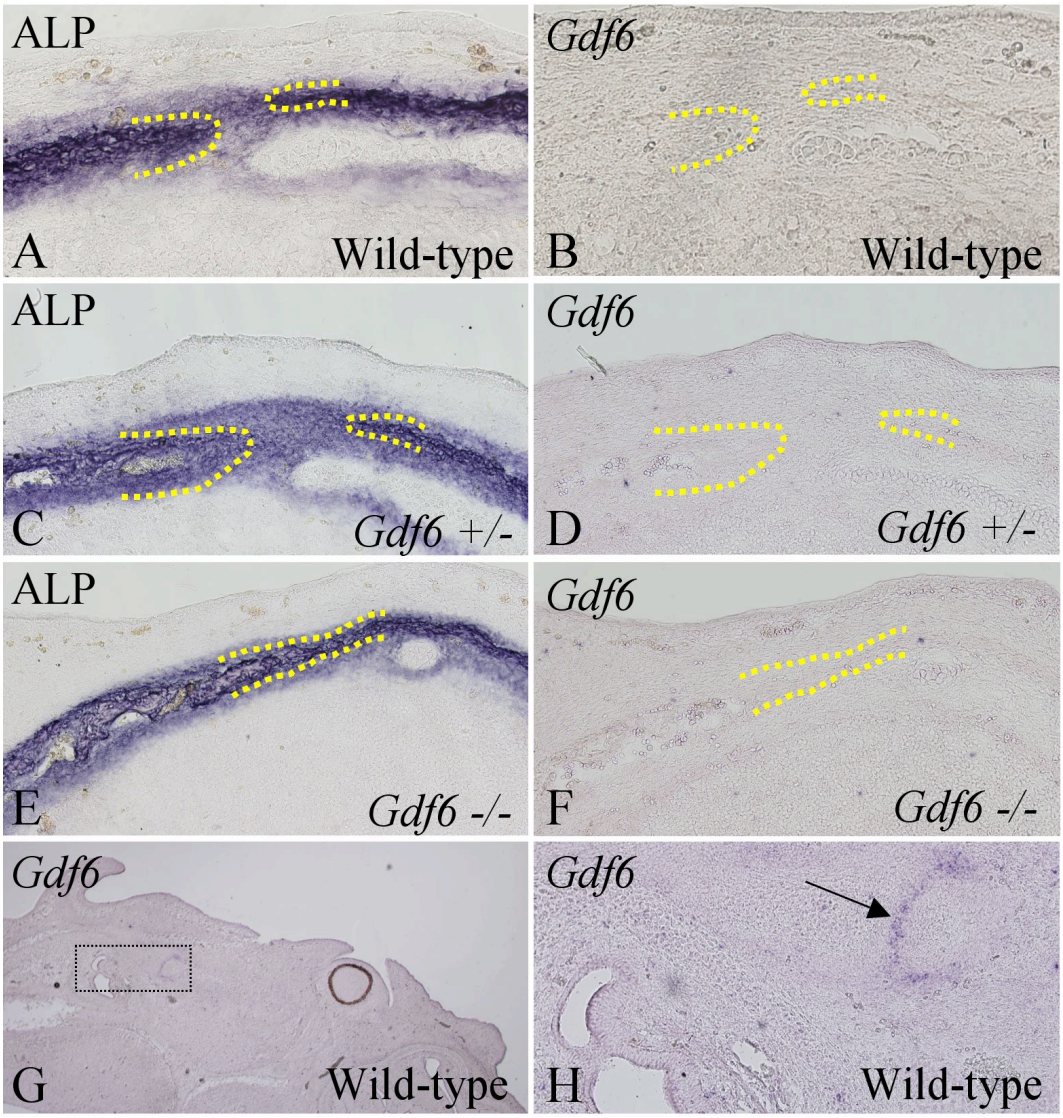

Figure 2.9. **Lack of *Gdf6* expression in the E14.5 coronal suture.** *Gdf6* transcription has ceased in the frontal bone by E14.5 in wild-type (B), *Gdf6*+/- (D), and *Gdf6*-/- embryos (F), with adjacent sections stained for ALP activity to highlight the location of the frontal and parietal bones (A, C, E, dotted lines). Previously reported expression in the middle ear bone joints is visible in sections from the same series, acting as a positive control (G,H arrow).

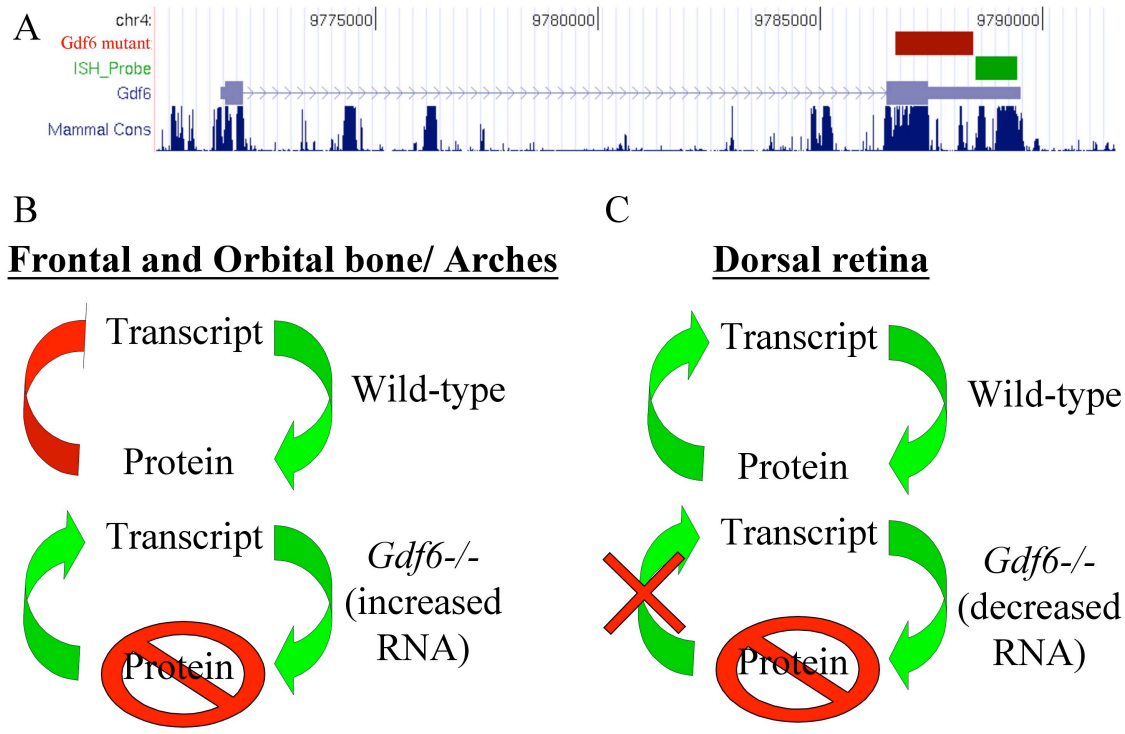

Figure 2.10 Autoregulation of *Gdf6* in the frontal bone primordia. A) Image from the UCSC genome browser denoting the region of the *Gdf6* gene replaced in the *Gdf6* mutant mouse by a *neomycin* cassette (red, mutant track) and the region targeted by the *Gdf6 in situ* hybridization probe (green, ISH_Probe track), which do not overlap, allowing us to detect *Gdf6* transcript in our mutant mice. B) Regulation of *Gdf6* in the frontal and orbital bone primordia and the branchial arches. In wild-type embryos, there might be a negative feedback loop to repress the continued transcription of *Gdf6* (upper). In the *Gdf6-/-* mouse, no functional protein is produced, and with the loss of negative feedback the *in situ* signal is increased (lower). C) Regulation of *Gdf6* in the adjacent dorsal retina. In wild-type embryos there is a positive feedback mechanism (upper), but this is lost in the *Gdf6* mutant, and with no positive feedback and the *in situ* signal is lost (lower).

feedback loop to repress continued *Gdf6* expression. However, in the *Gdf6-/-* embryo, no functional protein is produced, and with the loss of the negative feedback the *in situ* signal is increased (Fig 2.10B). However, transcript was observed in the dorsal retina wild-type and *Gdf6+/-* embryos (Fig 2.8K,L), but was lost in *Gdf6-/-* embryos (Fig 2.8M), suggesting a tissue-specific effect. Therefore, in the case of the dorsal retina, there is normally a positive feedback loop. However, in the *Gdf6-/-* mice, with no functional protein being made, there is no positive feedback to induce *Gdf6* expression (Fig 2.10C), resulting in the elimination of the *in situ* signal. Therefore, *Gdf6* appears to have two opposite modes of regulation in two adjacent structures, the dorsal retina and the frontal bone primordia.

Gdf6 protein has the ability to stimulate differentiation in vivo

In order to test for a direct effect of Gdf6 *in vivo*, agarose beads soaked in Gdf6 were implanted into the suture region of wild-type E12.5 embryos. The effect of the implanted bead on the differentiation process was assessed through staining for ALP activity. When a Gdf6-soaked bead was implanted into a region with endogenous ALP activity, such as the frontal bone (Fig 2.11B) or osteogenic cranial mesenchyme (Fig 2.11C) it was found that Gdf6 was able to stimulate ALP activity in the region immediately surrounding the bead when compared to beads soaked in BSA (Fig 2.11A). The BSA and Gdf6-soaked beads had a reduced ability to stimulate ALP activity (Fig 2.11C, red arrow) when implanted in non-osteogenic tissues, such as cranial cartilage (Fig 2.11C, asterix), brain, or ectoderm (not shown). Although this apparent ability of Gdf6 to stimulate differentiation was in contrast to the increased differentiation in the

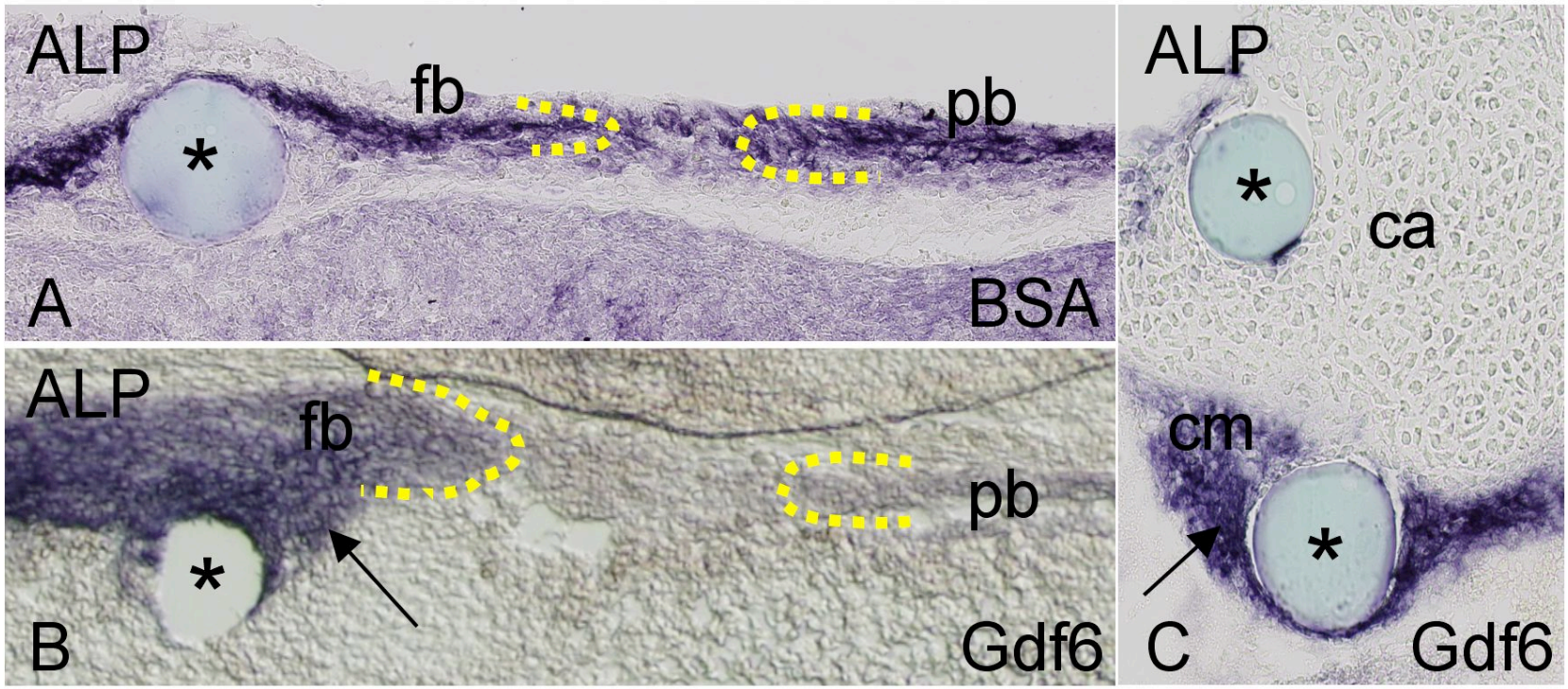

Figure 2.11. ***In vivo*** **activity of Gdf6 protein in the frontal bone primordia**. Beads soaked in BSA (control) (A) or Gdf6 protein (B,C) were implanted into the suture region of E12.5 embryos. The BSA-soaked bead had no effect on ALP activity when implanted into the frontal bone primordia (A, asterix). Beads soaked in Gdf6 increased ALP activity in the area immediately surrounding the bead (arrow) when implanted into the frontal bone primordia (B) or other cranial regions with endogenous ALP activity (C, arrow), but reduced activity (red arrow) when implanted into a region of cranial cartilage (C, asterix). ca, cranial cartilage; cm, cranial mesenchyme; fb, frontal bone primordia; pb, parietal bone primordia.

Gdf6-/- mice, it is likely that the inhibitory activity of Gdf6 on the suture mesenchyme is context dependent or moderated by a secondary factor.

Discussion

Here we present data indicating that *Gdf6* is genetically required for osteogenic differentiation in the developing CS during its formation. *Gdf6* is absolutely required for formation of the suture, as in *Gdf6-/-* embryos there is an initial failure to establish a region of delayed differentiation between the frontal and parietal condensations. Since *Gdf6* mRNA is strongly downregulated in wild-type calvaria by E14.5, *Gdf6* may not be required at later stages to maintain patency of the established suture. The question of whether *Gdf6* plays a role in suture maintenance will require examination of Gdf6 protein stability and localization, and/or conditional deletion of *Gdf6* at later stages.

Gdf6 represses osteogenic differentiation but not boundary formation in the coronal suture

We found no evidence for disruption in the frontal/parietal cell boundary in *Gdf6-/-* mice. This is in contrast to the mechanism of suture fusion in the *Twist+/-* and *Epha4-/-* mice where, before E14.5, osteogenic cells from the frontal bone abnormally cross into the suture mesenchyme (Merrill et al., 2006). In *Twist+/-* mice, ALP expression in the frontal/parietal rudiments is normal up to E14.5. In contrast, ALP expression abnormalities are detectable by E12.5 in *Gdf6-/-* embryos, before ephrin ligands are expressed in the frontal/parietal region (Merrill et al., 2006). Therefore *Gdf6* is required for a mechanism that is distinct from that controlled by the *Twist/Ephrin* pathway. *Twist*

also regulates osteogenic condensation via interaction with *Msx2* (Ishii et al., 2003). Our data does not exclude *Gdf6/Twist* interactions during osteogenic differentiation, although a combined reduction of *Twist* and *Msx2* levels was shown to primarily affect differentiation of the frontal, but not the parietal bone (Ishii et al., 2003).

Somewhat surprisingly, *Gdf6* mRNA was not detected in the suture mesenchyme itself but in the frontal bone primordia. This is in contrast to the sites of wrist and ankle joint fusion in *Gdf6-/-* embryos, where *Gdf6* is clearly expressed in the developing joint interzones (Settle et al., 2003). However, several studies suggest that the action of GDFs in limb joint development is not explained by direct autocrine suppression of chondrogenesis; for example, both the direct application of GDF5 protein to developing limb cartilage and transgenic Gdf5 overexpression are pro-chondrogenic (Storm and Kingsley, 1999; Tsumaki et al., 1999), although in limb joints the pro-chondrogenic effects of GDFs are probably inhibited by Noggin (Brunet et al., 1998). A unifying theme of both limb joints and the frontal bone is that both are important paracrine signaling centers for adjacent targets (that is, cartilage in the limb and the suture mesenchyme in the cranium). Paracrine effects of *Gdf6* are also demonstrated in other structures, including the thyroid cartilage. *Gdf6-/-* mice have hypoplastic thyroid cartilage, however, *Gdf6* is not expressed in the cartilage itself, but in the surrounding mesenchyme (Settle et al., 2003).

Phenotypic restriction to the coronal suture

With *Gdf6* expression occurring in the frontal bone primordia, this leads to the question of why the CS is the only suture affected and not the interfrontal suture, which

resides between the paired frontal bones? One possibility could relate the different origins of the bones and suture. The interfrontal suture resides at a boundary between two neural crest-derived bones, while the CS is a boundary between bones of mixed origin. We have already demonstrated that *Gdf6* has different effects in the frontal bone primordia and the suture mesenchyme, and therefore it is plausible that *Gdf6* could have different signaling properties in tissues of different origins.

Furthermore, the signaling in the interfrontal suture is distinct from the signaling within the other sutures. As discussed in detail in Chapter I, the interfrontal suture is the only suture in mice to undergo nonpathological postnatal fusion (Opperman, 2000), involving mechanisms that are distinct from the other sutures. In addition, the frontal and parietal bone ossification centers meet almost immediately at E14.5 (Fig 2.2E,G), much earlier than the bone fronts meet at the remaining sutures later in embryonic and postnatal development and long after expression of *Gdf6* has turned off at E14.5 (Fig 2.9).

Effects of Gdf6 signaling in the developing calvarium

Gdf5/6/7 form a closely related subfamily of BMPs, sharing >80% identity in their mature C-terminal signaling domains (Storm et al., 1994). The strong similarity of *Gdf5* and *Gdf6* suggest they share similar signaling properties. Given the *Gdf6* expression in developing calvaria, we conclude that *Gdf6* signals in a paracrine manner to regulate suture development. The simplest model is that *Gdf6* expression in the frontal bone signals to the suture mesenchyme to inhibit osteogenic differentiation and maintain suture patency (Fig 2.12A). Therefore, when the Gdf6 signal is lost, the suture mesenchyme differentiates and the suture space is obliterated by bone. Although this is

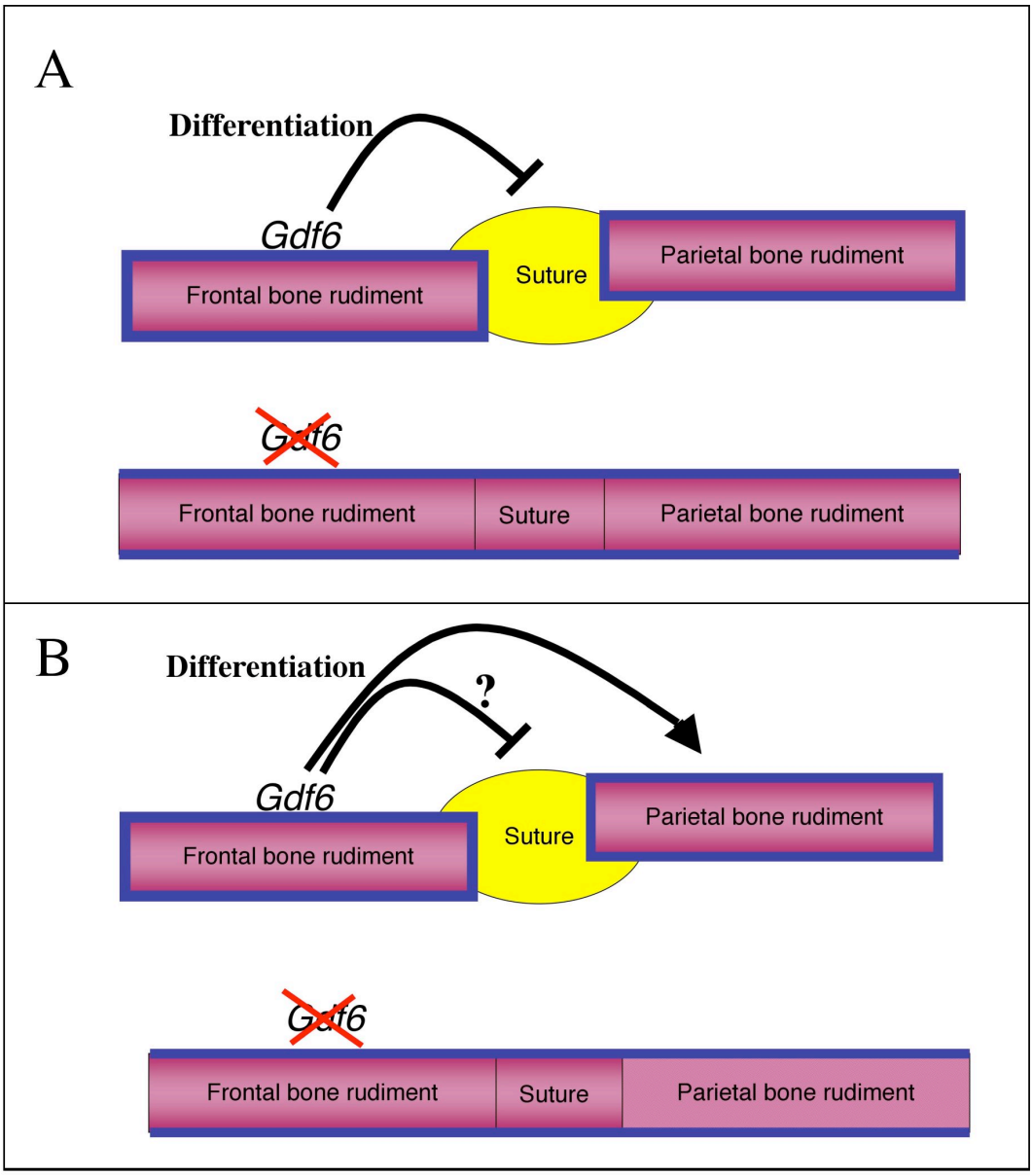

Figure 2.12. Alternative models for the function of *Gdf6* in suture development. A) *Gdf6* expression in the frontal bone provides a paracrine signal to the suture mesenchyme to inhibit osteogenic differentiation. With the loss of *Gdf6*, the suture mesenchyme differentiates into bone. B) *Gdf6* is pro-osteogenic, signaling to the parietal bone to promote differentiation. The inhibitory effect on differentiation of the suture mesenchyme is modulated through interactions with secondary factors. With the loss of *Gdf6*, the suture mesenchyme differentiates, but the differentiation of the parietal bone is delayed.

consistent with our analysis of increased ALP and *Runx2* in the suture mesenchyme of *Gdf6-/-* embryos, it seems to contradict our data showing that when beads soaked in Gdf6 protein are implanted into the frontal bone they stimulate differentiation of the primordia. Previous studies demonstrated that beads soaked in Bmp4 protein increased tissue volume when placed at the bone fronts or within the suture mesenchyme, but had no effect on suture closure (Kim et al., 1998a). Therefore, it is not yet clear if this inhibitory effect occurs via direct signaling or through indirect effects transmitted by downstream effectors. Interestingly, the onset of ALP activity is delayed in the parietal, but not frontal, primordia in *Gdf6-/-* embryos. Since *Gdf6* is expressed in the frontal but not parietal primordia, this suggests *Gdf6* signaling from the frontal primordium also acts in a paracrine manner to influence maturation of the parietal. In this view, Gdf6 actually stimulates osteogenic maturation of the parietal rudiment, although it is not clear if this effect is direct or indirect (for example, it could be a secondary effect mediated by Gdf6 regulating a separate factor in the suture mesenchyme) (Fig 2.12B). Homozygous mutants for *Noggin*, an antagonist of BMP signaling, also present with delayed ossification of the parietal bone, with no parietal bone ossification center evident at E14.5 (Tylzanowski et al., 2006). The frontal and parietal bone are derived from different tissues (the cranial neural crest and paraxial mesoderm) and therefore it is possible that different tissues respond differently to Gdf6 signal. *Msx1-/-; Msx2-/-* compound mutant mice also have defects in the ossification of both the frontal and parietal bones, although they are only expressed together in the frontal bones. This affect is possibly due to the loss of these genes in the dura, which is also derived from the cranial neural crest (Han et al., 2007).

Therefore, data regarding Gdf6's possible roles in skeletal differentiation are important for interpretation of our results. Several reports indicate that like Gdf5, Gdf6 can stimulate chondrogenic differentiation in cell culture models (Nochi et al., 2004). Whether Gdf6 is pro- or anti-osteogenic is less clear. Some studies indicate that in vitro, Gdf6 can have pro-osteogenic effects on osteoblastic cells in similar manner to Gdf5, albeit its ability to induce osteoblast markers is much less than that of the "canonical" osteogenic BMPs such as BMP2 or BMP7 (Bobacz et al., 2006). However, Gdf6 can inhibit ALP activity and mineralization in bone marrow-derived mesenchymal stem cells (Shen et al., 2009a). *In vitro* experiments must be interpreted with caution, due to potential differences in expression of BMP receptors and/or inhibitors across cell lines. In general, *in vitro* studies indicate that Gdf6 seems consistently capable of promoting differentiation of chondrogenic cells but relatively poor, or inhibitory, at promoting osteogenesis.

Injection of GDF5 into perinatal mouse calvaria *in vivo* led to increased bone formation after 2 weeks (Yoshimoto et al., 2006). While this suggests that GDFs can have stimulatory effects on calvarial osteogenic differentiation, the different timing and context of GDF5 application may not lead to the same effects as *Gdf6* in the prenatal calvaria and Gdf6 may have distinct signaling effects compared to Gdf5, despite similar receptor usage (Mazerbourg et al., 2005). Other studies indicate that the effects of *Gdf6* on ALP induction are context-dependent (Williams et al., 2008), which coincides with our own bead implantation studies.

This effect may be mediated by receptor subunit combinations, interactions with inhibitors such as *Noggin*, or even heterodimerization with other BMP family members.

Noggin is expressed in a layer surrounding the developing frontal and parietal bones and can bind Gdf6 (Chang and Hemmati-Brivanlou, 1999). Noggin can repress BMP signaling in the CS (Warren et al., 2003a), so it likely inhibits Gdf6-mediated signaling. However, Noggin is not required for suture formation, as *Noggin* -/- embryos do form CSs (described in detail in Chapter V) despite having other severe cranial defects. *Xenopus* GDF6 can heterodimerize with other BMPs, such as BMP2, *in vivo* (Chang and Hemmati-Brivanlou, 1999; Lyons et al., 1995) and other BMP heterodimers can have distinct and potent effects as compared to homodimers (Butler and Dodd, 2003).

One theory in suture development states that the position of the suture is determined by a growth factor gradient established by the advancing bone fronts (Lenton et al., 2005). It is possible that the relative temporal development of the frontal and parietal rudiments is critical for this process, and that the relative delay of the parietal ossification sequence leads indirectly to failure of suture establishment. However, the onset of *Runx2* transcription is not delayed in *Gdf6-/-* embryos, suggesting *Gdf6* is not required for temporal control of *Runx2* mRNA in calvarial rudiments. We postulate that the suture mesenchyme and the parietal rudiment may be differentially sensitive to *Gdf6* signaling.

Gdf6 autoregulation and interaction with other BMPs

We observed that *Gdf6* transcription is increased in frontal bone but reduced in eyes of *Gdf6-/-* embryos. This suggests differential, tissue-specific autoregulation of *Gdf6*. Interestingly, *Gdf5* represses its own transcription in limb joints (Storm and Kingsley, 1999). Bmp4 also shows evidence of temporal autoregulation in osteoblast

cultures derived from rat calvaria, with Bmp4 causing a temporary increase in *Bmp4* transcript followed by a clear inhibition of *Bmp4* expression (Pereira et al., 2000). We propose that *Gdf6* autoregulates itself in the frontal bone and that Gdf6/BMP signaling levels are fine-tuned during normal CS development to coordinate proper differentiation and morphogenesis. Interestingly, *Bmp4* and *Gdf6* are co-expressed in both the dorsal retina and the frontal bone primordia (Danesh et al., 2009; Mortlock et al., 2003). Mutations in *Bmp4* and *Gdf6* independently disrupt eye development (Asai-Coakwell et al., 2007; den Hollander et al.; Dunn et al., 1997). Although *Gdf6* is expressed in the frontal bone rudiment, there is no evidence for a frontal bone defect in *Gdf6-/-* mice. This is likely due to compensation by *Bmp4*. *Bmp4+/-; Gdf6-/-* mice at E18.5 do in fact have a frontal bone defect, with the persistence of large foramina that is not observed in either single heterozygotes (discussed in Chapter III). We speculate that these two BMP ligands cooperate to regulate suture and/or calvarial development.

Conclusions

In summary, we found that *Gdf6* is required to control an early stage of repressed osteogenic differentiation in the CS. Not only does this suggest potential new mechanisms for this BMP family member in regulating bone growth, it nominates *Gdf6* as a candidate gene harboring mutations in individuals with coronal craniosynostosis. *Gdf6* mutations in humans have been associated with eye and postcranial skeletal abnormalities although these effects are characterized by incomplete penetrance and phenotypic heterogeneity (Asai-Coakwell et al., 2007; Tassabehji et al., 2008). Interestingly, a literature search for genomic lesions in the GDF6 genomic region

identified Nablus mask-like facial syndrome (Raas-Rothschild et al., 2009; Salpietro et al., 2003; Shieh et al., 2006) which is a complex multigene deletion syndrome characterized by loss of a critical region just proximal to *Gdf6*. In one of only two known patients where the genomic deletion included *Gdf6*, coronal craniosynostosis was observed (Raas-Rothschild et al., 2009; Salpietro et al., 2003). We propose that some individuals having coronal craniosynostosis with unknown etiology may harbor mutations in *GDF6*.

CHAPTER III

BMP4 AND GDF6 COOPERATIVELY CONTROL THE FORMATION OF THE CORONAL SUTURE

Introduction

The mammalian cranial vault is mainly composed of flat bones separated by the cranial sutures; joints composed of fibrous connective tissue that act as the main sites for cranial growth during development (Cohen, 2005). As the cranial bones expand, new bone is deposited at the growing ends of the bones, or bone fronts, while the suture mesenchyme remains undifferentiated (Lana-Elola et al., 2007). Sutures provide flexible joints for passage through the birth canal, act as shock absorbers, prevent separation of the cranial bones, and accommodate room for the rapidly growing brain (Cohen, 2005). With the exception of the metopic suture, human sutures normally do not fuse until the third or fourth decade of life (Furuya et al., 1984), when the undifferentiated mesenchyme of the suture space becomes obliterated by bone.

Craniosynostosis is defined as the premature fusion of one or more of the cranial sutures and occurs in approximately 1 in 2,500 live births (Wilkie, 1997). When a suture fuses prematurely, cranial growth ceases perpendicular to site of suture fusion while compensatory growth increases in the remaining sutures, producing a dysmorphic skull shape (Slater et al., 2008). Craniosynostosis of the CS, the joint that separates the frontal and parietal bones, accounts for approximately 30% of the documented cases of cranial suture fusion (Kabbani and Raghuveer, 2004). The CS also serves as a tissue boundary,

with the frontal bones being derived from the cranial neural crest and the parietal bones derived from the paraxial mesoderm (Jiang et al., 2000).

Growth Differentiation Factor -6 (Gdf6) and *Bone Morphogenetic Protein-4 (Bmp4)* are both members of the Bone Morphogenetic Protein (BMP) family of secreted signaling molecules. The GDF subgroup is highly conserved in vertebrates and play a critical role in limb joint formation and chondrogenesis (Storm and Kingsley, 1999). The *Gdf6* mutant mouse displays multiple joint-associated defects, including fusion in the bones of the wrist and ankle, hypoplasia of the thyroid cartilage, defects in the bones of the middle ear, and craniosynostosis of the CS (Settle et al., 2003).

In Chapter II, we demonstrated that the CS in the *Gdf6-/-* developing embryo is fused by E14.5, the earliest timepoint when ossification of the cranial bones can be detected through alizarin red staining. At E12.5, several days before ossification begins, an increase in the expression and activity of early bone markers *Runx2* and ALP indicated the loss of the undifferentiated mesenchyme occupying the suture. The suture mesenchyme must remain undifferentiated in order for the suture to remain patent and a functioning center of growth. This suggests a paracrine Gdf6 signal from the frontal bone primordia, the site of *Gdf6* expression, in inhibiting differentiation of the suture mesenchyme. However, experiments in which beads soaked in Gdf6 protein were implanted into the frontal bone showed that Gdf6 is actually able to stimulate differentiation of the frontal bone in the area immediately surrounding the bead. Therefore, the ability of Gdf6 to prevent ossification of the suture mesenchyme is likely accomplished through interactions with other unidentified factors.

It is possible that *Gdf6* may interact with other members of the BMP family, particularly *Bmp4*. *Gdf6* and *Bmp4* utilize the same type I (BMPR1a and BMPR1b) and type II (BMPR2 and ACVR2A) receptors (Mazerbourg et al., 2005). While *Bmp4* has not been directly associated with a craniosynostosis phenotype, it is known to be involved in the signaling dynamics at the suture. The posterior interfrontal suture in mice is a common model to study the events which contribute to craniosynostosis, since it is the only suture in mice which undergoes predictable fusion during postnatal development (Opperman, 2000). *Bmp4* is expressed in the suture mesenchyme and bone fronts of both patent and fusing posterior interfrontal sutures, where it is believed to stimulate the expression of its own antagonist, *Noggin*. *Noggin* in turn is expressed in patent, but not fusing sutures, suggesting a role for *Noggin* in the maintenance of suture patency (Warren et al., 2003a).

The aim of this chapter was to determine if *Gdf6* was interacting with *Bmp4* in the development of the CS. We found that like *Gdf6*, *Bmp4* is expressed in the frontal bone primordia from E10.5-E12.5. Furthermore, *Bmp4 lacZ/+; Gdf6 +/-* compound mutant mice reproduce the coronal craniosynostosis phenotype found in *Gdf6* homozygous mutants. Unlike the *Gdf6-/-* embryos, a portion of the *Bmp4 lacZ/+; Gdf6 +/-* embryos do initially form a CS, but the aberrant differentiation of the suture mesenchyme is only delayed. *Bmp4-lacZ/+; Gdf6-/-* embryos have an additional defect in the ossification of the frontal bone that is not observed in single or compound heterozygotes, or the *Gdf6-/-* embryo. This suggests that *Gdf6* and *Bmp4* function cooperatively in the development of the CS and likely also the differentiation of the frontal bones.

Materials and Methods

Mouse crosses

Methodology for the *Gdf6-/-* mouse is described in the methods section of Chapter II. The *Bmp4-lacZ* mice (Lawson et al., 1999) were generously provided by Dr. Brigid Hogan. The *Bmp4-lacZ* mice were crossed to the *Gdf6+/-* mice to generate *Bmp4lacZ/+*; *Gdf6+/-* compound mutants, then again crossed to *Gdf6+/-* mice to produce wild-type, *Gdf6+/-* and *Bmp4-lacZ/+* single heterozygotes, *Bmp4-lacZ/+; Gdf6+/-* compound mutants, *Gdf6-/-* homozygous mutants, and *Bmp4lacZ/+*; *Gdf6-/-* progeny. Embryonic age was determined through detection of the vaginal plug, with noon of that day observed as E0.5.

DNA preparations and Genotyping

DNA preparation methods were described in detail in the methods section of Chapter II. *Bmp4-lacZ* mice were genotyped using the *lacZ* primers 5'-TTTCCATGTTGCCACTCGC-3' and 5'-AACGGCTTGCCGTTCAGCA-3' to generate a 375 base-pair product. The PCR program used for these primers included the following steps: 94^{o}C 5 minutes, 10x [98^{o}C 5 minutes, 94^{o}C 30 seconds, 60^{o}C 1 minute, 72^{o}C 40 seconds], 24x [94^{o}C 30 seconds, 56^{o}C 1 minute, 72^{o}C 40 seconds], 72^{o}C 5 minutes. Alternatively, tails snips or portions of the embryos could be stained with X-gal to genotype for the lacZ allele.

Whole-mount alizarin red skeletal preparations

P21: Weanling mice were collected 21 days after birth. Mice were sacrificed in a CO_2 chamber for approximately 5 minutes. The mice carcasses were then skinned, starting with the head and moving caudally, including careful removal of the skin from the paws. All organs were removed except for the brain: although the brain will sometimes expand during the staining procedure, it was left in place in order to maintain the integrity of the cranial vault. Nylon string was tied around the spine below the ribs and labeled with the cage, litter, and mouse number is order to match skeletal preps with their genotype information. Multiple carcasses were placed in a 1 liter bottle filled with 95% ethanol for 2 days. Skeletal preps were then moved to the alcian blue staining solution for 7-10 days. The alcian blue solution [20% glacial acetic acid (Sigma) and 0.15 mg/ml alcian blue 8GX (Sigma) in 95% ethanol] was incubated in a 37^{o} water bath then stirred vigorously on a stir plate for approximately 1 hour in order to help dissolve the blue stain. Skeletal preps were then de-stained for 2 days in 95% ethanol. Carcasses were rinse with tap water and then transferred to a 1 liter bottle of 1% potassium hydroxide (KOH). A 2% KOH solution was also used quicker clearing, however, care was taken to prevent the skeleton from disintegrating into individual bones. The 1% KOH was replaced with a fresh solution every day. This was continued for 7-10 days or until the bones were white and readily visible through the cleared muscle tissue. 2 ml of alizarin red stock solution [0.25 g alizarin red, 0.5 g KOH, and 50 ml dH2O] was then added to the 1 liter 1% KOH solution. Solution initially had a dark pink color, which lightens as the skeletal preps absorbed the stain. The skeletal preps were incubated in alizarin red / 1% KOH solution for 1 day. Preparations were rinsed with tap water and transferred to a graded glycerol

series (25%, 50%, 70%, 80%, 90%, 100% glycerol in 1X PBS pH 7.4). All incubations were done on a shaker or a stir plate with constant, but gentle, stirring. Specimens were imaged under a dissection microscope in a dish of water, prior to glycerol staging, or 100% glycerol after staging. If imaged in glycerol, the skeletal prep and glycerol solution were rocked overnight to avoid streaking of the glycerol.

E18.5. The same protocol was used as described above for P21 skeletons with the following exceptions: 1) each embryo was processed in its own 50 ml conical tube instead of multiple preps in a 1 liter bottle, 2) 0.5% KOH was used for clearing, 3) because of the delicate skeletons of the embryonic preps, alizarin red was added initially along with the 0.5% KOH and incubated for only 2 days.

E14.5/E15.5/E16.5. The same protocol was used as described above for P21 skeletons with the following exceptions: 1) each embryo was processed in its own 50 ml conical tube instead of multiple preps in a 1 liter bottle, 2) 0.25% KOH was used for clearing, 3) because of the delicate skeletons of embryonic preps, alizarin red was added initially along with the 0.25% KOH and incubated overnight, 4) no skinning was necessary since staining solution are able to penetrate the skin.

Additional methods

Detailed methodology for the following techniques was described in Chapter II: Whole-mount and slide *in situ* hybridization, 3-Aminopropyltriethoxysilane treatment of slides, and alkaline phosphatase staining of sections.

LacZ staining

Embryos were fixed in 4% PFA pH 7.4 for 1 hour at 4 degrees, followed by 3x30 minute washes with Wash Buffer [2mM $MgCl_2$, 0.01% deoxycholic acid, 0.02% nodidet-P40 (Roche), 23 mM monobasic sodium phosphate pH 7.3, 77 mM dibasic sodium phosphate pH 7.3 in H_2O], rocking at room temperature. Enough X-gal stain [0.6 mg/ml X-gal (Sigma) in dimethylformamide, 0.2 mM K-ferrocyanide, 0.2 mM K-ferricyanide, 1mM Tris pH 7.5, in Wash Buffer] was applied to cover the embryo and incubated overnight, rocking at room temperature. The next day, embryos were washed 3x 1 hour with 1X PBS, then post-fixed with 4% PFA.

Results

Gdf6 *and* Bmp4 *are co-expressed in the frontal bone primordia*

As shown in the Chapter II, *Gdf6* is expressed in the frontal bone primordia from E10.5-E12.5 (Fig 3.1 D-F, arrow), a triangular region just above the developing eye. *Bmp4* is co-expressed with *Gdf6* in multiple sites in the cranial region, as determined by lacZ transgene expression in the *Bmp4-lacZ/+* embryo from E10.5-E12.5. These include the branchial arches (Fig 3.1 A-B, D-E asterix) and the dorsal retina (Fig 3.1 C, F), but also in the frontal bone primordia (Fig 3.1 A-C, arrows). This is several days before ossification centers for the frontal and parietal bones are visible by alizarin red staining at E14.5, but corresponds to the timepoint at E12.5, when the first markers for osteoblasts differentiation are visible (ALP and *Runx2)* in the frontal and parietal bone primordia

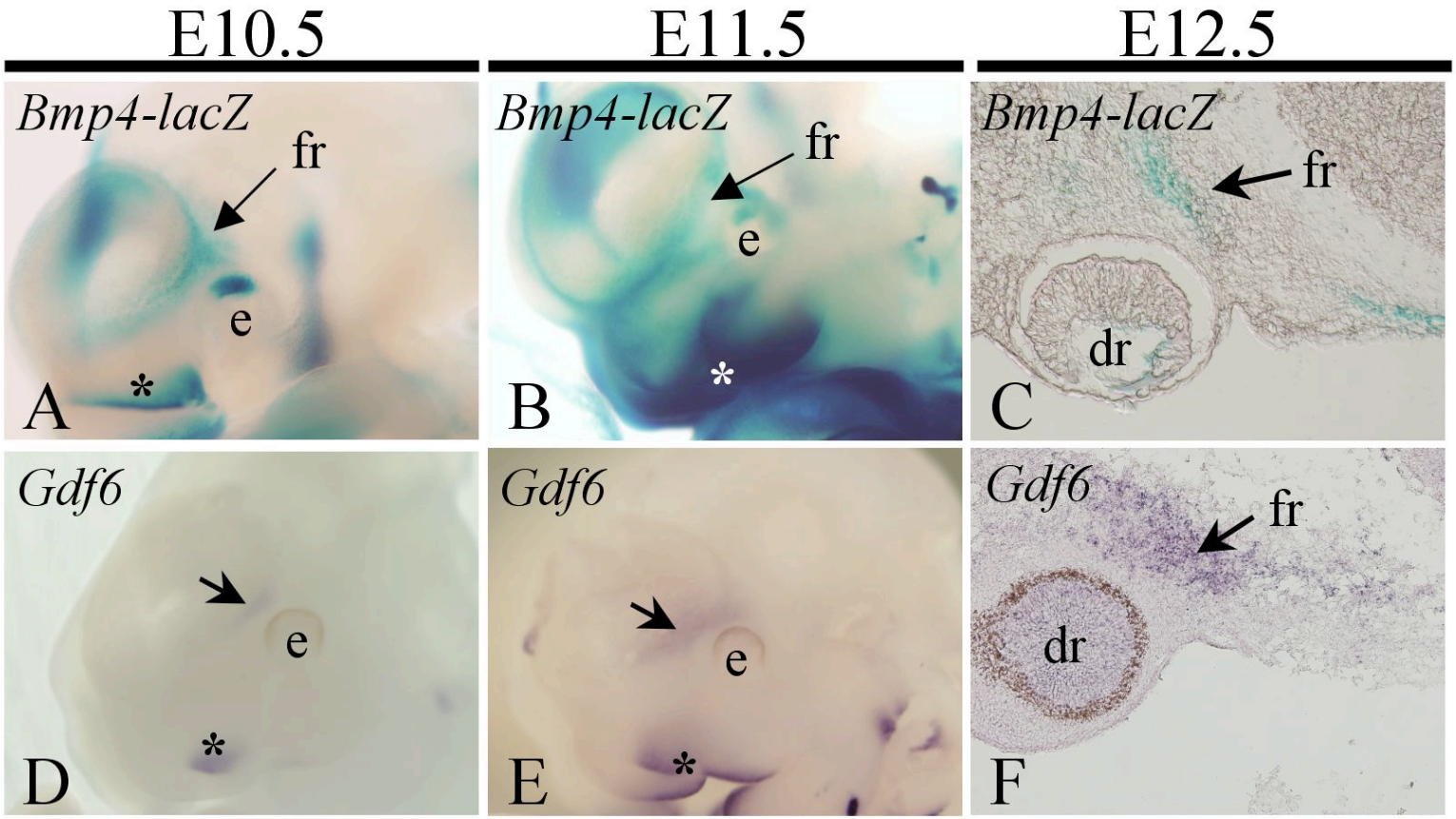

Figure 3.1. *Bmp4* and *Gdf6* are co-expressed in the frontal bone primordia. *LacZ* highlights the expression of *Bmp4* in the *Bmp4-lacZ* embryo at E10.5 (A), E11.5 (B), and E12.5 (C) just above the developing eye. *Gdf6* in the frontal bone primordia is seen in wild-type embryos through *in situ* hybridization at E10.5 (D), E11.5 (E), and E12.5 (F). Co-expression of *Bmp4* and *Gdf6* is also seen in the branchial arches at E10.5 and E11.5 (A-B, D-E asterix) dorsal retina at E12.5 (C,F). E, eye; dr, dorsal retina; fr, frontal bone primordia.

(Fig 2.5 A,D). E12.5 is also the timepoint when the first changes in suture mesenchyme differentiation are apparent in the *Gdf6-/-* embryo (Fig 2.4 C,F). At this stage, the undifferentiated state of the CS is already specified. This suggests that the loss of *Bmp4,* like *Gdf6*, could result in premature suture mesenchyme differentiation early in CS development.

Bmp4/Gdf6 *compound mutant mice present with coronal craniosynostosis*

To determine if *Gdf6* and *Bmp4* interact during suture development, *Gdf6+/-* and *Bmp4-lacZ/+* mice were crossed to produce compound heterozygotes (*Bmp4-lacZ/+; Gdf6+/-*). Mice were collected at P21 and stained with alcian blue, which stains cartilage, and alizarin red, which stains bone. The CS is the joint that separates the frontal and parietal bones in wild-type mice (Fig 3.2A, arrow). Both the *Gdf6+/-* and *Bmp4-lacZ/+* mice had normal CSs (Fig 3.2B-C, arrows). However, the *Gdf6+/-; Bmp4-lacZ/+* compound mutants had complete fusion of the CS (Fig 3.2 E). This defect was identical to the *Gdf6-/-* mouse (Fig 3.2 D), with the CS being the only cranial suture affected (the P21 *Gdf6-/-* mouse used as a reference in Figure 3.2 was collected prior to backcrossing the *Gdf6* line to a C57BL/6J background; on a mixed strain background some *Gdf6-/-* mice survived postnatally. No evidence of partial or total fusion was observed in the sagittal, squamosal, interfrontal, or lambdoid sutures (not shown). Also like the *Gdf6-/-* mouse, the fusion between the frontal and parietal bones appears as a continuous surface at this point in development (Fig 3.2 D,E). The craniosynostosis phenotype was highly penetrant in our cross (93%, 26/28), and no fusion events were

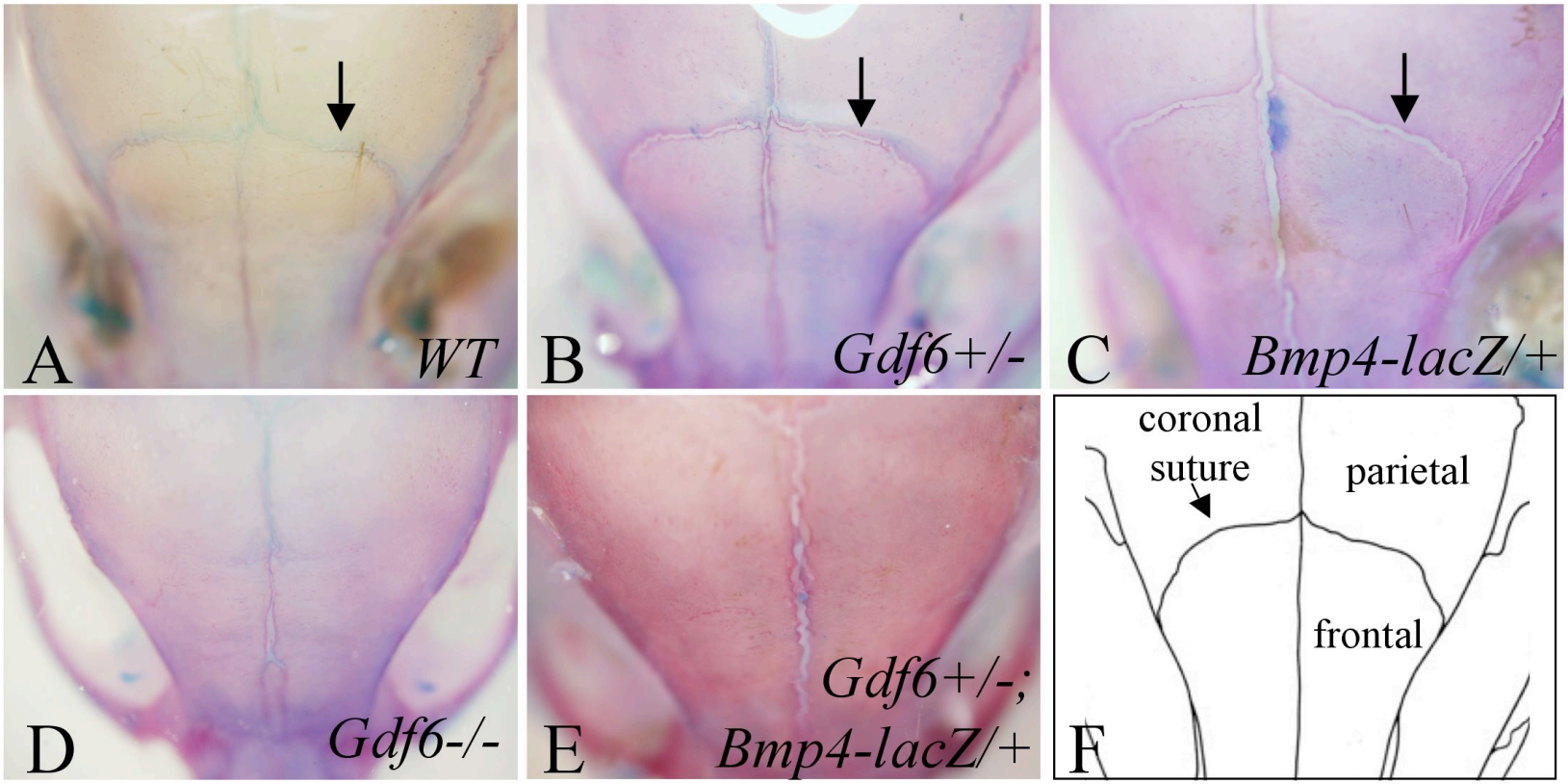

Figure 3.2. Coronal craniosynostosis in *Bmp4-lacZ/+; Gdf6+/-* compound mutant mice. P21 mice from a *Bmp4-lacZ/+* by *Gdf6+/-* cross were stained with alcian blue (cartilage) and alizarin red (bone). While wild-type (A, arrow), *Gdf6+/-* (B, arrow), and *Bmp4-lacZ/+* (C, arrow) single heterozygotes have normal coronal sutures, the *Bmp4-lacZ/+; Gdf6+/-* mouse (E) has complete fusion of only the coronal suture, like the *Gdf6-/-* mouse (D).

Table 3.1. Analysis of suture fusion in the *Bmp4-lacZ/+* by *Gdf6+/-* cross

Gdf6+/- x Bmp4-lacZ/+ cross		
Genotype	Total no. analyzed	Total with suture fusion
Wild-type	24	0
Gdf6+/-	31	0
Bmp4-lacZ/+	41	0
Gdf6+/-; Bmp4-lacZ/+	28	26

observed in the wild-type (n=24), *Gdf6*+/- (n=41), or *Bmp4-lacZ*/+ (n=31) mice (Table 3.1).

Determining the timing of fusion in the Bmp4/Gdf6 *compound heterozygote embryo*

There are two steps to producing a stable, functioning suture; the formation of the suture structure and the maintenance of an existing suture. Although the CS is fused by day P21 in the *Bmp4-lacZ/+; Gdf6*+/- mice, we wanted to determine if *Bmp4* and *Gdf6* were operating in the same steps of suture formation by establishing the timing of fusion in the *Bmp4-lacZ/+; Gdf6*+/- embryos compared the *Gdf6*-/- embryos.

As discussed in Chapter II, fusion of the CS in the *Gdf6*-/- embryo occurs prior to the onset of ossification of the cranial bones at E14.5 (Fig 2.2 E-H). Embryos from a *Gdf6*+/- by *Bmp4-lacZ/+; Gdf6*+/- cross were collected at increasingly early timepoints, stained with alizarin red, and assessed for fusion of the CS. The analysis of suture fusion is summarized in Table 3.2. At E18.5, the frontal and parietal bones overlap, with the frontal bone underlying the parietal bone, highlighting the location of the suture (Fig 3.3A, arrow). The *Bmp4-lacZ*/+ (Fig 3.3B) and *Gdf6*+/- (Fig 3.3C) embryos have normal CSs compared to wild-type (Fig 3.3A).

At E18.5, we observed varying phenotypes in the *Bmp4-lacZ/+; Gdf6*+/- embryos. In half of the embryos collected of this genotype (5/10), there was complete fusion of the frontal and parietal bones (Fig 3.3E), with a seamless surface between the two bones, as seen previously in the *Gdf6*-/- embryos. However in some embryos, although the suture is fused, the morphological remnants of a CS structure can still be seen (Fig 3.3D, yellow arrow). Although evidence of a remnant suture was never

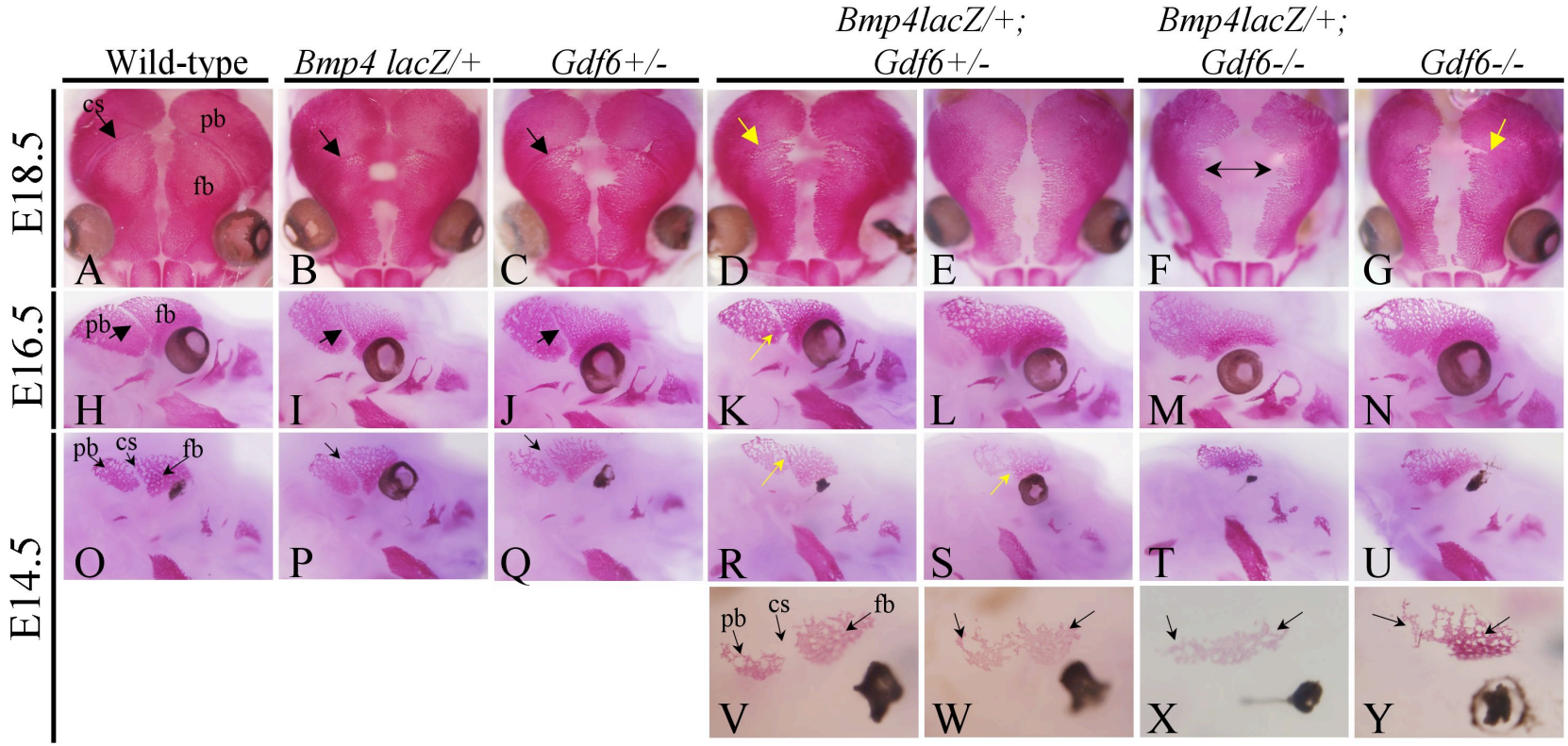
Wild-type
Bmp4 lacZ/+
Gdf6+/-
Bmp4lacZ/+; Gdf6+/-
Bmp4lacZ/+; Gdf6-/-
Gdf6-/-
E18.5
E16.5
E14.5
cs
pb
fb
A
B
C
D
E
F
G
H
I
J
K
L
M
N
O
P
Q
R
S
T
U
V
W
X
Y

Figure 3.3. Analysis of the timing of suture fusion in Bmp4-lacZ/+; Gdf6+/- compound mutants. Embryos were collected at E18.5 (A-G), E16.5 (H-N), and early (V-Y) and late (O-U) stage E14.5. At E18.5, wild-type (A, arrow), *Bmp4-lacZ/+* (B, arrow), and *Gdf6 +/-* (C, arrow) have normal coronal sutures. In the *Bmp4-lacZ/+; Gdf6+/-* embryos, there were mixed phenotypes. Some embryos had complete fusion of the coronal suture (E), while others had remnants of a previously existing suture (D). Remnants of the suture were also visible in *Gdf6-/-* embryos, suggesting an effect of the mixed genetic background. The *Bmp4-lacZ/+; Gdf6-/-* embryos also had a fused coronal suture, but also the added phenotype of a large frontal foramen (F, double arrow). A reduced frontal bone was also seen at earlier timepoints (M, T, X). At E16.5, mixed results were again seen in the *Bmp4-lacZ/+; Gdf6+/-,* with 3/3 embryos having a completely fused suture on one side (L) and the other side had evidence of early fusion (K, yellow arrow). Panels K and L of Figure 3.3 are taken from each side of the same embryo. In the *Bmp4-lacZ/+; Gdf6+/-* embryos at E14.5 the frontal and parietal ossification centers are distinct, but show evidence of beginning-stage fusion (S) or a ridge between the two bones (R). This differs from the *Gdf6-/-* (U) and *Bmp4-lacZ/+; Gdf6-/-* (T) embryos which have a smooth surface between the two bones. The asymmetrical fusion is also been as the very earliest stages of E14.5, when the bone centers first appear (V,W).

Table 3.2. Analysis of suture fusion in the *Bmp4-lacZ/+* by *Bmp4-lacZ/+; Gdf6-/-* cross

Gdf6+/- x Bmp4-lacZ/+;Gdf6+/- cross (Fused Suture/Total)										
	Wild-type	*Bmp4-lacZ/+*	*Gdf6+/-*	*Bmp4-lacZ/+; Gdf6+/-*			*Bmp4-lacZ/+; Gdf6-/-*	*Gdf6-/-*		
					Remnants	Partial			Remnants	Partial
E18.5	0/5	0/6	0/2	10/10	5	0	3/3	2/2	1	0
E16.5	0/5	0/2	0/4	3/3	1	1	3/3	1/1	0	0
E14.5 (late)	0/3	0/7	0/7	2/3	1	1	11	6/6	0	0
E14.5 (early)	0/3	0/3	0/2	1/1	1	0	2/2	2/2	0	0

observed in our *Gdf6*+/- by *Gdf6*+/- crosses discussed in Chapter II, it was very rarely observed in the *Gdf6*-/- embryos (Fig 3.3G, yellow arrow) collected from the *Gdf6*+/- by *Bmp4-lacZ*/+; *Gdf6*+/- crosses, but only at P21. This perhaps suggests an affect of the genetic background, as the original *Gdf6*+/-; *Gdf6*+/- crosses were all performed on a C57BL/6J background, while the *Gdf6*+/- by *Bmp4-lacZ*/+; *Gdf6*+/- crosses were a mixed C57BL/6J and CD1 background.

Not surprisingly, the *Bmp4-lacZ*/+; *Gdf6*-/- embryos had complete fusion of the CS (Fig 3.3F), with no evidence of a remnant suture. However, these embryos presented with persistence of large frontal foramina (Fig 3.3F, double arrow), which was not seen in the *Bmp4-lacZ*/+; *Gdf6*+/- and *Gdf6*-/- embryos. The foramen is the widest at the point where the CS should reside. A reduced size of the fused frontal-parietal bone was also noted at E14.5 in the *Bmp4-lacZ*/+; *Gdf6*-/- embryos compared to all the other genotypes (Fig 3.3 T,X). It is especially noticeable at E16.5, where the anterior frontal portion of the fused bone is smaller compared to the posterior parietal portion (Fig 3.3M). The delay in ossification of the frontal and parietal bones (particularly the frontal bone) producing the large frontal foramina at E18.5 likely starts very early in development. This would be consistent with the early expression of *Gdf6* and *Bmp4* in the E10.5-E12.5 frontal bone primordia, prior to the initiation of ossification. This is the first evidence that *Gdf6* and *Bmp4* may also play a role in ossification of the frontal bone along with the parietal bone and the formation of the suture.

Timepoint E16.5 was very similar to E18.5, with CS clearly observed in wild-type (Fig 3.3H), *Bmp4-lacZ*/+ (Fig 3.3I), and *Gdf6*+/- (Fig 3.3J) embryos. At this timepoint complete fusion of the CS was observed in the *Bmp4-lacZ*/+; *Gdf6*-/- embryos (Fig

3.3M), just like the *Gdf6-/-* embryo (Fig 3.3N). Again, like the CS at E18.5, mixed results were observed in the *Bmp4-lacZ/+; Gdf6+/-* compound heterozygotes. 3/3 embryos of the *Bmp4-lacZ/+; Gdf6+/-* genotype all had suture fusion delayed on one side. In this case, the left side had complete fusion of the frontal and parietal bones (Fig 3.3L), while the right side had a clear existing CS, with some evidence of fusion at the most lateral aspects of the suture (Fig 3.3K, yellow arrow). In 2/3 *Bmp4-lacZ/+; Gdf6+/-* embryos fusion was delayed in the right side, and in 1/3 fusion was delayed on the left side (not shown). This delay might explain why remnants of the suture may persist until E18.5.

The ossification centers for the frontal and parietal bones are first observed on E14.5. However, there are often slight variations in the degree of ossification even between embryos within the same litter. When we collected multiple litters of embryos at E14.5, in some cases ossification had progressed to where the CS was readily visible (Fig 3.3 O-U) and in other embryos the ossification centers for the frontal and parietal bones had just begun to form (Fig 3.3V-Y). When comparing the degree of ossification of the cranial bones to that in other skeletal elements, such as the mandible, it is clear that these are distinct developmental stages that we could use to further define the timing of suture fusion. In the advanced ossification of E14.5 embryos, the *Bmp4-lacZ/+; Gdf6+/-* embryos do show evidence of CS fusion. This fusion appears to begin at the earliest stages (Fig 3.3S, yellow arrow), where the bones are beginning to fuse at their most lateral aspects, but the frontal and parietal bones are still distinguishable as individual elements. In some cases the CS is completely fused, but a ridge is observed at the site of fusion that marks the boundary between the two bones (Fig 3.3R, yellow arrow). The

existence of a ridge between the bones suggests that a suture initially formed, followed by fusion of the two bones. This clearly differs from the fusion in the *Gdf6-/-* embryo (Fig 3.3U) and *Bmp4-lacZ/+; Gdf6-/-* embryo (Fig 3.3T) where there is a continuous surface between the two bones and no evidence of suture.

By looking embryos collected at E14.5, but were developmentally slightly delayed based on the cranial ossification sequence, in which the bones centers first appear, the same observations are seen, with one side forming a normal CS at least initially (Fig 3.3V) and the other side the ossification centers never appearing as separate frontal and parietal bone elements (Fig 3.3W). As discussed in Chapter II, this contrasts with the phenotype of the *Gdf6-/-* (Fig 3.3Y) and *Bmp4-lacZ/+; Gdf6-/-* (Fig 3.3X) E14.5 embryos, where the ossification centers are never seen as distinct structures. Although the suture is completely fused by P21, it is difficult to determine the precise timepoint when the suture in the *Bmp4-lacZ/+; Gdf6+/-* compound mutant can first be defined as fused due to variability in timing of suture fusion within this genotype. However, like the *Gdf6-/-* suture, evidence of ossification through the suture space is sometimes evident even at the earliest stage of cranial ossification (e.g. Fig 3.3W).

Differentiation of the suture mesenchyme is delayed in Bmp4/Gdf6 *compound mutant embryos compared to* Gdf6-/- *embryo*

In the *Gdf6-/-* embryo, failure of suture formation is evident even prior to the onset of ossification since we observed from E12.5 to E14.5 increased activity of alkaline phosphatase (ALP) and *Runx2*, both early markers for osteoblasts differentiation; namely, these markers are expressed continuously in the frontal bone, through the region where the CS should form, and into the parietal bone (Fig 2.5C,F). The *Gdf6+/-* embryo is

characterized by increased ALP activity within the suture and reduced distance between the frontal and parietal bone primordia (Fig 2.5B). Although this increase in ALP activity does not reach a threshold in the *Gdf6+/-* embryo required for suture fusion, it does demonstrate a dosage effect, where the *Gdf6+/-* phenotype is intermediate between the *Gdf6-/-* and wild-type suture.

Similar results were found in a *Gdf6+/-* by *Bmp4-lacZ/+; Gdf6+/-* cross. At E14.5, the wild-type suture is evident as a space between the ALP-stained frontal and parietal bone rudiments, with a bridge of light ALP staining spanning the suture (Fig 3.4B). The phenotype in the *Bmp4-lacZ/+* suture (Fig 3.4D) was similar to the *Gdf6+/-* suture (Fig 3.4C), with increased ALP activity within the suture mesenchyme. As previously shown in the Chapter II, in the *Gdf6-/-* embryo, there is continuous strong expression of ALP from the frontal to the parietal bone through where the suture "should" reside (Fig 3.4E). However, the *Bmp4-lacZ/+; Gdf6+/-* suture was yet a further intermediate phenotype between *Gdf6+/-* and *Bmp4-lacZ/+* single heterozygotes and the *Gdf6-/-* suture, with a clearly reduced distance between the frontal and parietal bone fronts and strong ALP activity through the suture (Fig 3.4F). However, unlike *Gdf6-/-* embryos (Fig 3.4E), the individual bony condensations could still be distinguished from the suture mesenchyme in the *Bmp4-lacZ/+; Gdf6+/-* compound heterozygotes. Since the CS eventually fuses in *Bmp4-lacZ/+; Gdf6+/-* mice, the threshold for increased differentiation within the suture mesenchyme that leads to a fused suture must reside at a level between the single heterozygote and compound heterozygote phenotypes.

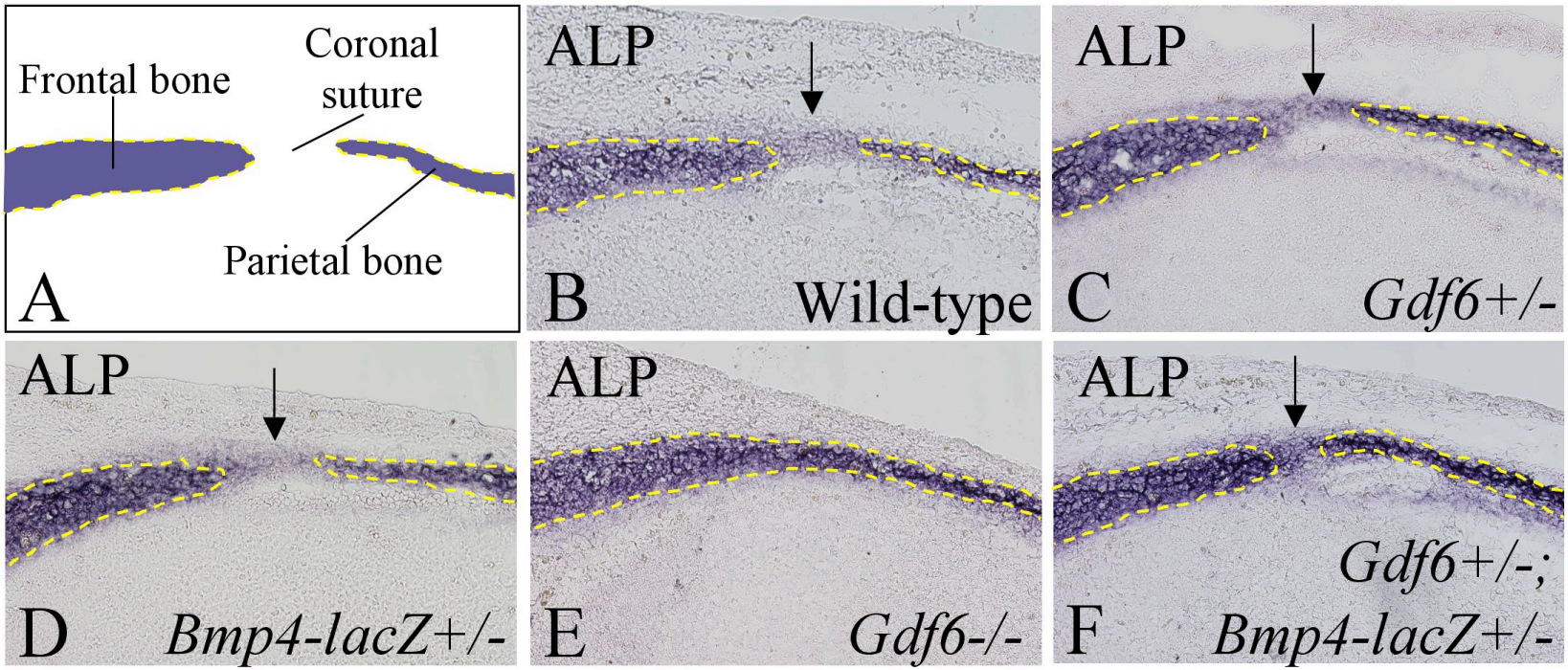

Figure 3.4. ALP activity in the coronal suture mesenchyme. In the wild-type E14.5 embryo, the coronal suture is evident as the space between the *ALP* labeled frontal and parietal bone primordia (B, arrow). In the *Gdf6*+/- (C, arrow) and *Bmp4-lacZ*/+ (D, arrow) single heterozygotes have slightly increased ALP activity within the suture mesenchyme. In the *Gdf6*-/- (E) there is continual strong ALP activity from the frontal and parietal bone primordia through the suture mesenchyme, making the two bones indistinguishable. The *Bmp4-lacZ*/+; *Gdf6*+/- suture (F, arrow) is a further intermediate phenotype between the *Gdf6*-/- (E) and the single heterozygotes (C,D) with reduced distance between the frontal and parietal bone primordia and strong ALP activity in the suture mesenchyme. Unlike the *Gdf6*-/- (E), the frontal and parietal bones are still distinguishable from the suture space.

Expression of Gdf6 *and* Bmp4 *in the compound mutants*

Chapter II described the autoregulation of *Gdf6* in the frontal bone primordia, with increased production of transcript in the *Gdf6-/-* embryo compared to wild-type embryos, with intermediate levels in the *Gdf6-/-* embryo *(*Fig 2.6). It has been previously reported the *Bmp4* is also autoregulated and regulated by other members of the BMP family, including Bmp2 and Bmp6 (Pereira et al., 2000). Because of their overlapping expression, it is possible that Gdf6 and Bmp4 could regulate each others' expression as well. To determine if *Gdf6* expression in the frontal bone primordia was also altered by the haploinsufficiency of *Bmp4*, E10.5 embryos from a *Gdf6+/-* by *Bmp4-lacZ/+* cross were analyzed through *in situ* hybridization for *Gdf6*. In wild-type embryos, the same triangle of *Gdf6* expression in the frontal bone primordia was observed as in previous *in situs* (Fig 2.6, Fig 3.5A, arrow). Quantitatively, the *in situ* signal for *Gdf6* expression in *Gdf6+/-* and *Bmp4-lacZ/+* single heterozygote embryos did not seem significantly increased compared to wild-type, although the domain expression was more defined, with an extension of the anterior border well past the borders of the eye (Fig 3.4 B,C, arrows).

Compared to the single heterozygotes, expression in the *Bmp4-lacZ/+; Gdf6+/-* compound mutant embryos was in a domain that was shorter in length (to the border of the eye) and broader in height, with less defined borders (Fig 3.4D, arrow). There also appears to be increased transcript in the *Bmp4-lacZ/+; Gdf6+/-* compound mutants compared to the single heterozygotes (B,C) and wild-type embryo (A).

To determine if *Bmp4* expression changes the haploinsufficiency of *Gdf6*, expression of *Bmp4* was examined using the lacZ reporter transgene in *Bmp4-lacZ/+* single heterozygotes and *Bmp4-lacZ/+; Gdf6+/-* compound mutants. However, no

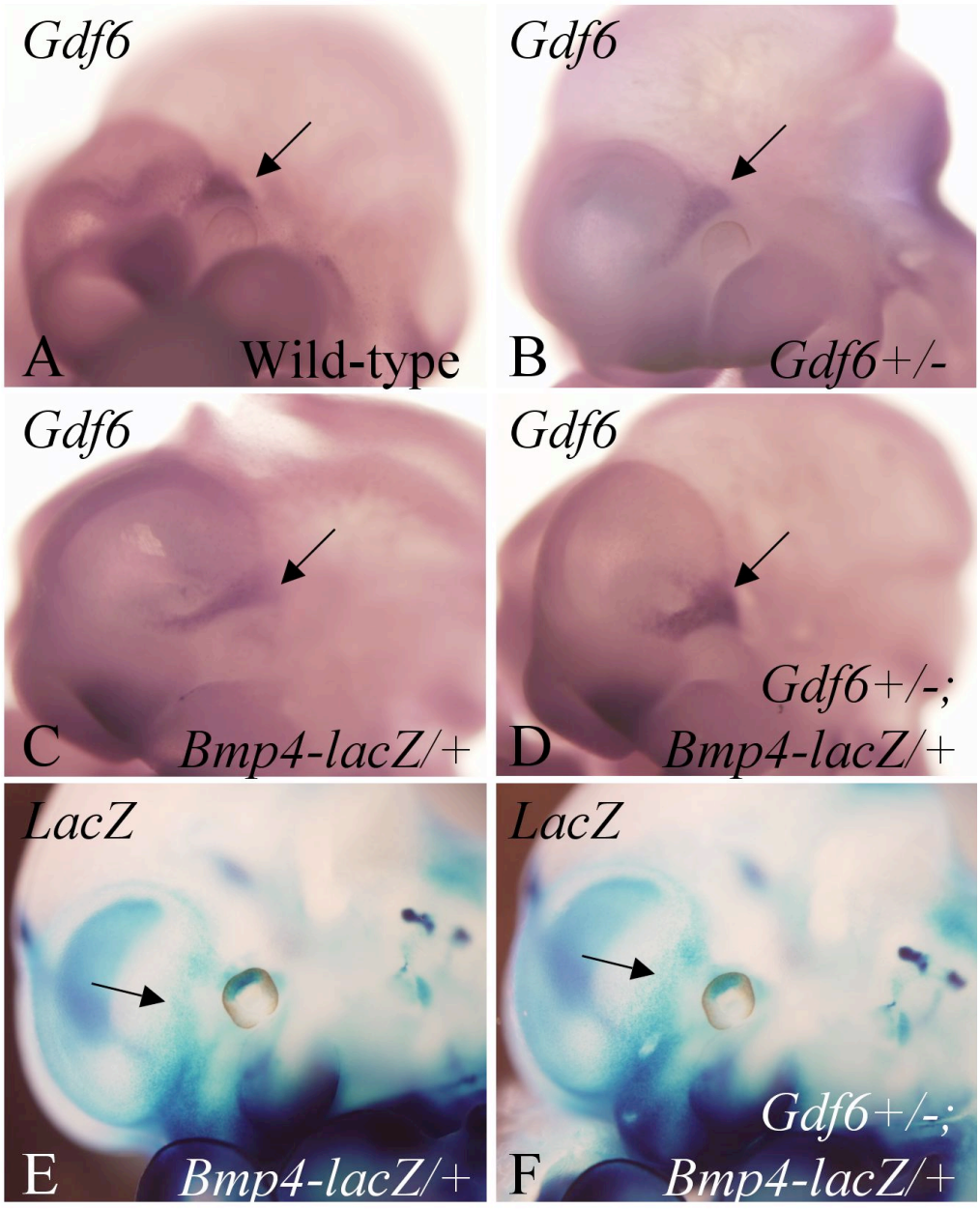

Figure 3.5. Expression of *Gdf6* and *Bmp4* in single and compound heterozygotes. (A-D) *Gdf6 in situ* hybridization on E10.5 embryos from a *Bmp4-lacZ*/+ by *Gdf6*+/- cross. *Gdf6* is expressed in the frontal bone primordia in wild-type embryos (A, arrow). This region is expanded ventrally in the *Gdf6*+/- (B, arrow) and *Bmp4-lacZ*/+ (C, arrow) embryos. In the *Bmp4-lacZ*/+*; Gdf6*+/- embryos the expression of *Gdf6* in the frontal bone primordia is shorter and broader with irregular borders (D, arrow) with increased level of transcript. (E-F) Expression of *Bmp4* by the *lacZ* transgene in E11.5 *Bmp4-lacZ*/+ (E, arrow) and *Bmp4-lacZ*/+*; Gdf6*+/- (F, arrow) embryos reveals no obvious differences in *Bmp4* expression in the frontal bone primordia.

changes in the domain of *Bmp4* expression were detected between *Bmp4-lacZ/+* (Fig 3.5E) and *Bmp4-lacZ/+;Gdf6+/-* embryos (Fig 3.5F). Together, this data does not provide conclusive evidence that Bmp4 or Gdf6 have the ability to regulate each other's expression at the transcriptional level.

Examination of Bmp4 *expression in the* Gdf6 *suture*

Although no changes were seen in whole-mount *Bmp4-lacZ* expression at E11.5 between *Bmp4-lacZ/+* single heterozygotes and *Bmp4-lacZ/+; Gdf6+-* compound mutants (Fig 3.5E,F), we also examined for subtle changes in *Bmp4-lacZ* expression at the suture level at E14.5, the timepoint when fusion of the frontal and parietal bone ossification centers is first visible through alizarin red staining. Embryos were collected from a *Gdf6+/-* by *Bmp4-lacZ/+; Gdf6+/-* cross and stained for lacZ to highlight sites of *Bmp4* expression. Sections were further stained for ALP activity to highlight the location of the bones and suture. In the E14.5 wild-type embryo, *Bmp4* is expressed in the frontal bone primordia, the underlying dura mater, and in the periosteum on the ectocranial side of the frontal bone (Fig 3.6A). The periosteal expression in the wild-type embryo appears to end within the suture mesenchyme (Fig 3.6A, arrow). In the *Gdf6+/-* suture, *Bmp4* is still expressed in the frontal bone, but the periosteal expression is retracted (Fig 3.6B, arrow) so it does not reach the suture mesenchyme. In the *Gdf6-/-* embryo, mixed results were found. In some embryos, no lacZ expression was detected in the frontal bones and the periosteal expression ended where the nasal bones end and frontal bones begin (not shown). In other embryos, expression of *Bmp4* was similar to expression in the wild-type and *Gdf6+/-* embryos and simply ended at the point where the frontal bone

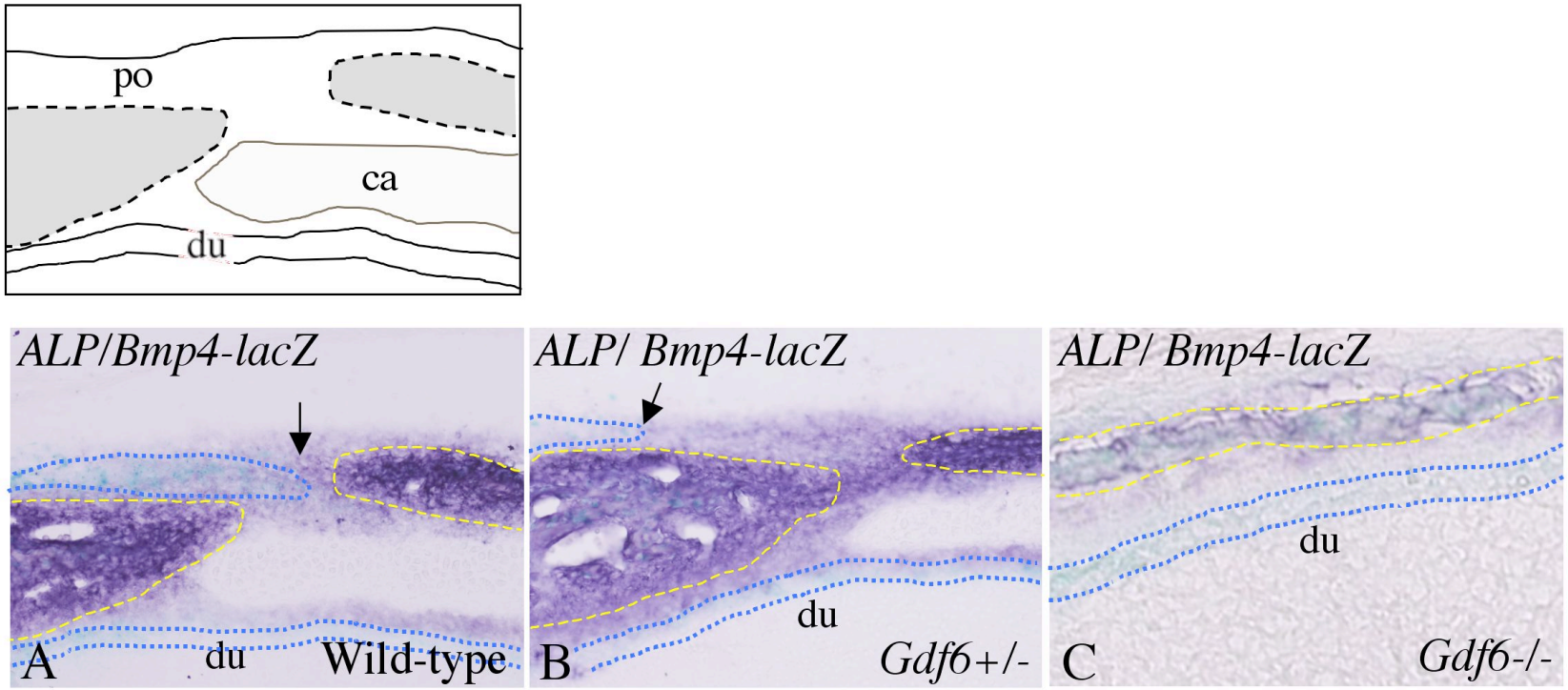

Figure 3.6. Expression of *Bmp4* in the *Gdf6* mutant suture. Embryos were collected from a *Gdf6+/-* by *Bmp4-lacZ/+; Gdf6+/-* cross and stained for *lacZ* to highlight sites of *Bmp4* expression and *ALP* to locate the suture. A) In the wild-type embryo, *Bmp4* is expressed in the frontal bone primordia, dura mater (lower blue line), and ectocranial periosteum (upper blue line), and ends in the suture mesenchyme (arrow). B) In the *Gdf6+/-* suture the periosteal expression is retracted (arrow) so it does not reach the suture mesenchyme. C) In some *Gdf6-/- embryos*, *Bmp4* expression continues from the frontal bone, through the site of the suture fusion, into the parietal bone. Yellow lines outline the bony condensations of the frontal and parietal bones.

fused to the parietal (not shown). And furthermore, in some *Gdf6-/-* sutures the *Bmp4* expression continues from the frontal bone, across the site of suture fusion into the parietal bone, and therefore was expressed in the entirety of the fused bone (Fig 3.6C). Although it appears that normal *Bmp4* expression is altered in the suture region of *Gdf6+/-* and *Gdf6-/-* embryos, it is difficult to draw conclusions about the mechanistic repercussions of such changes in expression due to the mixed results of *Bmp4* expression in the *Gdf6* homozygous mutant embryos.

Discussion

Cooperative function of Bmp4 *and* Gdf6 *in coronal suture development*

In this study we found evidence that *Gdf6* and *Bmp4* function together in the earliest stages of CS formation. Both *Gdf6* and *Bmp4* are co-expressed in the frontal bone primordia from E10.5-E12.5, several days prior to the onset of ossification. This corresponds to the timepoint when the suture mesenchyme loses its undifferentiated state in the *Gdf6-/-* embryo. Furthermore, the haploinsufficiency of both genes leads to complete craniosynostosis of the CS.

Increased differentiation of the suture mesenchyme is evident at E14.5 in the *Bmp4-lacZ/+; Gdf6+/-* compound mutant (Fig 3.4F) as an intermediate phenotype between the *Gdf6-/-* embryos (Fig 3.4E) and *Gdf6+/-* and *Bmp4-lacZ/+* single heterozygotes (Fig 3.4C-D), suggesting a slight delay in suture fusion in the compound mutants. This delay was also evident in alizarin red staining of embryos at several points in development, with partially fused sutures (Fig 3.3K,S), unilateral fusion of one side

(Fig 3.3K,L), or remnants of a previously existing suture (Fig 3.3D,R). This leads to the question: why is fusion delayed in the *Bmp4-lacZ/+; Gdf6* compound mutants if *Bmp4* and *Gdf6* are functioning at the same timepoints in the same processes?

One possibility is that while *Gdf6* functions primarily in the very early stages of suture formation, *Bmp4* cooperatively functions with *Gdf6* to form the suture by inhibiting osteogenic differentiation of the suture mesenchyme, but also plays a later role in development separate from *Gdf6* in the maintenance of the suture. This would explain why evidence of suture fusion and suture mesenchyme differentiation are evident at the early stages, and although they are not as severe as the complete fusion seen in the *Gdf6-/-* mice; the additional failure to maintain the suture ultimately leads to craniosynostosis. In addition to the expression we observed of *Bmp4* in the frontal bone primordia, *Bmp4* is also expressed in the periosteum, frontal bone, suture mesenchyme, and dura at E14.5, when *Gdf6* expression is undetectable in the suture region (Fig 3.6). Other publications have described *Bmp4* expression throughout embryonic development to E18.5 in the osteogenic fronts (Kim et al., 1998b). The expression of *Bmp4* in the dura is of note due to the importance of the dura in osteogenesis and suture maintenance. Some studies have suggested that the suture mesenchyme does not provide autocrine signals that help keep the suture in an undifferentiated state, but instead remains "primed" to receive signals from the surrounding tissues, including the dura mater, that serve this function. For example, the posterior interfrontal suture, which normally fuses in mice postnatally, only expressed osteoid markers when cultured together with the adjacent underlying dura mater. When suture mesenchymal cells were grown separate from the dura mater, gene

expression analysis was identical to the sagittal suture mesenchyme, which remains patent for the lifespan of the animal (Spector et al., 2000).

The delay in suture fusion in the *Bmp4/Gdf6* compound mutants might also be attributed to a more critical role of *Gdf6* in suture formation than *Bmp4*. Bmp4 and Gdf6 due use the same BMP receptors (Bmpr1a, Bmpr1b, BmprII, and AcvrIIa), however, the affinity for Bmp4 and Gdf6 for the receptors has not been compared. One study did compare affinities closely related family members Bmp2 and Gdf5 and found that Gdf5 had a higher affinity with the Bmpr1b receptor than Gdf5 (Heinecke et al., 2009). Considering that Gdf5 and Gdf6 likely have similar properties, perhaps if Bmpr1b was the predominant receptors in the suture region, this could explain why Gdf6 appears to be more required than Bmp4. Since *Bmp4* expression in the frontal bone primordia was assayed using the *Bmp4-lacZ* line, and direct comparison between the expression levels of *Bmp4* and *Gdf6* was not performed. Alternatively, perhaps *Bmp4* is expressed at lower levels than *Gdf6* in the frontal bone primordia.

Although suture differentiation in the *Bmp4/Gdf6* compound mutants reaches the threshold to produce suture fusion, enough undifferentiated suture mesenchymal cells remain to allow the suture to persist past the timing of suture fusion in the more severe *Gdf6-/-* case. This hypothesis is outlined in Figure 3.7. Both *Gdf6* and *Bmp4* are expressed in the frontal bone, providing a paracrine signal to the suture mesenchyme to inhibit osteogenic differentiation (Fig 3.7A). In the *Bmp4/Gdf6* compound mutant, the inhibitory signal is reduced, allowing for increased suture mesenchyme differentiation (Fig 3.7B). However, in the *Bmp4-lacZ/+; Gdf6-/-* suture, the inhibitory signal is

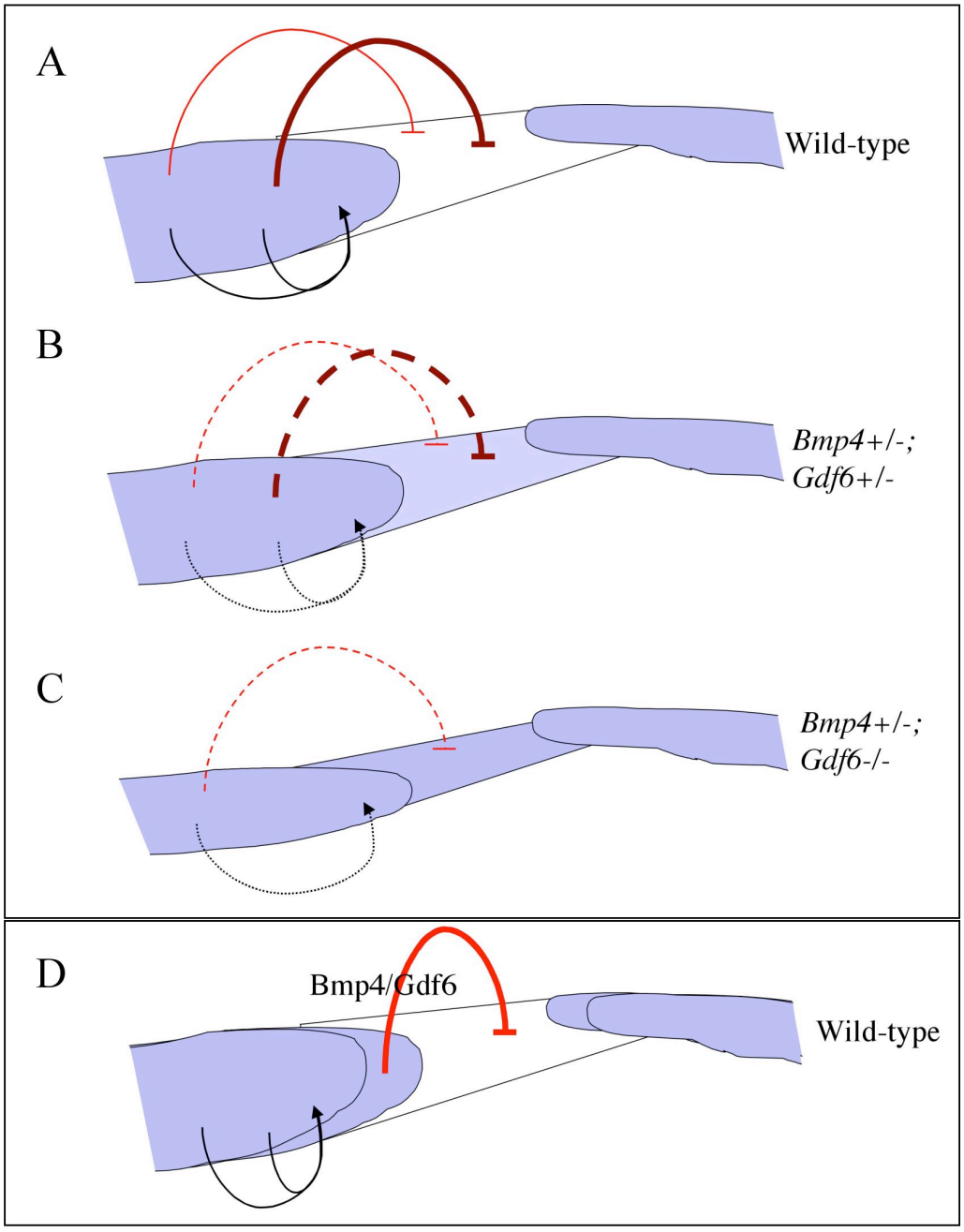
A
Wild-type
B
Bmp4+/-;
Gdf6+/-
C
Bmp4+/-;
Gdf6-/-
D
Bmp4/Gdf6
Wild-type

Figure 3.7. Model of *Bmp4* and *Gdf6* function in suture development. A) In wild-type embryos, *Bmp4* (light red) and *Gdf6* (dark red) expression in the frontal bone provides a paracrine signal to the suture mesenchyme to inhibit osteogenic differentiation. Because the phenotype of the *Gdf6-/-* is more severe than the *Bmp4/Gdf6* compound heterozygote, it seems that the *Gdf6* signal is more required than *Bmp4*. *Bmp4* and *Gdf6* also signal to the parietal bone primordia to promote proliferation and differentiation. B) In the*Bmp4/Gdf6* compound heterozygote, the inhibitory signal is reduced, increasing the differentiation of the suture mesenchyme to produce suture fusion, but allows the suture to persist longer than the *Gdf6-/-* embryo. C) In the *Bmp4-lacZ/+; Gdf6-/-* embryo, the inhibitory signal is reduced to so that the suture mesenchyme is immediately differentiated. The stimulatory effect of *Bmp4* and *Gdf6* in the frontal bone primordia is also reduced, resulting in the frontal bone foramina. D) Possible mechanism involving Bmp4/Gdf6 heterodimers. Bmp4/Gdf6 heterodimers in the frontal bone fronts provide a paracrine signal to inhibit differentiation of the suture mesenchyme. Bmp4 and Gdf6 homodimers in the frontal bone have a separate function, to promote proliferation of the frontal bone. In the case of reduction or elimination and Bmp4 and/or Gdf6, the heterodimers are reduced or eliminated, leading to differentiation of the suture mesenchyme. However, in the frontal bone, Bmp4 and Gdf6 can compensate for one another, so a bone defect is only seen with extreme reduction of the combined signal, as in the *Bmp4-lacZ/+; Gdf6-/-* embryos.

reduced to such a great extent that suture mesenchyme differentiation occurs rapidly and completely, hence there is never evidence of an existing suture space.

Due to the co-expression of *Gdf6* and *Bmp4* in the frontal bone primordia at E10.5-E12.5 (Fig 3.1) and the similarity in the ectopic suture mesenchyme differentiation between the *Gdf6*+/- and *Bmp4-lacZ*/+ embryos (Fig 3.4 C,D), it is likely that *Gdf6* and *Bmp4* are operating at the same timepoints in suture development. There are several possible explanations for the differences, albeit inconsistent, seen in *Bmp4* expression in *Gdf6-/-* mice. One possibility is that it could be a secondary result of morphological changes in the suture. Without the structure of the suture, the boundary between the frontal and parietal bone is indistinguishable, and therefore signals, which normally delineate the boundary, are likely also disrupted. Reduced *Bmp4* expression in the periosteum could result from the elimination of signals which usually emanate from the suture mesenchyme.

It is also possible that *Bmp4* or *Gdf6* does not directly play a role in suture development, but instead one could be involved in the regulation of the other (or another BMP). For example, if Bmp4 normally induces the expression of *Gdf6*, the loss of Bmp4 would reduce levels of *Gdf6*, which are already reduced due to haploinsufficiency in the *Bmp4/Gdf6* compound mutants. This would produce a phenotype similar to the *Gdf6-/-* mouse without Bmp4 having a direct affect on the suture. The same could be said if Gdf6 regulated *Bmp4* expression.

However, we found no conclusive evidence that Bmp4 or Gdf6 regulate each other's expression. When we compared *Gdf6* expression in the *Bmp4/Gdf6* compound mutant, it is possible the difference in the area occupied by *Gdf6* expression (Fig 3.5)

could contribute to the suture phenotype, where *Gdf6* is being ectopically expressed beyond the frontal bone primordia or the morphology of the frontal bone primordia itself has been altered. However, this could also be a secondary effect from an overall morphological change in the cranial region. For example, changes in eye development in the compound heterozygotes (discussed in detail in Chapter IV) could impact craniofacial morphology and the shape of the frontal bone primordia. The examination of *Bmp4* expression in *Gdf6-/-* mice failed to produce consistent results. Again, this could be due to strain background effects. The *Bmp4/Gdf6* compound mutants were generated on a mixed C57Bl/6J and CD1 genetic background, and therefore the presence of modifier in genes within the *Bmp4* and *Gdf6* pathways may alter the suture phenotype.

Additional experiment could be done to further explore the *Bmp4/Gdf6* interaction. For example, a conditional deletion of *Bmp4* using *Wnt1-Cre* and a floxed allele of *Bmp4* would eliminate *Bmp4* expression in the neural crest, including the frontal bone primordia. In addition, using the bead implantation methodology discussed in Chapter II, beads soaked in Bmp4 protein could be implanted into the suture region. In both these cases, possible changes in the expression of *Gdf6* could be examined through *in situ* hybridization.

Role of homodimers and heterodimers in suture development

The mechanism for *Gdf6/Bmp4* interaction may be more complicated then a simple additive model of signaling activity. The role of molecular heterodimers in the formation of the CS is a new area of investigation. Haploinsufficiency of *TWIST1* is associated with Saethre-Chotzen syndrome, characterized by coronal craniosynostosis.

Twist1 forms both homodimers and heterodimers with E2A E-proteins. The ratio of Twist1 homodimers to heterodimers is control by the helix-loop-helix transcription factor inhibitor Id proteins, which are induced by BMP signaling (Rice et al., 2005). The Id proteins, localized to the bone fronts, competes with Twist1 in dimerization with E proteins, forcing the formation of homodimers. In the suture mesenchyme where there is no Id protein, Twist1 can heterodimerize with E proteins. These dimers activate different sets of genes; the homodimers activate FGFR2, promoting differentiation, where the heterodimers induce TSP-1, which is involved in the maintenance of suture patency. In *Twist1+/-* mice, the ratio of homodimers to heterodimers is altered with increased homodimers in the bone fronts, extending the bone fronts in the suture mesenchyme and leading to synostosis of the suture (Connerney et al., 2006).

BMPs can form heterodimers, but only when they are expressed in the same cells, as dimerization proceeds secretion (Chang and Hemmati-Brivanlou, 1999). Gdf6 was able to heterodimerize with Bmp2 in frogs (Chang and Hemmati-Brivanlou, 1999), and given the high homology between Bmp2 and Bmp4, it would not be surprising if Gdf6 also formed heterodimers with Bmp4. In fact, a dominant-negative form of Gdf6 blocked mesodermal and epidermal induction by Bmp4 when co-injected into the same embryos (Chang and Hemmati-Brivanlou, 1999). In some cases, these BMP heterodimers, including Bmp2/Bmp7, have been found to have a more potent effect than homodimers (Xiao, 2007). Bmp4 can also heterodimerize with Bmp7, with significantly increased activity compared to the Bmp4 homodimer (Aono et al., 1995; Hazama et al., 1995). Bmp4 and Bmp7 homodimers alone, and even a mixture of Bmp4 and Bmp7

homodimers together, act as poor inducers of mesoderm. Yet Bmp4/Bmp7 heterodimers act as strong inducers of mesoderm in *Xenopus* embryos (Suzuki et al., 1997).

In many tissues the expression domains of *Bmp2, Bmp4,* and *Bmp7* overlap, however, the homozygous mutant phenotypes are very different (Hogan, 1996). If heterodimers had a unique function separate from the homodimers, you might expect there is be some overlap among the mutant phenotypes. BMP heterodimers have been generated *in vivo*, and it's possible that these could be acting as antagonists by competing with the homodimers for receptor binding (Hogan, 1996).

In the case of *Bmp4* and *Gdf6*, we have found multiple sites in addition to the CS where the phenotype of the compound mutant is more severe than that of each single heterozygote (discussed in Chapter IV). One could hypothesize that *Gdf6* and *Bmp4* do have the ability to form heterodimers, and the function of these heterodimers could be quite different than the function of homodimers. This hypothesis is summarized in Figure 3.7D. For example, it is possible that while Bmp4 and Gdf6 homodimers function primarily in the proliferation of the frontal bone, Bmp4/Gdf6 heterodimers function in the inhibition of the suture mesenchyme or vice versa. Like the case with Twist1 dimer formation, a secondary factor could limit the formation of Bmp4/Gdf6 heterodimers, or at least their diffusion of activity, to the bone fronts, closest in proximity to the suture mesenchyme. This would explain why CS fusion is seen in the *Bmp4/Gdf6* compound mutants, but not the frontal bone defect: in the proliferation of the frontal bone, Bmp4 and Gdf6 can compensate for one another, but both are required for the formation of heterodimers and therefore the inhibition of suture differentiation.

Total and partial fusion of the coronal suture

In the original design to assess suture formation in the *Gdf6/Bmp4* compound mutants, we planned to score the suture phenotype based on severity: the total percentage of the suture that has undergone fusion by P21. This is due to the fact that a coronal craniosynostosis phenotype as complete as that seen in the *Gdf6-/-* embryo is rare, where the frontal and parietal bones are completely fused and there is no evidence of at least partial suture formation. In our *Gdf6-/-* embryos, and liveborn *Gdf6-/-* mice analyzed on a mixed strain background (Settle et al., 2001), penetrance of the craniosynostosis phenotype was 100% (Fig 3.8E). In our *Bmp4-lacZ/+; Gdf6+/-* compound mutants the penetrance was 93% (Figure 3.8E). This is still remarkably high compared to other mouse models, demonstrating the importance of *Gdf6* in suture development. In the case of the *Twist1+/-* mutant, the mechanism for suture fusion is traced back to the formation of the boundary between the neural crest-derived frontal bone and the paraxial mesoderm-derived parietal bone, a boundary that forms around E9.5. Even so, suture fusion is often incomplete, unilateral, and/or not present until postnatal stages (Fig 3.8B) (Merrill et al., 2006). In the case of *EphA4-/-* mice, approximately 25% of the suture is fused and in the *Twist1+/-; EphA4+/-* mice only 50% of the suture was fused (Ting et al., 2009). The fact that in all cases of the *Gdf6-/-* and *Bmp4/Gdf6* compound mutant at P21 the entire length of the suture is fused, speaks to the severity of the defect in these mice. By P21 in the *Bmp4-lacZ/+; Gdf6+/-* compound mutants, the suture is completely fused, with no evidence of a partially fused or remnant suture (Fig 3.2E). Partial fusion is seen in the embryonic stages (Fig 3.3D,K,R), however, we believe that this is distinct

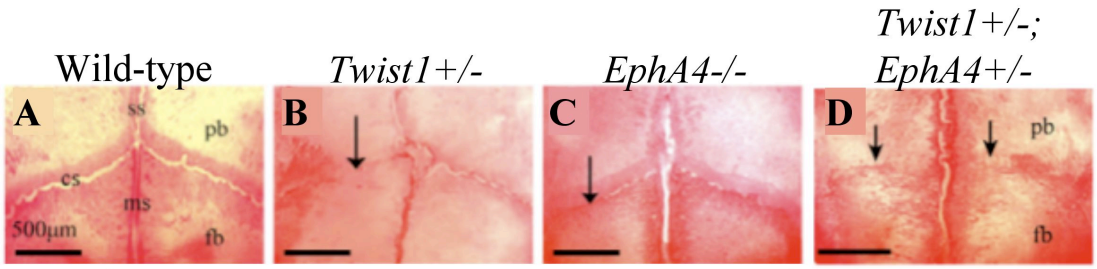

E

Genotype	Penetrance	% Penetrance
EphA4-/-	8/20	40%
Twist1+/-	19/26	73%
Twist1+/-; EphA4+/-	31/33	94%
Gdf6-/-	12/12	100%
Gdf6+/-; Bmp4+/-	26/28	93%

Figure 3.8. Penetrance and severity of the defects in mouse models for craniosynostosis. *Twist1+/-* (B), *EphA4-/-* (C), and *Twist11+/-; EphA4+/-* (D) mice all present with partial or unilateral fusion of the coronal suture. The penetrance in these models ranges from 40-94% (E). This is compared to the *Gdf6-/-* and *Bmp4-lacZ/+; Gdf6+/-* compound mutants which have a 100% and 93% penetrance respectively (E), and also complete fusion of the coronal suture.

Panels A-D adapted from Ting et al 2009.

from the partial fusion observed in other mouse craniosynostosis models. During the initial steps of formation of the suture, the ossification centers meet beginning at the most lateral aspects of the calvaria, and move "zipper-like" up toward the midline, as seen with the lateral regions of the suture being more histologically mature than the medial regions (Rice, 2008). The partial fusions observed in our *Bmp4-lacZ/+; Gdf6+/-* compound mutants were always evident at the most lateral aspects of the suture, with the suture remnants being localized to the medial aspects, next to the sagittal suture (Fig 3.3 D,K,S yellow arrows). This is most likely due to the initiation of fusion moving laterally toward the midline as the suture mesenchyme matures at each site.

However, we did see some remnant suture in the *Gdf6-/-* E18.5 embryos (Fig 3.3G) in our *Gdf6+/-* by *Bmp4-lacZ/+* crosses that were not seen in our *Gdf6+/-* by *Gdf6+/-* crosses. We attributed this to the mixed CD1/C57Bl/6J background of the former cross and the inbred C57Bl/6J background of the later. More specifically, this could be due to strain dependent differences in the genes (e.g. Noggin), which encode proteins that bind and inactivate Bmp4 and/or Gdf6, in the activity of receptors or downstream effectors of BMP signaling, or in the activity of redundant genes (Dunn et al., 1997).

Coronal craniosynostosis in the *Gdf6-/-* embryo and *Bmp4/Gdf6* compound mutant also stands out in the early appearance of the defect. In the *Gdf6-/-* embryo, the defect is apparent by E12.5 with the increased differentiation of the suture mesenchyme. Even in the *Twist1+/-* mouse, no changes in the suture can be detected until E14.5, although ossification through the suture may not be evident until postnatal stages (Merrill

et al., 2006). *Axin2-/-* homozygous mutants have normal sutures at birth and then the process of fusion initiates (Yu et al., 2005).

Additional role for Bmp4 *and* Gdf6 *in frontal bone growth*

Although *Gdf6* is expressed exclusively in the frontal bone primordia, no frontal bone defect is observed in the *Gdf6-/-* embryo at any timepoint. When we measured the size of the frontal and parietal bones in relation to the size of the occipital bone (which is presumably unaffected by changes in *Gdf6*), there was no significant difference between wild-type and *Gdf6-/-* embryos in relation to the size of the frontal ($p=0.77$) or parietal ($p=0.25$) bones, at least at E15.5 when the bones were measured. It is not until one further eliminates a *Bmp4* allele (in the *Bmp4-lacZ/+; Gdf6-/-* embryos) that a frontal bone defect is observed with the persistence of a frontal foramen (Fig 3.3F). This perhaps also demonstrates a cooperative function between *Gdf6* and *Bmp4* in the development of this structure. In Chapter II, we did see a difference between cellular proliferation between the frontal bones of wild-type and heterozygous embryos at E13.5 that trended toward significance ($p=0.056$) (proliferation specifically in the frontal bone of *Gdf6-/-* embryos could not be examined since the boundary between the frontal and parietal bones cannot be distinguished). In addition, beads soaked in Gdf6 protein promoted osteogenic differentiation when implanted into the frontal bone primordia (Fig 2.11B). This suggests that *Gdf6*, and *likely Bmp4*, play a role in the proliferation and differentiation of the embryonic frontal bone. Also of note was a decrease in the size of the interparietal bone in the *Gdf6-/-* embryo compared to wild-type (Fig 2.2 C, D), generating a wider lambdoid suture. This appears to particularly affect the portion of the

interparietal bone that is neural crest derived (Fig 1.3C), suggesting a specific function of Gdf6 on the growth of neural crest-derived cranial bones. A more detailed analysis of the occipital bone defect could be carried out by comparing the width and length of the bone between wild-type and *Gdf6-/-* embryos.

It is interesting to note that several other craniosynostosis-associated genes are not only also expressed in the frontal bone primordia, but also promotes frontal bone osteogenesis. This is the case with *Msx1* and *Msx2*, both of which are expressed in the frontal bone primordia at the same timepoints as *Gdf6* and *Bmp4* (E10.5-E12.5) (Han et al., 2007). Various combinations of single and compound mutants (*Msx1-/-, Msx1-/-; Msx2+/-; Msx1+/-; Msx2-/-*) all result in frontal foramina, while the *Msx1-/-; Msx2-/-* double mutants fail to generate any calvarial bones (Han et al., 2007). The frontal foramina phenotype in the *Msx2* mutants is also made more severe combined with the haploinsufficiency of *Twist1,* another craniosynostosis-associated gene expressed in the frontal bone primordia (Ishii et al., 2003).

Although not yet supported experimentally, it was originally hypothesized that the suture forms in response a growth factor gradient generated by the approximation of the advancing ossification centers. It is possible that CS fusion is a secondary result of the frontal bone defect. A lag in osteogenesis of the frontal bone could alter the position where it approximates the parietal bone, forming the CS. There is also evidence that the position where CS forms is also determined through signals from the dura and coincides with the cellular boundary between the neural-crest derived frontal bone and the paraxial mesoderm parietal bone. Perhaps the meeting of the frontal and parietal bones needs to occur at the position determined by these other factors, and if not, a suture defect would

result. In this case, the suture would fail to form and the mesenchyme undergo differentiation as though it was just part of the expanding bones.

CHAPTER IV

INTERACTIONS BETWEEN GDF6 AND BMP4 IN THE DEVELOPMENT OF MULTIPLE SKELETAL ELEMENTS

Introduction

In the previous chapter we showed that the CS phenotypes of *Bmp4-lacZ/+; Gdf6+/-* compound mutant resembles that of *Gdf6-/-* mice, with complete fusion of the CS (Fig 3.2). *Gdf6* and *Bmp4* are co-expressed in the frontal bone primordia early in cranial development (Fig 3.1). Furthermore, both the *Gdf6-/-* embryo and the *Bmp4/Gdf6* compound mutants show evidence of ossification through the suture at E14.5 (Fig 3.3) and erroneous differentiation of the suture mesenchyme (Fig 3.4). This has led us to conclude that these two BMP family members work cooperatively in the development of the CS.

There is much evidence in literature for BMP family members with cooperative functions in development. Due to the high homology between BMPs, it is likely that in some developmental processes they are able to compensate for one anther. In addition to the CS, other sites where *Gdf6* and *Bmp4* function cooperatively may be elucidated through the thorough examination of the compound mutants. Several phenotypes became apparent in *Gdf5/Gdf6* compound mutants that were not detectable in the *Gdf6-/-* mutant; including reductions and fusions of the phalanges, carpal and tarsal bones, and scoliosis of the spine (Settle et al., 2001). *Gdf5/Bmp5* compound mutants presented with phenotypes which demonstrated both an additive effect on the length of some skeletal structures (e.g. certain long bones) in addition to a synergistic effect in formation of

specific structures (fibula, knee) (Storm and Kingsley, 1996). While *Bmp2/Bmp7* and *Bmp5/Bmp7* compound heterozygotes have no reported abnormal skeletal phenotypes, *Bmp4/Bmp7* compound mutants have defects and abnormalities in the limbs and rib cage. These include misalignment of the ribs, defective ossification of the sternum, a split xiphoid process, and preaxial polydactyl of the limb. All these phenotypes were rarely observed in the single heterozygotes (Katagiri et al., 1998).

The goal of this study was to determine if *Bmp4* and *Gdf6* were cooperating in the formation of structures apart from the CS. To address this question we generated *Bmp4* and *Gdf6* compound mutants and analyzed the mice for skeletal phenotypes. We found that in the *Gdf6/Bmp4* compound mutants there are defects present in the single heterozygotes that are made more severe in the compound mutants and phenotypes that are only present in the compound mutants. Phenotypes in the compound mutants included sternal anomalies, hypoplasia of the pelvis and thyroid cartilage, preaxial polydactyly of the hindlimb, and microphthalmia. These phenotypes demonstrate a genetic interaction between *Bmp4* and *Gdf6* that affects multiple skeletal and non-skeletal structures and various developmental mechanisms.

Materials and Methods

Mouse crosses

Details for the *Gdf6* and *Bmp4* lines are discussed in detail in the methods section of Chapters II and III. The *Gdf6* BAC line (also termed Dβgeo or 125L11) was generated by Doug Mortlock by inserting a cassette containing a internal ribosome entry

site fused to the βgeo gene into the second exon of *Gdf6* in a 129/SvJ mouse BAC (Mortlock et al., 2003).

Additional methods

The following protocols were outlined in previous chapters: DNA preparations and genotyping (Chapters II and III), whole-mount alizarin red skeletal preparations (Chapter III), whole-mount and slide *in situ* hybridization (Chapter II), 3-aminopropyltriethoxysilane treatment of slides (Chapter II), and lacZ staining Chapter III).

Results

Increased presentation of the manubriosternal joint in Bmp4/Gdf6 *compound mutants*

The mouse sternum begins to form around E12 as a pair of mesenchymal condensations that elongate and form a cartilage precursor. The cartilage segments move towards the midline and fuse to form a cartilaginous rod. The rod segments as a result of hypertrophy of the cartilage cells in the intercostal regions and ossifies through the expansion of six ossification centers (Chen, 1952).

The thoracic bones in mice consist of the manubrium, six sternal segments, and the xiphoid cartilage. The manubrium and first sternal segment unite at a site known as the manubriosternal joint (Fig 4.1A, arrow). The manubrium and sternum form from a cartilage precursor, however, like the cranial sutures the manubriosternal joint forms at the interface between two joining ossification centers, one in the manubrium and one in

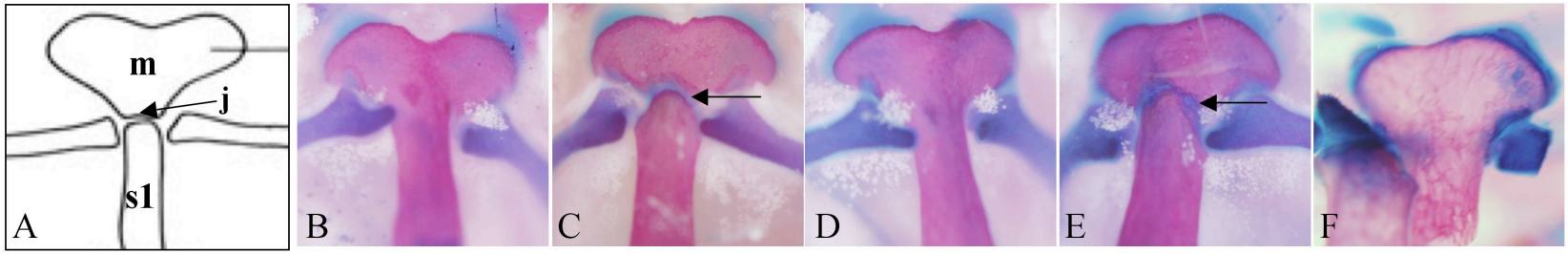

WT	*Bmp4-lacZ/+*	*Gdf6+/-*	*Bmp4-lacZ/+; Gdf6+/-*	*Gdf6-/-*
0/21	6/28 (21%)	0/35	18/30 (60%)	0/2

Figure 4.1. Increased presentation of the manubriosternal joint in *Bmp4/Gdf6* compound mutants. The manubrium and first sternal segment of the sternal body are fused together in wild-type (B) and *Gdf6*+/- (D) mice. In 21% of *Bmp4*+/- mice the manubriosternal joint is present (C). This is increased to 60% in *Bmp4-lacZ/+; Gdf6*+/- mice (D). No manubriosternal joint was present in *Gdf6*-/- mice (F). Panel F was imaged from a mouse collected at a different timepoint and litter from the remaining genotypes due to the perinatal lethality of *Gdf6*-/- mice on the C57BL/6J background, which caused the difference in intensity of alizarin red staining. M, manubrium; s1, first sternal segment; j, manubriosternal joint.

the first sternal segment of the body (Gray and Lewis, 1918). In the *Bmp4*+/- mice the manubriosternal joint was present at P21 in 21% of the animals (6/28) (Fig 4.1C), whereas the manubriosternal joint was never observed in the wild-type (0/21) and *Gdf6*+/- mice (0/35) (Fig 4.1B,D), with the manubrium and the sternum fused into a single bone. The incidence of the manubriosternal joint was increased to 60% in the *Bmp4*+/-;*Gdf6*+/- compound mutant mice (18/30) (Fig 4.1E). The difference in the penetrance of the manubriosternal joint phenotype between the *Bmp4-lacZ*/+ heterozygotes and *Bmp4-lacZ*/+; *Gdf6*+/- compound mutants was statistically significant (p=0.03, Chi-squared test). Although the *Gdf6*-/- allele is perinatal lethal on our C57BL/6J background, in two adult mice collected and saved when the *Gdf6* line was on a mixed background, no manubriosternal joint was observed (Fig 4.1F) (panel F of figure 4.1 was imaged from a mouse collected at a different time and litter from the remaining genotypes due to the perinatal lethality of *Gdf6*-/- mice on the C57BL/6J background, which caused the difference in intensity of alizarin red staining).

Hypoplasia of the ischium and the pubis

Two bones of the lower os coxae, the ischium and the pubis, join together below the large obturator foramen (Fig 4.2I). In wild-type mice at P21, these two bones meet and fuse together (Fig 4.2A, arrow). In *Gdf6*+/- and *Bmp4-lacZ*/+ mice, there is a small gap remaining between the two pelvic bones (Fig 4.2B,C arrows). The width of the gap between the bones is increased in the *Bmp4-lacZ*/+; *Gdf6*+/- compound mutant mice (Fig 4.2D, arrow). The timing and location of *Bmp4* and *Gdf6* expression in the pelvic region is unknown.

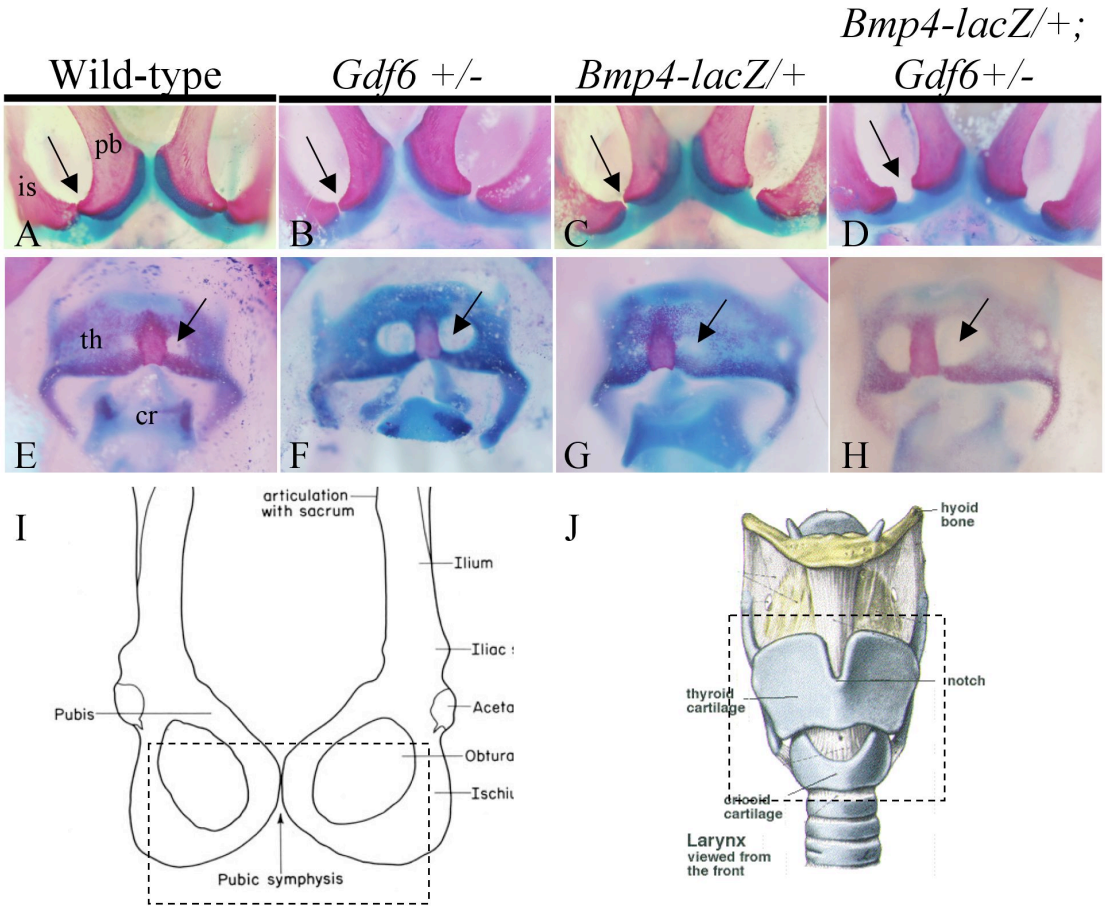

Figure 4.2. Hypoplasia of the pelvic bones and thyroid cartilage. Two bones of the lower os coxae, the ischium and the pubis, join together below the large obturator foramen (I). In wild-type mice, these two bones meet and fuse together (A, arrow). In *Gdf6*+/- (B) and *Bmp4-lacZ*/+ (C) mice, there is a small gap remaining between the two pelvic bones (arrows). The width of the gap is increased in the *Bmp4-lacZ*/+*; Gdf6*+/- mice (D, arrow). The thyroid cartilage is the largest cartilage of the larynx, consisting of two wings fused at the midline of the neck (J). In wild-type mice, chondrogenesis of the two wings is almost complete, with only small gaps close to the midline yet to form (E, arrow). In the *Gdf6*+/- mice, there are large holes on either wing lacking cartilage formation (F, arrow). The *Bmp4-lacZ*/+ phenotype more closely resembles wild-type (G, arrow). The area lacking cartilage in the *Bmp4/Gdf6* compound heterozygotes is larger than either of the single heterozygotes (H, arrow). Cr, cricoid cartilage; is, ischium; pb, pubis.

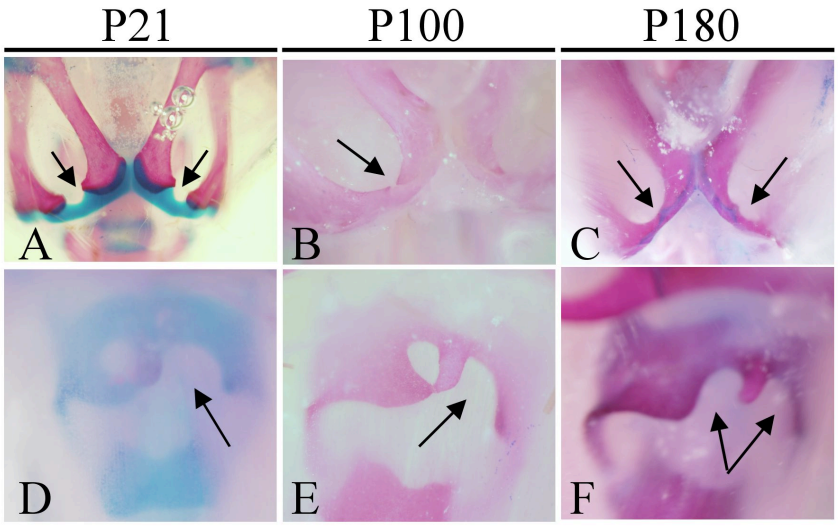

Figure 4.3. Persistence of hypoplasia through adulthood. A) In some *Bmp4/Gdf6* compound heterozygotes, a large portion of the cartilage fails to fuse along the midline. At both at P100 (B) and P180 (C), there is no change in the severity of the cartilage formation defect, and therefore this is a persisting defect established early in the development. The ischium and the pubis do appear to touch during adulthood (E,F arrows), however, the area of bone in which they unite it much thinner than found in wild-type mice (not shown).

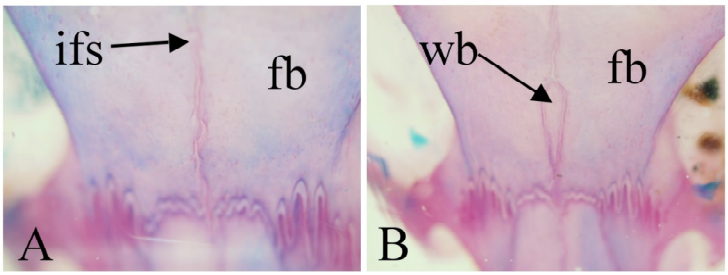

Figure 4.4. Wormian bones in the interfrontal suture. Wormian bones are small calvarial bones that develop from additional ossification centers, separate and at a distance from the ossification centers of the main cranial bones. In the *Gdf6+/-* by *Bmp4-lacZ/+* crosses, these ectopic bones were often observed in the most anterior portion of the interfrontal suture (B), the suture that separates the paired frontal bones (A). Fb, frontal bone; ifs, interfrontal suture; wb, wormian bone.

This leads to the question of whether this represents a permanent defect or simply a lag in the growth of these structures. To address this possibility, we also collected adult *Bmp4-lacZ/+; Gdf6+/-* compound mutants at P100 (Fig 4.3B) and Pz180 (Fig 4.3C). Although later in adulthood, the ischium and the pubis do appear to touch (Fig 4.3C,D arrows), the area of bone in which they unite it much thinner than found in wild-type mice, even at P21 (Fig.4.2A). This suggests that although the pelvic bones continue to grow past P21, the lag in growth fails to catch up with wild-type.

Hypoplasia of the thyroid cartilage

The thyroid cartilage is the largest cartilage of the larynx, consisting of two wings fused at the midline of the neck (Gray and Lewis, 1918) (Fig 4.2J). Previously collected *Gdf6-/-* adult mice had severe hypoplasia the thyroid cartilage and epiglottis, along with abnormal fusion of the arytenoids cartilages (not shown). We found that in wild-type P21 mice, chondrogenesis of the two wings of the thyroid cartilage is almost complete, with only small gaps close to the midline (Fig 4.2E, arrow). In the *Gdf6+/-* mice, there are large holes on either wing lacking cartilage formation (Fig 4.2F, arrow). While the *Bmp4-lacZ/+* phenotype more closely resembles wild-type then the *Gdf6+/-* mice (Fig 4.2G), the area of failed cartilage formation in the *Bmp4/Gdf6* compound mutant (Fig 4.2H, arrow) is larger than either of the single heterozygotes (Fig 4.2F,G, arrow). In some *Bmp4/Gdf6* compound mutants, a large portion of the cartilage fails to fuse along the midline (Fig 4.3D). Looking at adult *Bmp4-lacZ/+; Gdf6+/-* compound mutant, both at P100 (Fig 4.3E) and P180 (Fig 4.3F), there is no change in the severity of the cartilage

formation defect. Therefore, by P21 the development of the thyroid cartilage is complete, resulting in a persisting defect.

Although expression of *Bmp4* in this structure is not reported, *Gdf6* is expressed in the mesenchyme adjacent to the thyroid cartilage at E14.5 (not shown). Therefore, it is likely the Gdf6 provides a paracrine signal from the adjacent mesenchyme to the thyroid cartilage to stimulate cartilage growth. Since the phenotype of *Bmp4-lacZ/+* mice was similar to the wild-type thyroid cartilage, but the severity appeared to increase from the *Gdf6+/-* to *Bmp4/Gdf6* compound mutants, this suggests a possible interaction of these two BMP family members in the growth of this structure.

Wormian Bones

Although there was no preference among single and compound heterozygotes, we often observed the presence of Wormian bones in our *Bmp4-lacZ/+*; *Gdf6+/-* intercross. Wormian bones are small calvarial bones that develop from additional ossification centers within the sutures or the fontanelles, most often in the lambdoid or squamosal sutures. These miniature cranial bones are formed from ossification centers that form *de novo*, separate and at a distance from the ossification centers of the main cranial bones (Rice, 2008). In the progeny of our *Gdf6+/-; Bmp4-lacZ/+* crosses, these ectopic bones were often observed in the most anterior portion of the interfrontal suture (Fig 4.4B), the suture that separates the paired frontal bones (Fig 4.4A).

Wormian bones can be associated with pathologies, such as osteogenesis imperfecta or hydrocephalus, in which the requirement for cranial growth outpaces the ability of the bones to grow or in which the sutural space is spread apart (Roybal et al.,

2010). There has also been some association with craniosynostosis (Sanchez-Lara et al., 2007). In Chapter III, a defect in frontal bone growth was observed in *Bmp4-lacZ/+; Gdf6-/-* embryos. It is possible that if *Gdf6* and *Bmp4* play a role in the proliferation of the frontal bone, that even slight delays in growth of the bones may contribute to the formation of these Wormian bones, even if a frontal bone abnormality is not evident in the single heterozygous mice.

Failed fusion of the vertebrae along the dorsal midline

During our *Bmp4-lacZ/+* by *Gdf6+/-* crosses, we observed an abnormal vertebrae phenotype in our *Bmp4-lacZ/+* and *Bmp4-lacZ/+; Gdf6+/-* compound mutants that had not been previously reported in descriptions of the *Bmp4* heterozygote mouse. As the vertebrae ossify, two broad plates of the neural arch, referred to as the laminae, direct backward and medial toward the dorsal midline. They fuse at the dorsal midline to form the spinous processes, which serve as attachment sites for muscles and ligaments (Gray and Lewis, 1918) (Fig 4.5A). In the *Bmp4-lacZ/+* single heterozygotes and the *Bmp4-lacZ/+; Gdf6+/-* P21 mice, the laminae of the lower thoracic vertebrae and upper lumbar vertebrae failed to fused along the dorsal midline and lack spinous processes (Fig 4.5 B,D). The penetrance and severity of the vertebral defects were not increased in the *Bmp4/Gdf6* compound mutants compared to the *Bmp4-lacZ/+* single heterozygotes, and therefore the phenotype is most likely due to *Bmp4* alone. However, this defect appears to be only a delay in ossification. At P180 (6 month) mice, the laminae have fused and the spinous processes are present (Fig 4.5E).

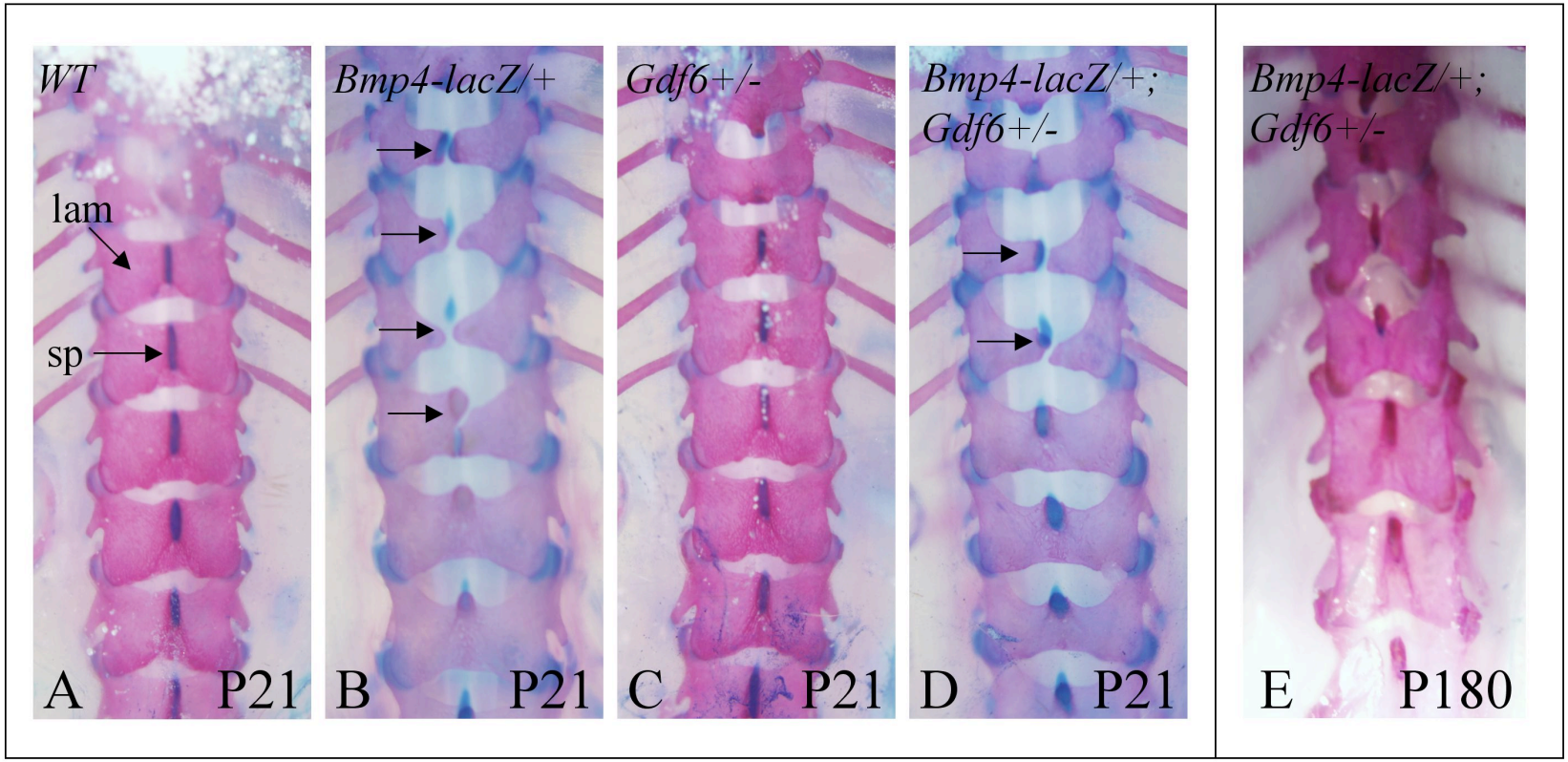

Figure 4.5. Failed fusion of the vertebrae along the dorsal midline. P21 mice presented with failed fusion of the lower thoracic and upper lumbar vertebrae along the dorsal midline in *Bmp4-lacZ/+* single heterozygotes (B) and *Bmp4-lacZ/+; Gdf6+/-* compound heterozygotes (D) and lack spinous processes. These defects were not seen in wild-type (A) or *Gdf6+/-* (C) and the vertebrae eventually did fuse during adulthood (E) by P180. There was no increase in the penetrance between *Bmp4-lacZ/+* (B) and *Bmp4-lacZ/+; Gdf6+/-* (D) mice.

Preaxial polydactyly of the hindlimb

The murine hindlimb skeleton is composed of ankle (tarsal) bones, metatarsals, phalanges, and claws (Fig 4.6A). Likewise, the joints between these segments are referred to as the tarsal-metatarsal, metatarsal-phalangeal, and phalangeal joints (Fig 4.6A). Both *Bmp4* (Fig 4.6I, arrows) and *Gdf6* (Fig 4.6J, arrows) are expressed in the anterior limb bud (shown at E11.5). *Bmp4-lacZ/+; Gdf6+/-* mice presented with preaxial polydactyly of the hindlimb (Fig 4.6C-H). This phenotype had been previously reported in *Bmp4* heterozygotes at a 12% penetrance (Dunn et al., 1997; Katagiri et al., 1998). In our crosses, no incidence of polydactyly was observed in wild-type (0/21) or *Gdf6+/-* mice (0/33) (Table 4.1). Polydactyly was present in 9% of the *Bmp4-lacZ/+* mice (2/23). This was increased to 77% in *Bmp4/Gdf6* compound mutants (24/31) (Table 4.1). This increase in the incidence of polydactyly between the *Bmp4-lacz/+* and *Bmp4/Gdf6* compound mutants was statistically significant (p=0.0017, Fisher's exact test). Since polydactyly was never observed in *Gdf6+/-* mice but the penetrance was drastically increased from the *Bmp4-lacZ/+* to *Bmp4/Gdf6* compound mutants, this suggests that these two BMP family members have a cooperative function in the patterning of the limb. No polydactyly was observed in the forelimb of any genotype. Although *Bmp4* and *Gdf6* are also expressed in the limb bud of the forelimb (Fig 4.6I, J, arrows), *Gdf6* is expressed at considerably reduced levels in the forelimb compared to the hindlimb (Fig 4.6J, arrows) and the *Gdf6-/-* mouse does not present with polydactyly (not shown), and therefore, *Bmp4* is likely more critical in limb patterning.

The analysis of the polydactyly phenotype is summarized in Table 4.1. The duplicated digit was always the first digit, however, there was variation in the site where

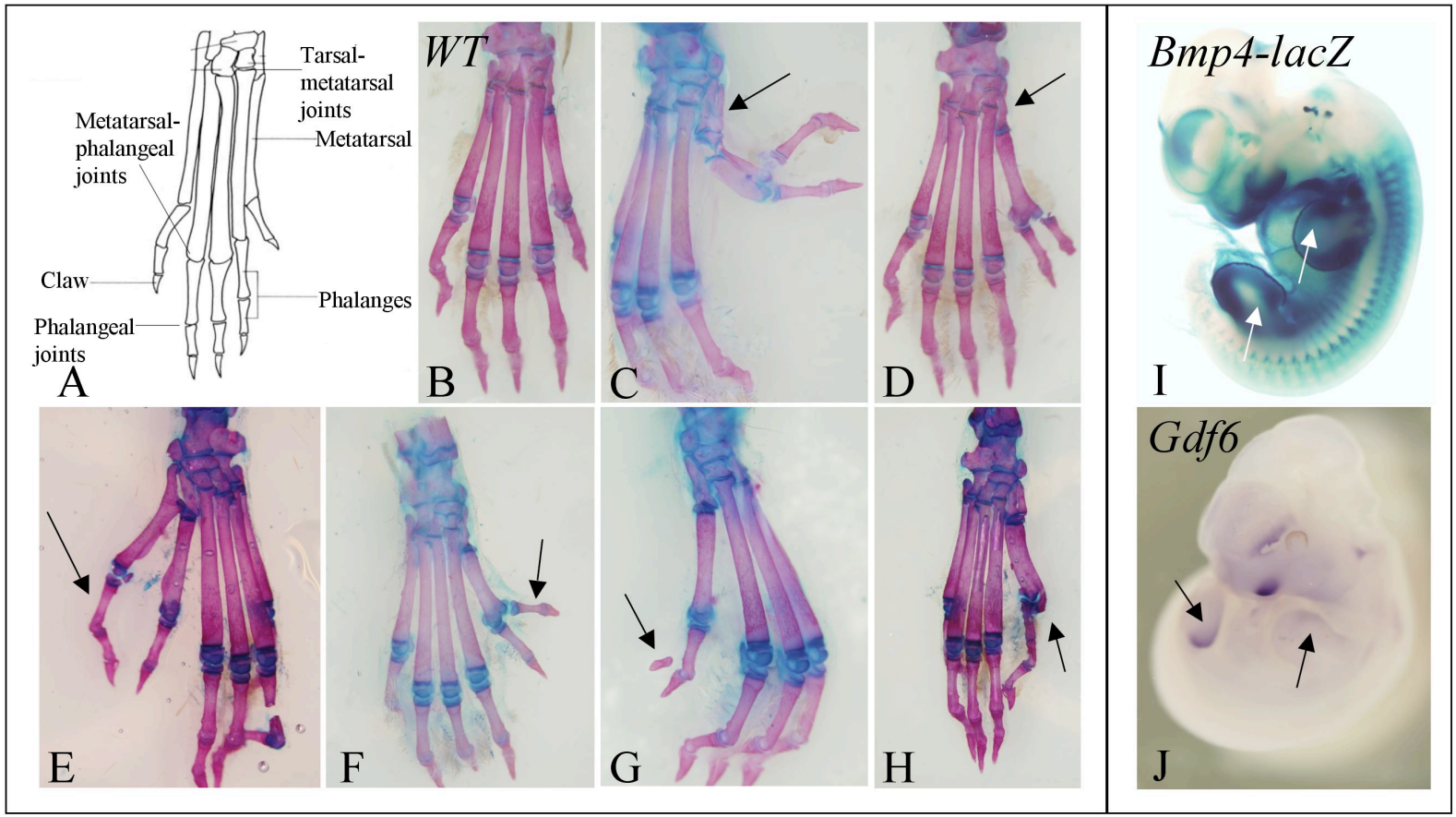

Figure 4.6. Pre-axial polydactyly of the hindlimb in *Bmp4/Gdf6* compound mutants. P21 mice stained with alzarin red/alcian blue. *Bmp4+/-; Gdf6+/-* mice present with pre-axial polydactyly of the hindlimb (C,D). In some cases the polydactyly occurred along with a duplicated first tarsal segment (C). There was also variation in the number of phalangeal segments in the duplicated digits, including three (E, arrow), two (F, arrow), or a single floating segment (G, arrow). In rare cases polydactyly was evident as a thickening of the first tarsal segment and the first metatarsal bone (H), but no extra digit. Co-expression of *Gdf6* and *Bmp4* in the anterior limb bud (arrows) was shown through *Gdf6 in situ* hybridization (I) and *lacZ* staining of *Bmp4-lacZ* embryos (J).

the duplication joined to the paw. The unction of the duplicated digit sometimes resided at the tarsal joints (47%, Fig 4.6E), the metatarsal joints (50%, Fig 4.6F), and rarely the phalangeal joints (3%, Fig 4.6G). In cases where the duplication initiated at the tarsal joint, the first tarsal segment was also duplicated (Fig 4.6C, arrow).

An interesting feature of polydactyly phenotype was that a duplicated digit was more often present in the right hindlimb than in the left. In the *Bmp4-lacZ/+* with polydactyly, 100% (2/2) had polydactyly in only the right hindlimb. In the *Bmp4-lacZ/+; Gdf6+/-* mice, 17% had unilateral polydactyly in the left limb (4/24), 50% had unilateral polydactyly of the right hindlimb (12/24), and 33% (8/24) had bilateral polydactyly (Table 4.1).

Lastly, there was also variation in the number of phalangeal segments present in the extra digit. In the *Bmp4/Gdf6* compound mutants, 31% had a complete extra digit with three phalangeal segments (10/32, Fig 4.6E), 59% had two phalangeal segments (19/32, Fig 4.6F), and 6% had a single "floating" phalangeal segment (2/32, Fig 4.6G). In one case (1/32), polydactyly was clearly evident by a duplicated tarsal segment, and a thickening of the first metatarsal bone, but there was no extra digit (Fig 4.6H).

Interaction of Gdf6 *and* Bmp4 *in the dorsal retina*

Although the phenotypic analysis of *Bmp4/Gdf6* compound mutants was focused on skeletal phenotypes, a defect in eye development was readily visible in our *Bmp4/Gdf6* compound mutants. In previous studies *Bmp4+/-* mice exhibited a threefold greater frequency of microphthalmia (small eyes) and anophthalmia (no eyes) compared to wild-type (Dunn et al., 1997). We did not observe any eye abnormalites in our wild-

type (Fig 4.7A), *Bmp4-lacZ/+* (Fig 4.7B), or *Gdf6+/-* (Fig 4.7C) embryos. However, microphthalmia was occasionally observed in *Gdf6-/-* (Fig 4.6E) and *Bmp4-lacZ/+; Gdf6+/-* embryos (not shown). Furthermore, the majority of the *Bmp4-lacZ/+; Gdf6-/-* embryos had unilateral or bilateral anophthalmia (Fig 4.7F, arrow), resulting in an almost complete failure of formation of rudimentary eye (Fig 4.7L) compared to the structure of the wild-type embryonic eye (Fig 4.7I). Expression of *Bmp4* is detected in the dorsal retina at E10.5 (Fig 4.7G, arrow) and E12.5 (Fig 4.7H) in the *Bmp4-lacZ* mouse. Expression of *Gdf6* in the dorsal retina is also clearly seen in the *Gdf6* Dβgeo reporter BAC line (Mortlock et al., 2003) at E10.5 (Fig 4.7J) and also through *in situ* hybridization at E12.5 (Fig 4.7K) (the section in panel K is taken more dorsally than panel H and therefore does not include the lens).

While the difference in eye size is visibly noticeable at fetal stages, we considered whether these defects persist into adulthood? Eyes from weanling mice were isolated and the diameter measured with microcalipers. At P21, there is virtually no difference in the average eye diameter between wild-type (2.53 mm, n=5), *Gdf6+/-* (2.50 mm, n=14), and *Bmp4-lacZ/+* (2.47 mm, n=4) mice. However, there is an approximately 10% reduction in average eye diameter in the *Bmp4-lacZ/+; Gdf6+/-* compound mutants (2.29 mm, n=6). An ANOVA detected no significant difference between the means of each group (p=0.087). However, a pair-wise T-test between each genotype group revealed a difference between the *Gdf6+/-* and *Bmp4-lacZ/+; Gdf6+/-* mice in the average eye diameter, with a p value= 0.0078, even with our small sample size (total n=29). The differences between the wild-type and *Gdf6+/- ;Bmp4-lacZ* (p=0.07) mice and between the *Bmp4-lacZ/+* and *Gdf6+/-; Bmp4-lacZ/+* (p=0.08) mice were trending toward

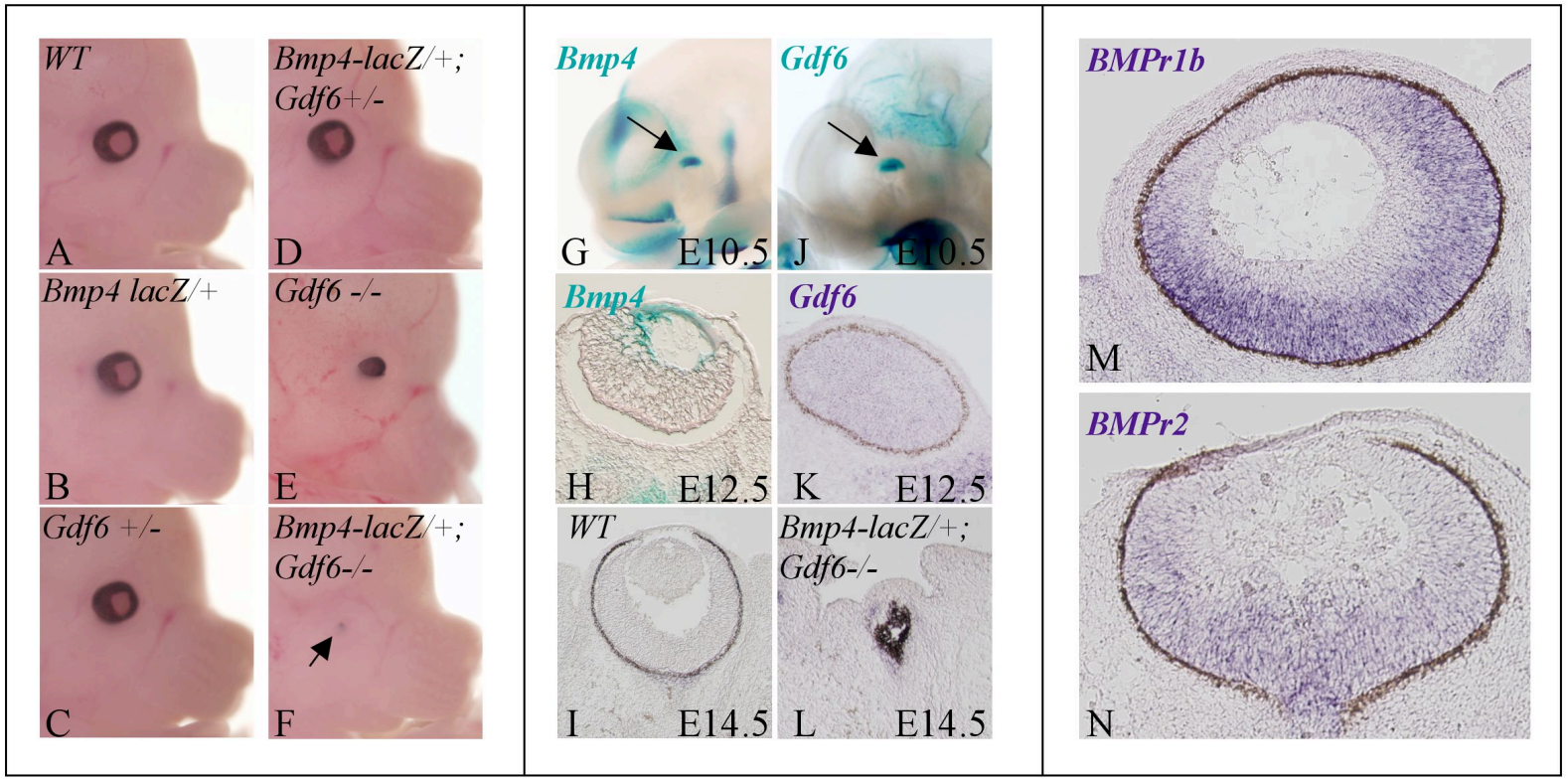

Figure 4.7. Anophthalmia in *Bmp4-lacZ/+; Gdf6-/-* embryos. While no defects in eye development were seen in wild-type (A), *Bmp4-lacZ/+* (B), or *Gdf6+/-* (C) E14.5 embryos, microphthalmia was rarely observed in *Bmp4-lacZ/+; Gdf6+/-* (not shown) and *Gdf6-/-* (F) embryos. *Bmp4-lacZ/+; Gdf6-/-* embryos often presented with unilateral or bilateral anophthalmia (F). *Bmp4* and *Gdf6* are co-expressed in the dorsal retina. This is seen in *Bmp4-lacZ* embryos at E10.5 (G, arrow) and E12.5 (H). Expression of *Gdf6* in the dorsal retina is seen in a *Gdf6 lacZ* reporter BAC line at E10.5 (J, arrow) and through *in situ* hybridization at E12.5 (K) (Panel K section is taken more dorsally than Panel H, and therefore does not include the lens). *Bmp4-lacZ/+; Gdf6-/-* embryos have complete failure to form the rudimentry eye (L) compared to the structure of the wild-type eye (I). BMPr1b (M) and BMPr2 (N), receptors shared by Bmp4 and Gdf6, are also expressed in the dorsal retina.

significance. Perhaps with a larger sample size the difference between wild-type, *Bmp4*+/-, and *Gdf6*+/-; *Bmp4-lacZ*/+ mice would also be statistically significant. All progeny were gathered from the same mating pair, so differences produced from their mixed background (C57Bl/6J and CD1) should be equal among groups. Since *Gdf6*-/- mice do not survive postnatally, the anophthalmia phenotype could not be examined in *Gdf6*-/-; *Bmp4-lacZ*/+ mice at adulthood.

Discussion

In this chapter we present data showing an interaction of *Gdf6* and *Bmp4* in the sternum, limb, thyroid cartilage, pelvis, and dorsal retina, demonstrating a cooperative function between these two related members of the BMP family. These multiple phenotypes further demonstrate the range of functional activity of these two BMP family members, including patterning (limb and dorsal retina), cartilage growth (thyroid cartilage and pelvis), and joint formation (CS and manubriosternal joint). In some cases, the interaction of *Bmp4* and *Gdf6* appears to fit a simply additive model, where a defect present in both single heterozygotes is increased in severity in the compound heterozygotes. This was the case in the pelvis, with a small gap between the ischium and the pubis in the single heterozygotes was further exaggerated in the *Bmp4/Gdf6* compound mutants. However, most of the abnormalities we observed were found in one of the single heterozygotes at a low frequency (manubriosternal joint and polydactyly in the *Bmp4*+/- mice and the thyroid cartilage and dorsal retina in the *Gdf6*+/- mice) increased in not only severity but also the penetrance. This suggests that although *Bmp4*

or *Gdf6* alone may play a more important role in the development of that structure, the two genes likely also have a cooperative function.

Commonality of multiple phenotypes

Although the multiple phenotypes observed in the *Gdf6/Bmp4* compound mutants appear unrelated, groups of these phenotypes occur together in certain individuals with birth defects. Many craniosynostosis syndromes also have clinical features of limb abnormalities, including syndactyly in the hands and/or feet (Apert and Saethre-Chotzen syndromes), broad thumbs (Pfeiffer syndrome), and broad toes and bony fusion in the feet (Jackson-Weiss syndrome) (Wilkie, 1997). Common molecular pathways are likely involved in the development of both craniofacial and limb structures. *Bmp7* homozygous mutants have preaxial polydactyly of the hindlimb but also defects in the sternum, with a missing fourth sternum ossification center and a failure to fully develop the cranial bones (Dudley et al., 1995). *Bmp4/Bmp7* compound mutants also have defective ossification of the sternum, a split xiphoid process, and preaxial polydactyl of the limb (Katagiri et al., 1998).

Klippel-Feil syndrome (KFS) is characterized by multiple skeletal defects including conductive hearing impairment, malformed thyroid cartilages, carpals and tarsal fusions, and eye anomalies (Clarke et al., 1995), which correspond closely with the abnormal phenotypes observed in the *Gdf6* homozygous mutant mouse. In a large family with KFS, the mutation was determined to be a paracentric inversion with the proximal breakpoint located 623 kb downstream of GDF6 (Tassabehji et al., 2008); in a region that likely includes multiple long-distance regulatory elements for *Gdf6* (Mortlock et al.,

2003). Klippel-Feil patients also have vertebral fusions not seen in *Gdf6-/-* mice, however, *Gdf5/Gdf6* compound mutant mice do have scoliosis, suggesting these two BMPs do play a role in vertebral growth (Settle et al., 2001). Vertebral defects were also seen in our *Bmp4+/-* mice (Fig 4.5B), although this was related to a delay in ossification rather than fusion between vertebrae, as seen in KFS (Clarke et al., 1998). Some KFS patients reportedly have cranial defects, including macrocephaly (large head), microcephaly (small head), and brachycephaly (round head), which could also be associated with growth of the cranial bones (Tassabehji et al., 2008).

It is also common for several members of the BMP family to be expressed in a subset of a larger structure and together work in its development. This appears to be the case in the sternum. We showed that *Bmp4/Gdf6* compound mutants have an increased presence of the manubriosternal joint, the joint the separates the manubrium and the first sternal segment (Fig 4.1), suggesting that the normal function of Bmp4 and Gdf6 is to promote ossification within this joint. *Gdf5/Bmp5* compound mutants also present with one or more missing sternal segments (Storm and Kingsley, 1996) where *Bmp4/Bmp7* mice have a sinusoidal sternum and a split xiphoid process (Katagiri et al., 1998). The *Bmp6* homozygous mutant mice possess a single known skeletal abnormality: a delay in the growth of the cartilage template and ossification of the bones of the sternum. However, *Bmp5-/-; Bmp6-/-* compound mutants present with a entirely new phenotype: the failure of the two sternal bands to fuse along the midline, leaving a gap in the center of each sternal segment (Solloway et al., 1998). Therefore, multiple BMPs have a role in different regions of the sternum to contribute to the overall patterning and growth of the structure.

BMPs in patterning of the limb

While the cranial sutures form with the approach of two separate growing ossification elements, the joints of the limb form through the splitting of larger cartilage precursor elements. This process occurs through the formation of "interzones": specialized regions that extend across cartilage elements and mark the future site of the joint. This is followed by apoptosis in the middle of the interzone region with differentiation of the articular cartilage at the edges of the interzone, and is finished with the formation of a fluid-filled space between the two opposing skeletal elements (Storm and Kingsley, 1996).

At E11.5, digit condensation can first be seen as individual elements and this is the stage where improper patterning can lead to the deletion or multiplication of the digits. *Bmp2, Bmp4,* and *Bmp7* are all expressed in the apical ectodermal ridge (AER) where they control cell proliferation and signal to the progress zone, an adjacent region of proliferating undifferentiated cells (Dunn et al., 1997; Katagiri et al., 1998). The reduction or absence of BMP expression can cause the abnormal expansion of the mesenchymal cell condensations. It is possible that *Gdf6* and/or *Bmp4* normally restrict cell proliferation in the limb mesenchyme, and with the loss of *Gdf6/Bmp4* enough mesenchyme is accumulated to generate an additional digit. However, this does not explain why the loss of *Gdf6* and *Bmp4* affects only the preaxial digit or why the remaining digits appear morphologically normal.

In general, the preaxial digit is most often affected in BMP mutants with polydactyly. Like our *Bmp4-lacZ/+; Gdf6+/-* compound mutants, *Bmp7* homozygous mutants also present with preaxial polydactyly of the hindlimb, although at a lower

penetrance (approximately 25%) (Dudley et al., 1995) compared to the 77% in our compound mutants. The authors also described the polydactyly as unilateral and generally a mirror image duplication of the second digit, or a duplication of the first digit along with the adjoining tarsal element (Dudley et al., 1995), as we described. *Bmp4/Gli3* compound mutants with polydactyly were lacking the preaxial apoptotic region while the postaxial region is sustained. Decreased apoptosis in the limb bud could allow for prolonged survival of the AER and allow for the secretion of more growth promoting FGFs (Dunn et al., 1997).

Previous reports describe polydactyly being present only in the right hindlimb of *Bmp4*+/- single heterozygotes (Dunn et al., 1997), which confirms our own observations (Table 4.1). Like our *Bmp4/Gdf6* compound mutant mice, *Bmp4/Gli3* and *Bmp4/Alx4* compound mutants have bilateral polydactyly with increased penetrance and severity over the *Bmp4*+/- single heterozygotes (Dunn et al., 1997). The nature of the interaction between *Bmp4* and *Gli3, Alx4,* and likely *Gdf6*, could be that they are components of the same pathway and regulate each other's activity. Another possibility is that they operate in parallel pathways or pathways which involve slightly different aspects of limb patterning. Due to the early embryonic lethality of *Bmp4* homozygous mutant mice due to failed mesoderm formation (Winnier et al., 1995), the role of *Bmp4* in limb formation must be assessed by other means. By crossing a *Bmp4*-floxed allele to the *Prx1-cre* driver, investigators have generated a conditional knock-out of *Bmp4* in the limb bud mesoderm. They found that polydactyly in the *Bmp4* mutants was associated with delayed induction and maturation of the AER, resulting in expanded *Shh* and prolonged *Fgf8* signaling (Selever et al., 2004). Prolonged *Fgf8* expression in the AER is associated

Table 4.1. Analysis of the polydactyly phenotype in *Bmp4/Gdf6* compound mutants.

Genotype	Number with polydactyly out of total	Site of origin for each affected limb			Extra tarsal segment	Asymmetry			Number of phalanges in extra digit			
		TA	MT	PH		L	R	LR	3	2	1	0
WT	0/21											
Bmp4+/-	2/23 (9%)		2/2 (100%)				2/2 (100%)		1/2 (50%)	1/2 (50%)		
Gdf6+/-	0/33											
Bmp4-lacZ/+; Gdf6+/-	24/31 (77%)	15/32 (47%)	16/32 (50%)	1/32 (3%)	15/32 (47%)	4/24 (17%)	12/24 (50%)	8/24 (33%)	10/32 (31%)	19/32 (59%)	2/32 (6%)	1/32 (3%)

with increases in the number of phalanges in chick limbs (Sanz-Ezquerro and Tickle, 2003). In this chapter we described variation in the number of phalangeal segments (Fig 4.6, Table 4.1) in the polydactyly limb of our *Bmp4/Gdf6* compound mutants. BMPs do influence digit number, but this is mediated by secondary affects through the AER and *Shh* (Drossopoulou et al., 2000). Since this appears to be the underlying mechanism contributing to polydactyly in the *Bmp4+/-* mouse, it is highly likely a similar effect would be seen in *Bmp4/Gdf6* compound mutants.

The majority (82%) of *Bmp7* mutant mice also present with preaxial polydactyly. However, in these mutants there were no changes in *Shh* expression in the limb mesenchyme, but *Hoxd-13* expression in the posterior hindlimb was restricted and weaker compared to wild-type (Luo et al., 1995). Both *Shh* and *Hoxd13* could be analyzed in the *Bmp4/Gdf6* compound mutants to determine if the patterning of the limb, rather than changes in the proliferation of the limb bud mesenchyme, is the underlying mechanism in polydactyly phenotype.

Left/right asymmetry

Interestingly, the preaxial polydactyly of the hindlimb in the *Bmp4-lacZ/+; Gdf6+/-* mice preferentially affected both hindlimbs (33%) or just the right hindlimb (50%) over the left hindlimb alone (17%). The same observation has been noted in studies of the *Bmp4/Bmp7* compound heterozygotes, which also have unilateral and bilateral polydactyly with a preference for preaxial polydactyly of the right hindlimb (Katagiri et al., 1998). Furthermore, previous studies have failed to detect left hindlimb

polydactyly in any *Bmp4*+/- mice (Katagiri et al., 1998), which was consistent with our findings.

The idea of a role in left/right asymmetry for BMP signaling was initiated with the finding that BMP family member *Nodal* is expressed asymmetrically, with one domain to the left of the notochord and another in the anterior lateral mesoderm on the left side of the embryo. The *Nodal* expression domain in the lateral mesoderm overlaps with the expression of *Shh*, and the misexpression of *Shh* on the right side of the embryo leads to the ectopic expression of *Nodal* (Hogan, 1996). *Bmp4* has also been found to be required for left right patterning: expression of *Bmp4* in on the right side induces *Fgf8*, which then represses *Shh* (Levin et al., 1995; Monsoro-Burq and Le Douarin, 2000). The loss of embryonic *Bmp4* results in the absence of left-side determinants including *Nodal* and *Lefty2* in the lateral plate mesoderm (Fujiwara et al., 2002), a population of cells that contributes to the skeletal portion of the limb (Gilbert, 2003). Furthermore, *Bmpr-1a* and the transcriptional modulator Smad1, which are utilized by both Bmp4 and Gdf6, are also asymmetrically expressed on the right side (Monsoro-Burq and Le Douarin, 2000). It is possible that the preference for polydactyly in the right hindlimb in both *Bmp4* single heterozygotes and *Bmp4/Gdf6* compound mutants is related to a disruption in the left-right patterning established in part by BMP signaling. However, polydactyly was the only abnormal phenotype in the *Bmp4/Gdf6* compound mutants with a noticeable preference for the left or right side.

Beyond the skeleton: BMPs and patterning of the dorsal retina

The occurrence of anophthalmia in the *Bmp4-lacZ/+; Gdf6-/-* embryos demonstrates an interaction of these two genes in the development of the eye, particularly the dorsal retina where *Bmp4* and *Gdf6* are co-expressed. *Bmp4* and *Gdf6* have both independently play a role in the formation of the eye, although this is the first evidence of an interaction between the different BMPs within the eye.

Ocular defects attributed to mutations in the BMPs, and Gdf6 in particular, have been well documented. After screening patients with ocular defects, including microphthalmia, anophthalmia, and coloboma, a total of seven heterozygous sequence changes were identified in the *GDF6* sequence, two located in the first exon and five located in the second exon (Asai-Coakwell et al., 2007). *Bmp4* has also been identified as an underlying genetic factor in human patients with anophthalmia and microphthalmia (Bakrania et al., 2008). The affect of *Gdf6* on ocular development has also been studied in zebrafish. A genome-wide duplication event during evolution produced multiple gene paralogs in the zebrafish genome, including two for *Gdf6*, referred to as *radar/gdf6a* and *dynamo/gdf6b*. Like *Gdf6* in the mouse, *radar* is also expressed in the dorsal retina (Rissi et al., 1995) and the knock-down of *radar* in zebrafish resulted in microphthalmia and coloboma (Asai-Coakwell et al., 2007).

In mice, the haploinsufficiency of *Bmpr1a* and *Bmpr1b* in the retina, the receptors utilized by both Bmp4 and Gdf6, resulted in abnormal retina dorso-ventral patterning (Murali et al., 2005). *Bmp4* expression in the dorsal retina is thought to affect retinal patterning by regulating the expression of transcription factor *Tbx5* in the optic cup and downregulating ventral markers *Vax* and *Pax2* (Koshiba-Takeuchi et al., 2000). The

disruption of these molecular signals also results in abnormal projections of the retina ganglion cell axons. Due to the co-expression of *Gdf6*, *Bmp4,* and BMP receptors 1a and 1b in the dorsal retina early in development, it is likely that *Gdf6* and *Bmp4* are also interacting in retinal patterning.

Unique role of Gdf6 *in the suture*

Much of the literature published on the Gdf family is related to cartilage growth. Although *Gdf5* is one of the earliest markers for joints, bead implanted into the chick limb actually stimulates cartilage growth (Storm and Kingsley, 1999). Due to the high homology between *Gdf5* and *Gdf6*, these two sub-family members likely have similar functions. Several defects in the *Bmp4/Gdf6* compound mutants are likely related to lack of growth and proliferation of the cartilage precursors, including failed union of the ischium and pubic bones and hypoplasia of the thyroid cartilage. However, *Gdf6* must have an activity separate from cartilage growth since the cranial bones form through intramembranous ossification, which occurs without a cartilage intermediate. This makes the study of *Gdf6* in the CS development particularly interesting.

CHAPTER V

CORONAL CRANIOSYNOSTOSIS IN THE GDF6 MUTANT MOUSE OCCURS INDEPENDENTLY OF THE BMP ANTAGONIST NOGGIN

Introduction

Craniosynostosis is defined as the premature fusion of one or more of the cranial sutures, the fibrous joints separating the flat bones of the cranial vault. These joints are the main sites for cranial growth during development, and premature fusion of a suture eliminates growth perpendicular to the site of craniosynostosis. In an attempt to compensate and maintain the volume of the skull vault, growth at the unaffected sutures increases. This produces a characteristic dysmorphic skull shape that is dependent on which sutures have undergone fusion (Slater et al., 2008).

In Chapters II and III we demonstrated a role of both *Gdf6* and *Bmp4,* members of the BMP family, in the earliest stages of CS development. By E14.5, fusion of the frontal and parietal ossification centers in *Gdf6-/-* and *Bmp4-lacZ/+; Gdf6+/-* embryos can be visualized through alizarin red staining. BMP signaling can be inhibited by several antagonists, including Cerbarus, Dan, Gremlin, Chordin, and Noggin (Xiao, 2007). Noggin binds to BMP dimers and inhibits their interaction with Type I and Type II receptors by blocking the binding epitopes for the receptors (Groppe et al., 2002). Noggin has been definitively shown to bind with high affinity to Bmp2 and Bmp4 and with less affinity to Bmp7 (Zimmerman et al., 1996). In Xenopus, the ability of GDF6 to induce epidermal genes and inhibit neural markers in animal caps was blocked by Noggin (Chang and Hemmati-Brivanlou, 1999). The investigators furthermore demonstrated that

GDF6 and Noggin directly bind with a high affinity, similar to that of BMP2 (Chang and Hemmati-Brivanlou, 1999).

The role of *Noggin* in the sutures has been largely restricted to the study of the interfrontal suture, the suture homologous to the human metopic suture. The posterior interfrontal suture in mice is a common model to study the events which contribute to fusion of a suture, since it is the only suture in mice which undergoes predictable fusion during postnatal development (Opperman, 2000). Previous studies demonstrated that *Noggin* is expressed postnatally in patent (the sagittal and coronal) sutures but not fusing sutures (the posterior interfrontal). *Bmp4* is expressed in the suture mesenchyme and bone fronts of both patent and fusing posterior interfrontal sutures. Although *Noggin* is an antagonist for BMPs, BMPs were able to actually stimulate *Noggin* expression in calvarial explants (Rice et al., 2005). The suppression of *Noggin* in the presence of *Bmp4* stimulation is achieved through FGF2, which is only expressed in the posterior interfrontal suture. The over-expression of FGF2 and the gain of function mutations in *FGFR2* that have been associated with Apert's and Crouzon craniosynostosis syndromes both inhibited *Noggin* expression and blocked *Bmp4*-mediated stimulation of *Noggin* (Warren et al., 2003a).

The *Noggin* homozygous mutant is lethal and the severity of the *Noggin* homozygous mutant phenotype was dependent on the genetic background (Tylzanowski et al., 2006). The homozygous loss of *Noggin* is lethal at birth in the DBA/1 and CDA strains (McMahon et al., 1998; Tylzanowski et al., 2006) or prior to day E14.5 in the C57Bl/6J (Tylzanowski et al., 2006). The homozygous mutants that survived to birth present with failed neural tube closure, broad limbs, loss of vertebrae, and shortened body

(McMahon et al., 1998). No abnormal suture phenotype has been reported in the *Noggin* homozygous mutants; however, this could have been impossible to examine due to the presence of exencephaly in a large portion of the *Noggin-/-* embryos, precluding analysis of intact calvarial joints. Furthermore, the expression and activity of *Noggin* in the suture during the earliest stages of suture development has been unreported. We identified expression of *Noggin* in the periosteum of the frontal and parietal bones at E14.5 (Fig 5.3), which corresponds to the timepoint when fusion of the ossification centers is first visible in the *Gdf6-/-* embryo.

BMPs are secreted signaling proteins, and with both *Gdf6* and *Bmp4* being expressed in the frontal bone primordia it is possible that these two family members may interact with *Noggin.* The mechanism leading to suture fusion in the *Gdf6-/-* embryo and *Bmp4-lacZ/+;Gdf6+/-* compound mutants could be directly related to *Noggin's* role in maintaining the patency of the suture mesenchyme. In the wild-type suture, *Gdf6* and *Bmp4* may stimulate *Noggin* expression through paracrine signaling from the frontal bone primordia, and in turn, *Noggin* maintains the suture mesenchyme in undifferentiated state by inhibiting the osteogenic affects of BMP signaling.

In the present chapter, we investigate the role of *Noggin* in early suture development, and the possible interaction with *Gdf6,* by examining the phenotype of *Gdf6* and *Noggin* compound mutants. In performing these crosses we tested three hypotheses to explain a possible *Gdf6/Noggin* interaction: 1) Along with *Gdf6, Noggin* plays an inhibitory role to maintain the suture mesenchyme in an undifferentiated state; 2) *Gdf6* and other BMPs stimulate *Noggin* expression in the suture and therefore

indirectly maintain the suture through *Noggin*; or 3) *Noggin* does not play a role in early embryonic suture development.

Despite the hypothesized important role of *Noggin* in the maintenance of suture patency discussed in the literature, we found no evidence of an early role of *Noggin* in the development of the CS. *Noggin-lacZ/lacZ* embryos without exencephaly phenotype form the cranial sutures, including the CS. Furthermore, no abnormal suture phenotype was observed in the *Gdf6+/-; Noggin-lacZ/+* mice and no rescue of CS fusion was observed in *Gdf6-/-; Noggin-lacZ/+* embryos other than a possible slight delay (still within the same embryonic day) in the fusion of the ossification centers. This upheld our third hypothesis that *Noggin* does not play a critical role in embryonic suture development. Therefore, the role of *Gdf6*, and likely that also of *Bmp4*, in the ectopic differentiation of the suture mesenchyme occurs independently of *Noggin*'s role in suture patency.

Materials and Methods

Mouse crosses

A mutation in the *Noggin* locus was generated by replacing the coding sequence with a lacZ reporter (Brunet et al., 1998). *Noggin-lacZ* mice were maintained on a CD1 outbred background. Embryonic age was determined through detection of the vaginal plug, with noon of that day observed as E0.5. To analyze *Noggin-lacZ/lacZ* homozygous mutants, *Gdf6+/-; Noggin-lacZ/+* compound mutants were crossed. For analysis of CS phenotype, *Gdf6+/-* mice were crossed to *Noggin-lacZ/+* mice to generate wild-type, *Gdf6+/-* and *Noggin-lacZ/+* heterozygotes, and *Gdf6+/-; Noggin-lacZ/+*

compound mutants. For analysis of suture phenotype at embryonic stages and for analysis of *Noggin* expression in the suture, *Gdf6+/-* mice were crossed to *Gdf6+/-; Noggin-lacZ/+* mice to produce wild-type, *Gdf6+/-* and *Noggin-lacZ/+* heterozygotes, *Gdf6+/-; Noggin-lacZ/+* compound mutants, *Gdf6-/-,* and *Gdf6-/-; Noggin-lacZ/+* embryos with 3 missing alleles. Mouse genotypes and crosses are summarized in Table 5.1. Genotypes highlighted in the gray boxes were crossed to produce the next generation. G1 and G2 were analyzed by alizarin red staining for suture phenotypes, and G1 was additional analyzed for other skeletal phenotypes. Genotypes highlighted in the yellow boxes in G2 were analyzed for changes in *Noggin-lacZ* expression among *Gdf6+/+* (wild-type for *Gdf6*), *Gdf6+/-,* and *Gdf6-/-* embryos (Table 5.1)

Genotyping

Samples were genotyped for Noggin to generate a 211 base-pair wild-type allele from primers Nog1 and Nog2 and a 160 base-pair mutant allele from primers Nog1 and Gal1. Primers: Nog1 5'-GCATGGAGCGCTGCCCCAGC-3', Nog2 5'-GAGCAGCGAGCGCAGCAGCG-3', Gal1 5'-AAGGGCGATCGGTGCGGGCC-3'. The PCR program included heating the samples to 93^{o}C for 90 seconds then 35 cycles of alternating between 93^{o}C for 30 seconds (denaturation) and 72^{o}C for 45 seconds (extension) (protocol from (McMahon et al., 1998)). Embryos could alternatively be genotyped for *Noggin-lacZ* by removing a limb from the embryo and staining for lacZ.

Table 5.1 Summary of *Gdf6/Noggin* mouse crosses and genotypes. Genotypes highlighted in the gray boxes were crossed to produce the next generation. G1 and G2 were analyzed by alizarin red staining for suture phenotypes, and G1 was additional analyzed for other skeletal phenotypes. Genotypes highlighted in the yellow boxes in G2 were analyzed for changes in *Noggin-lacZ* expression among *Gdf6+/+* (wild-type for *Gdf6*), *Gdf6+/-,* and *Gdf6-/-* embryos.

Parental Genotypes	G1 Genotypes	G2 Genotypes
Gdf6+/-	WT	WT
Noggin-lacZ/+	*Gdf6+/-*	*Gdf6+/-*
	Noggin-lacZ/+	*Noggin-lacZ/+*
	Gdf6+/-; Noggin-lacZ/+	*Gdf6+/-; Noggin-lacZ/+*
		Gdf6-/-
		Gdf6-/-; Noggin-lacZ/+

Additional methods

Information of the following methods were discussed in previous chapters: whole-mount alizarin staining of skeletal preparations (Chapter III), DNA preparations (Chapter II), histology (Chapter II), lacZ staining (Chapter III), and 3-aminopropylsilane treatment of slides (Chapter II).

Results

Haploinsufficiency of Gdf6 *and* Noggin *does not produce coronal craniosynostosis*

Three alternative results were hypothesized for the interaction of *Gdf6* and *Noggin* in suture development. The first was that, like *Gdf6*, *Noggin* plays an inhibitory role to maintain the CS in an undifferentiated state. To test this hypothesis, we crossed *Gdf6*+/- and *Noggin-lacZ*/+ heterozygotes to produce compound heterozygotes, which would theoretically remove two inhibitory factors and result in differentiation of the suture mesenchyme and premature suture fusion.

The established genotyping strategy for the *Gdf6* line consists of a duplex PCR, with one primer pair detecting the wild-type allele and a second detecting the *neo* cassette inserted into the mature signaling region of the targeted locus. However, the *Noggin-lacZ* line also contains a *neo* cassette. This made it impossible to distinguish *Noggin-lacZ*/+ single heterozygotes and *Gdf6*+/-; *Noggin-lacZ*/+ compound mutant animals using the conventional *Gdf6* PCR protocol. Attempts were made to generate allele-specific primers for the *Gdf6* locus, spanning the border between the wild-type sequence and the *neo* cassette. However, the *Gdf6* locus is extremely GC rich and the precise

boundary of the targeted allele was never well defined or previously described, making attempts for primer design unsuccessful. Fortunately, by looking at the phenotype and Mendelian ratios, conclusions could still be drawn from the collected data.

Mice from a *Gdf6*+/- by *Noggin*+/- cross were collected at P21 and stained with alizarin red. A total of 25 animals were analyzed (Table 5.2). None of the wild-type (0/7) (Fig 5.1F) or *Gdf6*+/- (0/5) (Fig 5.1G) mice presented with coronal craniosynostosis. Due to the genotyping issues discussed above, a total of 13 animals were determined to be either *Noggin-lacZ*/+ single heterozygotes or *Gdf6*+/-; *Noggin-lacZ*/+ compound mutants, and none of them presented with any suture defects (Fig 5.1H). On the basis of Mendelian ratios, at least half of the 13 animals were likely to be compound heterozygotes, and therefore we concluded that compound mutants for *Gdf6* and *Noggin* did not produce suture fusion. In this group of mice that were either *Noggin-lacZ*/+ single heterozygotes or *Gdf6*+/-; *Noggin-lacZ*/+ compound mutants, a portion had fusions in the wrist and ankle (Fig 5.5) that had not been previously reported in *Gdf6* or *Noggin* heterozygotes, and therefore, we were confident that a portion of these mice were in fact *Gdf6/Noggin* compound mutants.

Haploinsufficiency of Noggin *does not rescue suture fusion in the* Gdf6-/- *embryo*

Our second hypothesis states that *Gdf6* and other BMPs stimulate *Noggin* expression in the suture and therefore indirectly maintain the suture through *Noggin*. To test this genetically, we produced *Gdf6-/-; Noggin-lacZ*/+ embryos. Although a homozygous mutant allele for *Gdf6* would normally result in erroneous differentiation of the suture mesenchyme, we hypothesized that the haploinsufficiency of *Noggin* would

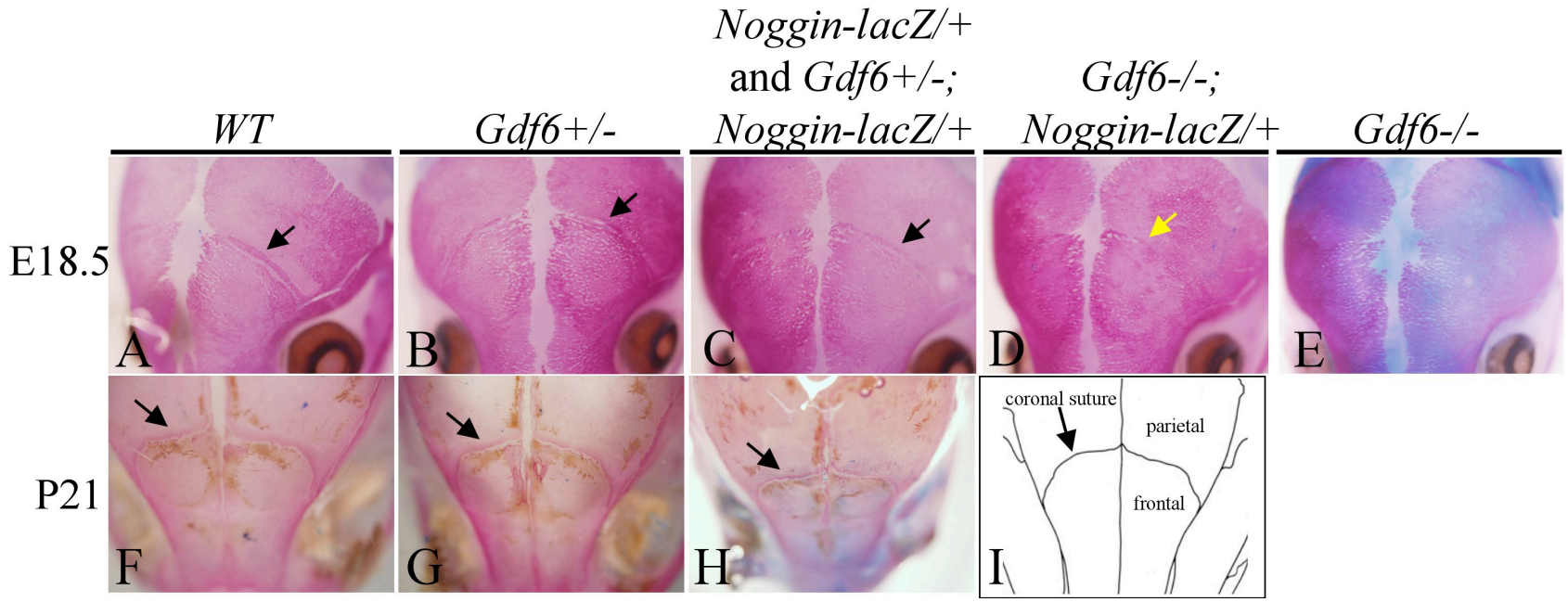

Figure 5.1. Analysis of suture fusion in *Gdf6/Noggin* compound mutants. At E18.5, wild-type (A), *Gdf6*+/- (B), *Noggin-lacZ/+,* and *Gdf6+/-; Noggin-lacZ/+ (C*) all have normal coronal sutures. *Gdf6-/-; Noggin-lacZ/+* embryos had fusion of specifically the coronal suture (D), showing the reduction of *Noggin* dosage was unable to rescue suture fusion in the *Gdf6*-/- embryo. Where the *Gdf6-/-* embryo has a continuous surface between the frontal and parietal bones (E), the possible remnants of a suture appear in the *Gdf6-/-*; *Noggin-lacZ/+* embryo (D, yellow arrow). At P21, no suture phenotype was observed in wild-type (F), *Gdf6*+/- (G), *Noggin-lacZ/+*, and *Gdf6+/-; Noggin-lacZ/+* (H) embryos. I) Location of the coronal suture, frontal, and parietal bones in the P21 mouse.

Table 5.2. Analysis of suture fusion in *Gdf6/Noggin* compound mutants.

Genotype	Total no. analyzed	Total with suture fusion
Gdf6+/- x Noggin-lacZ/+ cross		
Wild-type	7	0
Gdf6+/-	5	0
Noggin-lacZ/+ or *Noggin-lacZ/+; Gdf6+/-*	13	0

reduce the inhibition of BMP signaling. This would allow for an increase in signaling by other members of the BMP family to compensate for the loss of *Gdf6*, thereby maintaining the undifferentiated suture mesenchyme and rescuing suture fusion in the *Gdf6-/-* embryo.

To test this second hypothesis, *Gdf6+/-* and *Gdf6+/-; Noggin-lacZ/+* mice were crossed. This cross generated wild-type, *Gdf6+-* and *Noggin-lacZ/+* heterozygotes, *Gdf6+/-; Noggin-lacZ/+* compound mutants, *Gdf6-/-*, and *Gdf6-/-; Noggin-lacZ/+* embryos within the same litter. Due to the fact that *Gdf6-/-* mice die at the perinatal stage, embryos were collected at E18.5 and stained with alizarin red and alcian blue. Despite our genotyping challenges we did have the advantage in this cross of being able to distinguish *Gdf6-/-; Noggin-lacZ/+* embryos from *Noggin-lacZ/+* and *Gdf6+/-; Noggin-lacZ/+* embryos, since they completely lack the *Gdf6* wild-type allele targeted by the PCR genotyping primers. In this cross, the wild-type, *Noggin-lacZ/+*, and *Gdf6+/-; Noggin-lacZ/+* embryos all had normal CSs (Fig 5.1A-C, arrows). However, the *Gdf6-/-; Noggin-lacZ/+* embryos did have fusion of specifically the CS (Fig 5.1D), showing the reduction of *Noggin* dosage was unable to rescue suture fusion in the *Gdf6-/-* embryo. Yet where the *Gdf6-/-* embryo has a continuous surface between the frontal and parietal bones (Fig 5.1E), the possible remnants of a suture appear in the *Gdf6-/-*; *Noggin-lacZ/+* embryo (Fig 5.1D, yellow arrow), as described in the *Bmp4-lacZ/+; Gdf6+/-* embryos. This suggests that although the suture still fuses in the *Gdf6-/-; Noggin-lacZ/+* embryo, the loss of *Noggin* may also delay the fusion event. If this were the case, the suture would initially form, unlike the *Gdf6-/-* embryo, but fuse sometimes prior to E18.5.

Slight delay in coronal suture fusion in the Gdf6-/-; Noggin-lacZ/+ *embryos*

In order to determine if the suture remnants in the *Gdf6-/-; Noggin-lacZ/+* embryos were indicative of delayed suture fusion, *Gdf6+/-* and *Gdf6+/-; Noggin-lacZ/+* mice were crossed and embryos were collected at various timepoints in development. As discussed in Chapters II and III, the frontal and parietal bones in the *Gdf6-/-*embryo are fused at E14.5, at the first appearance of the ossification centers for the frontal and parietal bones (Fig 2.2 E-H), where complete fusion in the *Bmp4-lacZ/+; Gdf6+/-* compound mutant can be delayed for several days but ultimately results in a completely fused suture (Fig 3.2, 3.3).

At the E14.5 timepoint, wild-type, *Gdf6+/-* and *Noggin-lacZ/+* single heterozygotes, and *Gdf6+/-; Noggin-lacZ/+* compound mutants have normal CSs (Fig 5.2A-C). Although the *Gdf6-/-; Noggin-lacZ/+* embryo showed signs of fusion even at this earliest timepoint (Fig 5.2D), the fusion did not appear as complete as in the *Gdf6-/-* embryo (Fig 5.2E). Where the *Gdf6-/-* frontal and parietal bones appeared as a single continuous bone, the *Gdf6-/-; Noggin-lacZ/+* embryo, bones could still be distinguished, with a small bridge of ossified bone between the two (Fig 5.2D, yellow arrow). This suggests that fusion in the *Gdf6-/-; Noggin-lacZ/+* embryos may be delayed, albeit very slightly (still within the E14 day), compared to the *Gdf6-/-* embryo. Although fusion was complete by E15.5, a ridge (Fig 5.2I, yellow arrow) was observed between the fused frontal and parietal bones that is not present in the smooth single fused bone in the *Gdf6-/-* embryo (Fig 5.2J) as a sign of a previously existing suture. No unilateral fusion, like that found in the *Bmp4-lacZ/+; Gdf6+-* embryos, was observed in the *Gdf6-/-; Noggin-*

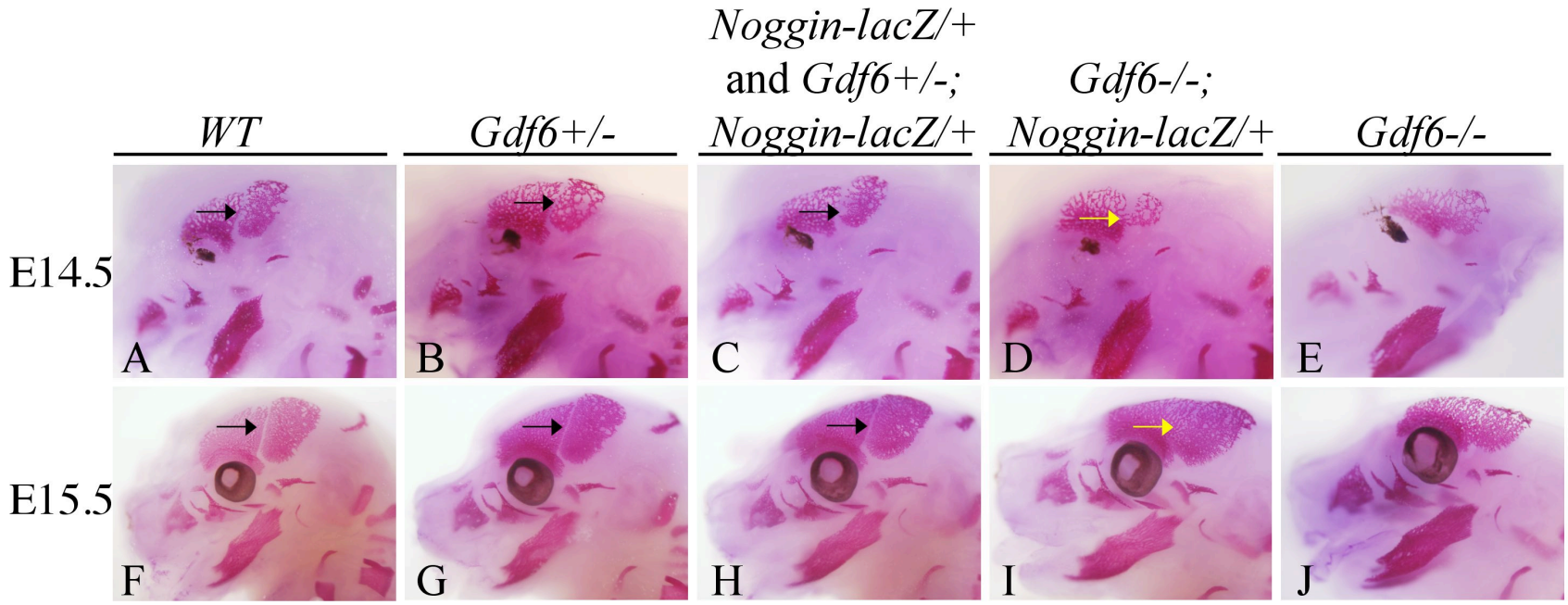

Figure 5.2. Timing of coronal suture fusion in *Gdf6/Noggin* compound mutants. At E14.5, wild-type (A), *Gdf6+/- (B)* and *Noggin-lacZ/+* and *Gdf6+/-; Noggin-lacZ/+* embryos (C) have normal coronal sutures. The *Gdf6-/-; Noggin-lacZ/+* embryo showed signs of fusion even at this earliest time-point (D, yellow arrow), but the fusion did not appear as complete as in the *Gdf6-/-* (E), suggesting that fusion in the *Gdf6-/-; Noggin-lacZ/+* embryos may be delayed, albeit very slightly (still within the E14 day), compared to the *Gdf6-/-*. Fusion was complete by E15.5 (I), a ridge was observed between the fused frontal and parietal bones (I, yellow arrow) as a sign of a previously existing suture.

lacZ/+ embryos after E14.5, despite having the same mixed background (C57BL/6J and CD1) as the *Bmp4-lacZ*/+ by *Gdf6*+/- crosses.

Noggin *expression is maintained in the E14.5 suture*

Although *Noggin* does not appear to play an important role in prenatal suture development, it is possible that there were more subtle changes in *Noggin* expression at the suture level that could contribute to the *Gdf6* craniosynostosis phenotype. Changes such as alterations in the levels or localization of *Noggin* expression may not be red staining, by utilizing the *Noggin-lacZ* line. In *Gdf6* wild-type embryos, *Noggin-lacZ* was expressed in the periosteal layer surrounding the frontal and parietal bones (Fig 5.3A), in addition to a cartilage element that underlies the suture (Fig 5.3A, B, asterix). *Noggin* appeared to be expressed at low levels within the suture mesenchyme, if at all (Fig 5.3A, arrow). *Noggin* is similarly expressed in the periosteum of the *Gdf6*+/- embryonic suture (Fig 5.3B). In the *Gdf6*-/- suture, the frontal and parietal bones are fused into a single bone, and likewise, *Noggin* is expressed continually in the periosteum across the fused portion where the suture should reside (Fig 5.3C, arrow). Other than the morphological changes cause by failed suture formation, there seems to be no difference in *Noggin* expression that correlates with the loss of *Gdf6.*

Noggin *does not play a critical role in early suture formation*

Although previous studies have reported the embryonic lethality of *Noggin* homozygous mutants occurs by E14.5, our *Gdf6* and *Noggin* crosses produced a mixed genetic background (C57BL/6J and CD1) allowing the *Noggin* homozygous mutants to

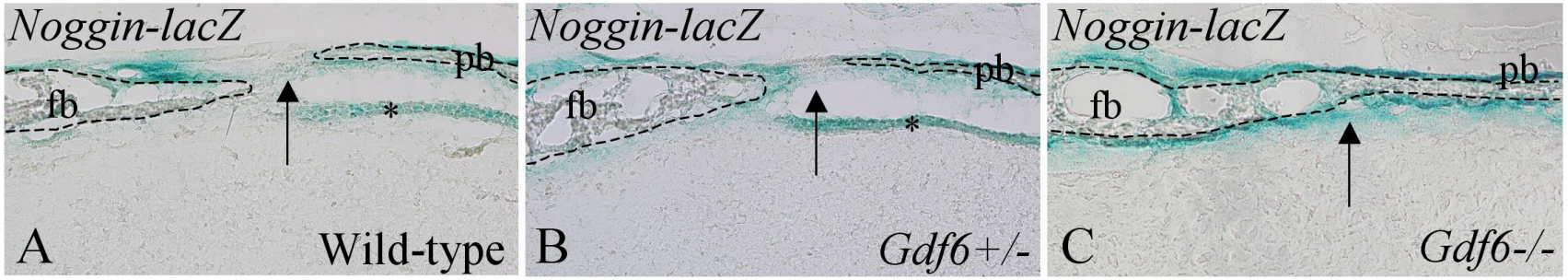

Figure 5.3. *Noggin* expression in the E14.5 *Gdf6* suture. In *Gdf6*+/+ embryos, *Noggin-lacZ* was expressed in the periosteal layer surrounding the frontal and parietal bones (A), in addition to a cartilage element that underlies the suture (A, B asterix). *Noggin* appeared to be expressed at low levels within the suture mesenchyme, if at all (A, arrow). *Noggin* is similarly expressed in the periosteum of the *Gdf6*+/- embryonic suture (B). In the *Gdf6*-/- suture, the frontal and parietal bones are fused into a single bone, and likewise, *Noggin* is expressed continually in the periosteum across the fused portion where the suture should reside (C, arrow). Fb, frontal bone; pb, parietal bone.

survive at least to E18.5. Although the CD1 strain is outbred, previously published works have described the *Noggin* homozygous mutant phenotype as highly stable on this background (Tylzanowski et al., 2006).

We observed similar phenotypes in our *Noggin* homozygous mutant embryos at E18.5 as has been previously reported (Brunet et al., 1998). The *Noggin* homozygous mutants had gross axial skeletal deformities, particularly in the vertebrae, ribs, sternae, and limbs, which were short and broad with multiple joint fusions (Fig 5.4B) compared to wild-type (Fig 5.4A). Although still deformed, the cranial vault appeared less significantly affected than the axial skeleton, although a large portion of the *Noggin-lacZ/lacZ* embryos presented with exencephaly and therefore no cranial bones or suture could be observed (Fig 5.4E). However, several *Noggin-lacZ/lacZ* embryos did have intact cranial bones. Although the bones appeared to have delayed ossification (Fig 5.4D) compared to wild-type littermates (Fig 5.4C), the cranial sutures, including the CS (Fig 5.4D, arrow) were present and readily visible. Therefore, although *Noggin* may play a critical role in the maintenance of a patent suture during adulthood, it does not appear to be required for the prenatal suture formation or maintenance.

Fusions in the carpal and tarsal bones of Gdf6/Noggin *compound mutants*

The cranial sutures are not the only anatomical location where a genetic interaction of *Gdf6* and *Noggin* could occur. To test to see if there were interactions between *Gdf6* and *Noggin* in non-cranial skeletal elements, P21 mice from the *Gdf6*+/- and *Noggin-lacZ*/+ cross were examined for abnormal skeletal phenotypes. Again, the genotyping problems caused by a *neo* cassette in both the *Gdf6* mutant and *Noggin-lacZ*

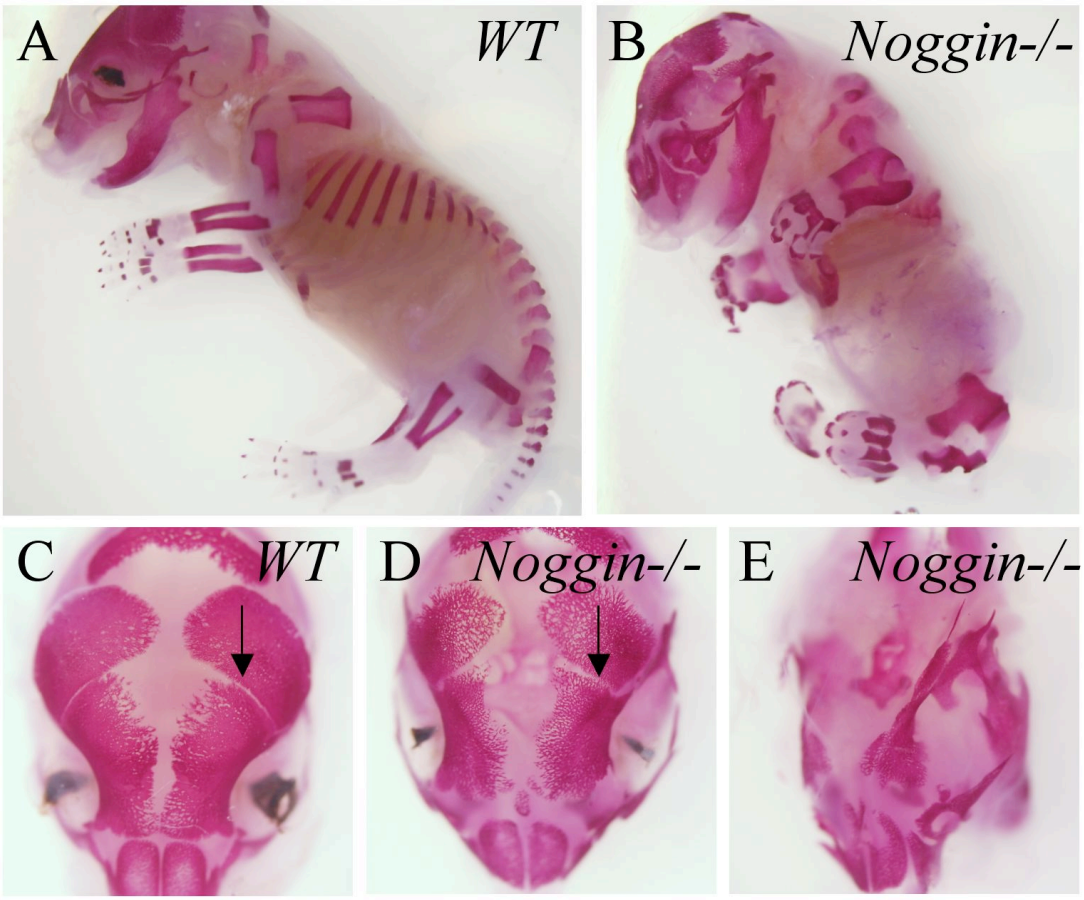

Figure 5.4. Skeletal phenotype of the Noggin homozygous mutant embryo. The *Noggin* homozygous mutant embryos had gross axial skeletal deformities, particularly in the vertebrae, ribs, sternae, and limbs, which were short and broad with multiple joint fusions (B) compared to wild-type (A). A large portion of the *Noggin-lacZ/lacZ* embryos presented with exencephaly and therefore no cranial bones or suture could be observed (E). Several *Noggin-lacZ/lacZ* embryos did have intact cranial bones with cranial sutures, including the coronal suture (D, arrow).

alleles prevented *Noggin-lacZ/+* and *Gdf6+-; Noggin-lacZ/+* mice from being distinguished. But through analysis of Mendelian ratios and previous published information on the *Noggin* phenotype, conclusions could still be drawn from the collected data.

When crossing *Gdf6+/-* and *Noggin+/-* mice to produce compound heterozygotes, limb abnormalities became evident or were exacerbated, including fusions in the carpal and tarsal bones of the wrist and ankle, a site where *Gdf6* has been previously shown to be expressed in developing joints (Settle et al., 2003). The wild-type wrist is composed of multiple articulating bones, including the metacarpals I-V, the 1, 2, 3, and 4/5 distal carpals, the central carpal bone (Fig 5.5A), the radiale and ulnare bones, and the radius and ulna. Out of a total of 31 animals analyzed from a *Gdf6+/-* and *Noggin+/-* cross, none of the wild-type animals presented with any wrist phenotype (9/9) (Fig 5.5A, Table 5.3). In the *Gdf6+/-* animals, 5/6 had fusion of the second and central carpals in at least one of the forelimbs (Fig 5.5B, Table 5.3) while 1/6 had an additional fusion of the second, third, and central carpals (Fig 5.5C, Table 5.3). In the animals that were genotyped to be either *Noggin-lacZ/+* heterozygotes or *Gdf6+/-; Noggin-lacZ/+* compound mutants, we observed unilateral or bilateral fusion of the second and central carpals in 9/16 animals (Fig 5.5B, Table 5.3) or unilateral or bilateral fusion of the second, third, and central carpals in 7/16 animals (Fig 5.5C, Table 5.3).

In the wild-type hindlimb, the bones of the ankle are composed of the metatarsals I-V, the distal tarsal bones 1-3 and 4/5, the central tarsal (Fig 5.5D), talus, and the calcaneous bones. When *Gdf6+/-* and *Noggin+/-* mice were crossed, a total of 33 animals were analyzed and ankle fusions were categorized by genotype and phenotypes

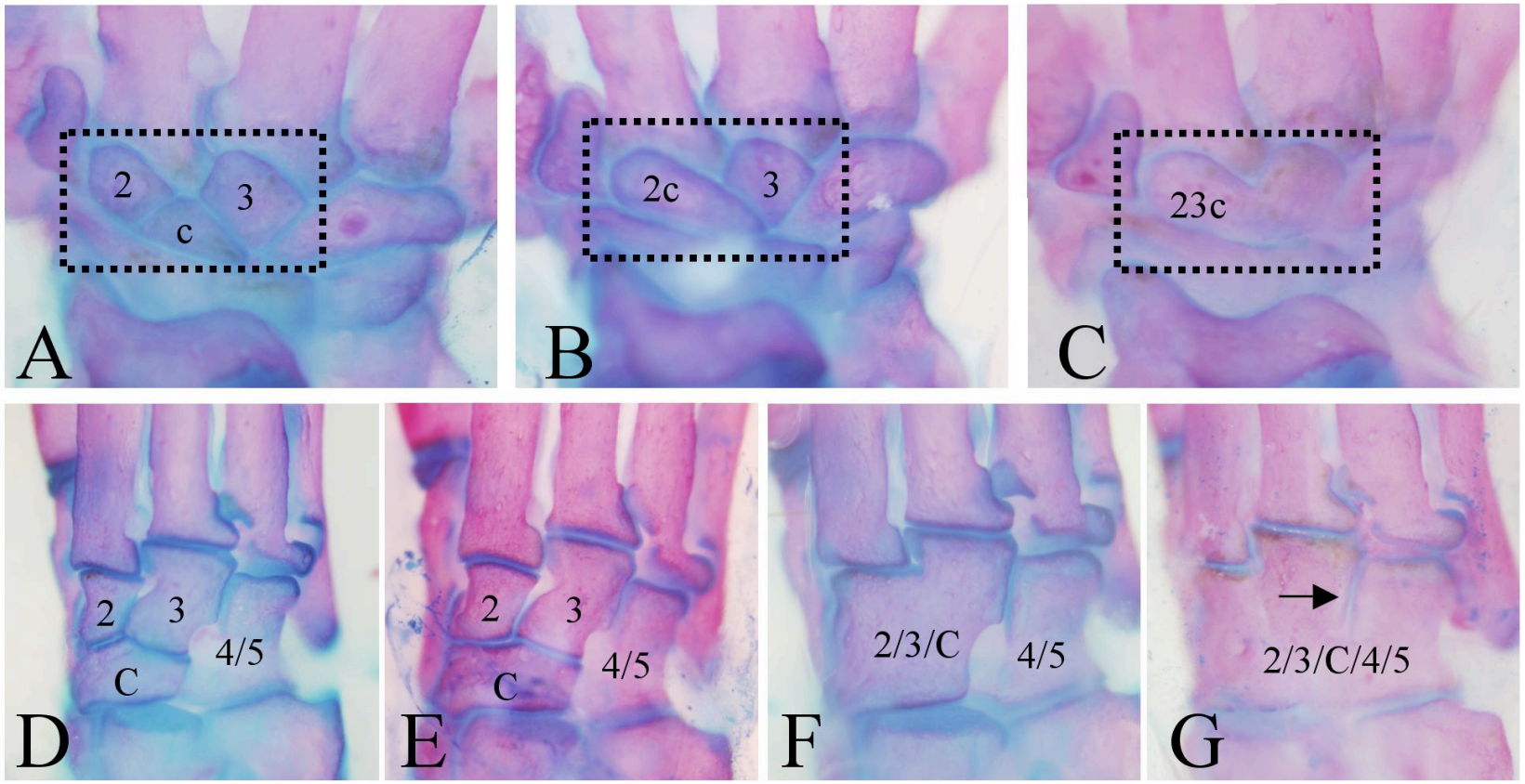

Figure 5.5. Carpal and tarsal fusions present in *Gdf6* and *Noggin* single and compound heterozygotes. A) Normal arrangement of carpals bones seen in wild-type mice, including the second. third, and central carpals. B) Fusion of the second and central carpals. C) Fusion of the second, third, and central carpals. D-E) Normal arrangement of the tarsal bones seen in wild-type (D) and *Gdf6*+/- (E) mice. F) Fusion of the second, third, and central tarsals. G) Fusion of the second, third, fourth/fifth, and central tarsals, with the persistence of a small joint between the third and fourth/fifth tarsal segments (arrow). c, central carpal; C, central tarsal.

Table 5.3. Analysis of carpal fusions in *Gdf6* and *Noggin* single and compound heterozygotes.

Genotype	Fusions (Left/Right)	Animals
Wild-type	None	9
Gdf6+/- N=6	None	1
	2c/none	4
	23c/2c	1
Noggin-lacZ/+ or *Gdf6*+/-; *Noggin-lacZ*/+ N=16	None	0
	2c/2c	8
	2c/none	1
	23c/2c	4
	23c/23c	3

Table 5.4. Analysis of tarsal fusions in *Gdf6* and *Noggin* single and compound heterozygotes.

Genotype	Fusions (Left/Right)	Animals
Wild-type	None	11
Gdf6+/- N=7	None	5
	23c/23c	1
	None	1
Noggin-lacZ/+ or *Gdf6*+/-; *Noggin-lacZ*/+ N=15	None	0
	23c/23c	6
	2345c/23c	1
	2345c/2345c	8

(Table 5.4). No ankle fusions (Fig 5.5D) were observed in the wild-type animals (11/11, Table 5.4). Most *Gdf6+/-* mice formed normal joints (Fig 5.5E), although fusion of the second, third, and central tarsals (Fig 5.5F) was rarely observed (1/6, Table 5.4). In the animals determined to be either *Noggin+/-* or *Gdf6+/-; Noggin-lacZ/+* mice, fusions of the second, third, and central tarsals were observed (Fig 5.5F) (6/16, Table 5.4) along with fusions of the second, third, fourth/fifth, and central tarsals (2345c) (Fig 5.5G) (8/16, Table 5.4) and combinations of the two fusions in the limbs of the same animal (1/16, Table 5.4). For animals in which the 2345c tarsal segments were fused, the entire central region of the ankle was a single block of bone, with only a small remnant of a joint remaining between the 3 and the 4/5 tarsal segments (Fig 5.5G, arrow).

Discussion

In this chapter, we report that *Noggin* does not play a critical role in the formation of the CS, due to the fact that *Noggin* homozygous mutant embryos do form cranial sutures, including the CS (Fig 5.4). In addressing our first and second hypotheses, the haploinsufficiency of *Noggin,* in addition to *Gdf6,* failed to alter suture phenotypes substantially in *Gdf6/Noggin* compound mutants and also failed to rescue coronal craniosynostosis in the *Gdf6*-/- embryo. This suggests that the mechanism leading to suture fusion in the *Gdf6* homozygous mutant occurs independently of *Noggin* activity in the suture.

Noggin *is not required for embryonic suture development*

There are several reasons that could explain this seemingly insignificant role of *Noggin* in early suture development. One could be the lack of expression of *Noggin* in the suture region during early suture development. Although *Noggin* expression was found in postnatal coronal and sagittal sutures (Warren et al., 2003a), no *Noggin* expression is detectable in the suture region of *Noggin-lacZ* embryos at the time when *Gdf6* and *Bmp4* are initially expressed in the frontal bone primordia at E10.5 (McMahon et al., 1998; Patel et al., 2006), but instead appears to be mostly restricted to the neural tube and caudal notochord (McMahon et al., 1998). According to lacZ expression in the *Noggin-lacZ* knock-in line at E14.5, when fusion of the ossification centers is visible in the *Gdf6-/-* embryo and beginning in the *Bmp4-lacZ/+; Gdf6+/-* embryo, *Noggin* appears to have little to no expression in the suture mesenchyme, but instead is expressed in the periosteum of the frontal and parietal bones (Fig 5.3). In the periosteum, *Noggin* could be regulating the growth of the frontal and parietal bones while not having a large role in maintaining suture patency at early developmental timepoints. In fact, multiple BMPs (*Gdf6, Bmp4)* and BMP effectors (*Msx2, Alx4, FoxC1)* are expressed in the frontal bone and/or are known to be associated with growth of the frontal bone (Maxson and Ishii, 2008), and therefore regulation of these BMPs by *Noggin* would not be unexpected. The postnatal expression of *Gdf6* in the suture region is not known, but *Bmp4* expression in the frontal bones is primarily embryonic and is downregulated after birth (Kim et al., 1998a).

Another possibility is that BMPs stimulate frontal bone growth but inhibit osteogenic differentiation in the suture. In Chapter II, we showed that reduced *Gdf6*

resulted in increased differentiation (Fig 2.5), and the same in Chapter III, with the reduction of both *Gdf6* and *Bmp4* leading to suture mesenchyme differentiation (Fig 3.4). However, the additive reduction of *Gdf6* and *Bmp4* in the *Bmp4-lacZ/+; Gdf6-/-* embryo does result in delayed ossification of the frontal bones (Fig 3.3). The effect of BMP signaling on the development of the cranial sutures might depend on the identity of the suture and the developmental stage. During embryonic development, reduced BMP signaling may promote synostosis while in postnatal stages reduced BMP signaling promotes an open and patent suture (Maxson and Ishii, 2008), and therefore postnatal loss or haploinsufficiency of *Noggin* during embryonic development may not have a phenotypic effect on the suture at that stage. Indeed, in most of the studies in which application of Noggin protein prevented suture fusion, the protein was applied ectopically and at postnatal stages (Shen et al., 2009b; Warren et al., 2003a). Interestingly, application of Noggin protein was able to prevent post-operative refusion of the CS in a rabbit craniosynostosis model (Cooper et al., 2007), but was unable to prevent the initial craniosynostosis event (Cray et al., 2011). This data together suggests that *Noggin* may not play a large role in the craniosynostosis phenotype, but a large role in bone wound healing, and the events that occur in the posterior interfrontal suture may not be indicative of all synostosis events.

Interaction of Gdf6 *and* Noggin *in carpal and tarsal joint formation*

Since *Noggin* is an antagonist of BMP signaling, the loss of *Noggin* should result in a global increase in BMP signaling. Indeed there are widespread skeletal defects in the *Noggin* homozygous mutant with the severity increasing caudally (Fig 5.4). The limbs

are short but broadened with fusions of the elbows and digit joints. The loss of joints in the *Noggin-/-* embryo correlates with failed upregulation of *Gdf5* in early joint development, suggesting a failure of joint specification, not a secondary fusion event (Brunet et al., 1998). The *Gdf6* homozygous mutant mouse also has multiple joint associated defects, including fusions in the carpal and tarsal joints (Settle et al., 2001). These joints generally form large precursors that subdivide into individual skeletal elements, but in the *Gdf6-/-* mouse the precursors fail to divide at sites of fusion. *Gdf5* specifies only a subset of the joints affected in the *Noggin* homozygous mutants, and therefore other genes are likely involved, such as fellow family member *Gdf6*. We were confident that a number of defects would be apparent in *Gdf6/Noggin* compound mutants, particularly in the limb.

Despite the severe skeletal defects present in the *Noggin* homozygous mutant embryo, the *Noggin* heterozygous mutant presents with more subtle phenotypes. Previous reports have described carpal and tarsal fusions in 100% of the animals examined, on three different background strains (CD1, Dba/1, and C57BL/6J) (Tylzanowski et al., 2006). These included fusions of the second, third, and central carpals (23c) or fusions of the third and central carpals (3c) (Tylzanowski et al., 2006). Previous work demonstrated that the *Gdf6* homozygous mutant mouse also presents with 23c carpal fusions (Settle et al., 2003), with no fusions present in the *Gdf6+/-* mice. We found slightly different results in our cross, with 5/6 *Gdf6+/-* mice having fusions of the second and central carpals (2c). These differences are likely attributed to differences in background. In the initial description of the *Gdf6* mutant phenotype, the mice were on a mixed 129/SvJ and C57BL/6J background (Settle et al., 2003), where the mice we

analyzed had been backcrossed onto a C57BL/6J line for more than 10 generations and then crossed to the *Noggin-lacZ* line, which is on the outbred CD1 background. It is possible that some protective alleles found in the 129/SvJ background were eliminated in our crosses.

Although we could not tell the difference between *Noggin-lacZ/+* and *Gdf6+/-; Noggin-lacZ/+* mice, Mendelian ratios would suggest that the 2c fusions were the *Noggin-lacZ/+* single heterozygotes (9/31), and the more severe 23c fusions were the *Gdf6+/-; Noggin-lacZ/+* compound mutants (7/31). While the haploinsufficiency of *Noggin* produced the similar 23c carpal fusion as the *Gdf6-/-* mouse (Settle et al., 2003), the ankle fusions were distinct. The *Gdf6-/-* mouse presents with fusion of the second and third tarsals (23) and fusion of the central tarsal and the talus (Settle et al., 2003). Previously reported work has described 23c tarsal fusion in the *Noggin* heterozygote (Tylzanowski et al., 2006). Although our study cannot distinguish between the *Noggin-lacZ/+* single heterozygotes and the *Gdf6+/-; Noggin-lacZ/+* compound mutants, the incidence of 23c tarsal fusion phenotype in our sample (6/16) is close to Mendelian ratios and likely present in only the *Noggin* heterozygotes (Table 5.4). The most extensive fusion of the second, third, fourth/fifth and central tarsals (2345c) is likely present in the *Gdf6+/-; Noggin-lacZ/+* compound mutants. The 2345c fusion in the compound mutants differs from the *Gdf6-/-* phenotype in that it includes the 4/5 tarsal segment, but excludes fusion with the talus. As mentioned above, the loss of the carpals and tarsal joints in the *Noggin* heterozygote has been attributed to the loss of *Gdf5* in the presumptive joints (Brunet et al., 1998; Tylzanowski et al., 2006). In fact, the *Gdf6+/-; Noggin-lacZ* phenotype more closely resembles the phenotype seen in the *Gdf5-/-* mouse, with failed

joint formation in the distal tarsals, producing a single large block of bone in the ankle (Settle et al., 2001).

In mice with 2/3/C/4/5 ankle fusion, predicted *Gdf6/Noggin* compound mutants, we observed a "T-shaped" joint remaining at the border between the third and fourth/fifth tarsal bones (Fig 5.5G, arrow). Interestingly, previous work also described a similar joint remaining in the fusion of the second, third, and central carpals at a site of known *Gdf5* expression (Tylzanowski et al., 2006). The authors attribute this to the persistence of a *Gdf5* expression. However, this joint is also a site of *Gdf6* expression, and therefore, it is equally likely that additive expression of *Gdf5* with *Gdf6* is able to compensate for one another. We also observed a similar "T-shaped" joint in the *Gdf6+/-; Noggin-lacZ/+* compound mutants between the third and fourth/fifth tarsals, where *Gdf6* and *Gdf5* are expressed at low levels, if at all (Settle et al., 2003). It is likely that with the complex expression of BMPs in the developing limb, there is some redundancy and compensation that allows specific joints or parts of joints to form.

Gdf6 *and* Noggin *likely interact in the formation of the middle ear bones*

Due to the profound role of BMPs in bone and joint formation, it is surprising that so few skeletal phenotypes were found in the *Noggin-lacZ/+* single heterozygote and our *Gdf6+/-; Noggin-lacZ/+* compound mutants. In our *Bmp4-lacZ/+* and *Gdf6+/-* crosses in Chapter IV, no fusions were observed in bones of the limbs (not shown). The *Gdf6-/-* mouse additionally has defects in the bones of the middle ear, the malleus, incus, and stapes, with changes in the shape of the articular surfaces and increased distances between the bones. This was thought to be caused by reduced cartilage growth and

proliferation at the articular surfaces (Settle et al., 2001). Klippel-Feil syndrome, a genetic disorder mapped to a paracentric inversion downstream of GDF6, is often characterized by conductive hearing loss (Tassabehji et al., 2008). Although *Noggin* does not appear to play a large role in prenatal suture development, *Noggin* haploinsufficiency has been reported to produce multiple abnormalities in humans, including symphalangism, multiple synostosis syndrome, and tarsal and carpal coalition syndrome (Tylzanowski et al., 2006). Several of these conditions are associated with missense mutations in *Noggin*, and like the *Noggin* heterozygous mice, are characterized by carpal and tarsal bone fusions, in addition to conductive hearing loss (Gong et al., 1999). On some genetic backgrounds, the *Noggin* heterozygote mouse had conductive hearing loss, caused by excess bone formation in the stapes (Hwang and Wu, 2008). This was attributed to chondrocyte hyperplasia from unregulated BMP signaling. We saw no evidence of a stapes malformation in our *Noggin-lacZ/+* single heterozygotes or *Gdf6+/-; Noggin-lacZ/+* mice (not shown), however our crosses were performed on a mixed C57BL/6J and CD1 background. *Noggin+/-* mice with conductive hearing loss were reported on a congenic C57BL/6J background but this phenotype was not reported when on a mixed C57BL/6J;FVB background (Hwang and Wu, 2008). In addition to *Gdf6*, *Bmp4, Bmp2,* and *Bmp7* are also expressed in the mesenchyme surrounding each bone of the middle ear (Hwang and Wu, 2008; Settle et al., 2001), and therefore the likely contribution of *Gdf6* and other BMPs in the development of the middle ear bones cannot be overlooked.

Activity of Gdf5 *in the joints of the limb resembles the activity of* Gdf6 *in the coronal suture*

In many ways the activity of *Bmp4* and *Gdf6* in the development of the CS seem contradictory. BMPs are known for their ability to induce bone formation, but the loss of these two genes leads to bone formation across the suture mesenchyme. Although *Noggin* was a good candidate for an intermediate factor in connecting BMP signaling to inhibited differentiation of the suture mesenchyme, in this chapter we demonstrated that *Noggin* does not play a role in embryonic suture development. Therefore, there are likely other unidentified secondary factors involved in the *Gdf6*- and *Bmp4*-mediated craniosynostosis phenotype.

The paradoxical role of *Gdf6* in suture development in many ways mirrors the role of the Gdf subfamily members in the limb. *Gdf5* is one of the earliest markers for joint development and thus was an early candidate as a repressor of the normal cartilage growth process (Storm et al., 1994). However, beads soaked in Gdf5 protein embedded into chick limbs in culture were found to stimulate the growth and differentiation of existing cartilage and localized fusion of joints (Storm and Kingsley, 1999), despite the fact that *Gdf5-/-* mice present with joint fusions (Storm and Kingsley, 1996). Therefore, Gdf5 cannot directly induce joint formation, but instead has chondrogenic roles and likely an indirect role in joint formation *in vivo*. Likewise in our studies, beads soaked in Gdf6 protein actually stimulated osteogenic differentiation when implanted into the frontal bone, even though the loss of *Gdf6* increases differentiation in the suture mesenchyme (Fig 2.11). In both the sutures and the limb, the seemingly contradictory functions could be attributed to different ligand concentrations, the localized expression of receptors or BMP antagonists, or the formation of heterodimers with other members of

the BMP family. The CS is a relatively simple system of study, with a defined set of tissues involved in the formation and maintenance of the suture structure and also a limited group of known genes to be involved in the signaling events. Thus, the suture may serve as a useful model in studying the complex activity and interaction of BMPs outside of simple osteogenic induction.

CHAPTER VI

CONCLUSION

Future Directions

In this body of work we have demonstrated a role of *Gdf6* (and *Bmp4)* in inhibiting premature differentiation of the CS mesenchyme. Although we addressed questions regarding the developmental timing of suture fusion and the underlying mechanism, many questions still remain: Are mutations in *Gdf6* found in human craniosynostosis patients? How does Gdf6 inhibit suture differentiation? What additional factors are involved in the Gdf6 signaling pathway? How does *Gdf6* interact with other pathways in the suture? Is *Gdf6* autoregulated? And are there regulatory elements driving *Gdf6* expression in the suture?

Are mutations in Gdf6 *found in human craniosynostosis patients?*

Despite the severity of the craniosynostosis phenotype in the *Gdf6* mutant mouse, *Gdf6* has not yet been implicated as a craniosynostosis-associated gene in humans. Preliminary work in sequencing *Gdf6* failed to identify mutations in humans with coronal craniosynostosis (David Kingsley, Max Muenke, and Simeon Boyd, personal correspondence). This could be attributed to the fact that CS fusion was only observed in *Gdf6-/-* mice, not in heterozygotes, making it a recessive and undoubtedly rare genotype in humans. However, a common theme in the BMP field is that mutations in BMPs that are often recessive in mice are dominant in humans (Ducy and Karsenty, 2000).

Therefore, mutations in the coding region of the *Gdf6* gene could explain some human craniosynostosis cases in which the etiology is still unknown. Furthermore, mutations in *Gdf6* could be one of several genes that contribute to a polygenic phenotype.

In the heterogeneous descriptions of Klippel-Feil Syndrome, which was mapped to a paracentric inversion downstream of *Gdf6,* some patients were reported to have microcephaly (Tassabehji et al., 2008). However, the presence or absence of craniosynostosis was not reported. Currently, the only connection between *Gdf6* and human craniosynostosis is a condition called Nablus mask-like facial syndrome, characterized by tight glistening facial skin, flat and broad nose, and a frontal upsweep of hair (Salpietro et al., 2003). Some patients also report digit defects, including short toes, clinodactyly, and a wide interdigit gap (Salpietro et al., 2003). In all the reported Nablus patients, the condition was mapped to a microdeletion in 8q21-22, where several genes are located, including *Gdf6* (Raas-Rothschild et al., 2009). However, only two of the patients had a deletion that included the *Gdf6* locus (Fig 6.1). Interestingly, one of these two patients had coronal craniosynostosis (Salpietro et al., 2003), a feature not found in Nablus patients where the deletion did not include *Gdf6*. Although the deletion is heterozygous, it is possible that the haploinsufficiency of *Gdf6* is particularly penetrant in human craniosynostosis.

A future goal of this project could be to search for *Gdf6* mutations in patients with craniosynostosis. Vanderbilt currently has a running DNA Databank called "BioVU", a repository of DNA samples extracted from patient blood samples that are available for Vanderbilt researchers. The samples are connected to the patient's medical record, but with de-identified information. Patients with non-syndromic craniosynostosis could be

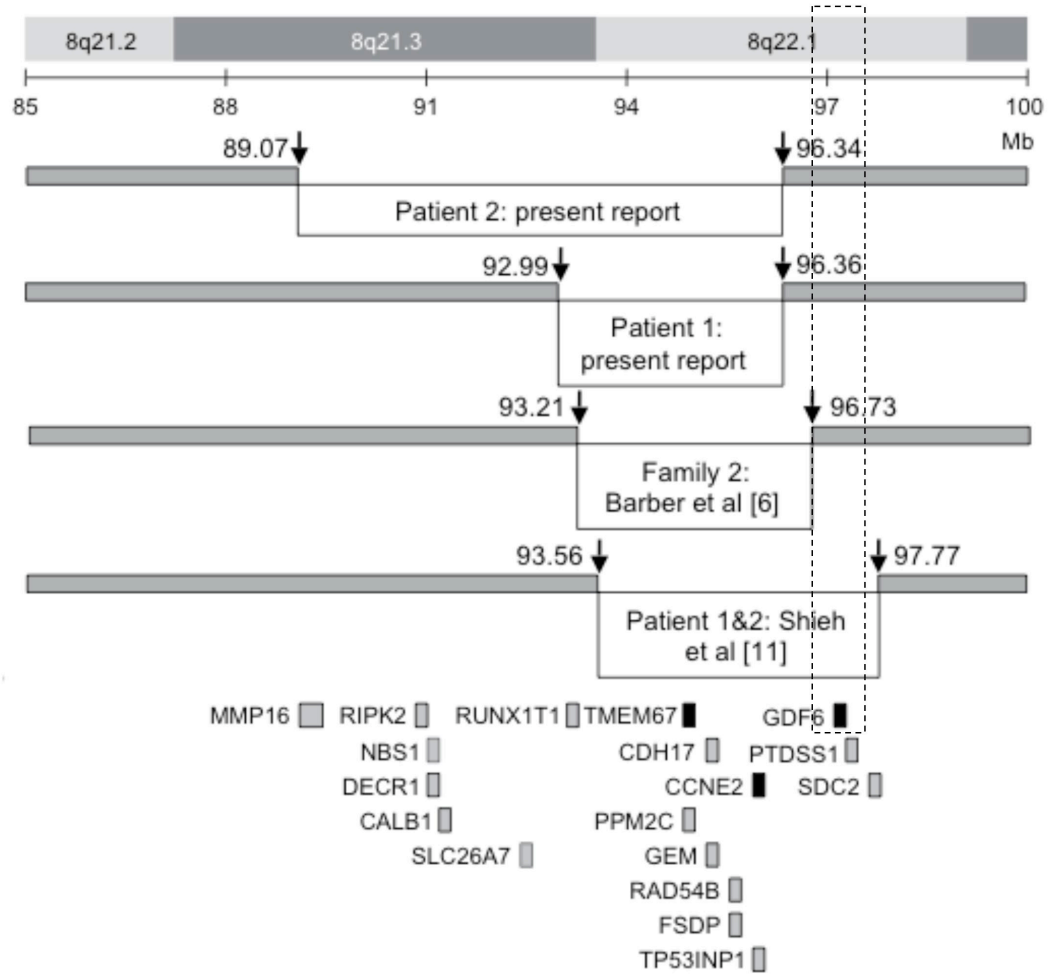

Figure 6.1. Genomic microdeletions of Nablus mask-like facial syndrome. Mapping of microdeletion in patients with Nablus mask-like facial syndrome. Patients 1&2 reported by Shieh et al. 2006 mapped the deletion to include the coding region for *Gdf6*. One of these two patients presented with coronal craniosynostosis. The red box denotes the region unique to these two patients.

Adapted from Raas-Rothschild et al 2009.

selected for targeted sequencing of *Gdf6* (and *Bmp4)*. Although known human *Gdf6* mutations are rare, it is possible that as an understudied member of the BMP family, the contribution of *Gdf6* to human disease has simply been overlooked.

Craniosynostosis is generally not diagnosed until infancy, with the appearance of a dysmorphic cranial shape. Furthermore, the majority of human cases are spontaneous, with no known family history. Therefore, in utero screening for craniosynostosis is not practical. However, identifying craniosynostosis-associated mutations in *Gdf6* can be useful as a diagnostic tool and provide insight and understanding to patients and their families.

With approximately 70% of craniosynostosis cases having no known etiology, this leaves much room for the identification of more craniosynostosis-associated genes. In addition to *Gdf6* and *Bmp4*, mutations in other members of the BMP family (e.g. *Bmp2*), BMP receptors, Smad proteins, and downstream effectors of BMP signaling may all contribute to premature fusion of a suture. In Chapters III and V we described some variation in the craniosynostosis phenotype in embryos from a mixed genetic background, suggesting the presence of modifier genes. These modifiers could affect the severity and penetrance of suture fusion. Using an unbiased approached to identify craniosynostosis genes, such as whole-exome sequencing of coronal craniosynostosis patients, could highlight some of these identified genetic interactions.

How does Gdf6 *inhibit suture differentiation?*

What tissues receive Gdf6 signal? In Chapter II we showed expression of *Gdf6* mRNA in the frontal bone primordia at E10.5-E12.5. However, Gdf6 is a secreted

signaling protein, and although it is expressed in the frontal bone primordia, several different tissues could be receiving a Gdf6 paracrine signal. These may include not only the suture mesenchyme, but also the parietal bone rudiment or periosteum. Perhaps partly due to the high homology between BMP family members (members of Gdf subfamily have almost 100% homology in the mature region), we were unable to find a commercially available Gdf6 antibody that functioned reliably in immunohistochemical approaches.

If the question of which cells receive Gdf6 signal cannot be address through Gdf6 protein localization, the answer could be addressed indirectly. One way to approach this question is through the examination of phospho-Smad 1/5/8. Binding of BMPs ligands to Type I and Type II receptors activate Smads 1/5/8, which translocate to the nucleus to activate a set of target genes (Ducy and Karsenty, 2000). By comparing the localization and levels of phospho-Smad in the suture region between wild-type and *Gdf6* mutant embryos, one could infer whether the suture mesenchyme is directly receiving a Gdf6 signal, or if the suture fusion is a secondary results of a frontal bone defect. This would also address the question of whether the increased differentiation of the suture mesenchyme in *Gdf6*-/- and *Bmp4/Gdf6* compound mutants is due to increased BMP osteogenic signals in the suture mesenchyme.

BMPs do signal through a non-canonical Smad-independent pathway (p38 mitogen-activated protein kinase (MAPK)). BMP receptors activate a downstream pathway that includes the adaptor protein XIAP, TAB1 (TAK1 binding protein), TAK1 (TGF-β activated kinase 1), and the p38/Jnk pathway (Botchkarev, 2003). Studies show that BMP-2 bonded to pre-formed receptors complexes activated the Smad pathway.

However, when BMP-2 induced the recruitment of receptors the p38 MAPK pathway was activated (Nohe et al., 2002). Bmp4 also activated the MAPK pathway in lymphocytes (Fiori et al., 2006). To address the possibility of non-canonical BMP signaling, the localization of phospho-p38 could also be examined.

We mentioned the possibility that premature suture fusion is a secondary affect of a frontal bone defect. Although *Gdf6* is only expressed in the frontal bone primordia, *Bmp4* is also expressed in the dura and suture mesenchyme. Due to the different origins of the frontal bone (neural crest) and the suture mesenchyme and parietal bones (mesoderm), Cre-drivers could be utilized to eliminate *Gdf6* and/or *Bmp4* in specific sub-structures of the suture. Although a Cre-loxP allele for *Gdf6* would have to be generated, Cre-drivers for the neural crest (*Wnt1-Cre*) (Danielian et al., 1998) and mesoderm (*Mesp1*) (Yoshida et al., 2008) and a conditional allele for *Bmp4* (*Bmp4-loxP*) (Jiao et al., 2003) are already available. Similar studies are reported with *Bmp4*. The conditional deletion of *Bmp4* in the neural crest through *Wnt1-Cre* produced a frontal bone defect (Maxson and Ishii, 2008), but no effect on the suture was reported. This could be due to the fact that the CS mesenchyme is mesoderm-derived, and therefore some *Bmp4* expression would be maintained in the suture region. The lack of a suture abnormality with the conditional deletion of *Bmp4* might also be attributed to compensation by *Gdf6.* Conditionally deleting combinations of *Gdf6* and *Bmp4* could further clarify their interaction.

Although we have demonstrated a genetic interaction between *Gdf6* and *Bmp4* in suture development, what is the nature of this interaction? Bmp4 and Gdf6 do share type I (Bmpr1a and Bmpr1b) and type II (BmprII and AcvrIIa) receptors (Mazerbourg et al.,

2005), although which receptors are expressed in the suture region, where, when, and in what combination has not been explored. We have already initiated some preliminary work on this question by designing *in situ* hybridization RNA probes specific for each of the shared type I and type II receptors (the design information for *Bmpr1b* and *BmprII* is described in Appendix B and demonstrated in the dorsal retina in Figure 4.7). Information on the localization of the BMP receptors in the suture region would also provide mechanistic insight, such as which tissues are competent to receive BMP signals at the timepoints when *Gdf6* and *Bmp4* are co-expressed (E10.5-E12.5).

Although no suture defects are reported in homozygous mutants for *Bmpr1b* and *AcvrIIa*, mutants for *Bmpr1a* and *BmprII* are embryonic lethal. Using Cre-drivers specific for neural crest or mesoderm-derived tissue (e.g. *Wnt1* and *Mesp1*) could be used to conditionally delete the BMP receptors or combination of the receptors from the suture region in order to identify those critical to suture development.

The signaling properties of Gdf6 might also be dependent upon the assembly of receptor complexes. Studies demonstrate that different signals can be transduced depending on whether the receptor complexes are pre-formed or assembled upon binding of the ligand, and furthermore, which receptor (type I or type II) does the ligand bind to first (Nickel et al., 2009). Gdf6 can bind multiple type I (Bmpr1a and Bmpr1b) and type II (BmprII and AcvrIIa), providing yet more complexity to the signaling pathway (Mazerbourg et al., 2005). This complexity might explain some the anti-osteogenic activity of Gdf6 in the suture mesenchyme versus the pro-osteogenic activity in the frontal bone. More information on the receptor usage in the suture region might shed some light on how Gdf6 functions in the suture region.

Do Gdf6 and Bmp4 form heterodimers? In Chapter III, we reported an interaction between *Gdf6* and *Bmp4* in the development of the CS. Bead implantation experiments involving Gdf6 (Chapter II) and Bmp4 (Kim et al., 1998b) showed an increase in differentiation and proliferation of the frontal bone, which is difficult to explain in the light of the increased differentiation of the suture mesenchyme we observed in our *Gdf6-/-* and *Bmp4-lacZ/+; Gdf6+/-* sutures. Another possible explanation for these different functions is that Gdf6 and Bmp4 form heterodimers. BMP homodimers and heterodimers can have different potencies and functions (Butler and Dodd, 2003). In the case of Twist1, the ratio of Twist1 homodimers to Twist1/E-protein heterodimers affects the patency of the suture mesenchyme (Connerney et al., 2006). It is known that Gdf6 forms heterodimers with Bmp2 in *Xenopus* (Chang and Hemmati-Brivanlou, 1999), and given the high homology between Bmp2 and Bmp4, it would not be surprising if Gdf6 was able to form heterodimers with Bmp4.

First, do Gdf6 and Bmp4 form heterodimers? A strategy that could be used to answer this question would be to express cDNAs encoding epitope-tagged versions of Gdf6 and Bmp4 in cells. Supernatants from transfected cells would then be analyzed for the presence of heterodimers through immunoprecipitation. If heterodimers were present, antibodies specific for Bmp4 would pull out both Bmp4 and Gdf6, which could be confirmed through western blot analysis. This was the strategy used to demonstrate that Gdf7 and Bmp7 form heterodimers (Butler and Dodd, 2003) and that Gdf6 and Bmp2 form heterodimers (Chang and Hemmati-Brivanlou, 1999). A similar strategy could be employed *in vivo* by injecting tagged Gdf6 RNA into a zebrafish embryo and test for a Gdf6-Bmp4 protein interaction by co-immunoprecipitation. Additional *in vivo*

techniques that could be utilized include FRET (Fluorescence Resonance Energy Transfer) and yeast two-hybrid.

Second, do Bmp4/Gdf6 heterodimers have a different activity than the homodimers? To test this, we would require purified Bmp4/Gdf6 heterodimers. One strategy to obtain purified heterodimers is to take supernatant from cells expressing recombinant Gdf6 and Bmp4 protein, each with a different epitope tag, and run it through sequential affinity columns specific for each tag. This would enable isolation of the heterodimers while eliminating the homodimers.

In our bead implantation studies, Gdf6 protein was able to stimulate ALP activity in the frontal bone primordia, however, Gdf6 alone is a poor inducer of osteogenesis (Bobacz et al., 2006). This opens the possibility that Bmp4/Gdf6 heterodimers could be more osteogenic than Gdf6 homodimers. Homodimer and heterodimer functions could be tested in osteoblast cell lines or primary calvaria cells, comparing their ability to induce matrix formation. Additionally, a bead implantation experiment, as described in Chapter II, could be carried out to examine the ability of Gdf6 and Bmp4 homodimers to promote frontal bone differentiation, through the analysis of bone differentiation markers ALP*, Runx2,* or *Bsp*, compared to differentiation in beads treated with Gdf6/Bmp4 heterodimers. To test our hypothesis that Gdf6 had context-dependent activity, additional implantations could be carried out with beads implanted into the suture mesenchyme and parietal bone primordia.

If Bmp4/Gdf6 heterodimers do have a different function from the homodimers, why does this occur? Are signaling cascades affected by which member of the dimer binds first? Do the heterodimers have different association, disassociation, degradation,

or diffusion rates from the monomers? These are all issues that might impact the activity of Gdf6/Bmp4 homodimers versus heterodimers and could be addressed in future studies.

What additional factors are involved in the Gdf6 pathway?

What are the downstream targets of Gdf6 signaling? Despite the large amount of research on members of the BMP family, the set of target genes activated by their signaling is still largely unknown. Changes in the expression of candidate genes in the *Gdf6-/-* embryo could be assessed through *in situ* hybridization or quantitative real-time PCR, although this would be restricting the study to known craniosynostosis genes (*FGFRs, Twist1, Msx2*, etc) or bone-related genes (*osterix, osteocalcin, bone sialo-protein*). Expanding the study to a large-scale analysis would allow for the detection of novel interactions or understudied genes, and thereby provide a clearer picture of the mechanism of Gdf6 signaling.

One approach that could be used is laser capture microdissection. In this methodology, *Gdf6* mice could be crossed to a reporter mouse line with fluorescently labeled tissues. In our case, we could again utilize the *Wnt1-Cre* (Danielian et al., 1998) and *R26R-YFP* lines (Srinivas et al., 2001) to fluorescently label derivatives of the neural crest, including the frontal bone primordia. We have previously performed crosses utilizing the *GNZ* (Stoller et al., 2008) line, a modified *R26R* allele with nuclear-localized *GFP* expression. However, this line failed to generate the fluorescent intensity necessary for histological analysis. Therefore, the more robust *R26R-YFP* line (Srinivas et al., 2001) would be better suited for this study. The *R26R-YFP* and *Wnt1-Cre* lines would be

crossed to the *Gdf6* mutant line in order to compare the differences in gene expression between wild-type, *Gdf6*+/-, and *Gdf6*-/- embryos.

At E12.5 in mice, the frontal bone primordia is still present but the suture mesenchyme is also its own distinct population of cells. In embryo sections, the frontal bone would be highlighted by fluorescence. Laser capture microdissection would be used to isolate cells from frontal bone or the adjacent suture mesenchyme from the sectioned material. Total RNA would be isolated from the microdissected tissue and converted to cDNA. To identify differentially expressed genes between the *Gdf6* genotypes, we could use high-throughput whole-transcriptome sequencing, also referred to a RNA-Seq (Mortazavi et al., 2008). This procedure would allow us to identify not only genes up or downregulated in the *Gdf6*-/- embryo compared to wild-type, but also differences in the frontal bone compared to the parietal.

We could also investigate the downstream activators of Gdf6 signaling through the Smad proteins, which transduce the signal to the nucleus. ChIP-sequencing could be used to compare sites of pSmad binding between untreated calvarial cells to those treated with Gdf6 protein, or even calvaria cells isolated from wild-type and *Gdf6*-/- embryos. This would highlight specific pathways and provide strong clues to the mechanisms of coronal craniosynostosis in the *Gdf6*-/- mouse.

Does Gdf6 interact with other BMP antagonists? In Chapter V we explored the possible interaction between *Gdf6* and the BMP antagonist *Noggin*. *Noggin* was a likely candidate for an interaction due to an important role in postnatal suture maintenance and the periosteal expression in embryonic cranial bones. However, *Noggin* is just one of the many antagonists of BMP signaling, which also include Cerbarus, Dan, Gremlin, and

Chordin (Yanagita, 2005). Mutant mice for Gremlin (Khokha et al., 2003), Dan (Dionne et al., 2001), and Cerbarus (Simpson et al., 1999) were generated but have no described cranial defects. Although Dan is an inefficient antagonist of BMP-2/4 signaling, an interaction between Dan and GDF-5 was demonstrated in frogs (Dionne et al., 2001). There is also a mouse mutant for Chordin, and although the mice do not have coronal craniosynostosis, they do have microcephaly (Bachiller et al., 2003). The expression of these BMP antagonists in the suture region or potential function in suture development is not reported. Although we saw no interaction between *Gdf6* and *Noggin*, it is possible that other BMP antagonists that are important in embryonic suture development.

How does Gdf6 *interact with other pathways in the suture?*

The complex signaling at the suture involves multiple pathways, including BMP, FGF, and WNT, and there is much evidences for indirect interactions between the pathways. Therefore, the suture defect in the *Gdf6-/-* mouse could be produced or exacerbated by affecting signaling in other pathways. Here are some examples of interactions between BMP and other pathways. *Msx2* and *Alx4* are downstream effectors of BMP signaling, and like *Gdf6,* they affect the proliferation and differentiation of the frontal bone (Antonopoulou et al., 2004; Ishii et al., 2003). *Msx2* and *Alx4* feed into the FGF pathways by affecting the expression of the FGFRs. We performed some preliminary work looking at the expression of *FGFR3* in *Gdf6* mutants and saw some evidence of increased *FGFR3* in the *Gdf6-/-* suture (not shown). Gain of function mutations in *FGFR3* are associated with premature suture fusion through increases in differentiation and proliferation at the bone fronts. BMPs also enhance FGF response in

the bone fronts through *Twist1*. Furthermore, the formation of Twist1 homodimers and heterodimers is affected by BMP signaling, and alterations in the ration of homodimers to heterodimers can generate a fused suture (Connerney et al., 2006). *Axin-2*, an inhibitor of the WNT pathway, promotes osteogenic differentiation in a positive feedback loop with BMPs (Liu et al., 2007). Examination of the affects of *Gdf6* on the expression of other members of these pathways would not only further the understanding of signaling in the suture but also the general interaction of multiple pathways.

Is Gdf6 *expression autoregulated?*

From *in situ* hybridization data presented in Chapter II, we suggested that *Gdf6* expression is autoregulated. In the frontal bone and brachial arches expression there appears to be a negative feedback mechanism with a positive feedback mechanism in the dorsal retina. What is causing these tissue-specific differences? Since Gdf6 is a secreted signaling factor, secondary factors must be modulating this autoregulation at the transcriptional level.

Gdf6 expression is driven by long-distance regulatory elements (Mortlock et al., 2003). Are some regulatory elements silenced in specific tissues? Or is tissue specificity affected by what transcription factors are present in that tissue? Such questions could be explored using ChIP (to determine what transcription factors bind to tissue-specific regulatory elements) or ChIP-ChIP (to determine if the chromatin in the region of the regulatory element is in an open and active conformation).

Does long-distance regulation affect Gdf6 *suture expression?*

Is there an enhancer driving *Gdf6* expression in the frontal bone rudiment? Like many members of the BMP family, *Gdf6* is flanked by a large gene desert that contains multiple distant non-coding *cis*-regulatory elements (Mortlock et al., 2003). Using overlapping Bacterial Artificial Chromosomes (BACs) in conjunction with a *lacZ* reporter, approximately 280 kilobases of the *Gdf6* locus was divided into five regulatory regions and tested for their ability to drive expression of the reporter in regions where *Gdf6* is expressed. These BAC lines were able to drive expression of *lacZ* in eleven anatomical sites, including the digit tips, whisker buds, dorsal retina, elbow joints, and larynx in mice (Fig 6.2A) (Mortlock et al., 2003).

One of these five BACs tested, referred to as D-βgeo or 125L11, drove expression of the *lacZ* reporter in ectoderm overlying the parietal bone at E9.5 (not shown) and E10.5 (Fig 6.2B, arrow). This is the same timepoint as *Gdf6* expression in the frontal bone primordia. Because the BACs are overlapping, this narrows down the area in which the regulatory element resides to an approximately 60 kb region 3' of the *Gdf6* coding region (Fig 6.2A, red box). Although expression of *Gdf6* in the parietal ectoderm was not detected through *in situ* hybridization studies, the *lacZ* reporter in the BAC construct may have the ability to highlight sites of low-level gene expression that cannot be detected through *in situ* analysis. Reduced Gdf6 signaling from the ectoderm to the underlying parietal bone rudiment and could contribute to the delay in parietal bone differentiation we observed in the *Gdf6-/-* embryos in Chapter II.

Regions of the *Gdf6* gene desert analyzed through BAC transgenic mice failed to drive expression of lacZ in the frontal bone or the suture mesenchyme. However, not all

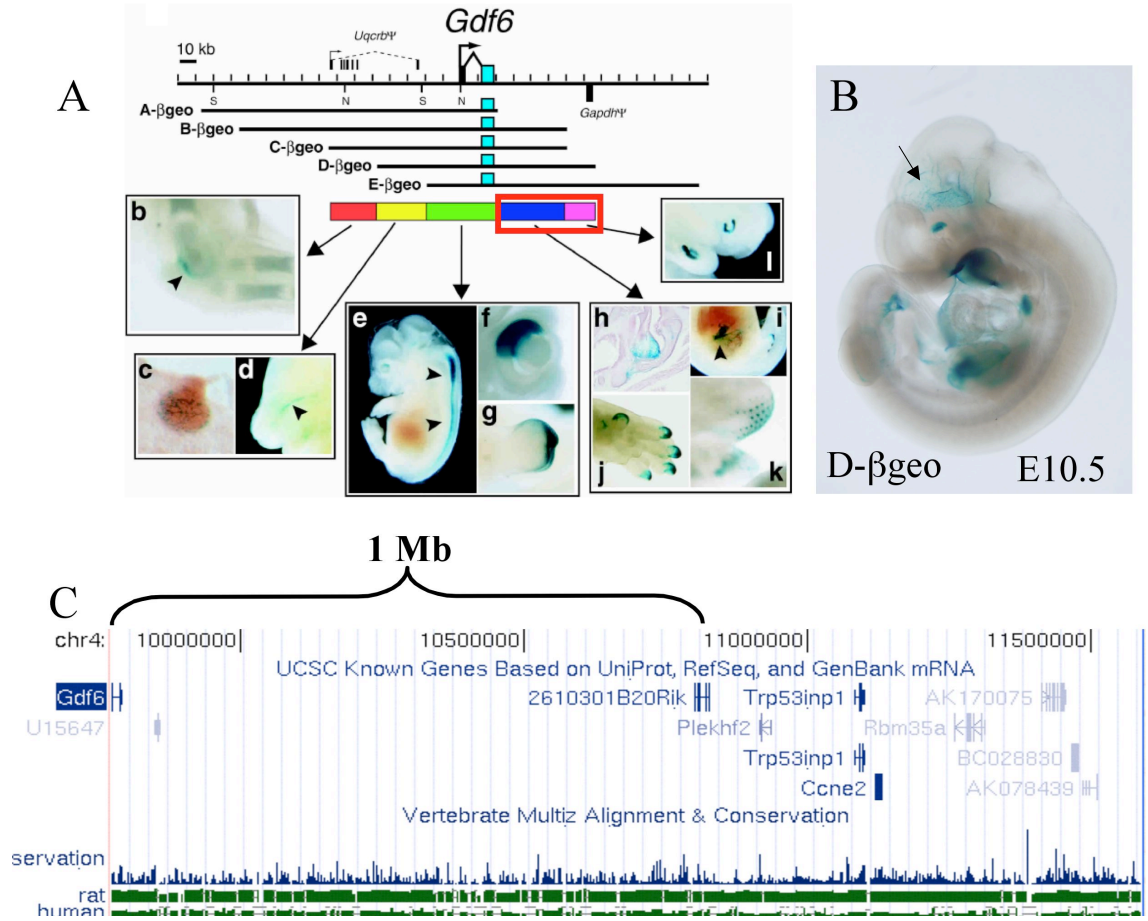

Figure 6.2. ***Cis*-regulatory elements in the *Gdf6* gene desert**. A) Using BACs with a *lacZ* reporter, approximately 280 kilobases of the *Gdf6* locus was divided into five regulatory regions and tested for their ability to drive expression of the reporter in region where *Gdf6* is expressed. These BAC lines were able to drive expression of *lacZ* in eleven anatomical sites adapted from Mortlock et al. 2003. B) The D-βgeo BAC drove expression of the *lacZ* reporter in ectoderm overlying the parietal bone at E10.5 (arrow). C) *Gdf6* is flanked by a 1 Mb gene desert where additional cis-regulatory elements may reside, including an element driving expression of *Gdf6* in the frontal bone primordia.

the lines produced were examined for expression at E10.5-E12.5 when *Gdf6* is expressed in the frontal bone primordia. Furthermore, this study did not identify *cis*-regulatory elements that corresponded to all sites of *Gdf6* expression, suggesting that additional regulatory elements reside even more distant from the *Gdf6* coding region and outside the region spanned by the BACs. Therefore, a future extension of this project could be to locate the likely *cis*-regulatory element that drives expression of *Gdf6* in the frontal bone primordia by examining the remaining BACs spanning the gene desert.

Could a mutation in a regulatory element contribute to craniosynostosis? In addition to the *Gdf6* coding region, mutations in the regulatory elements could explain some of the cases of human craniosynostosis in which the etiology is unknown. Locating a *Gdf6* regulatory element specific for the suture region would allow for more targeted sequence analysis. In humans, mutations in *cis*-regulatory sequences for *SHH* and *SOST* are associated with abnormal limb development or Van Buchem disease respectively (Loots et al., 2005; Sagai et al., 2005), demonstrating the contribution of *cis*-regulatory elements to human disease.

This is likely also the case for *Gdf6*. *Tcm* is an autosomal dominant mouse mutant characterized by microphthalmia. Genetic mapping reduced the critical region to a 1.3 Mb region containing five known genes, including *Gdf6* (Wang et al., 2005). Because of the expression of *Gdf6* in the dorsal retina and the microphthalmia and anophthalmia phenotypes observed in our own crosses, *Gdf6* is a likely candidate for the *Tcm* mutation. None of the candidate genes had mutations in the coding region, therefore the mutation most likely resides in a regulatory element for *Gdf6*. In collaboration with Dr. Dwight Stombolian, our lab found that *Gdf6* is upregulated in the eyes of *Tcm* mice

relative to wild-type (Y. Hou, D. Clendenning, and D. Mortlock, unpublished results). In addition, a familial case of Klippel-Feil syndrome has been attributed to a paracentric inversion that interrupts the *GDF6* gene desert, although the coding region is unaffected (Clarke et al., 1995; Tassabehji et al., 2008). Therefore, the phenotype is likely due to several *Gdf6 cis*-regulatory elements that are affected by the change in genomic positioning; resulting in altered chromatin structure, changes in the position of repressing elements, or separation of *Gdf6* from regulatory elements located past the inversion site. Since all these changes could produce variation in gene expression without affecting the coding region, it would be important to know the location of the non-coding sequence or sequences that drive expression of *Gdf6* in the suture region. Such elements would also be candidates for screening potential sites of mutations in human craniosynostosis patients. However, due to the large number of polymorphisms that likely reside within the one megabase gene desert for *Gdf6*, the regulatory elements would have to first be identified. The identification of tissue-specific regulatory elements could also be useful for the development of tools for further study of cranial suture development, such as transgenic lines made to drive expression in the frontal bone rudiment.

Thesis Summary and Conclusions

The goal this work was to gain a developmental understanding of *Gdf6* in the formation of the CS through the study of the initiation of the suture phenotype, the timing and location of *Gdf6* cranial expression, and the interaction of *Gdf6* with other BMP family members. Although the phenotype of the *Gdf6* mutant mouse was published almost a decade ago (Settle et al., 2003), the study of craniosynostosis has remained restricted to a small set of genes, including *FGFR1-3*, *Twist1*, *Msx2*, the *Ephrins*, *Nell-1,* and *Axin2*. BMPs are widely known for their role in skeletal patterning and osteogenesis, but their role in the dynamics at the suture has been less clear. Even less was known about the *Gdf* sub-family and how the members function.

This study shows the importance of *Gdf6* in the development of the CS in that it is one of the earliest, most penetrant, and most severe of the mouse craniosynostosis models. A suture defect is evident in *Gdf6-/-* mice even prior to the onset of ossification with the loss of the undifferentiated suture mesenchyme by E12.5, resulting in complete fusion of the CS by E14.5. We characterized the expression of *Gdf6* in the frontal bone primordia from E10.5-E12.5, and showed evidence for auto-regulation of *Gdf6* in this structure. We also demonstrated an interaction of *Gdf6* and *Bmp4* in the development of the CS, a relationship that is carried over to multiple skeletal (sternum, thyroid cartilage, pelvis) and non-skeletal (dorsal retina) structures. Although *Noggin* has been noted as an important factor in suture patency (Warren et al., 2003a), we demonstrated that it does not play in important role in early prenatal suture formation and the removal of *Noggin* has no effect on the *Gdf6* suture phenotype.

Clinical applications of Gdf6 in the suture

Although our work described only an embryonic role of *Gdf6* in the development of the CS, we did not examined the possible role of *Gdf6* in postnatal suture patency. When fused sutures are excised from infants with craniosynostosis, the defect that led to premature suture fusion is still present and it is common for the new suture space to re-fuse. Therefore, finding treatments to prevent this re-fusion event would eliminate the need for additional cranial surgeries. In rats, when beads soaked in recombinant Noggin were implanted into the space generated after removal of a fused suture, the bead inhibited suture re-fusion (Cooper et al., 2009; Shen et al., 2009b). From our data suggesting an inhibitory effect of Gdf6 on suture mesenchyme differentiation, a similar strategy could be utilized with Gdf6 protein.

BMPs are especially attractive to be used in therapeutic manipulation because they are secreted factors. Several BMPs, particularly rhBMP2 and rhBMP7, are already being used to treat patients with breaks and fractures, spinal fusion, and mandibular defects. Even rhGDF5 is being developed as a potential clinical tool in spinal fusions and injections into mice show stimulation of cranial bone growth (Moore et al., 2010). *Gdf-5, -6,* and *–7* mutants all have defects in the tendons and new studies show that it could also have clinical applications to humans (Mikic, 2004). BMP treatments are beneficial in that they eliminate the need to harvest bone grafts from the patient and are able to stimulate healing at sites of non-union between two bones.

Due to the highly osteogenic nature of BMP-2, a continued problem associated with clinical applications is finding a way to deliver physiologically relevant levels of protein. Large concentrations of protein can result in excess bone formation at undesired

sites, while the clearance of low levels of protein might occur too fast to produce an effect *in vivo* (Groeneveld and Burger, 2000). Almost a decade after BMP-2 began to be use in patients, research showed that the patients had a five times higher risk for developing malignant cancer after treatment (Carragee et al., 2011). Previous studies demonstrated that compared to Bmp2 and Bmp7, Gdf6 is weakly osteogenic (Bobacz et al., 2006). Since the function of the Gdfs is mostly related to cartilage growth, and the cranial bones are formed without a cartilage intermediate, this suggests that Gdf6 could be more specific as a clinical tool than other members of the BMP family in the treatment of craniosynostosis by providing a signal to inhibit suture mesenchyme differentiation without the strong ectoptic induction of bone formation.

Mutations in *Gdf6* have been associated with several human phenotypes, including Nablus mask-like facial syndrome (Raas-Rothschild et al., 2009; Salpietro et al., 2003; Shieh et al., 2006), Klippel-Feil Syndrome (Tassabehji et al., 2008), and ocular defects (Asai-Coakwell et al., 2007; Gosse and Baier, 2009). As we gain a more thorough understanding of the function of BMPs in the etiology of craniosynostosis, clinical applications to other conditions could also be attainable.

Advancing the understanding of BMP signaling

The suture offers a useful model for the study of BMP signaling. The suture region has the advantages of involving few tissues (bone, bone fronts, suture mesenchyme, and dura), with known BMP expression, and are known to signal to each other. Although BMPs are widely studied in endochondral bone, the suture provides a system to also study BMPs involvement in intramembranous ossification. There is

already evidence for indirect interactions between BMPs and other pathways in the suture (FGF and WNT). The suture can be used to address large questions in the BMP field, including how do BMPs interact? How do so many ligands transmit signals utilizing only a few receptors? What are the downstream effectors of BMP signaling? It is clear that not only will the study of the suture expand the understanding of BMPs, but also highlight the critical yet diverse role of this family of proteins.

APPENDIX A

GENOTYPING PCR PRIMERS FOR VARIOUS MOUSE LINES

Mouse Line	Allele	Genotyping Primers	Product Size
Gdf6	Wild-type	5'-AGCTCTTGGTCATGGATGTTTCTC-3' 5'-CTGATGTAGCCCTTCCACCTTTC-3'	176 bp
	Targeted allele	5'-TGGAGAGGCTATTCGGCTATGAC-3' 5'-TACTTTCTCGGCAGGAGCAAGG-3'	310 bp
Bmp4-lacZ	LacZ	5'-TTTCCATGTTGCCACTCGC-3' 5'-AACGGCTTGCCGTTCAGCA-3'	375 bp
Wnt1-Cre	Transgene	5'-ATTCTCCCACCGTCAGTACG-3' 5'-CGTTTTCTGAGCATACCTGGA-3'	475 bp
R26R	Wild-type & Mutant	5'-AAAGTCGCTCTGAGTTGTTAT-3' 5'-GCGAAGAGTTTGTCCTCAAGG-3' 5'-GGAGCGGGAGAAATGGATATG-3'	500 bp (WT) 250 bp (Mut)
Noggin-lacZ	Wild-type & Mutant	5'-GCATGGAGCGCTGCCCCAGC-3' 5'-GAGCAGCGAGCGCAGCAGCG-3' 5'-AAGGGCGATCGGTGCGGGCC-3'	211 bp (WT) 160 bp (Mut)

APPENDIX B

IN SITU HYBRIDIZATION PROBES, PRIMERS, AND CONDITIONS

RNA Probe Target	Primers	Probe	Linearization enzyme	RNA Polymerase	Product Size	Hybridization Temperature
Gdf6	5'- AAGCATGGAAGGAGGATGAAAGGG- 3' 5'- CGACCTCCAGTAACTTTAGTGTTGTCA –3'	Antisense Sense	NotI SpeI	Sp6 T7	937	65°C
ColIIa	Metsaranta et al., 1991	Antisense	EcoRI	T7	405	65°C
Runx2	5'- AAAGCTTCAGAACTCTTAGAATGA-3' 5'-ATCATATTAAAAAGCCAAGCACAAG-3'	Antisense	SpeI	T7	672	63°C
BMPR1b	5'- AACCCTTGCCAAAATGTCAG – 3' 5'- GGTGTGTCGGGCAGTAAGTT –3'	Antisense	SacII	Sp6	506	65°C
BMPR2	5'- GTGACAGGGCAGTCCATTCT –3' 5'- CAGCAATCCATTGTTTTTGC –3'	Antisense	SacII	Sp6	424	65°C

APPENDIX C

SUMMARY OF DEFECTS AND ABNORMALITIES IN ANALYZED MOUSE MUTANTS

	Gdf6+/-	***Gdf6-/-***	***Bmp4-lacZ/+***	***Bmp4-lacZ/+; Gdf6+/-***	***Bmp4-lacZ/+; Gdf6-/-***	***Gdf6+/-; Noggin-lacZ/+***
Long bones		Femur, Elbow				
Digits			Polydactyly	Polydactyly		
Cranial		Middle ear bones, CS fusion		CS fusion	CS fusion	
Manbrio-sternal joint			Unfused (21%)	Unfused (60%)		
Carpals	2c fusion	23c fusion				2c, 23c fusions
Tarsals		2/3 and CT fusions			23c, 2345 fusions	23c, 2345 fusions
Vertebrae			Unfused	Unfused		
Eye		Microph-thalmia		Microph-thalmia	Anopthalmia	
Thyroid cartilage	Hypoplasia	Hypoplasia		Hypoplasia		
Pelvic bones	Small ischium/ pubis gap		Small ischium/ pubis gap	Larger ischium/ pubis gap		

REFERENCES

Agresti, M., Gosain, A. K., 2005. Detection of apoptosis in fusing versus nonfusing mouse cranial sutures. J Craniofac Surg. 16**,** 572-8.

Antonopoulou, I., Mavrogiannis, L. A., Wilkie, A. O., Morriss-Kay, G. M., 2004. Alx4 and Msx2 play phenotypically similar and additive roles in skull vault differentiation. J Anat. 204**,** 487-99.

Aono, A., Hazama, M., Notoya, K., Taketomi, S., Yamasaki, H., Tsukuda, R., Sasaki, S., Fujisawa, Y., 1995. Potent ectopic bone-inducing activity of bone morphogenetic protein-4/7 heterodimer. Biochem Biophys Res Commun. 210**,** 670-7.

Asai-Coakwell, M., French, C. R., Berry, K. M., Ye, M., Koss, R., Somerville, M., Mueller, R., van Heyningen, V., Waskiewicz, A. J., Lehmann, O. J., 2007. GDF6, a novel locus for a spectrum of ocular developmental anomalies. Am J Hum Genet. 80**,** 306-15.

Bachiller, D., Klingensmith, J., Shneyder, N., Tran, U., Anderson, R., Rossant, J., De Robertis, E. M., 2003. The role of chordin/Bmp signals in mammalian pharyngeal development and DiGeorge syndrome. Development. 130**,** 3567-78.

Bakrania, P., Efthymiou, M., Klein, J. C., Salt, A., Bunyan, D. J., Wyatt, A., Ponting, C. P., Martin, A., Williams, S., Lindley, V., Gilmore, J., Restori, M., Robson, A. G., Neveu, M. M., Holder, G. E., Collin, J. R., Robinson, D. O., Farndon, P., Johansen-Berg, H., Gerrelli, D., Ragge, N. K., 2008. Mutations in BMP4 cause eye, brain, and digit developmental anomalies: overlap between the BMP4 and hedgehog signaling pathways. Am J Hum Genet. 82**,** 304-19.

Behr, B., Longaker, M. T., Quarto, N., 2010. Differential activation of canonical Wnt signaling determines cranial sutures fate: a novel mechanism for sagittal suture craniosynostosis. Dev Biol. 344**,** 922-40.

Behr, B., Longaker, M. T., Quarto, N., 2011. Craniosynostosis of coronal suture in twist1 mice occurs through endochondral ossification recapitulating the physiological closure of posterior frontal suture. Front Physiol. 2**,** 37.

Bobacz, K., Ullrich, R., Amoyo, L., Erlacher, L., Smolen, J. S., Graninger, W. B., 2006. Stimulatory effects of distinct members of the bone morphogenetic protein family on ligament fibroblasts. Ann Rheum Dis. 65**,** 169-77.

Botchkarev, V. A., 2003. Bone morphogenetic proteins and their antagonists in skin and hair follicle biology. J Invest Dermatol. 120**,** 36-47.

Boyadjiev, S. A., 2007. Genetic analysis of non-syndromic craniosynostosis. Orthod Craniofac Res. 10**,** 129-37.

Brugger, S. M., Merrill, A. E., Torres-Vazquez, J., Wu, N., Ting, M. C., Cho, J. Y., Dobias, S. L., Yi, S. E., Lyons, K., Bell, J. R., Arora, K., Warrior, R., Maxson, R., 2004. A phylogenetically conserved cis-regulatory module in the Msx2 promoter is sufficient for BMP-dependent transcription in murine and Drosophila embryos. Development. 131**,** 5153-65.

Brunet, L. J., McMahon, J. A., McMahon, A. P., Harland, R. M., 1998. Noggin, cartilage morphogenesis, and joint formation in the mammalian skeleton. Science. 280**,** 1455-7.

Butler, S. J., Dodd, J., 2003. A role for BMP heterodimers in roof plate-mediated repulsion of commissural axons. Neuron. 38**,** 389-401.

Canalis, E., Economides, A. N., Gazzerro, E., 2003. Bone morphogenetic proteins, their antagonists, and the skeleton. Endocr Rev. 24**,** 218-35.

Candia, A. F., Watabe, T., Hawley, S. H., Onichtchouk, D., Zhang, Y., Derynck, R., Niehrs, C., Cho, K. W., 1997. Cellular interpretation of multiple TGF-beta signals: intracellular antagonism between activin/BVg1 and BMP-2/4 signaling mediated by Smads. Development. 124**,** 4467-80.

Carragee, E. J., Hurwitz, E. L., Weiner, B. K., 2011. A critical review of recombinant human bone morphogenetic protein-2 trials in spinal surgery: emerging safety concerns and lessons learned. Spine J. 11**,** 471-91.

Chai, Y., Jiang, X., Ito, Y., Bringas, P., Jr., Han, J., Rowitch, D. H., Soriano, P., McMahon, A. P., Sucov, H. M., 2000. Fate of the mammalian cranial neural crest during tooth and mandibular morphogenesis. Development. 127**,** 1671-9.

Chang, C., Hemmati-Brivanlou, A., 1999. Xenopus GDF6, a new antagonist of noggin and a partner of BMPs. Development. 126**,** 3347-57.

Chen, J. M., 1952. Studies on the morphogenesis of the mouse sternum. I. Normal embryonic development. J Anat. 86**,** 373-86.

Chen, L., Li, D., Li, C., Engel, A., Deng, C. X., 2003. A Ser252Trp [corrected] substitution in mouse fibroblast growth factor receptor 2 (Fgfr2) results in craniosynostosis. Bone. 33**,** 169-78.

Choi, K. Y., Kim, H. J., Lee, M. H., Kwon, T. G., Nah, H. D., Furuichi, T., Komori, T., Nam, S. H., Kim, Y. J., Ryoo, H. M., 2005. Runx2 regulates FGF2-induced Bmp2 expression during cranial bone development. Dev Dyn. 233**,** 115-21.

Clarke, R. A., Catalan, G., Diwan, A. D., Kearsley, J. H., 1998. Heterogeneity in Klippel-Feil syndrome: a new classification. Pediatr Radiol. 28**,** 967-74.

Clarke, R. A., Singh, S., McKenzie, H., Kearsley, J. H., Yip, M. Y., 1995. Familial Klippel-Feil syndrome and paracentric inversion inv(8)(q22.2q23.3). Am J Hum Genet. 57**,** 1364-70.

Cohen, M. M., Jr., 2005. Editorial: perspectives on craniosynostosis. Am J Med Genet A. 136A**,** 313-26.

Connerney, J., Andreeva, V., Leshem, Y., Muentener, C., Mercado, M. A., Spicer, D. B., 2006. Twist1 dimer selection regulates cranial suture patterning and fusion. Dev Dyn. 235**,** 1345-57.

Cooper, G. M., Curry, C., Barbano, T. E., Burrows, A. M., Vecchione, L., Caccamese, J. F., Norbutt, C. S., Costello, B. J., Losee, J. E., Moursi, A. M., Huard, J., Mooney, M. P., 2007. Noggin inhibits postoperative resynostosis in craniosynostotic rabbits. J Bone Miner Res. 22**,** 1046-54.

Cooper, G. M., Usas, A., Olshanski, A., Mooney, M. P., Losee, J. E., Huard, J., 2009. Ex vivo Noggin gene therapy inhibits bone formation in a mouse model of postoperative resynostosis. Plast Reconstr Surg. 123**,** 94S-103S.

Cray, J., Jr., Burrows, A. M., Vecchione, L., Caccamese, J. F., Jr., Losee, J. E., Moursi, A. M., Siegel, M. I., Cooper, G. M., Mooney, M. P., 2011. Blocking bone morphogenetic protein function using in vivo noggin therapy does not rescue premature suture fusion in rabbits with delayed-onset craniosynostosis. Plast Reconstr Surg. 127**,** 1163-72.

Dahmann, C., Oates, A. C., Brand, M., 2011. Boundary formation and maintenance in tissue development. Nat Rev Genet. 12**,** 43-55.

Daluiski, A., Engstrand, T., Bahamonde, M. E., Gamer, L. W., Agius, E., Stevenson, S. L., Cox, K., Rosen, V., Lyons, K. M., 2001. Bone morphogenetic protein-3 is a negative regulator of bone density. Nat Genet. 27**,** 84-8.

Danesh, S. M., Villasenor, A., Chong, D., Soukup, C., Cleaver, O., 2009. BMP and BMP receptor expression during murine organogenesis. Gene Expr Patterns. 9**,** 255-65.

Danielian, P. S., Muccino, D., Rowitch, D. H., Michael, S. K., McMahon, A. P., 1998. Modification of gene activity in mouse embryos in utero by a tamoxifen-inducible form of Cre recombinase. Curr Biol. 8**,** 1323-6.

den Hollander, A. I., Biyanwila, J., Kovach, P., Bardakjian, T., Traboulsi, E. I., Ragge, N. K., Schneider, A., Malicki, J., Genetic defects of GDF6 in the zebrafish out of sight mutant and in human eye developmental anomalies. BMC Genet. 11**,** 102.

Dionne, M. S., Skarnes, W. C., Harland, R. M., 2001. Mutation and analysis of Dan, the founding member of the Dan family of transforming growth factor beta antagonists. Mol Cell Biol. 21**,** 636-43.

Drossopoulou, G., Lewis, K. E., Sanz-Ezquerro, J. J., Nikbakht, N., McMahon, A. P., Hofmann, C., Tickle, C., 2000. A model for anteroposterior patterning of the vertebrate limb based on sequential long- and short-range Shh signalling and Bmp signalling. Development. 127**,** 1337-48.

Ducy, P., Karsenty, G., 2000. The family of bone morphogenetic proteins. Kidney Int. 57**,** 2207-14.

Ducy, P., Zhang, R., Geoffroy, V., Ridall, A. L., Karsenty, G., 1997. Osf2/Cbfa1: a transcriptional activator of osteoblast differentiation. Cell. 89**,** 747-54.

Dudley, A. T., Lyons, K. M., Robertson, E. J., 1995. A requirement for bone morphogenetic protein-7 during development of the mammalian kidney and eye. Genes Dev. 9**,** 2795-807.

Dunn, N. R., Winnier, G. E., Hargett, L. K., Schrick, J. J., Fogo, A. B., Hogan, B. L., 1997. Haploinsufficient phenotypes in Bmp4 heterozygous null mice and modification by mutations in Gli3 and Alx4. Dev Biol. 188**,** 235-47.

Evans, D. J., Noden, D. M., 2006. Spatial relations between avian craniofacial neural crest and paraxial mesoderm cells. Dev Dyn. 235**,** 1310-25.

Fiori, J. L., Billings, P. C., de la Pena, L. S., Kaplan, F. S., Shore, E. M., 2006. Dysregulation of the BMP-p38 MAPK signaling pathway in cells from patients with fibrodysplasia ossificans progressiva (FOP). J Bone Miner Res. 21**,** 902-9.

Fujiwara, T., Dehart, D. B., Sulik, K. K., Hogan, B. L., 2002. Distinct requirements for extra-embryonic and embryonic bone morphogenetic protein 4 in the formation of the node and primitive streak and coordination of left-right asymmetry in the mouse. Development. 129**,** 4685-96.

Furtwangler, J. A., Hall, S. H., Koskinen-Moffett, L. K., 1985. Sutural morphogenesis in the mouse calvaria: the role of apoptosis. Acta Anat (Basel). 124**,** 74-80.

Furuya, Y., Edwards, M. S., Alpers, C. E., Tress, B. M., Ousterhout, D. K., Norman, D., 1984. Computerized tomography of cranial sutures. Part 1: Comparison of suture anatomy in children and adults. J Neurosurg. 61**,** 53-8.

Gilbert, S. F., 2003. Developmental biology. Sinauer Associates, Sunderland, Mass.

Gong, Y., Krakow, D., Marcelino, J., Wilkin, D., Chitayat, D., Babul-Hirji, R., Hudgins, L., Cremers, C. W., Cremers, F. P., Brunner, H. G., Reinker, K., Rimoin, D. L., Cohn, D. H., Goodman, F. R., Reardon, W., Patton, M., Francomano, C. A., Warman, M. L., 1999. Heterozygous mutations in the gene encoding noggin affect human joint morphogenesis. Nat Genet. 21**,** 302-4.

Gosse, N. J., Baier, H., 2009. An essential role for Radar (Gdf6a) in inducing dorsal fate in the zebrafish retina. Proc Natl Acad Sci U S A. 106**,** 2236-41.

Gray, H., Lewis, W. H., 1918. Anatomy of the human body. Lea & Febiger, Philadelphia and New York,.

Groeneveld, E. H., Burger, E. H., 2000. Bone morphogenetic proteins in human bone regeneration. Eur J Endocrinol. 142**,** 9-21.

Groppe, J., Greenwald, J., Wiater, E., Rodriguez-Leon, J., Economides, A. N., Kwiatkowski, W., Affolter, M., Vale, W. W., Belmonte, J. C., Choe, S., 2002. Structural basis of BMP signalling inhibition by the cystine knot protein Noggin. Nature. 420**,** 636-42.

Han, J., Ishii, M., Bringas, P., Jr., Maas, R. L., Maxson, R. E., Jr., Chai, Y., 2007. Concerted action of Msx1 and Msx2 in regulating cranial neural crest cell differentiation during frontal bone development. Mech Dev. 124**,** 729-45.

Hanken, J., Gross, J. B., 2005. Evolution of cranial development and the role of neural crest: insights from amphibians. J Anat. 207**,** 437-46.

Hazama, M., Aono, A., Ueno, N., Fujisawa, Y., 1995. Efficient expression of a heterodimer of bone morphogenetic protein subunits using a baculovirus expression system. Biochem Biophys Res Commun. 209**,** 859-66.

Heinecke, K., Seher, A., Schmitz, W., Mueller, T. D., Sebald, W., Nickel, J., 2009. Receptor oligomerization and beyond: a case study in bone morphogenetic proteins. BMC Biol. 7**,** 59.

Hogan, B. L., 1996. Bone morphogenetic proteins: multifunctional regulators of vertebrate development. Genes Dev. 10**,** 1580-94.

Hwang, C. H., Wu, D. K., 2008. Noggin heterozygous mice: an animal model for congenital conductive hearing loss in humans. Hum Mol Genet. 17**,** 844-53.

Iseki, S., Wilkie, A. O., Morriss-Kay, G. M., 1999. Fgfr1 and Fgfr2 have distinct differentiation- and proliferation-related roles in the developing mouse skull vault. Development. 126**,** 5611-20.

Ishii, M., Merrill, A. E., Chan, Y. S., Gitelman, I., Rice, D. P., Sucov, H. M., Maxson, R. E., Jr., 2003. Msx2 and Twist cooperatively control the development of the neural crest-derived skeletogenic mesenchyme of the murine skull vault. Development. 130**,** 6131-42.

Jiang, X., Iseki, S., Maxson, R. E., Sucov, H. M., Morriss-Kay, G. M., 2002. Tissue origins and interactions in the mammalian skull vault. Dev Biol. 241**,** 106-16.

Jiang, X., Rowitch, D. H., Soriano, P., McMahon, A. P., Sucov, H. M., 2000. Fate of the mammalian cardiac neural crest. Development. 127**,** 1607-16.

Jiao, K., Kulessa, H., Tompkins, K., Zhou, Y., Batts, L., Baldwin, H. S., Hogan, B. L., 2003. An essential role of Bmp4 in the atrioventricular septation of the mouse heart. Genes Dev. 17**,** 2362-7.

Kabbani, H., Raghuveer, T. S., 2004. Craniosynostosis. Am Fam Physician. 69**,** 2863-70.

Katagiri, T., Boorla, S., Frendo, J. L., Hogan, B. L., Karsenty, G., 1998. Skeletal abnormalities in doubly heterozygous Bmp4 and Bmp7 mice. Dev Genet. 22**,** 340-8.

Khokha, M. K., Hsu, D., Brunet, L. J., Dionne, M. S., Harland, R. M., 2003. Gremlin is the BMP antagonist required for maintenance of Shh and Fgf signals during limb patterning. Nat Genet. 34**,** 303-7.

Kim, H., Peterson, T. G., Barnes, S., 1998a. Mechanisms of action of the soy isoflavone genistein: emerging role for its effects via transforming growth factor beta signaling pathways. Am J Clin Nutr. 68**,** 1418S-1425S.

Kim, H. J., Rice, D. P., Kettunen, P. J., Thesleff, I., 1998b. FGF-, BMP- and Shh-mediated signalling pathways in the regulation of cranial suture morphogenesis and calvarial bone development. Development. 125**,** 1241-51.

Knecht, A. K., Bronner-Fraser, M., 2002. Induction of the neural crest: a multigene process. Nat Rev Genet. 3**,** 453-61.

Koshiba-Takeuchi, K., Takeuchi, J. K., Matsumoto, K., Momose, T., Uno, K., Hoepker, V., Ogura, K., Takahashi, N., Nakamura, H., Yasuda, K., Ogura, T., 2000. Tbx5 and the retinotectum projection. Science. 287**,** 134-7.

Lana-Elola, E., Rice, R., Grigoriadis, A. E., Rice, D. P., 2007. Cell fate specification during calvarial bone and suture development. Dev Biol. 311**,** 335-46.

Lawson, K. A., Dunn, N. R., Roelen, B. A., Zeinstra, L. M., Davis, A. M., Wright, C. V., Korving, J. P., Hogan, B. L., 1999. Bmp4 is required for the generation of primordial germ cells in the mouse embryo. Genes Dev. 13**,** 424-36.

Lee, K. J., Mendelsohn, M., Jessell, T. M., 1998. Neuronal patterning by BMPs: a requirement for GDF7 in the generation of a discrete class of commissural interneurons in the mouse spinal cord. Genes Dev. 12**,** 3394-407.

Lenton, K. A., Nacamuli, R. P., Wan, D. C., Helms, J. A., Longaker, M. T., 2005. Cranial suture biology. Curr Top Dev Biol. 66**,** 287-328.

Levin, M., Johnson, R. L., Stern, C. D., Kuehn, M., Tabin, C., 1995. A molecular pathway determining left-right asymmetry in chick embryogenesis. Cell. 82**,** 803-14.

Liu, B., Yu, H. M., Hsu, W., 2007. Craniosynostosis caused by Axin2 deficiency is mediated through distinct functions of beta-catenin in proliferation and differentiation. Dev Biol. 301**,** 298-308.

Loots, G. G., Kneissel, M., Keller, H., Baptist, M., Chang, J., Collette, N. M., Ovcharenko, D., Plajzer-Frick, I., Rubin, E. M., 2005. Genomic deletion of a long-range bone enhancer misregulates sclerostin in Van Buchem disease. Genome Res. 15**,** 928-35.

Luo, G., Hofmann, C., Bronckers, A. L., Sohocki, M., Bradley, A., Karsenty, G., 1995. BMP-7 is an inducer of nephrogenesis, and is also required for eye development and skeletal patterning. Genes Dev. 9**,** 2808-20.

Lyons, K. M., Hogan, B. L., Robertson, E. J., 1995. Colocalization of BMP 7 and BMP 2 RNAs suggests that these factors cooperatively mediate tissue interactions during murine development. Mech Dev. 50**,** 71-83.

Mabbutt, L. W., Kokich, V. G., 1979. Calvarial and sutural re-development following craniectomy in the neonatal rabbit. J Anat. 129**,** 413-22.

Mansukhani, A., Bellosta, P., Sahni, M., Basilico, C., 2000. Signaling by fibroblast growth factors (FGF) and fibroblast growth factor receptor 2 (FGFR2)-activating mutations blocks mineralization and induces apoptosis in osteoblasts. J Cell Biol. 149**,** 1297-308.

Marie, P. J., Kaabeche, K., Guenou, H., 2008. Roles of FGFR2 and twist in human craniosynostosis: insights from genetic mutations in cranial osteoblasts. Front Oral Biol. 12**,** 144-59.

Matsuoka, T., Ahlberg, P. E., Kessaris, N., Iannarelli, P., Dennehy, U., Richardson, W. D., McMahon, A. P., Koentges, G., 2005. Neural crest origins of the neck and shoulder. Nature. 436**,** 347-55.

Matzuk, M. M., Kumar, T. R., Bradley, A., 1995. Different phenotypes for mice deficient in either activins or activin receptor type II. Nature. 374**,** 356-60.

Maxson, R., Ishii, M., 2008. The Bmp pathway in skull vault development. Front Oral Biol. 12**,** 197-208.

Mazerbourg, S., Sangkuhl, K., Luo, C. W., Sudo, S., Klein, C., Hsueh, A. J., 2005. Identification of receptors and signaling pathways for orphan bone morphogenetic protein/growth differentiation factor ligands based on genomic analyses. J Biol Chem. 280**,** 32122-32.

McMahon, J. A., Takada, S., Zimmerman, L. B., Fan, C. M., Harland, R. M., McMahon, A. P., 1998. Noggin-mediated antagonism of BMP signaling is required for growth and patterning of the neural tube and somite. Genes Dev. 12**,** 1438-52.

Merrill, A. E., Bochukova, E. G., Brugger, S. M., Ishii, M., Pilz, D. T., Wall, S. A., Lyons, K. M., Wilkie, A. O., Maxson, R. E., Jr., 2006. Cell mixing at a neural crest-mesoderm boundary and deficient ephrin-Eph signaling in the pathogenesis of craniosynostosis. Hum Mol Genet. 15**,** 1319-28.

Metsaranta, M., Toman, D., De Crombrugghe, B., Vuorio, E., 1991. Specific hybridization probes for mouse type I, II, III and IX collagen mRNAs. Biochim Biophys Acta. 1089**,** 241-3.

Mikic, B., 2004. Multiple effects of GDF-5 deficiency on skeletal tissues: implications for therapeutic bioengineering. Ann Biomed Eng. 32**,** 466-76.

Monsoro-Burq, A., Le Douarin, N., 2000. Left-right asymmetry in BMP4 signalling pathway during chick gastrulation. Mech Dev. 97**,** 105-8.

Moore, Y. R., Dickinson, D. P., Wikesjo, U. M., 2010. Growth/differentiation factor-5: a candidate therapeutic agent for periodontal regeneration? A review of pre-clinical data. J Clin Periodontol. 37**,** 288-98.

Morriss-Kay, G. M., 2001. Derivation of the mammalian skull vault. J Anat. 199**,** 143-51.

Morriss-Kay, G. M., Wilkie, A. O., 2005. Growth of the normal skull vault and its alteration in craniosynostosis: insights from human genetics and experimental studies. J Anat. 207**,** 637-53.

Mortazavi, A., Williams, B. A., McCue, K., Schaeffer, L., Wold, B., 2008. Mapping and quantifying mammalian transcriptomes by RNA-Seq. Nat Methods. 5**,** 621-8.

Mortlock, D. P., Guenther, C., Kingsley, D. M., 2003. A general approach for identifying distant regulatory elements applied to the Gdf6 gene. Genome Res. 13**,** 2069-81.

Moss, M. L., 1960. Inhibition and stimulation of sutural fusion in the rat calvaria. Anat Rec. 136**,** 457-67.

Murali, D., Yoshikawa, S., Corrigan, R. R., Plas, D. J., Crair, M. C., Oliver, G., Lyons, K. M., Mishina, Y., Furuta, Y., 2005. Distinct developmental programs require different levels of Bmp signaling during mouse retinal development. Development. 132**,** 913-23.

Nacamuli, R. P., Fong, K. D., Lenton, K. A., Song, H. M., Fang, T. D., Salim, A., Longaker, M. T., 2005. Expression and possible mechanisms of regulation of BMP3 in rat cranial sutures. Plast Reconstr Surg. 116**,** 1353-62.

Nickel, J., Sebald, W., Groppe, J. C., Mueller, T. D., 2009. Intricacies of BMP receptor assembly. Cytokine Growth Factor Rev. 20**,** 367-77.

Nochi, H., Sung, J. H., Lou, J., Adkisson, H. D., Maloney, W. J., Hruska, K. A., 2004. Adenovirus mediated BMP-13 gene transfer induces chondrogenic differentiation of murine mesenchymal progenitor cells. J Bone Miner Res. 19**,** 111-22.

Nohe, A., Hassel, S., Ehrlich, M., Neubauer, F., Sebald, W., Henis, Y. I., Knaus, P., 2002. The mode of bone morphogenetic protein (BMP) receptor oligomerization determines different BMP-2 signaling pathways. J Biol Chem. 277**,** 5330-8.

Opperman, L. A., 2000. Cranial sutures as intramembranous bone growth sites. Dev Dyn. 219**,** 472-85.

Ornitz, D. M., Marie, P. J., 2002. FGF signaling pathways in endochondral and intramembranous bone development and human genetic disease. Genes Dev. 16**,** 1446-65.

Passos-Bueno, M. R., Serti Eacute, A. E., Jehee, F. S., Fanganiello, R., Yeh, E., 2008. Genetics of craniosynostosis: genes, syndromes, mutations and genotype-phenotype correlations. Front Oral Biol. 12**,** 107-43.

Patel, S. R., Gordon, J., Mahbub, F., Blackburn, C. C., Manley, N. R., 2006. Bmp4 and Noggin expression during early thymus and parathyroid organogenesis. Gene Expr Patterns. 6**,** 794-9.

Pereira, R. C., Rydziel, S., Canalis, E., 2000. Bone morphogenetic protein-4 regulates its own expression in cultured osteoblasts. J Cell Physiol. 182**,** 239-46.

Poliakov, A., Cotrina, M., Wilkinson, D. G., 2004. Diverse roles of eph receptors and ephrins in the regulation of cell migration and tissue assembly. Dev Cell. 7**,** 465-80.

Quarto, N., Longaker, M. T., 2005. The zebrafish (Danio rerio): a model system for cranial suture patterning. Cells Tissues Organs. 181**,** 109-18.

Raas-Rothschild, A., Dijkhuizen, T., Sikkema-Raddatz, B., Werner, M., Dagan, J., Abeliovich, D., Lerer, I., 2009. The 8q22.1 microdeletion syndrome or Nablus mask-like facial syndrome: report on two patients and review of the literature. Eur J Med Genet. 52**,** 140-4.

Rice, D. P., 2008. Developmental anatomy of craniofacial sutures. Front Oral Biol. 12**,** 1-21.

Rice, D. P., Kim, H. J., Thesleff, I., 1999. Apoptosis in murine calvarial bone and suture development. Eur J Oral Sci. 107**,** 265-75.

Rice, R., Rice, D. P., Olsen, B. R., Thesleff, I., 2003. Progression of calvarial bone development requires Foxc1 regulation of Msx2 and Alx4. Dev Biol. 262**,** 75-87.

Rice, R., Rice, D. P., Thesleff, I., 2005. Foxc1 integrates Fgf and Bmp signalling independently of twist or noggin during calvarial bone development. Dev Dyn. 233**,** 847-52.

Rissi, M., Wittbrodt, J., Delot, E., Naegeli, M., Rosa, F. M., 1995. Zebrafish Radar: a new member of the TGF-beta superfamily defines dorsal regions of the neural plate and the embryonic retina. Mech Dev. 49**,** 223-34.

Roybal, P. G., Wu, N. L., Sun, J., Ting, M. C., Schafer, C. A., Maxson, R. E., 2010. Inactivation of Msx1 and Msx2 in neural crest reveals an unexpected role in suppressing heterotopic bone formation in the head. Dev Biol. 343**,** 28-39.

Sagai, T., Hosoya, M., Mizushina, Y., Tamura, M., Shiroishi, T., 2005. Elimination of a long-range cis-regulatory module causes complete loss of limb-specific Shh expression and truncation of the mouse limb. Development. 132**,** 797-803.

Sahar, D. E., Longaker, M. T., Quarto, N., 2005. Sox9 neural crest determinant gene controls patterning and closure of the posterior frontal cranial suture. Dev Biol. 280**,** 344-61.

Salpietro, C. D., Briuglia, S., Rigoli, L., Merlino, M. V., Dallapiccola, B., 2003. Confirmation of Nablus mask-like facial syndrome. Am J Med Genet A. 121A**,** 283-5.

Sanchez-Lara, P. A., Graham, J. M., Jr., Hing, A. V., Lee, J., Cunningham, M., 2007. The morphogenesis of wormian bones: a study of craniosynostosis and purposeful cranial deformation. Am J Med Genet A. 143A**,** 3243-51.

Sanz-Ezquerro, J. J., Tickle, C., 2003. Fgf signaling controls the number of phalanges and tip formation in developing digits. Curr Biol. 13**,** 1830-6.

Selever, J., Liu, W., Lu, M. F., Behringer, R. R., Martin, J. F., 2004. Bmp4 in limb bud mesoderm regulates digit pattern by controlling AER development. Dev Biol. 276**,** 268-79.

Settle, S., Marker, P., Gurley, K., Sinha, A., Thacker, A., Wang, Y., Higgins, K., Cunha, G., Kingsley, D. M., 2001. The BMP family member Gdf7 is required for seminal vesicle growth, branching morphogenesis, and cytodifferentiation. Dev Biol. 234**,** 138-50.

Settle, S. H., Jr., Rountree, R. B., Sinha, A., Thacker, A., Higgins, K., Kingsley, D. M., 2003. Multiple joint and skeletal patterning defects caused by single and double mutations in the mouse Gdf6 and Gdf5 genes. Dev Biol. 254**,** 116-30.

Shapiro, R., Robinson, F., 1976. Embryogenesis of the human occipital bone. AJR Am J Roentgenol. 126**,** 1063-8.

Shen, B., Bhargav, D., Wei, A., Williams, L. A., Tao, H., Ma, D. D., Diwan, A. D., 2009a. BMP-13 emerges as a potential inhibitor of bone formation. Int J Biol Sci. 5**,** 192-200.

Shen, K., Krakora, S. M., Cunningham, M., Singh, M., Wang, X., Hu, F. Z., Post, J. C., Ehrlich, G. D., 2009b. Medical treatment of craniosynostosis: recombinant Noggin inhibits coronal suture closure in the rat craniosynostosis model. Orthod Craniofac Res. 12**,** 254-62.

Shieh, J. T., Aradhya, S., Novelli, A., Manning, M. A., Cherry, A. M., Brumblay, J., Salpietro, C. D., Bernardini, L., Dallapiccola, B., Hoyme, H. E., 2006. Nablus mask-like facial syndrome is caused by a microdeletion of 8q detected by array-based comparative genomic hybridization. Am J Med Genet A. 140**,** 1267-73.

Simpson, E. H., Johnson, D. K., Hunsicker, P., Suffolk, R., Jordan, S. A., Jackson, I. J., 1999. The mouse Cer1 (Cerberus related or homologue) gene is not required for anterior pattern formation. Dev Biol. 213**,** 202-6.

Slater, B. J., Lenton, K. A., Kwan, M. D., Gupta, D. M., Wan, D. C., Longaker, M. T., 2008. Cranial sutures: a brief review. Plast Reconstr Surg. 121**,** 170e-8e.

Solloway, M. J., Dudley, A. T., Bikoff, E. K., Lyons, K. M., Hogan, B. L., Robertson, E. J., 1998. Mice lacking Bmp6 function. Dev Genet. 22**,** 321-39.

Soriano, P., 1999. Generalized lacZ expression with the ROSA26 Cre reporter strain. Nat Genet. 21**,** 70-1.

Spector, J. A., Mehrara, B. J., Greenwald, J. A., Saadeh, P. B., Steinbrech, D. S., Smith, L. P., Longaker, M. T., 2000. A molecular analysis of the isolated rat posterior frontal and sagittal sutures: differences in gene expression. Plast Reconstr Surg. 106**,** 852-61; discussion 862-7.

Srinivas, S., Watanabe, T., Lin, C. S., William, C. M., Tanabe, Y., Jessell, T. M., Costantini, F., 2001. Cre reporter strains produced by targeted insertion of EYFP and ECFP into the ROSA26 locus. BMC Dev Biol. 1**,** 4.

Stoller, J. Z., Degenhardt, K. R., Huang, L., Zhou, D. D., Lu, M. M., Epstein, J. A., 2008. Cre reporter mouse expressing a nuclear localized fusion of GFP and beta-galactosidase reveals new derivatives of Pax3-expressing precursors. Genesis. 46**,** 200-4.

Storm, E. E., Huynh, T. V., Copeland, N. G., Jenkins, N. A., Kingsley, D. M., Lee, S. J., 1994. Limb alterations in brachypodism mice due to mutations in a new member of the TGF beta-superfamily. Nature. 368**,** 639-43.

Storm, E. E., Kingsley, D. M., 1996. Joint patterning defects caused by single and double mutations in members of the bone morphogenetic protein (BMP) family. Development. 122**,** 3969-79.

Storm, E. E., Kingsley, D. M., 1999. GDF5 coordinates bone and joint formation during digit development. Dev Biol. 209**,** 11-27.

Suzuki, A., Kaneko, E., Maeda, J., Ueno, N., 1997. Mesoderm induction by BMP-4 and -7 heterodimers. Biochem Biophys Res Commun. 232**,** 153-6.

Tassabehji, M., Fang, Z. M., Hilton, E. N., McGaughran, J., Zhao, Z., de Bock, C. E., Howard, E., Malass, M., Donnai, D., Diwan, A., Manson, F. D., Murrell, D., Clarke, R. A., 2008. Mutations in GDF6 are associated with vertebral segmentation defects in Klippel-Feil syndrome. Hum Mutat. 29**,** 1017-27.

Ting, K., Vastardis, H., Mulliken, J. B., Soo, C., Tieu, A., Do, H., Kwong, E., Bertolami, C. N., Kawamoto, H., Kuroda, S., Longaker, M. T., 1999. Human NELL-1 expressed in unilateral coronal synostosis. J Bone Miner Res. 14**,** 80-9.

Ting, M. C., Wu, N. L., Roybal, P. G., Sun, J., Liu, L., Yen, Y., Maxson, R. E., Jr., 2009. EphA4 as an effector of Twist1 in the guidance of osteogenic precursor cells during calvarial bone growth and in craniosynostosis. Development. 136**,** 855-64.

Tsumaki, N., Tanaka, K., Arikawa-Hirasawa, E., Nakase, T., Kimura, T., Thomas, J. T., Ochi, T., Luyten, F. P., Yamada, Y., 1999. Role of CDMP-1 in skeletal morphogenesis: promotion of mesenchymal cell recruitment and chondrocyte differentiation. J Cell Biol. 144**,** 161-73.

Tyler, M. S., 1983. Development of the frontal bone and cranial meninges in the embryonic chick: an experimental study of tissue interactions. Anat Rec. 206**,** 61-70.

Tylzanowski, P., Mebis, L., Luyten, F. P., 2006. The Noggin null mouse phenotype is strain dependent and haploinsufficiency leads to skeletal defects. Dev Dyn. 235**,** 1599-607.

Urist, M. R., 1965. Bone: formation by autoinduction. Science. 150**,** 893-9.

Wang, K. S., Zahn, L. E., Favor, J., Huang, K. M., Stambolian, D., 2005. Genetic and phenotypic analysis of Tcm, a mutation affecting early eye development. Mamm Genome. 16**,** 332-43.

Warren, S. M., Brunet, L. J., Harland, R. M., Economides, A. N., Longaker, M. T., 2003a. The BMP antagonist noggin regulates cranial suture fusion. Nature. 422**,** 625-9.

Warren, S. M., Greenwald, J. A., Nacamuli, R. P., Fong, K. D., Song, H. J., Fang, T. D., Mathy, J. A., Longaker, M. T., 2003b. Regional dura mater differentially regulates osteoblast gene expression. J Craniofac Surg. 14**,** 363-70.

Warren, S. M., Longaker, M. T., 2001. The pathogenesis of craniosynostosis in the fetus. Yonsei Med J. 42**,** 646-59.

Wilkie, A. O., 1997. Craniosynostosis: genes and mechanisms. Hum Mol Genet. 6**,** 1647-56.

Williams, J. A., Paddock, S. W., Vorwerk, K., Carroll, S. B., 1994. Organization of wing formation and induction of a wing-patterning gene at the dorsal/ventral compartment boundary. Nature. 368**,** 299-305.

Williams, L. A., Bhargav, D., Diwan, A. D., 2008. Unveiling the bmp13 enigma: redundant morphogen or crucial regulator? Int J Biol Sci. 4**,** 318-29.

Winnier, G., Blessing, M., Labosky, P. A., Hogan, B. L., 1995. Bone morphogenetic protein-4 is required for mesoderm formation and patterning in the mouse. Genes Dev. 9**,** 2105-16.

Xiao, Y. T., Xiang, L. X., Shao, J. Z., 2007. Bone morphogenetic protein. Biochem Biophys Res Commun. 362**,** 550-3.

Yanagita, M., 2005. BMP antagonists: their roles in development and involvement in pathophysiology. Cytokine Growth Factor Rev. 16**,** 309-17.

Yi, S. E., Daluiski, A., Pederson, R., Rosen, V., Lyons, K. M., 2000. The type I BMP receptor BMPRIB is required for chondrogenesis in the mouse limb. Development. 127**,** 621-30.

Yoshida, T., Phylactou, L. A., Uney, J. B., Ishikawa, I., Eto, K., Iseki, S., 2005. Twist is required for establishment of the mouse coronal suture. J Anat. 206**,** 437-44.

Yoshida, T., Vivatbutsiri, P., Morriss-Kay, G., Saga, Y., Iseki, S., 2008. Cell lineage in mammalian craniofacial mesenchyme. Mech Dev. 125**,** 797-808.

Yoshimoto, T., Yamamoto, M., Kadomatsu, H., Sakoda, K., Yonamine, Y., Izumi, Y., 2006. Recombinant human growth/differentiation factor-5 (rhGDF-5) induced bone formation in murine calvariae. J Periodontal Res. 41**,** 140-7.

Yu, H. M., Jerchow, B., Sheu, T. J., Liu, B., Costantini, F., Puzas, J. E., Birchmeier, W., Hsu, W., 2005. The role of Axin2 in calvarial morphogenesis and craniosynostosis. Development. 132**,** 1995-2005.

Zhang, H., Bradley, A., 1996. Mice deficient for BMP2 are nonviable and have defects in amnion/chorion and cardiac development. Development. 122**,** 2977-86.

Zhang, X., Kuroda, S., Carpenter, D., Nishimura, I., Soo, C., Moats, R., Iida, K., Wisner, E., Hu, F. Y., Miao, S., Beanes, S., Dang, C., Vastardis, H., Longaker, M., Tanizawa, K., Kanayama, N., Saito, N., Ting, K., 2002. Craniosynostosis in transgenic mice overexpressing Nell-1. J Clin Invest. 110**,** 861-70.

Zimmerman, L. B., De Jesus-Escobar, J. M., Harland, R. M., 1996. The Spemann organizer signal noggin binds and inactivates bone morphogenetic protein 4. Cell. 86**,** 599-606.